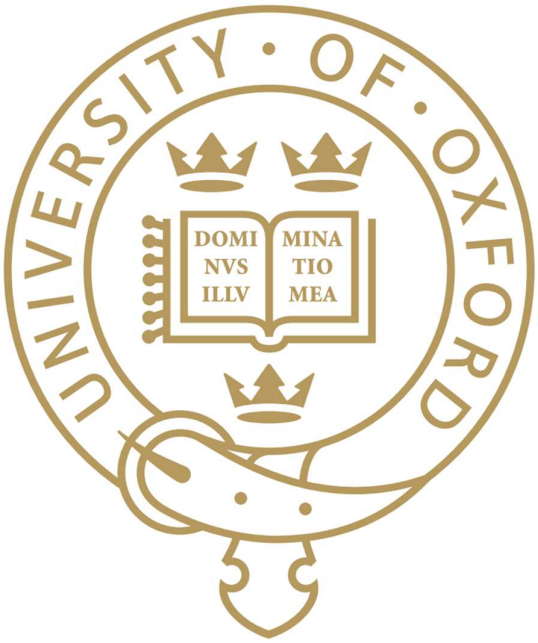


The effects of Galectin-3 on hippocampal neurogenesis and neuroinflammation

Doctor of Philosophy Thesis

Jun Ong

St Cross College

Department of Physiology Anatomy and Genetics

Trinity Term 2025

For my parents.

Abstract

Galectin-3 (Gal-3) is upregulated in Alzheimer's Disease (AD) patients and has been shown to contribute to Beta-amyloid (Aβ) deposition in mouse models of Alzheimer's Disease. Genetic removal of Gal-3 in these models have shown reduction in plaque load and rescue of cognitive deficits. In the subventricular zone (SVZ), Gal-3 regulates postnatal gliogenesis and migration of neural progenitors through the rostral migratory stream. However, less is known about the effects of Gal-3 on hippocampal neurogenesis.

In my thesis, I firstly show that Gal-3 is present in the hippocampus and its neurogenic subgranular zone (SGZ) in healthy adult mice. I then show *in vitro* that Gal-3 decreases neural stem cell proliferation without affecting their differentiation. However, genetic ablation of Gal-3 did not significantly affect hippocampal neurogenesis in healthy adult mice. Next, I show that Gal-3 knockout altered hippocampal microglial morphology in healthy adult mice but did not affect expression of disease associated microglial genes *in vitro*. However, Gal-3 increased expression of disease associated astrocytic genes by astrocytes. Functionally, Gal-3 increased microglial phagocytosis of Aβ, but only when co-cultured with astrocytes. I show that this was due to Gal-3 increasing astrocytic secretion of amyloid degrading enzymes including Matrix metalloproteinase 9 (MMP9). Lastly, I show that intrahippocampal co-injections of truncated Gal-3 without the oligomerisation domain (Gal-3C) with Aβ managed to induce Aβ deposits, but I also show that this was due to host upregulation of full length Gal-3. Hence showing that Gal-3C was not sufficient to induce Aβ deposition. I then show that this was likely due to the fact that only full length Gal-3 could promote high molecular weight oligomers of Aβ.

In conclusion, my thesis provides insight into the effects of Gal-3 on hippocampal neurogenesis and on Aβ clearance by glial cells.

Acknowledgements

This thesis would not have been possible without the kind and patient guidance of Prof Francis Szele. I look up to Francis not just scientifically, but especially in the way he mentors his students. He is never too busy to answer questions or to have discussions about new findings. I have been very lucky to have worked with you and I look forward to working together in the future.

My heartfelt gratitude goes out to all members of the Szele lab both past and present. Some of you have performed experiments which contributed towards this thesis, but all have made my life in Oxford much more enjoyable. A special mention to Dr Luana Soares, who helped me with the surgeries amidst other techniques in the lab. To Adam Packer and the members of his lab who have guided me when I was learning 2P microscopy, thank you for kindly hosting me and showing me the ropes.

My work in the Biomedical Science Building would have been much more tedious without the help from the NACWOs Laura and Agata. A big thank you also to the animal technicians who ensured my colonies were maintained with the utmost care,

I would also like to express my gratitude towards Prof Emma Mead and Prof Daniel Anthony for their kind comments during my confirmation, and providing direction towards the completion of my thesis.

The Agency for Science, Technology and Research Singapore (A*STAR) has provided me funding for my DPhil studies. They have allowed me to fully immerse myself in the culture here in Oxford and without them, I would not have been able to pursue my doctoral training.

My time in Oxford has been marked with mostly peaks but also some troughs. During the toughest of times, I am glad to have friends that I can depend on, be it for a phone call, or to have someone to stay with for a night. To Joycelyn, thank you for always lending a listening ear, however far away you may be. To Alexis Dorier, thank you for the late nights, the adventures, and the friendship. I enjoyed sharing our DPhil journey together; the best thing we got from college was that one cookie!

To Lana, my partner, thank you for being my pillar of support, you always manage to find ways to make even the most tiresome of tasks entertaining. Thank you for sharing my joys and my pains, and I look forward to starting the next Chapters of our lives together.

To my parents I owe too much. Growing up, you made sure that I never had to worry. To Mum, thank you for your sacrifices for me as I was growing up. Taking a career break to look after me full time must not have been an easy decision. To Dad, who had to work tirelessly as a taxi driver, thank you for all the hard work you've put in to keep our family going.

And lastly, to Brownie, losing you was not what I had thought would happen before I submitted my thesis. Thank you for choosing me and I hope I was able to give you a rather happy life, because your presence made all the difference in mine.

Authorship statement

I designed the experiments outlined in this thesis under the supervision of Prof Francis Szele, my supervisor. I have highlighted in my thesis where undergraduate students have contributed to the experiments. These were performed under my supervision and guidance.

In Chapter 3, Zubaida Mukthar contributed to the immunohistochemistry and quantification of DCX^+ cells in middle-aged mice. She also contributed towards immunohistochemistry of a set of brains which I have injected with Aβ, for which the results are outlined in Chapter 7.

In Chapter 3, Hannah Rosenheim contributed towards the immunohistochemistry and quantification of $BrdU^+DCX^+$ cells.

In Chapter 4, Sofia Savastano contributed towards the qPCR experiments in BV2 microglia. She also worked on the phagocytosis assay with BV2 cells in Chapter 5.

In Chapter 6, Dr Daniel Rand performed the i.p. injections of LPS into mice and collected the brains.

Jun Ong

11/10/2025

Table of Contents

List of Abbreviations 18

Chapter 1: Introduction 20

1.1 Alzheimer’s Disease (AD) 21

1.1.1 Beta-Amyloid (Aβ) 21

1.1.2 Tau 22

1.1.3 Neuroinflammation 22

1.1.4 Decreased adult hippocampal neurogenesis (AHN) 24

1.1.5 Cognitive decline 26

1.1.6 Conclusion 27

1.2 Galectin-3 and Alzheimer's Disease 27

1.2.1 Galectin-3 Biology 27

1.2.2 Galectin-3 and Beta-amyloid 29

1.2.3 Galectin-3 and Tau 29

1.2.4 Galectin-3 and inflammation 30

1.2.5 Galectin-3 and phagocytosis 31

1.2.6 Galectin-3 and neurogenesis 31

1.2.7 Galectin-3 and cognitive decline 32

1.3 Aims of project 33

Chapter 2: Materials and Methods 35

2.1 Animals 36
2.1.1 Galectin-3 knockout mice (Lgals3<tm1Poi>/129Sv) 36
2.1.2 Galectin-3 knockout mice (Lgals3<tm1Ftl>) 36
2.1.3 Cx3cr1-GFP mice 37
2.2 Preparation of Beta Amyloid 37
2.2.1 Monomerisation of Aβ from lyophilised stock 37
2.2.2 Preparation of Aβ oligomers for *in vitro* assays 38
2.3 Surgeries 38
2.4 Immunofluorescence 40
2.4.1 Sectioning of brains with intrahippocampal injections 40
2.4.2 Immunohistochemistry without antigen retrieval 40
2.4.3 Immunohistochemistry with antigen retrieval 41
2.4.4 Immunohistochemistry with Sudan Black B (SBB) quenching 41
2.4.5 Immunocytochemistry 41
2.5 Neurosphere experiments 42
2.5.1 Isolation of primary neurospheres from P2 – P4 pups 42
2.5.2 Passaging of neurospheres 42
2.5.3 Neurosphere proliferation assay 43
2.5.4 Neurosphere differentiation assay 43
2.6 Glial cell culture 44
2.6.1 Poly-d-lysine (PDL)-coating of flasks and plates 44

2.6.2 Isolation of primary murine glia 44

2.6.3 Subculturing of mixed glial cultures 45

2.6.4 Subculturing of microglia and astrocytes 45

2.6.5 pHrodo phagocytosis assays 46

2.7 Western blot 47

2.7.1 Sample collection 47

2.7.2 Sodium dodecyl sulfate–polyacrylamide gel electrophoresis (SDS-PAGE) and transfer 48

2.7.3 Immunoblotting 48

2.8 Reverse Transcription quantitative Polymerase Chain (RT-qPCR) 49

2.8.1 Sample collection and purification 49

2.8.2 cDNA synthesis 49

2.8.3 qPCR 50

2.9 Thioflavin T assay 50

Chapter 3: The effect of Galectin-3 on hippocampal neurogenesis 52

3.1 Galectin-3 is expressed in the hippocampus in WT mice by 10 weeks of age. 53

3.2 Galectin-3 decreases neural stem cell proliferation but does not affect differentiation *in vitro* 59

3.2.1 Neural stem cell proliferation is decreased by Galectin-3, but is not affected by Galectin-3 inhibitor in medium 60

3.2.2 Neural stem cell differentiation is not affected by presence of Galectin-3 or Galectin-3 inhibitor in medium 61

3.3 Galectin-3 knockout did not significantly alter adult hippocampal neurogenesis in young adult mice on a Sv129 background 64

3.3.1 Galectin-3 knockout did not affect the transient amplifying progenitor or neuroblast population in young adult mice 64

3.4 Galectin-3 knockout did not significantly alter hippocampal neurogenesis in young adult mice 66

3.4.1 Galectin-3 knockout did not affect slow dividing label retaining cell 66

3.4.2 Galectin-3 knockout trended towards increased neuroblast generation in young adult mice 68

3.4.3 Galectin-3 knockout did not affect number of post-mitotic neurons generated 69

3.4.4 Galectin-3 knockout did not affect location of $BrdU^+/NeuN^+$ cells within the DG 70

3.5 Galectin-3 knockout in middle-aged mice did not alter generation of newborn neurons in WTs 72

3.6 Discussion 73

3.6.1 Galectin-3 expression is detectable in the hippocampus and SGZ of C57Bl6 mice from 10 weeks. 73

3.6.2 On the use of recombinant Galectin-3 and TD-139 over Galectin-3 overexpression and silencing via nucleofection of plasmids 73

3.6.3 Galectin-3 effects on different neuronal populations 74

3.6.4 Discrepancies between *in vitro* neurosphere assays and *in vivo* mouse models 75

3.6.5 Use of two different mouse strains 78

3.6.6 Future directions..... 79

3.6.7 Conclusion 80

Chapter 4: The effect of Galectin-3 on Glial cells..... 81

4.1 Introduction 82

4.1.1 Sholl analysis 82

4.1.2 Disease associated microglia genes 83

4.1.3 Disease associated astrocyte genes 83

4.2 Galectin-3 expressing microglia are not morphologically distinct from non-Galectin-3 expressing microglia 84

4.3 In C57Bl6 mice, microglia from young mice do not significantly differ from microglia from middle-aged mice..... 89

4.4 Microglia from Galectin-$3^{-/-}$ mice are more ramified than microglia from Galectin-$3^{+/+}$ mice 91

4.5 The effect of Galectin-3 knockout on DAM gene expression..... 97

4.5.1 Galectin-3 knockout did not alter DAM gene expression in primary murine microglia 97

4.5.2 Treatment of BV2 microglia with Galectin-3 or TD-139 did not affect expression of DAM genes 98

4.6 The effect of Galectin-3 modulation on Disease Associated Astrocyte (DAA) gene expression..... 99

4.6.1 Exogenous Galectin-3 increased expression of a subset of DAA genes in primary murine astrocytes 99

4.7 Discussion 101

4.7.1 Galectin-3 expression did not alter microglial morphology in young or middle-aged C57Bl6 mice 101

4.7.2 Galectin-3 knockout increases microglial ramification in middle-aged male mice, and to a smaller extent in young adult male mice. 102

4.7.3 Galectin-3 did not significantly alter disease associated microglial gene expression *in vitro* 103

4.7.4 Galectin-3 altered expression of Disease Associated Astrocyte (DAA) genes *in vitro* 104

Chapter 5: Galectin-3 increases microglial phagocytosis of pHrodo-Aβ_{1-42} via astrocyte secreted factors 107

5.1 Introduction 108

5.2 Oligomerisation of Beta-Amyloid and Characterisation by western blot and transmission electron microscopy (TEM) 109

5.3 Addition of Galectin-3 or its inhibitor to microglial cultures did not alter phagocytosis of pHrodo-AβO_{1-42} 110

5.3.1 Galectin-3 did not alter phagocytosis of pHrodo-AβO_{1-42} by BV2 microglia 110

5.3.2 Galectin-3 did not alter phagocytosis of pHrodo-AβO_{1-42} by primary murine microglia from Cx3cr1-GFP$^{+/-}$ mice 112

5.4 Galectin-3 mediates microglial phagocytosis of pHrodo-AβO_{1-42} in mixed glial cultures 114

5.5 Galectin-3 increases microglial phagocytosis of pHrodo-AβO$_{1-42}$ through astrocyte secreted factors 117

5.6 Galectin-3 increases microglial phagocytosis of pHrodo-AβO$_{1-42}$ in mixed glial cultures via matrix metalloproteinases (MMPs) 121

5.6.1 Addition of MMP inhibitor Marimastat to mixed glial cultures decreased microglial phagocytosis of pHrodo-AβO$_{1-42}$ 124

5.6.2 Addition of MMP inhibitor Marimastat to mixed glial cultures abrogated the Galectin-3 mediated increase in microglial phagocytosis of pHrodo-AβO$_{1-42}$ .. 124

5.7 Galectin-3 increased expression of amyloid degrading enzymes (ADEs) in astrocytes 125

5.8 Galectin-3 increased levels of pro-MMP9 and cleaved MMP9 in Galectin-3$^{+/+}$ and Galectin-3$^{-/-}$ primary murine glia 127

5.9 Discussion 129

5.9.1 Aβ uptake pathways in microglia 129

5.9.2 Possible pathways of MMP9 upregulation by Galectin-3 in astrocytes:.. 131

5.9.3 Use of WT Aβ over mutant Aβ 132

5.9.4 Inhibition of Galectin-3 increased expression of Mme (Neprilysin)..... 133

5.9.5 Limitations 133

Chapter 6: Galectin-3 increases MMP9 *in vitro* 136

6.1 Introduction 137

6.2 Galectin-3 knockout decreased LPS-mediated increase in MMP9 levels in primary murine glia 138

6.3 LPS and Galectin-3 knockout have sex dependent effects on MMP9 levels 139

6.3.1 Peripheral LPS increased MMP9 levels in the brain 141

6.3.2 Galectin-3 knockout in males did not have a significant effect on LPS-induced MMP9 levels 141

6.3.3 Galectin-3 knockout in females increased LPS-mediated increase in MMP9 levels 142

6.3.4 LPS increased Galectin-3 levels in male mice 142

6.4 Discussion 143

6.4.1 Possible mechanisms of interaction between Galectin-3 and LPS to induce MMP9 levels 143

6.4.2 Sex difference in LPS-induced MMP9 levels *in vivo* 144

6.4.3 Sex difference in how Galectin-3 knockout alters LPS-induced MMP9 levels *in vivo* 144

6.4.4 Peripheral Galectin-3 vs. brain Galectin-3 144

6.4.5 Implications for AD 146

6.4.6 Limitations and future work 146

Chapter 7: Galectin-3 Promotes Beta Amyloid deposition *in vivo* 148

7.1 Introduction 149

7.2 Galectin-3 Promotes Aβ Deposition *in vivo* 149

7.2.1 Injections of Aβ alone do not result in deposit formation 149

7.2.2 Co-injections of Aβ with Galectin-3 result in deposits 150

7.2.3 Co-injections of Aβ with Galectin-3C result in deposits 151

7.3 Exogenous Galectin-3, without host Galectin-3, is sufficient to promote Aβ deposition 153

7.3.1 Injections of Aβ alone into Galectin-$3^{-/-}$ mice did not result in Aβ deposits 153

7.3.2 Injections of Aβ with Galectin-3 into Galectin-$3^{-/-}$ mice resulted in Aβ deposition 154

7.3.3 Injections of Aβ and Galectin-3C did not result in formation of Aβ deposits 155

7.4 Galectin-3 promotes Aβ oligomerisation *in vitro* 156

7.4.1 Amyloid Beta oligomerisation is induced by incubation with Galectin-3.. 157

7.4.2 Incubation with Galectin-3C does not promote formation of high molecular weight oligomers of Aβ 157

7.4.3 Thioflavin T assay shows increased aggregation with Galectin-3 but not Galectin-3C..... 158

7.5 Discussion..... 159

7.5.1 Key differences between previous work on the role of Galectin-3 and Aβ aggregation..... 159

7.5.2 Galectin-3C together with Aβ was sufficient to induce host expression of Galectin-3 160

7.5.3 Galectin-3C did not result in HMW oligomers of Aβ. 161

7.5.4 Full length Galectin-3, but not Galectin-3C, was sufficient to promote Aβ deposition in Galectin-$3^{-/-}$ mice..... 162

7.5.5 Limitations 162

Chapter 8: Final discussion 165

8.1 Overview and mechanistic model 166

8.2 Galectin-3 and hippocampal neurogenesis 167

8.3 Galectin-3 and glial biology 168

8.4 Astrocyte–microglia crosstalk and Aβ uptake 169

8.5 MMP9 as part of a broader protease network 170

8.6 MMP9 as a context-dependent modulator of Aβ processing and neurodegeneration 171

8.6.1 MMP9 can contribute to AD pathologies 171

8.6.2 MMP9 leads to blood brain barrier (BBB) breakdown in AD and other neurological conditions 172

8.7 Galectin-3, inflammation, and MMP9 *in vivo* 173

8.8 Galectin-3 and Aβ aggregation 174

8.9 Integrating Galectin-3, Aβ aggregation, MMP9, and neurogenesis 175

8.10 Galectin-3 and ageing 176

8.11 Galectin-3 in AD patients 177

8.12 Implications for Galectin-3 as a therapeutic target 178

8.12.1 Clinical trials with Galectin-3 as a target 178

8.12.2 Galectin-3 inhibition as a BBB protective therapy 179

8.12.3 Galectin-3 inhibition could reduce neuroinflammation 180

8.12.4 Galectin-3 inhibition could increase neurogenesis 180

8.13 Limitations of current work 181

8.13.1 Cx3cr1-GFP mice 181

8.13.2 Primary glial cultures 181

8.13.3 Use of human rGalectin-3 and $A\beta_{1-42}$ in murine models..... 184

8.13.4 Aβ-galectin-3 pre-incubation conditions 184

8.13.5 Limitations of pHrodo labelled Aβ 185

8.13.6 Sex-dependent effects 186

Chapter 9: References 189

Appendix 207

List of Abbreviations

AD	Alzheimer's disease
Aβ	Beta Amyloid
$A\beta O_{1-42}$	oligomerized beta amyloid (1-42)
BrdU	5-bromo-2'-deoxyuridine
DAA	disease associated astrocyte
DAM	disease associated microglia
DAPI	4',6-diamidino-2-phenylindole
DCX	doublecortin
DG	dentate gyrus
EGF	epidermal growth factor
FGF	fibroblast growth factor
Gal-3-	non-Galectin-3 expressing
Gal-3+	Galectin-3 expressing
GCL	granule cell layer
GFAP	glial fibrillary acidic protein
GFP	green fluorescent protein
hiPSC	human induced pluripotent stem cell
i.p.	intraperitoneal
IBA1	ionized calcium-binding adapter molecule 1
IHC	immunohistochemistry
LPS	lipopolysaccharide
MMP	matrix metalloproteinase
NeuN	neuronal nuclei
NSC	neural stem cell
PB	phosphate buffer

PBS	phosphate buffered saline
PDL	poly-D-lysine
PFA	paraformaldehyde
RT-qPCR	Reverse Transcription quantitative Polymerase Chain
SEM	standard error of the mean
SGZ	subgranular zone
SRI	Schoenen ramification index
SVZ	subventricular zone
ThT	thioflavin T
WT	wild type

Chapter 1: Introduction

1.1 Alzheimer's Disease (AD)

Alzheimer's Disease is the leading cause of dementia, accounting for over 60% of cases. With the leading risk factor for AD being age, dementia cases are expected to almost triple globally between 2019 and 2050 (Nichols et al., 2022). First observed more than a century ago by Alois Alzheimer, the pathological hallmarks of AD include the presence of Beta Amyloid (Aβ) plaques and Tau neurofibrillary tangles (NFTs). More recently, in addition to Aβ and Tau NFTs, alterations to hippocampal neurogenesis and neuroinflammation have been observed in AD.

1.1.1 Beta-Amyloid (Aβ)

1.1.1.1 Production of Aβ from Amyloid precursor protein (APP)

APP and its cleavage products have roles in neural development and neurogenesis (Nicolas & Hassan, 2014). Non-amyloidogenic α-cleavage of APP by α-secretase produces sAPPα which has been shown to promote neurogenesis (Ohline et al., 2022) and even been proposed to be a possible therapeutic agent (Dar & Glazner, 2020).

The amyloidogenic pathway involves sequential cleavage, first by β-secretase to generate sAPPβ and CTF99 (C-terminal fragment). Cleavage of the CTF by the γ-secretase complex then results in the release of free Aβ which can range from 38 – 43 amino acids in length. These include $Aβ_{1-40}$, the most abundant form of Aβ in the brain, and $Aβ_{1-42}$, the most well-studied isoform of Aβ in AD.

1.1.1.2 The amyloid cascade hypothesis

Under the amyloid cascade hypothesis, accumulation and aggregation of Aβ is proposed to drive AD pathology. This is supported by the fact that monomers of Aβ have not been considered as toxic (Sarkar et al., 2013), and have even been proposed as neuroprotective by promoting survival of mature neurons (Giuffrida et al., 2009). Multiple genes associated with increased risk of AD have been shown to encode proteins which promote Aβ aggregation, including ApoE and ApoJ (Hashimoto et al., 2012), and aggregated species of Aβ correlated with disease severity in AD (Tomic et al., 2009). Aβ could cause cognitive decline by inducing

neuroinflammation in microglia and astrocytes (discussed in 1.1.3), or by directly affecting neurons and neurogenesis (discussed in 1.1.4). Importantly, Aβ accumulation drives downstream Tau pathology (Oddo et al., 2003); *in vivo* imaging using 2-photon microscopy demonstrates that Aβ plaques induce local dystrophic neurites (Meyer-Luehmann et al., 2008).

1.1.2 Tau

Tau is a microtubule-associated protein in axons of neurons. Under homeostatic conditions, Tau binds to and stabilises microtubules, facilitating axonal transport. In AD, hyperphosphorylation of Tau can lead to its aggregation and cytotoxicity. In addition to loss of homeostatic functions, aggregation of Tau can result in the formation of seed-competent species which lead to the spreading of Tau pathology. Like Aβ, Tau can result in glial reactivity (discussed in 1.1.3) and is correlated with cognitive decline (discussed in 1.1.5).

1.1.3 Neuroinflammation

Inflammation and cellular senescence have been proposed as hallmarks of ageing (Lopez-Otin et al., 2023), with senescent cells having a secretory phenotype that can promote “inflammaging”, chronic low-grade inflammation that increases with age (Olivieri et al., 2018). In AD, increased levels of pro-inflammatory cytokines such as Tumour Necrosis Factor alpha (TNFα), Interleukin 6 (IL-6) have been described, with microglia and astrocytes being the major contributors towards this neuroinflammatory phenotype.

Both $A\beta_{1\text{-}42}$ and Tau NFTs have been shown to increase glial activation and expression of pro-inflammatory genes (Zaheer et al., 2008), furthermore, activated glia have been shown to propagate AD-related pathologies, resulting in a positive feedback loop which may aggravate neuroinflammation and induce further Aβ plaques and Tau NFTs.

1.1.3.1 Microglial activation in AD

Microglia are the tissue-resident macrophages in the brain, maintaining homeostasis by surveilling for pathogens and clearing debris from dead and dying cells. In AD, microglia acquire a reactive phenotype, with a subset of microglia (termed disease associated microglia,

DAM) in the 5xFAD mouse model strongly upregulating genes related to the phagocytosis/lysosomal pathway and immune response (Keren-Shaul et al., 2017).

The pathological features of AD have been shown to result in microglial activation. Aβ binds to receptors on microglia including Toll-like receptors (TLRs) and Scavenger receptors; while these interactions promote phagocytic clearance of Aβ by microglia, they can also induce microglial secretion of pro-inflammatory cytokines including IL-6 and nitric oxide (Walter et al., 2007). Microglia which have phagocytosed Aβ *in vivo* upregulate genes for inflammatory processes (Grubman et al., 2021), showing a specific subset of reactive microglia in response to Aβ. Tau activates the cyclic GMP–AMP synthase–stimulator of interferon genes (cGAS-STING) pathway, driving nuclear factor kappa B (NFκB) transcription of pro-inflammatory genes such as Tnfa and Isg54 (Jin et al., 2021). Hence, the microglial activation seen in AD can be driven by Aβ and Tau pathologies.

Concurrently, microglial activation can also propagate AD pathologies, with reactive microglia contributing to Tau seeding and spreading (Maphis et al., 2015). Failure of microglia to clear Aβ intracellularly leads to its accumulation in lysosomes, causing apoptosis of microglia and further plaque formation (Baik et al., 2016). Altogether, these suggest that microglial activation is not only a result of AD pathologies such as Aβ and Tau but can also contribute to the pathologies, resulting in a positive feedback cycle.

1.1.3.2 Astrocytic activation in AD

Astrocytes have important roles in ion and metabolite homeostasis, and they regulate the blood-brain barrier as their endfeet are connected to the brain vasculature.

Like microglia, astrocytes have also been shown to acquire a disease associated phenotype in AD (Disease associated astrocytes, DAA) (Habib et al., 2020). Aβ-treatment of cultured astrocytes has been shown to result in increased nitric oxide levels and Interleukin-1 beta (IL-1β) expression (Hu et al., 1998; Schubert et al., 2009), along with increased activation as seen from stellate morphology.

In vitro, primary murine astrocytes increased pro-inflammatory cytokine expression after Tau pre-formed fibril (PFF) stimulation in a NfκB-dependent manner (Wang & Ye, 2021). Furthermore, conditioned medium from both Tau PFF and monomer pre-treated astrocytes increased neuronal cell death (Wang & Ye, 2021), suggesting astrocytes secreted neurotoxic factors in response to Tau. Astrocytes derived from P301S mice, when co-cultured with neurons from either wild type (WT) or P301 mice, decreased neuronal survival when compared to astrocytes derived from WT mice (Sidoryk-Wegrzynowicz et al., 2017). This is supported by the decreased levels of glutamine synthetase and glial glutamate transporter in P301S mice along with increased levels of glial fibrillary acidic protein (GFAP) (Sidoryk-Wegrzynowicz et al., 2017). Such increases in astrogliosis are also seen in other mouse models of tauopathy such as the Thy22 (Gomez-Murcia et al., 2020). In conclusion, astrocytes are also activated in AD, and this can be a result of Aβ and Tau pathology.

1.1.4 Decreased adult hippocampal neurogenesis (AHN)

In adults, neurogenesis is restricted to two niches – the ventricular-subventricular zone (V-SVZ) and the sub-granular zone (SGZ) of the hippocampus. In the SGZ, Neural Stem Cells (NSCs, $GFAP^+$) divide either symmetrically for self-renewal (generating two NSCs), or asymmetrically to generate one NSC and one neural progenitor cell (Achaete-scute family bHLH transcription factor 1, $ASCL1^+$). Neural progenitors then divide and differentiate into neuroblasts (doublecortin, DCX^+) which then further differentiate into neurons which integrate into the dentate gyrus. In AD, AHN is decreased (Moreno-Jimenez et al., 2019), and hence multiple studies have tried to identify novel and natural substances which will promote AHN in an attempt to rescue the cognitive deficits of AD (Ong et al., 2025). In mice, increasing AHN has shown promise, with compounds increasing neurogenesis also rescuing cognitive deficits in AD models (Sasaki et al., 2019).

The pathological hallmarks of AD can decrease AHN. Soluble extracts from the hippocampi of 6-month old amyloid precursor protein/presenilin-1 (APP/PS1) mice (containing Aβ)

decreased neural stem cell proliferation in the neurosphere assay (Baglietto-Vargas et al., 2017). The authors confirmed the effect of Aβ by showing that hippocampal extracts immuno-depleted of Aβ did not alter neurosphere diameters (Baglietto-Vargas et al., 2017). The effect of Aβ on hippocampal neurogenesis was also seen *in vivo* with intracerebroventricular injections of Aβ into WT mice, which resulted in decreased neuronal nuclei-positive ($NeuN^+$) cell density in the dentate gyrus (Amber et al., 2020), and with intrahippocampal injection of $Aβ_{1-42}$ oligomers which decreased 5-bromo-2′-deoxyuridine-positive ($BrdU^+$) proliferative cells in the SGZ (Zheng et al., 2013). Aggregation-prone Tau resulted in the thinning of the dentate gyrus pyramidal layer (Sydow et al., 2011), suggesting decreased hippocampal neurogenesis. Pro-inflammatory cytokines released by reactive glia can also decrease neurogenesis. Adult rat neural stem cells treated with IL-6 decreased differentiation and increased apoptosis (Monje et al., 2003). TNFα decreased proliferation of murine neural stem cells in a tumour necrosis factor receptor 1 (TNFR1) dependent manner, and also decreased differentiation of neural stem cells into Dcx+ neuroblasts (Chen & Palmer, 2013). The authors also showed that injections of TNF into the dentate gyrus decreased the generation of neurons *in vivo* (Chen & Palmer, 2013). Since activated microglia and astrocytes can secrete IL-6, the increased glial cell activation could increase the levels of pro-inflammatory cytokines in the brain, decreasing neurogenesis. In conclusion, the abovementioned characteristics of AD can all contribute towards alterations in hippocampal neurogenesis.

While neurogenesis in mice is widely accepted to continue throughout life, adult hippocampal neurogenesis (AHN) in humans is still contested. While some have contested the existence of AHN (Franjic et al., 2022; Sorrells et al., 2018), multiple lines of evidence suggest that neurogenesis in the hippocampus continues throughout life in humans, including C_{14} dating observations (Spalding et al., 2013), immunohistochemical analyses (Alonso-Moreno et al., 2025), and single cell RNA sequencing (Tobin et al., 2019).

1.1.5 Cognitive decline

Plasma levels of Aβ and Tau have been correlated with cognitive decline in Mild Cognitive Impairment (MCI) patients (Chen et al., 2019). Concurrently, levels of AHN are decreased in aged adults with MCI and AD (Cao et al., 2024; Tobin et al., 2019). Hence AD pathologies could lead to cognitive deficits by decreasing AHN. Additionally, AD pathologies have also been shown to directly alter synaptic function. Injections of Aβ were sufficient to induce cognitive deficits in C57BL/6 mice (Faucher et al., 2015). Aggregates of Aβ have been hypothesized to cause cognitive decline by disrupting synaptic plasticity and increasing synaptic toxicity. Aβ disrupts glutamatergic receptors and their function, such as by activating N-methyl-D-aspartate (NMDA) and α-amino-3-hydroxy-5-methyl-4-isoxazolepropionic acid (AMPA) receptors and increasing intracellular Ca^{2+} levels to sensitize neurons to glutamate (Mattson et al., 1992). Concurrently, Aβ can also block long term potentiation (LTP) by decreasing re-uptake of glutamate (Li et al., 2009). Hence, in addition to decreasing hippocampal neurogenesis and increasing neuroinflammation, Aβ oligomers can directly disrupt synapses and cause loss of LTP, all of which could contribute to the learning and memory deficits seen in AD.

In both control and AD brains, Tau NFT containing neurons have lower synaptophysin than non-NFT containing neighbours (Callahan & Coleman, 1995). Mice expressing aggregation-prone Tau also performed worse on hippocampal-dependent tasks such as the Morris Water Maze and passive avoidance test (Sydow et al., 2011). Lipopolysaccharide (LPS)-induced neuroinflammation can increase microglial Complement component 1q (C1q) and decrease dendritic spine density of neurons in the CA1 (Wu et al., 2023), resulting in cognitive impairment. A similar upregulation of C1q and aberrant synaptic engulfment is seen in an AD mouse model (De Schepper et al., 2023). Chronic, low-dose LPS also induces astrocytic activation and result in alterations to glutamate homeostasis (Schirmbeck et al., 2023), decreased expression of genes related to these processes can cause excitotoxicity and loss

of synapses. Altogether, these suggest that the pathologies seen in AD can contribute towards cognitive decline, either directly by disrupting synapses, or indirectly via inflammation.

1.1.6 Conclusion

In section 1.1, the pathological hallmarks of AD have been outlined. The interactions between neuroinflammation, Aβ pathology and Tau NFTs have been highlighted, with *in vitro* and *in vivo* evidence showing that Aβ and Tau pathologies can be worsened by glial activation and vice versa. Importantly, these features can lead to decreased hippocampal neurogenesis, which has been correlated to cognitive impairment in humans. Furthermore, they can also directly disrupt synaptic function which leads to cognitive deficits.

1.2 Galectin-3 and Alzheimer's Disease

Recently, Galectin-3 has become of interest in the context of AD as it has been shown to be upregulated in patient sera (Ashraf & Baeesa, 2018; Wang et al., 2015) and CSF (Ashraf & Baeesa, 2018; Boza-Serrano et al., 2022). Additionally, Gal-3 levels are negatively correlated with cognitive scores (Ashraf & Baeesa, 2018; Wang et al., 2015) and colocalise with Aβ deposits and Tau tangles in AD brains (Boza-Serrano et al., 2022). In the 5xFAD model, Galectin-3 is upregulated in DAM (Keren-Shaul et al., 2017)

1.2.1 Galectin-3 Biology

Galectins are evolutionarily conserved proteins characterised by a carbohydrate recognition domain (CRD) and have multiple roles in innate immunity, inflammation, differentiation and apoptosis. While the prototypic subfamily (Gal-1, 2, 7, 10, 11, 13, 14, 15) contains only one CRD which can form homodimers, the tandem repeat subfamily (Gal-4, 5, 6, 8, 9, 12) have two distinct CRDs which form heterodimers. Galectin-3 is the only chimeric member in the Galectin family, having a unique N-terminal oligomerisation domain linked to the C-terminus CRD by a collagen-like sequence (CLS).

Pentamerisation of Galectin-3 is triggered by binding to glycoproteins (Zhao et al., 2021) and is mediated by prolines in the N-terminal, the positions of which are highly conserved across species. This occurs through a process similar to liquid-liquid phase separation as the CRD is hydrophilic while the N-terminal is hydrophobic.

Human and mouse Galectin-3 (hGal-3 and mGal-3, respectively) share a highly conserved sequence (77% identity, 82% positives), with the CRD having even higher conservation (88% identity, 93% positives). While there are differences in the CLS, the positions of prolines remain highly similar. Together, these suggest that hGal-3 and mGal-3 are likely to function similarly.

Galectin-3 is conserved between mouse and human:

```
Mouse  1    MADSFSLNDALAGSGNPNPQGYPGAWGNQP-GAGGYPGAAYPGAYPGQAPPGAYPGQAPP  59
            MAD+FSL+DAL+GSGNPNPQG+PGAWGNQP GAGGYPGA+YPGAYPGQA         PP
Human  1    MADNFSLHDALSGSGNPNPQGWPGAWGNQPAGAGGYPGASYPGAYPGQA---------PP  51

Mouse  60   GAYPGQAPPSAYPGPTAPGAYPGPTAPGAYPGQPAPGAFPGQPGAPGAYPQ-----CSGG  114
            GAYPGQAPP AYPG           APGAYPG PAPG +PG P  PGAYP       +G
Human  52   GAYPGQAPPGAYPG----------APGAYPGAPAPGVYPGPPSGPGAYPSSGQPSATGA  100

Mouse  115  YPAAGPYGVPAGPLTVPYDLPLPGGVMPRMLITIMGTVKPNANRIVLDFRRGNDVAFHFN  174
            YPA GPYG PAGPL VPY+LPLPGGV+PRMLITI+GTVKPNANRI LDF+RGNDVAFHFN
Human  101  YPATGPYGAPAGPLIVPYNLPLPGGVVPRMLITILGTVKPNANRIALDFQRGNDVAFHFN  160

Mouse  175  PRFNENNRRVIVCNTKQDNNWGKEERQSAFPFESGKPFKIQVLVEADHFKVAVNDAHLLQ  234
            PRFNENNRRVIVCNTK DNNWG+EERQS FPFESGKPFKIQVLVE DHFKVAVNDAHLLQ
Human  161  PRFNENNRRVIVCNTKLDNNWGREERQSVFPFESGKPFKIQVLVEPDHFKVAVNDAHLLQ  220

Mouse  235  YNHRMKNLREISQLGISGDITLTSANHAMI  264
            YNHR+K L EIS+LGISGDI LTSA++ MI
Human  221  YNHRVKKLNEISKLGISGDIDLTSASYTMI  250
```

Furthermore, this similarity is increased for just the C-terminal CRD:

```
Mouse  1    PLPGGVMPRMLITIMGTVKPNANRIVLDFRRGNDVAFHFNPRFNENNRRVIVCNTKQDNN  60
            PLPGGV+PRMLITI+GTVKPNANRI LDF+RGNDVAFHFNPRFNENNRRVIVCNTK DNN
Human  1    PLPGGVVPRMLITILGTVKPNANRIALDFQRGNDVAFHFNPRFNENNRRVIVCNTKLDNN  60

Mouse  61   WGKEERQSAFPFESGKPFKIQVLVEADHFKVAVNDAHLLQYNHRMKNLREISQLGISGDI  120
            WG+EERQS FPFESGKPFKIQVLVE DHFKVAVNDAHLLQYNHR+K L EIS+LGISGDI
Human  61   WGREERQSVFPFESGKPFKIQVLVEPDHFKVAVNDAHLLQYNHRVKKLNEISKLGISGDI  120

Mouse  121  TLTSANHAMI  130
             LTSA++ MI
Human  121  DLTSASYTMI  130
```

1.2.2 Galectin-3 and Beta-amyloid

Boza-Serrano and colleagues show that by knocking out Gal-3 in 5xFAD mice, Aβ plaque burden is decreased, while conversely the co-injection of Aβ with Gal-3 induced Aβ deposition (Boza-Serrano et al., 2019). Remarkably, this reduction in plaque burden is recapitulated in the APP/PS1 model with Gal-3 knockdown (Tao et al., 2020). Gal-3 is known to bind to β-galactosidated proteins such as Aβ, and a co-immunoprecipitation showed that Gal-3 indeed binds to Aβ (Tao et al., 2020). Furthermore, both studies also show cognitive benefits from reducing Gal-3 levels (Boza-Serrano et al., 2019; Tao et al., 2020). Microglia which have phagocytosed Aβ show increased Galectin-3 expression (Grubman et al., 2021). Altogether, these show that Galectin-3 directly interacts with Aβ and increases its deposition.

1.2.3 Galectin-3 and Tau

Another crucial hallmark of AD is the presence of Tau neurofibrillary tangles (NFTs). More recently, Siew and colleagues show that Gal-3 not only binds to phosphor-Tau (pTau), but also promotes Tau fibrillation (Siew et al., 2024). The knockout of Gal-3 in THY-Tau22 mice also reduced Tau deposition and rescued cognitive defects in the tauopathy mouse model (Siew et al., 2024). Since Aβ pathology also drives Tau aggregation (Gotz et al., 2001), Galectin-3 could also be promoting Tau aggregation indirectly by increasing Aβ aggregation. In humans, Galectin-3+ microglia are observed to be associated with pTau in post-mortem brain samples and Galectin-3 levels are correlated with both pTau and total Tau levels (Boza-Serrano et al.,

2022). Taken together, these show that Galectin-3 has similar effects on the aggregation of Tau as it has on Aβ.

1.2.4 Galectin-3 and inflammation

Galectin-3 was first described to be expressed in macrophages after strong inflammatory challenges (Ho & Springer, 1982). Galectin-3 is also upregulated by BV2 microglia and in the brain after LPS treatment (Burguillos et al., 2015).

1.2.4.1 Microglia

Primary murine microglia from Galectin-3$^{-/-}$ mice showed decreased secretion of pro-inflammatory cytokines after LPS stimulation (Burguillos et al., 2015) and after treatment with Aβ fibrils (Boza-Serrano et al., 2019). iPSC-derived microglia also decreased pTau-induced secretion of IL1α, IL1β, IL-6 and TNFα when treated with the Galectin-3 inhibitor TD-139 (Siew et al., 2024). Addition of Galectin-3 directly to primary microglia also increased release of proinflammatory cytokines in a TLR4 dependent manner (Burguillos et al., 2015). *in vivo*, Galectin-3 knockout decreased the density of CD68^{+} cells in response to peripheral LPS, suggesting that loss of Galectin-3 attenuated LPS-induced microglial activation (Espinosa-Oliva et al., 2021).

These findings show that Galectin-3 is a crucial mediator of microglial activation both intracellularly and extracellularly. In the latter, Galectin-3 can act as a TLR4 ligand (Burguillos et al., 2015), inducing paracrine activation of neighbouring cells.

1.2.4.2 Astrocytes

Galectin-3 is upregulated in astrocytes after traumatic brain injury (TBI) and marks a subset of proliferative astrocytes with neurosphere-forming potential (Sirko et al., 2015). However, it has not been characterised whether Galectin-3 can also result in astrocytic activation. The effect of Galectin-3 on astrocytic activation in neurodegenerative diseases is also not well characterized.

1.2.5 Galectin-3 and phagocytosis

Galectin-3 acts as a pattern-recognition receptor, opsonising bacteria for phagocytosis by microglia upon binding to MerTK (Cockram et al., 2019; Nomura et al., 2017). In demyelinating disease, Galectin-3 is expressed by microglia which phagocytose myelin, and inhibition of Galectin-3 with galactose decreased myelin phagocytosis (Reichert et al., 1994). Hence, it appears that Galectin-3 promotes the phagocytosis of cargo by microglia. However, less is understood about how Galectin-3 regulates Aβ phagocytosis. Currently, only one study has examined the effect of Galectin-3 on Aβ phagocytosis. Addition of Galectin-3 simultaneously with cargo increased uptake of monomeric Aβ (mAβ), but not fibrillar Aβ (fAβ); however, 30 minute pre-treatment of primary microglia with Galectin-3 prior to addition of cargo decreased uptake of fAβ, but not mAβ (Boza-Serrano et al., 2019). While the increased uptake of mAβ in the presence of Galectin-3 is consistent with the role of Galectin-3 as an opsonin, the results seen with pre-treatment of Galectin-3 suggests a more complex role of Galectin-3 in Aβ phagocytosis which warrants further investigation.

1.2.6 Galectin-3 and neurogenesis

In the SVZ, neural stem cells divide and differentiate into DCX^+ neuroblasts which migrate along the rostral migratory stream (RMS) towards the olfactory bulb (OB) where they differentiate into NeuN+ neurons. Here, Galectin-3 is expressed by $GFAP^+$ astrocytes, ependymal cells and a subset of $Mash1^+$ intermediate progenitors (Comte et al., 2011). Galectin-3 KO reduces the number of neurons in the OB by altering neuroblast migration along the RMS (Comte et al., 2011).

By electroporation of either an shGal-3 construct into WT animals, or a Cre construct into Galectin-$3^{flox/flox}$ animals, previous work in the Szele lab established that Galectin-3 knockdown decreased gliogenesis in the SVZ (Al-Dalahmah, Campos Soares, et al., 2020). Overexpression of Gal-3 increased the proportion of $GFAP^+$ and $S100\beta^+$ cells while decreasing the number of $Olig2^+$ cells, suggesting a shift of fate choice away from oligodendrogenesis

and towards astrogenesis (Al-Dalahmah, Campos Soares, et al., 2020). Together, these show that in the postnatal SVZ, Galectin-3 is expressed by glial cells and a subset of neural progenitors, and that Galectin-3 has cell-autonomous roles in fate choice between astrocytes and oligodendrocytes.

It is not known whether Galectin-3 regulates hippocampal neurogenesis, or if cells expressing Galectin-3 can be detected in the SGZ. The cell types expressing Galectin-3, if present, are also to be determined. Nevertheless, most regulators of neurogenesis affect both SVZ and SGZ neurogenesis (such as fibroblast growth factor 2, FGF2 (Kang & Hebert, 2015; Woodbury & Ikezu, 2014)). Other Galectins have been shown to regulate hippocampal neurogenesis, with Galectin-1 being expressed by the neural stem cells ($GFAP^+$, $Nestin^+$, $FABP7^+$ or $Msi1^+$) in the SGZ, where it inhibits proliferation of NSCs under homeostatic conditions (Imaizumi et al., 2011).

Hence, I hypothesized that Galectin-3 would decrease neurogenesis in the SGZ.

1.2.7 Galectin-3 and cognitive decline

As mentioned, Galectin-3 is negatively correlated with cognitive scores. Galectin-3 genetic variants rs4644, rs4652 and rs1009977 were associated with lower cognitive performances even after adjusting for increased C-reactive protein levels (Trompet et al., 2012). Experimentally, Galectin-3 overexpression impaired hippocampal-dependent fear memory in rats (Chen et al., 2017). The authors also showed that knockout of Galectin-3 improved fear memory in mice (Chen et al., 2017), and that this was not due to decreased levels of pro-inflammatory cytokines IL6 and TNFα (Chen et al., 2017). While the authors also reported that Galectin-$3^{-/-}$ mice had enhanced spatial acquisition in the Morris Water Maze compared to male Galectin-$3^{+/+}$ mice (Chen et al., 2017), other studies did not find improvements in Morris Water Maze (MWM) performance from Galectin-3 knockout on a WT background (Siew et al., 2024; Tao et al., 2020). Hence, Galectin-3 may also affect memory and cognitive functions directly independent of its effects on glial reactivity and pro-inflammatory cytokine levels.

1.3 Aims of project

Galectin-3 is expressed by microglia and is strongly upregulated after brain injury and in neurodegenerative diseases including Alzheimer's Disease. While it has been shown to increase oligomerisation and deposition of beta-amyloid, its effects on neural cells are less clear. I aimed to test the overarching hypothesis that Galectin-3 is deleterious to AD pathology.

Galectin-3 can modulate cognitive performance independent of neuroinflammatory markers IL-6 and TNFα (Chen et al., 2017). Hippocampal neurogenesis is decreased in AD patients, and galectin-3 can modulate neurogenesis and gliogenesis in the SVZ (Al-Dalahmah, Campos Soares, et al., 2020; Comte et al., 2011). Hence, chapter 3 aims to test the hypothesis that secreted galectin-3 can directly decrease hippocampal neurogenesis *in vitro* via the neurosphere assay and *in vivo* using galectin-3 knockout mice.

Since Galectin-3 is mainly expressed by reactive microglia, I sought to test if Galectin-3 expression alters microglial activation. In Chapter 4, I first test the hypothesis that Galectin-3 knockout would decrease the expression of disease-related and pro-inflammatory genes in microglia. Next, microglial morphology has been used as a measure of microglial reactivity, with reactive microglia having decreased ramification. Hence, I hypothesized that Galectin-3 expressing microglia would have decreased ramification. In addition to being expressed by reactive microglia, Galectin-3 can also act as a paracrine signal to neighbouring cells. I tested the hypothesis that galectin-3 knockout mice would have increased microglial ramification compared to wildtype counterparts. I also tested the hypothesis that astrocytes would upregulate disease-associated genes upon treatment with Galectin-3.

While Galectin-3 has been shown to increase Beta-amyloid deposition, it is not clear whether Galectin-3 does this solely by promoting oligomerisation of Beta-amyloid or if it also alters microglial clearance of Beta-amyloid. In chapter 5, I test the hypothesis that Galectin-3 would decrease phagocytosis of Aβ oligomers, hence leading to its accumulation.

In some disease contexts, Galectin-3 has been shown to be neuroprotective, with the Carbohydrate recognition domain (CRD) possibly contributing to re-myelination. Hence, I aimed to determine if the CRD is sufficient to promote oligomerisation and deposition of Beta-amyloid. Since the N-terminal tail mediates oligomerisation of Galectin-3, I hypothesized that without the N-terminal, Galectin-3 will have reduced ability to promote oligomerisation and deposition.

In conclusion, my thesis aims to show that Galectin-3 negatively influences hippocampal neurogenesis, amyloid clearance and glial cell activation.

Chapter 2: Materials and Methods

2.1 Animals

2.1.1 Galectin-3 knockout mice (Lgals3<tm1Poi>/129Sv)

Galectin-3 knockout mice (Lgals3<tm1Poi>) were generated by Francoise Poirier, Paris, and kindly gifted to the Szele lab for a previous study on SVZ neurogenesis (Comte et al., 2011). Brains had previously been extracted after transcardiac perfusion with phosphate buffered saline (PBS) and 4% paraformaldehyde (PFA), and then post-fixed in 4% PFA overnight before being equilibrated in 30% sucrose in PBS. The brains were then frozen prior to sectioning. I obtained posterior brains from approximately –1.0mm w.r.t. Bregma (containing the hippocampus). Coronal sections of 30µm were obtained using a Leica microtome and sections were stored in cryoprotectant (ethylene glycol, glycerol, 0.1M phosphate buffer, pH 7.4, 1:1:1:2 by volume). All sections were stored in cryoprotectant at –20°C until immunohistochemistry commenced. These brains were obtained for comparison of neurogenesis between WT and Galectin-3 knockout mice.

2.1.2 Galectin-3 knockout mice (Lgals3<tm1Ftl>)

Galectin-3 knockout mice (Lgals3<tm1Ftl>) were a kind gift from the Bethan Psaila/Adam Mead labs. Homozygous knockout mice were first crossed with C57Bl6 to produce F1 heterozygotes. The F1 generation were then mated as sibling trios to generate 25% Galectin-$3^{+/+}$, 50% Galectin-$3^{+/-}$, and 25% Galectin-$3^{-/-}$ F2 generation. F2 mice were earclipped and genotyped (Transnetyx) at 3 weeks of age. These brains were obtained for comparison of neurogenesis between WT and Galectin-3 knockout mice, and for experiments involving intrahippocampal injection of Aβ.

2.1.2.1 BrdU injections

10 mg/ml BrdU stock was prepared (Abcam, ab142567) and kept at –20 °C. At 2 months of age, mice were given 100 mg/kg (10 µl/g of 10 mg/ml stock) BrdU daily for 10 days via intraperitoneal (i.p.) injections. For the neuroblast cohort, this was followed by a 10-day

washout before sacrifice via transcardiac perfusion. For the Label-Retaining Cell (LRC) cohort, BrdU injections were followed by a 30-day washout period before sacrifice.

Brains were dissected and fixed with 4% PFA overnight at 4°C before being equilibrated in 30% w/v sucrose. 30 µm sections were taken using a Leica microtome and sections were stored in cryoprotectant (ethylene glycol, glycerol, 0.1 M phosphate buffer, pH 7.4, 1:1:1:2 by volume). All sections were stored in cryoprotectant at –20 °C until immunohistochemistry was performed.

2.1.3 Cx3cr1-GFP mice

A breeder trio of Cx3cr1-GFP$^{+/-}$ mice were obtained as a gift from the Domingos lab. Cx3cr1-GFP$^{+/-}$ were crossed to produce Cx3cr1-GFP$^{+/+}$ mice. Mice were used as breeders to produce Cx3cr1-GFP+/- pups, from which glial cells were extracted (see section 2.6.2).

2.2 Preparation of Beta Amyloid

2.2.1 Monomerisation of Aβ from lyophilised stock

To ensure monomerization of Aβ, lyophilised $Aβ_{(1-42)}$ (CAS 107761-42-2) was obtained from Cambridge Biosciences (H7442.1000) and dissolved in 221 µl 1,1,1,3,3,3-Hexafluoro-2-propanol (HFIP; VWR International Ltd, 354861000) (Stine et al., 2003). The solution was sonicated for 45 minutes in a bath sonicator. After the solution was clear, an Eppendorf Repeater Plus pipette with a 0.1 ml tip was used to aspirate the $Aβ_{(1-42)}$ monomer solution. 20 µl was aliquoted into each tube quickly to minimise evaporation of the HFIP. Any remaining solution was dispensed back into the original tube as a control to test for oligomerisation. The tubes were left in a fume cabinet overnight to allow the HFIP to evaporate. The tubes were then spun for 2 hours under vacuum in a DNA concentrator to ensure all HFIP was evaporated to leave the $Aβ_{(1-42)}$ monomers as a film on the bottom of each tube. The tubes were stored at –80 °C until further use.

2.2.2 Preparation of Aβ oligomers for *in vitro* assays

The protocol was kindly provided by Chris Bohlen (Haney et al., 2018).

To one tube of $A\beta_{1-42}$ monomer film, 8.88 µL of dimethyl sulfoxide (DMSO) (Sigma, D4540-500ML) was added and dissolved completely by gentle pipetting (12.5 mg/ml Aβ in DMSO). The solution was bath sonicated for 10 minutes. 102 µl of filtered PBS (ThemoFisher, 14190250) was added to the tube, giving 110.8 µl of 0.903mg/ml (200µM) Aβ solution in PBS/8% DMSO. The tube was vortexed for 15 seconds before incubation at 4 °C for 24 hours. The solution was centrifuged at 17 000 *g* for 1 minute before the supernatant was aliquoted into single use aliquots. The $A\beta_{1-42}$ oligomer solution was kept at –80 ºC until experiments. During the day of the phagocytosis assay, an aliquot was thawed on ice. 1 µl of pHrodo-SE (Thermo Fisher, P36600; 10 mg/ml in DMSO) was added and the sample was incubated in the dark on a rocker for 15 minutes. The labelled oligomer solution was centrifuged at 17 000 *g* for 1 minute and the supernatant was transferred to a fresh tube.

2.3 Surgeries

To determine the effects of Galectin-3 and Galectin-3C (truncated Galectin-3 with only the carbohydrate recognition domain) on Aβ deposition in mice, cranial injections of the following preparations were performed according to the protocol from Boza-Serrano and colleagues (Boza-Serrano et al., 2019):

1) $A\beta_{1-42}$
2) $A\beta_{1-42}$ + Galectin-3 (Abcam, ab50236-50ug)
3) $A\beta_{1-42}$ + Galectin-3C (R&D Systems, 10110-GA)

Preparing Galectin-3/Galectin-3C solutions:

1) 100 µg of HFIP-treated $A\beta_{1-42}$ was dissolved in 140 µl of saline for injection.
2) The peptide was allowed to rehydrate and the solution was sonicated for 10 minutes.
3) The tube was centrifuged for 1 minute at 17 000 *g* to remove precipitates and fibrils.

4) The supernatant (monomer solution) was aliquoted into 7µl aliquots and stored at –80 °C until further use.
5) On the days of surgery, aliquots were thawed on ice and prepared as follows:
    a. $A\beta_{1-42}$: 3 µl saline + 7 µl $A\beta_{1-42}$ solution
    b. $A\beta_{1-42}$ + Galectin-3: 1 µl saline + 2 µl 500 µg/ml Galectin-3 + 7 µl $A\beta_{1-42}$ solution
    c. $A\beta_{1-42}$ + Galectin-3C: 1 µl saline + 2 µl 307.7 µg/ml Galectin-3C + 7µl $A\beta_{1-42}$ solution
6) The solutions were mixed and incubated at 37 °C for 1 hour before being kept on ice.
7) Solutions were then transferred into a pulled glass pipette using a 10 µl Hamilton syringe (701RN)

2 month old male and female Galectin-$3^{+/+}$ (C57Bl6) and Galectin-$3^{-/-}$ (Lgals3<tm1Ftl>) mice were anaesthetised in an induction chamber using 3% isofluorane before being transferred to a stereotaxic frame with a rodent heating mat (Stoelting, 53800M). Anaesthesia was maintained with 1.5% isofluorane administered through a snout-fitted conical tube. Mouse heads were shaved and mice were given 0.05 ml of 0.25% Marcaine subcutaneous (s.c.) and 5 mg/kg of Metacam i.p.. The surgical site was cleaned with 2% chlorhexidine in 70% ethanol (Clinell) and the incision was made. The skull was dried with sterile cotton buds to expose the targeted region. The needle was used to measure the following coordinates with respect to Bregma – anterior-posterior (AP): -2.0 mm, mediolateral (ML): +1.5 mm – and a Dremel drill was used to make a small hole to expose the brain. The needle was lowered to 2.5 mm below Bregma before being raised to 2.0mm below Bregma. 2 µl of the designated preparation was injected intracranially to coordinates (corresponding to 0.1 µg of Aβ and 10 µmol of either Galectin-3 or Galectin-3C, if present). Injection was done at 0.5 µl/minute and the needle was left in place for 2 minutes after the injection before being retracted over 4 minutes. The skin incision was then closed with Vetbond (3M) and allowed to dry for 1 minute and the animal

was allowed to recover. Mice were allowed access to Metacam jellies for 3 days post-surgery. Mice were kept for 1 month from the date of injection and then sacrificed via transcardiac perfusion with saline and then 4% PFA in PBS. The brains were dissected and fixed in 4% PFA overnight at 4 °C before being transferred into 30% w/v sucrose and allowed to equilibrate. Brains were then frozen at –80 °C until sectioning.

2.4 Immunofluorescence

2.4.1 Sectioning of brains with intrahippocampal injections

30µm sections were taken using a Leica microtome as before. Where present, olfactory bulb (OB) sections were taken and separated into left and right OBs. SVZ and anterior hippocampal sections were kept. At AP –1.25mm (with reference to Bregma), the first serial section was placed into well 1, second section into well 2, and so on until the 8th section into well 8. The 9th serial section was placed into well 1 and 10th into well 2. This was continued until the 40th section, giving 8 serial wells of 5 evenly spaced sections from -1.25mm to -2.45mm w.r.t. Bregma. More posterior sections were obtained for staining controls. All sections were stored in cryoprotectant at –20 °C until immunohistochemistry.

2.4.2 Immunohistochemistry without antigen retrieval

For immunohistochemical detection of all antigens excluding BrdU, and in mice without intracranial surgeries. Sections were transferred into PBS in a well plate. They were washed five times in PBS for 7 minutes each before being incubated in glycine for 15 minutes. Sections were incubated in blocking buffer (BB, 10% Donkey Serum in PBS with 0.05% Triton-X100) for 1 hour at room temperature, after which the primary antibody solution (antibodies diluted in BB) was added, and the plates were incubated on a rocking platform at 4 °C overnight. Primary antibody solution was collected the next day and the sections were washed 3 times for 10 minutes each in PBS with 0.05% Triton-X100 (PBS-T). The secondary antibody solution was then added, and the plates were incubated on a rocking platform at room temperature

(RT) for 1 hour in the dark. The sections were then washed 3 times for 10 minutes each in PBS-T before 4′,6-diamidino-2-phenylindole (DAPI) solution (10 µg/ml DAPI in PBS) was added. The sections were washed in PBS and mounted onto glass slides and allowed to dry before Fluorsave (Millipore, 345789) was added and the slides were coverslipped. List of antibodies used and their concentrations can be found in the appendix.

2.4.3 Immunohistochemistry with antigen retrieval

For immunohistochemical detection of BrdU, antigen retrieval was required. Sections were transferred into PBS in a well plate. They were washed five times in PBS for 7 minutes each before being incubated in glycine for 15 minutes. The sections were then transferred into 1.5 ml tubes with 2 M HCl and incubated at 37 °C for 30 minutes for antigen retrieval. After antigen retrieval, sections were transferred back into the well plates and rinsed with PBS before BB was added. The remaining protocol followed the immunohistochemistry protocol above.

2.4.4 Immunohistochemistry with Sudan Black B (SBB) quenching

For sections from mice injected with Aβ (see section 2.3), SBB was used to quench lipofuscin-like autofluorescence. The protocol from 2.4.3 was followed except for SBB quenching between DAPI counter-staining and mounting. After rinsing off DAPI staining solution, sections were first equalised into 70% ethanol for 5 minutes, then incubated with 0.3% SBB in 70% ethanol. The sections were then washed five times with 70% ethanol for 1 minute each. The sections were then transferred to PBS before being mounted as per 2.4.3.

2.4.5 Immunocytochemistry

For cell culture experiments, immunocytochemical detection was performed with the same protocol as 2.4.3 but with the removal of the glycine step.

2.5 Neurosphere experiments

2.5.1 Isolation of primary neurospheres from P2 – P4 pups

Pups were sacrificed by overdose of pentobarbital and checked for pedal reflexes before confirmation by cervical dislocation. After decapitation, the brains were isolated and immediately placed in cold Neurobasal medium (Gibco, 21103049) and kept on ice. Brains were sliced coronally at 400 µm with the Mcilwain tissue chopper and the slices were placed back in cold Neurobasal medium. The dentate gyri were isolated using 27G needles, and a P200 pipette was used to transfer the dentate gyri (DG/DGs) to a 15ml tube with Neurobasal medium and kept on ice; DGs from 6 – 8 brains were pooled into each replicate. The medium was aspirated and 1 – 2 ml of 1X Accutase (Stemcell, 07920) was added to the tissue and the tube was incubated at 37 °C for 10 minutes. The cells were gently triturated with a P1000 pipette to dissociate the DGs into a single cell suspension. 10 ml of Neurobasal A+ medium (Neurobasal + B27 + Glutamax + penicillin/streptomycin) with growth factors (GFs; 20 ng/mL epidermal growth factor [EGF] and 20 ng/mL FGF2) was added and the cells were plated into a non-tissue culture (non-TC) treated 6-well plate with 2 ml per well. The next day, a medium change was performed by transferring the cells into a 50 ml tube and rinsing the wells with calcium- magnesium-free (CMF) PBS. The cells were centrifuged at 300 *g* for 10 minutes and the supernatant was discarded. 12 ml of fresh Neurobasal A+ medium with GFs was added to the tube and the neurospheres were gently mixed with a 10 ml serological pipette. 2 ml of the suspension was added to each well of a fresh non-TC treated 6-well plate. The neurospheres were observed daily over a week and passaged when the neurospheres were approximately 200 µm in diameter.

2.5.2 Passaging of neurospheres

The neurosphere suspension was transferred into a 50 ml tube, and the culture flask or wells were rinsed with PBS to remove all neurospheres. The suspension was centrifuged and the supernatant discarded before 2 ml of Accutase was added to the pellet. The cells were gently

triturated and then incubated at 37 °C for 10 minutes. The cell suspension was then triturated into a single cell suspension before 8 ml of medium was added to neutralise the Accutase. After cell counting Trypan blue-positive and negative cells, the cell suspension was centrifuged to remove the Accutase and fresh medium was added to dilute the suspension to 10^6 live cells per ml. After thorough mixing, the cells were transferred either to non-TC treated plate or Poly(2-hydroxyethyl methacrylate) (poly-HEMA) treated T75-flasks. The cells were observed daily until the next passage or treatment.

2.5.3 Neurosphere proliferation assay

On day 0 (D0), the cells were passaged as before. A single cell suspension was obtained and 4 ml of Neurobasal A+ medium was added before cell counting.

Using serial dilution, 0.5 x 10^5 cells were transferred to a 1.5 ml tube per condition before they were centrifuged and the supernatant aspirated. 1 ml of the appropriate medium with GFs was added and the cells gently resuspended evenly. 9 x 100 µl of the suspension was seeded onto a single poly-HEMA treated 96-well plate at a final seeding concentration of 5.0 x 10^4 cells/ml.

Wells were imaged on days 4 and 7. Thereafter, all neurospheres were pooled and centrifuged. The supernatant was discarded before 500 µl of Accutase was added and the samples were incubated at 37 °C for 10 minutes. The cell suspension was gently triturated into single cells and 2.5 ml of Neurobasal medium was added. The suspension was mixed thoroughly and 10 µl of it was added to 30 µl of Trypan Blue for cell counting.

2.5.4 Neurosphere differentiation assay

On D0, the cells were passaged as before. A single cell suspension was obtained and 4ml of Neurobasal A+ medium was added before cell counting. 2.5 x 10^5 cells were transferred to a 1.5 ml tube per condition before being centrifuged and the supernatant aspirated. 1 ml of the medium (without GFs) was added and the cells gently resuspended evenly. 3 x 100 µl of the suspension was seeded onto 3 separate Poly-L-ornithine and laminin coated plates (final

seeding concentration 2.5 x 10^5 live cells/ml). Plates were fixed on D5 with 4% PFA and kept at 4 °C until immunocytochemistry.

2.6 Glial cell culture

2.6.1 Poly-d-lysine (PDL)-coating of flasks and plates

15 mm glass coverslips were placed into 24-well plates and sterilised with 70% ethanol for one minute. The wells were rinsed twice with distilled water before coating. Cell culture plates (96-well, 24-well and 6-well) and T75 flasks were coated with Poly-D-Lysine (PDL, 10 µg/ml) for 2 hours at room temperature. The flasks and plates were then rinsed thrice with distilled water to remove any remaining PDL before being air-dried. Unused plates or flasks were then parafilmed and stored at 4 °C.

2.6.2 Isolation of primary murine glia

P0 – P2 mice were sacrificed and their brains were extracted. The olfactory bulbs were dissected and removed; this was followed by peeling the cortices and hippocampi. Two to three half cortices were pooled into one 1.5 ml tube with 500 µl of ice cold DMEM. After all brains were dissected, the brains were minced with a pair of sharp scissors and then rinsed thrice with cold DMEM. A final rinse with PBS was performed before 500 µl of 0.25% Trypsin was added to the tubes. The samples were incubated at 37 °C for 10 minutes before being triturated to break up the tissue. 1 ml of glial cell medium was added to neutralise the trypsin and the samples were gently mixed. The samples were centrifuged at 300 *g* for 5 minutes and the supernatant was discarded. The cell pellets were resuspended in the appropriate amount of glial cell medium and seeded onto PDL-coated T75 flasks. Each T75 flask contained two to three half brains. The flasks were kept in a humidified incubator at 37 °C. The following day, the medium was aspirated and the flask was rinsed with PBS. Fresh medium was added and the flasks were returned to the incubator and checked twice weekly until they were confluent. After 5 – 7 days of culture, a confluent layer of astrocytes was observed and microglia started

to proliferate on top of the astrocytic layer. The cultures were then passaged either as mixed glial co-cultures, or as separate microglia and astrocyte cultures.

2.6.3 Subculturing of mixed glial cultures

When the primary cultures were confluent, the medium was aspirated and the flasks were rinsed with PBS before 0.25% trypsin was added. The flasks were then incubated at 37 °C for 10 minutes until the cells detached. The remaining cells were rinsed off the flask with glial cell medium and the cell suspension was gently mixed in a 15 ml tube. The tube was then centrifuged at 300 *g* for 5 minutes before the supernatant was discarded. The cell pellet was resuspended and the cells were counted. Cells were seeded onto PDL-treated coverslips and well plates at 10^5 cells/cm^2 (10^6 cells/well in 6-well plates, 2 x 10^5 cells/well in 24-well plates, and 3.5 x 10^4 cells/well in 96-well plates). The cultures were placed back in the incubator overnight and the medium was changed the next day into treatment medium.

2.6.4 Subculturing of microglia and astrocytes

2.6.4.1 Microglia cultures

Microglia begin to proliferate on top of the confluent astrocytic layer. Hence, for pure microglial cultures, primary mixed glial cultures were shaken on an orbital shaker for 2 hours and then tapped hard to release any microglia. The medium was transferred into a 15 ml tube and the flask was rinsed with PBS to harvest any remaining microglia. Thereafter, 0.25% trypsin was added to the flasks for subculturing of astrocytes. The microglia suspension was centrifuged at 300 *g* for 5 minutes and the supernatant was discarded. The cell pellet was resuspended for cell counting and then diluted in glial cell medium to the appropriate concentration. Cells were seeded at 5 x 10^4 cells/cm^2 into PDL-coated plates or coverslips (10^5 cells/well in 24-well plates, and 1.75 x 10^4 cells/well in 96-well plates). The plates were returned to the incubator and the medium was changed the next day to treatment medium.

2.6.4.2 Astrocyte cultures

After lifting of microglia and then addition of 0.25% trypsin, the flasks were incubated at 37 °C for 10 minutes until the astrocytes lifted. Thereafter, the cell suspension was transferred into a 15 ml tube and the flask was rinsed with glial cell medium before the cell suspension was gently mixed. The cell suspension was centrifuged at 300 *g* for 5 minutes and the supernatant was discarded. The cell pellet was resuspended in glial cell medium for cell counting. Cells were seeded at 5 x 10^4 cells/cm^2 into PDL-coated plates or coverslips (10^5 cells/well in 24-well plates, and 1.75 x 10^4 cells/well in 96-well plates). The plates were returned to the incubator, and the medium was changed the next day to treatment medium.

2.6.5 pHrodo phagocytosis assays

Cx3cr1-GFP$^{+/-}$ glial cells were obtained from pups and cultured as outlined in 2.6.4. Labelled AβO_{1-42} (pHrodo-AβO_{1-42}) was prepared as outlined in 2.2.2. After obtaining either microglia or mixed glia cultures in 96-well plates, the cells were treated with the appropriate conditions and then immediately placed into a humidified imaging chamber (OKO labs). Images were acquired every hour over 24 hours. After 24 hours, the cells were rinsed with PBS and lysed with Buffer RLT with beta-mercaptoethanol (β-ME) before the lysates were frozen at –80°C.

2.6.5.1 Image analysis

For BV2 microglia phagocytosis assay, bright-field images at the endpoint were thresholded and the area of cells was measured. pHrodo area at each timepoint was also thresholded and the phagocytic index was determined as the pHrodo area/cell area. This was plotted over 24 hours.

For primary glia assays, both GFP and pHrodo images were thresholded and the fluorescence area was measured. To obtain the phagocytic index at each timepoint, the pHrodo area was divided by the GFP area. This was then plotted over 24 hours.

2.7 Western blot

2.7.1 Sample collection

2.7.1.1 Cell culture

6-well plates were rinsed once in ice cold PBS and kept on ice. All PBS was aspirated and 100 µl of radioimmunoprecipitation assay (RIPA) buffer with phosphatase and protease inhibitors was added to each well. The plate was kept on ice while each well was scraped with a cell scraper and the lysates were collected into 1.5 ml tubes. The lysates were centrifuged at 17 000 *g* for 20 minutes before the supernatant was transferred to a fresh tube. 5 µl of each sample was then diluted in 45 µl of PBS for quantification of protein concentration via Bradford assay.

After samples were equalised, 4x Laemmli buffer with 50 mM dithiothreitol (DTT) was added to the samples (30 µl of Laemmli buffer ,LB to 90 µl of sample). The samples were then boiled for 10 minutes before being placed on ice. Unused samples were stored at –20 °C until immunoblotting.

2.7.1.2 Tissue

Mice were perfused with saline and the brain was dissected. Half of the brain was immediately snap-frozen in liquid nitrogen and then kept at – 80 °C until further processing. Brains were allowed to thaw gently on ice prior to extraction. Ice-cold RIPA buffer with phosphatase and protease inhibitors was added at a ratio of 700µl RIPA per 100mg of tissue. The brain was minced with scissors before being triturated with a P1000 tip. Brains were kept on ice and vortexed occasionally for 30 minutes. Brains were then sonicated on ice for 2 minutes (10 seconds on 10 seconds off, total 60 seconds sonication time). Samples were centrifuged for 30 minutes at 4 °C and maximum speed on the centrifuge. Two 360 µl, two 180 µl and two 90 µl aliquots were made for samples and stored at –80 °C for future analyses. 5µl of each sample was used for bicinchoninic acid (BCA).

Samples were then equalised with RIPA buffer before 4x Laemmli buffer with 50 mM DTT was added to the samples (30 µl of LB to 90 µl of sample). The samples were then boiled for 10 minutes before being placed on ice. Unused samples were stored at –20 °C until immunoblotting.

2.7.2 Sodium dodecyl sulfate–polyacrylamide gel electrophoresis (SDS-PAGE) and transfer

Samples were loaded onto 4 – 20% mPAGE gels at 30 µg per lane. 4 µl of PageRuler pre-stained ladder was used. The gel was run with 3-(N-morpholino) propane sulfonic acid (MOPS) buffer at 100V for 2 hours until the dye front reached the end of the gel. A polyvinylidene difluoride (PVDF) membrane was activated with 100% methanol and placed onto a transfer sandwich comprising of the following in order: negative electrode, foam pad, filter paper, gel, membrane, filter paper, foam pad, positive electrode. The wet transfer was run at 300 mA for 60 minutes.

2.7.3 Immunoblotting

After the transfer, the membrane was removed from the sandwich and blocked with 5% skim milk in PBS-T (PBS with 0.05% Tween-20) for 1 hour at room temperature. Primary antibodies were diluted in the blocking buffer. The membrane was then cut according to the molecular weights of the proteins of interest and incubated overnight with primary antibody solutions at 4 °C with gentle rocking. The following day, the primary antibody solution was collected and recycled, and the membranes were washed thrice with PBS-T for 10 minutes each on an orbital shaker. The corresponding horseradish peroxidase (HRP)-conjugated antibodies were diluted in blocking buffer and added to membranes for 1 hour at room temperature. The membranes were washed thrice with PBS-T for 10 minutes each on an orbital shaker. The membranes were then incubated with the appropriate HRP substrate and visualised with Chemidoc XRS.

2.8 Reverse Transcription quantitative Polymerase Chain (RT-qPCR)

2.8.1 Sample collection and purification

RNA was collected and purified using the RNeasy minikit (Qiagen, 74104) with genomic DNA digest (Qiagen, 79254). Samples were collected with Buffer RLT with β-ME and either processed immediately or frozen at –80 °C until RNA purification.

RNase-free DNase was prepared by adding 10 µl of DNase stock solution to 70 µl of buffer RDD per sample and the solution was flicked to mix before being kept on ice. 70% Ethanol was added to the lysate at a 1:1 ratio. The mixture was mixed gently with a pipette and then transferred to the spin column. The columns were centrifuged at 8000 *g* for 1 minute and the flow through was discarded. 350 µl of buffer RW1 was added to the tubes and the columns were centrifuged at 8000 *g* for 1 minute. The flow through was discarded and the DNase solution was added directly to the spin column filter membrane. The columns were incubated for 15 minutes at room temperature before 350 µl of buffer RW1 was added and the columns were centrifuged at 8000 *g* for 1 minute. The flow through was discarded and 500 µl of buffer RPE was added to the tubes. The columns were centrifuged at 8000 *g* for 1 minute and the flow through was discarded. The RPE wash step was repeated. The columns were then centrifuged at 17 000 *g* with the lids open to air dry the membrane. Nuclease-free water was added directly to the membrane and the tubes were incubated at room temperature for one minute before RNA was collected by centrifuging the tubes at 8 000 *g* for 1 minute. The RNA was immediately kept on ice. The samples were quantified using a Nanodrop spectrophotometer. RNA samples were stored at –80 °C until cDNA synthesis.

2.8.2 cDNA synthesis

cDNA was synthesised with the iScript™ cDNA synthesis kit (BioRad, 1708891) according to manufacturer's recommendations. cDNA was diluted to 1 ng/µl after cDNA synthesis.

2.8.3 qPCR

qPCR primers were designed and purchased from Thermo Fisher, and diluted to 100 µM (forward and reverse) working solutions. The sequences used are provided in the appendix. qPCR was run with LUNA Universal qPCR (New England Biolabs, M3003). Final concentrations of primers were 10 µM or 50 µM (see table 2.8.3) and each reaction contained 2ng of cDNA. qPCR was run on either Quantstudio5 or Quanstudio3 qPCR machines with the



following parameters:

The Cq values were then compared to determine relative gene expression levels.

2.9 Thioflavin T assay

Thioflavin T (ThT) stock was prepared by dissolving 500mg of ThT in 78.4 ml of ethanol (20 mM). 100 µl of ThT stock was added to 900 µl of cold PBS and kept on ice. Galectin-3 was dissolved in PBS at a concentration of 500 µg/ml (19.23 µM); Galectin-3 CRD was dissolved in PBS at a concentration of 307.7 µg/ml (19.23 µM). Both solutions were kept on ice. A black non-binding 96-well plate was used for the assay and was kept on ice until it was placed in the shaking incubator. Galectin-3, Galectin-3CRD and PBS were added to the appropriate wells in the volumes below:

Blank:	10 µl ThT + 90 µl PBS
Control:	10 µl ThT + 10 µl PBS + 80 µl Aβ42
2 µg Galectin-3:	10 µl ThT + 4 µl Galectin-3 + 80 µl Aβ42 + 6 µl PBS
1.23 µg Galectin-3CRD:	10 µl ThT + 4 µl Galectin-3C + 80 µl Aβ42 + 6 µl PBS

$A\beta_{1-42}$ films prepared as per 2.2.1 were used for thioflavin T assays. One aliquot of $A\beta_{1-42}$ monomer (100 µg) was dissolved in 640 µl of ice cold PBS (250ug/ml, 55.38µM). The peptide was allowed to re-hydrate and sonicated for 3 minutes. The tube was centrifuged at 17 000 *g* for 5 minutes at 4ºC and the supernatant was added to a fresh tube containing 84 µl of 2 mM ThT and the tube was flicked to mix. 90 µl of the solution (10 µl ThT + 80 µl $A\beta_{1-42}$) was added to each well. The plate was sealed with optical film and placed into a BMG PHERAstar FSX plate reader. Fluorescence signal was monitored at Ex/Em= 440/484 nm every 15 minutes at 37 ºC with 15 seconds shaking between reads.

Chapter 3: The effect of Galectin-3 on hippocampal neurogenesis

3.1 Galectin-3 is expressed in the hippocampus in WT mice by 10 weeks of age.

Galectin-3 expression becomes robust in the brain after brain injury and models of brain disease. However, Galectin-3 in healthy mice is below the level of immunodetection in most parts of the brain, except notably in the SVZ. In C57Bl6J mice, Galectin-3 expression was previously reported to be observed in the hippocampus of 7 month old mice (Tao et al., 2020). However, most of the Galectin-3 immunoreactivity appears to be in the CA1 region and it was unclear whether there were Galectin-3 expressing (Galectin-3+) cells in the SGZ neurogenic niche. Secondly, while the authors show that Galectin-3 was colocalised with ionized calcium-binding adaptor molecule 1 (IBA1) and not GFAP in middle-aged adults (Tao et al., 2020), it was not certain which cells in the SGZ, if any, express Galectin-3. Lastly, it is not known if younger adult mice show expression of Galectin-3 in the hippocampus.

Hence, to address the above questions, I co-immunostained coronal sections of Galectin-$3^{+/+}$ and Galectin-$3^{-/-}$ mice with Galectin-3, IBA1 and GFAP. This allowed me to determine the identity of the cells expressing Galectin-3, and to determine if young adult mice express Galectin-3.

Mice from two different cohorts were used: young adults (average age: Galectin-$3^{+/+}$ 2.61 months, Galectin-$3^{-/-}$ 2.71 months), or middle-aged (average age: Galectin-$3^{+/+}$ 7.55 months, Galectin-$3^{-/-}$ 7.43 months). Table 3.1 shows the ages of the mice used.

Galectin-3$^{+/+}$			Galectin-3$^{-/-}$		
Young adult					
Male	Average	2.47	Male	Average	2.82
	n	3		n	3
	SEM	0.23		SEM	0.22
Female	Average	2.82	Female	Average	2.59
	n	2		n	3
	SEM	0.42		SEM	0.28
Total	Average	2.61	Total	Average	2.71
	n	5		n	6
	SEM	0.20		SEM	0.17
Middle-aged					
Male	Average	7.55	Male	Average	7.43
	n	4		n	3
	SEM	0.45		SEM	0.23

Table 3.1: Ages (in months) of Galectin-3$^{+/+}$ and Galectin-3$^{-/-}$ mice used. In the young adult cohort, both male and female mice were used. For middle-aged mice, only males were used.

The SVZ has been previously characterised by the lab to have strong Galectin-3 expression (Comte et al., 2011). To ascertain that Galectin-3$^{-/-}$ do not express Galectin-3, I immunostained sections containing the dorsal ventricles from a subset of the mice. I also performed western blot analysis of whole brain lysates on mice from the same colony.

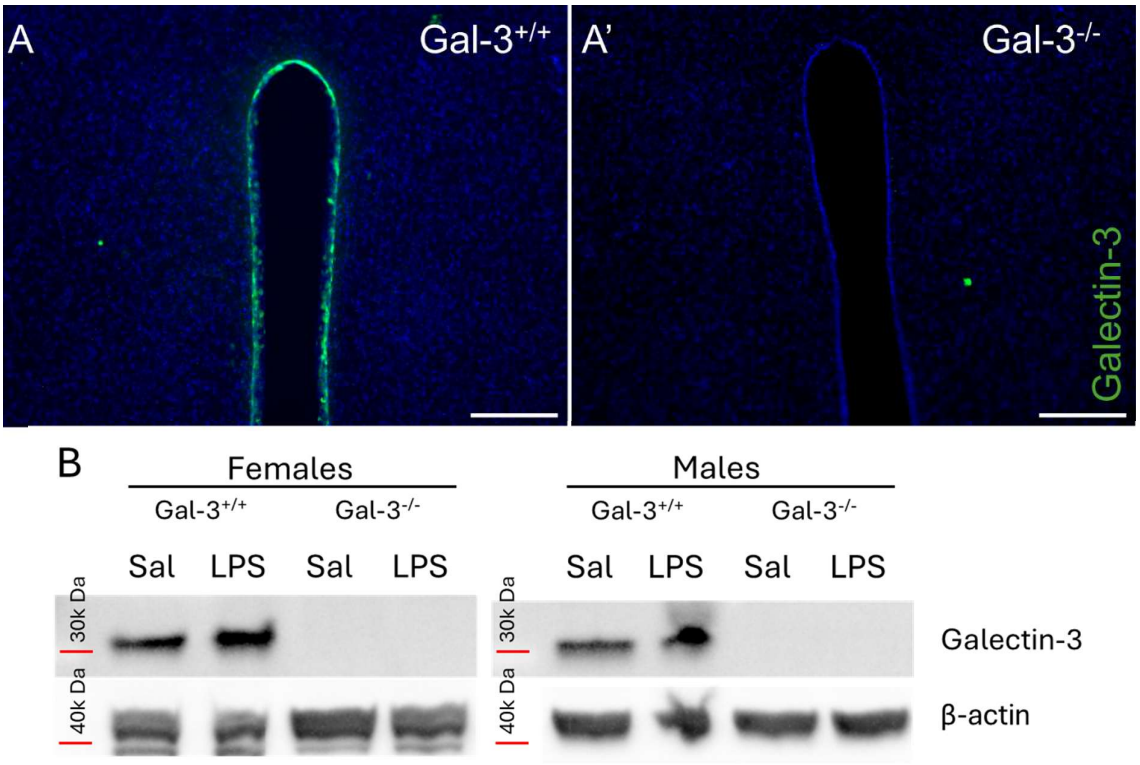


Figure 3.1.1: Verification that Galectin-3 knockout mice do not express detectable levels of Galectin-3. (A) Galectin-3 immunoreactivity is observed in the ventricles of Galectin-3$^{+/+}$ mice but not Galectin-3$^{-/-}$ mice.

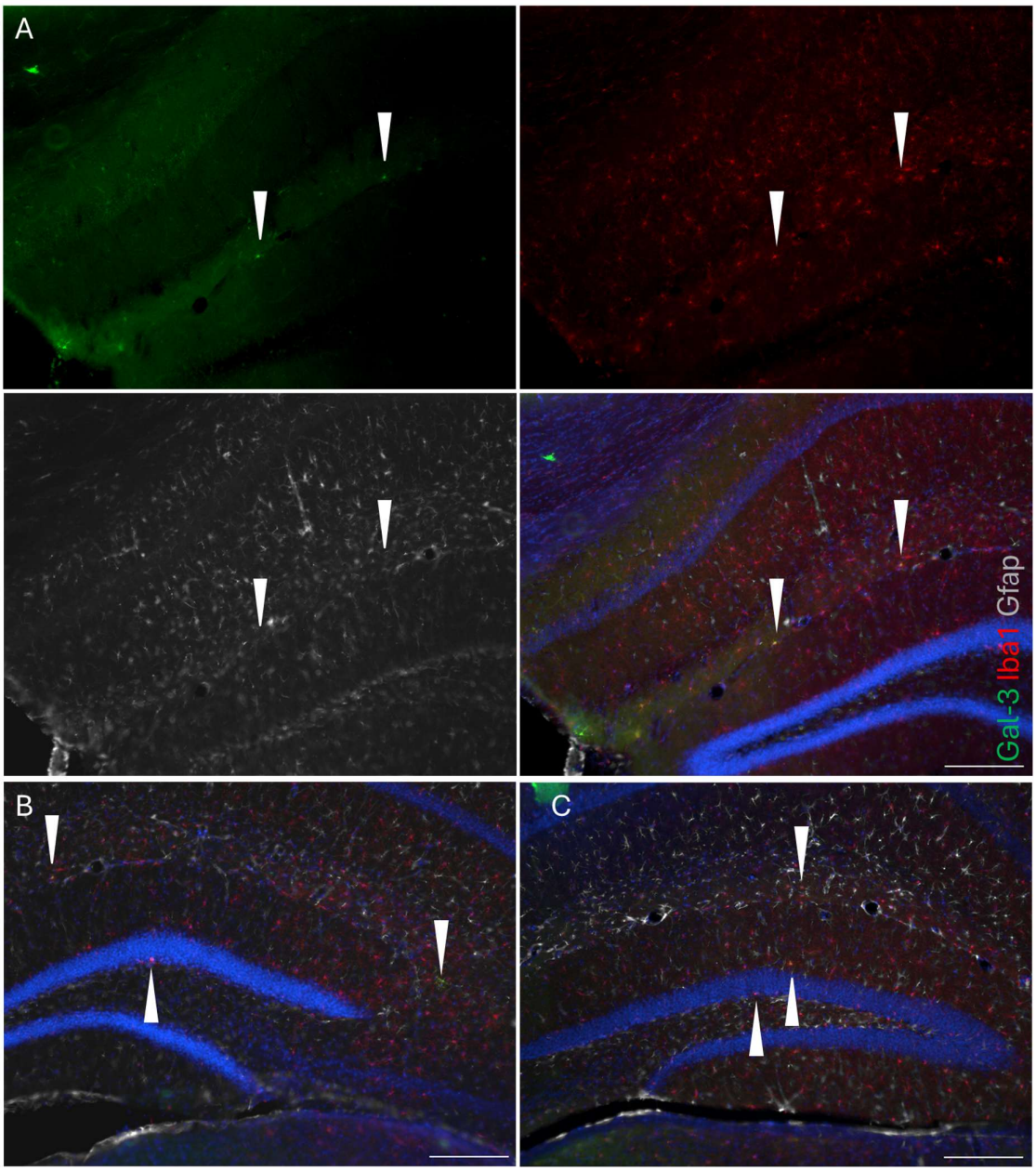


Figure 3.1.2: Galectin-3 is expressed in a small number of cells in the hippocampus of young adult mice. Galectin-3+ cells (white arrowheads) are mostly seen in the molecular layer of the CA1 in the hippocampus, but can also be seen in the SGZ (B & C), in the molecular layer of the CA3 (B) and in the molecular layer of the dentate gyrus (C). Galectin-3+ cells are seen in both male (B) and female (C) mice. Scale bars represent 200 µm.

In young adult Galectin-3$^{+/+}$ mice, I found that expression of Galectin-3 can be observed in the hippocampus. This was surprising as most work in the lab and field suggested Galectin-3 was not expressed in healthy mice. Most of the Galectin-3 immunoreactivity was observed in the molecular layer of the CA1 (Figure 3.1.2), with just over half of Galectin-3+ cells residing in the CA1. Galectin-3 was also detected with antibodies in the molecular layer of the CA3 and DG (Figure 3.1.2B and C) and in the hilus. Importantly, Galectin-3+ cells are present within the granule cell layer where newborn neurons are produced and maturing, and within the SGZ where NSCs reside.

Co-labelling of Galectin-3 with IBA1 and GFAP shows that in the hippocampus, Galectin-3 is almost exclusively expressed by IBA1^{+} microglia, but a single GFAP^{+}Galectin-3^{+} cell was observed in the CA1. However, since the CA1 is not a neurogenic niche, it is unlikely that the Galectin-3^{+}GFAP^{+} cell observed represents a neural stem cell. Hence, in young adult mice, Galectin-3+ cells are restricted to a small number of glial cells and can mostly be found in microglia.

In 7 – 9M Galectin-3$^{+/+}$ male mice, expression of Galectin-3 can be observed in the hippocampus. While most of the expression is still seen in the molecular layer of the CA1 (Figure 3.1.3), Galectin-3 immunofluorescence is also observed just lateral to the granule cell layer (GCL) of the DG in the CA3 and in the SGZ of the DG. The density of Galectin-3+ cells also appears to be higher in middle-aged mice as compared to younger mice.

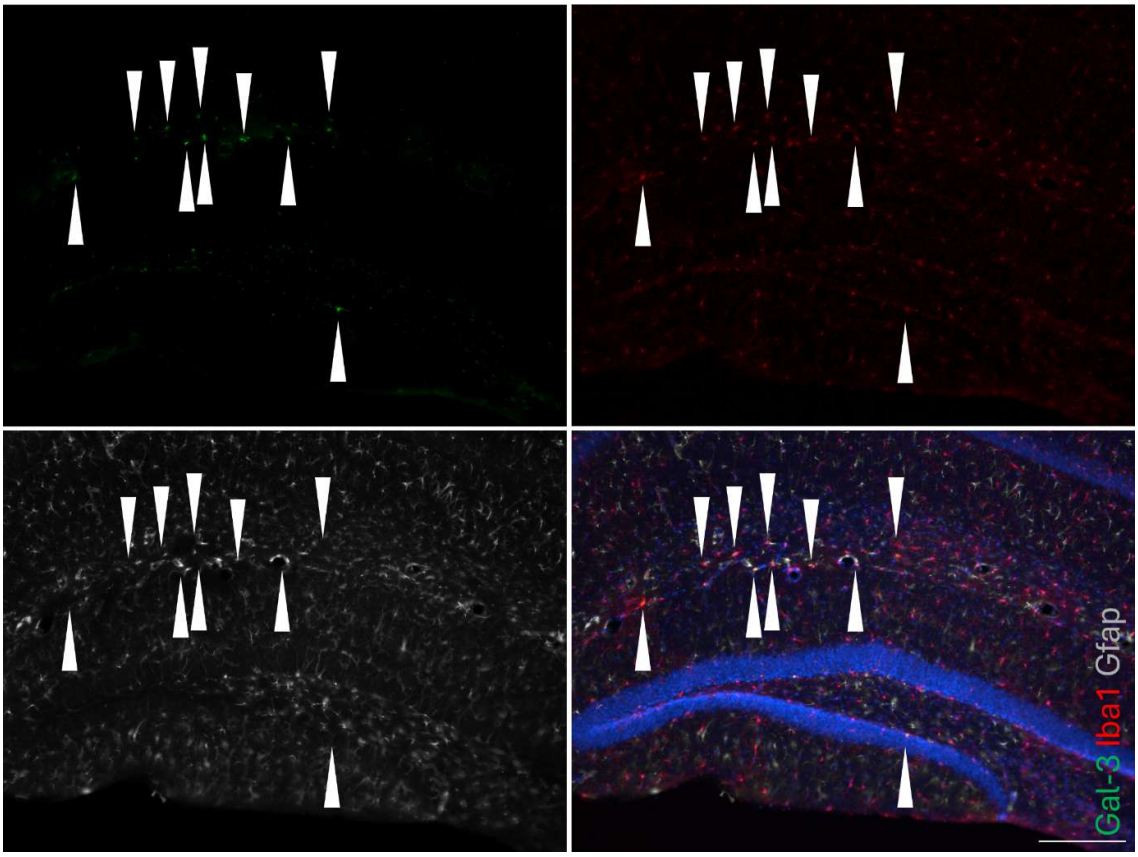


Figure 3.1.3: Galectin-3+ cells are observed in the hippocampus of middle-aged C57Bl6 mice. Most of the Galectin-3 immunoreactivity is observed in the molecular layer of the CA1, but Galectin-3+ cells are also seen in the SGZ of the DG. Notably, there are more Galectin-3+ cells as compared to younger adults. Scale bar represents 200 μm.

In Galectin-3$^{-/-}$ mice, no Galectin-3 expression is seen in the hippocampus in both young adult mice and middle-aged mice (Figure 3.1.4).

As Galectin-3 can be secreted into the extracellular space, microglia in the vicinity of the SGZ may release Galectin-3 which could affect neighbouring cells. Additionally, Galectin-3 transcripts may be detectable by qPCR in the hippocampus even if undetectable by immunohistochemistry. As such, I asked if Galectin-3 may act directly on neural stem cells of the hippocampus to affect neurogenesis.

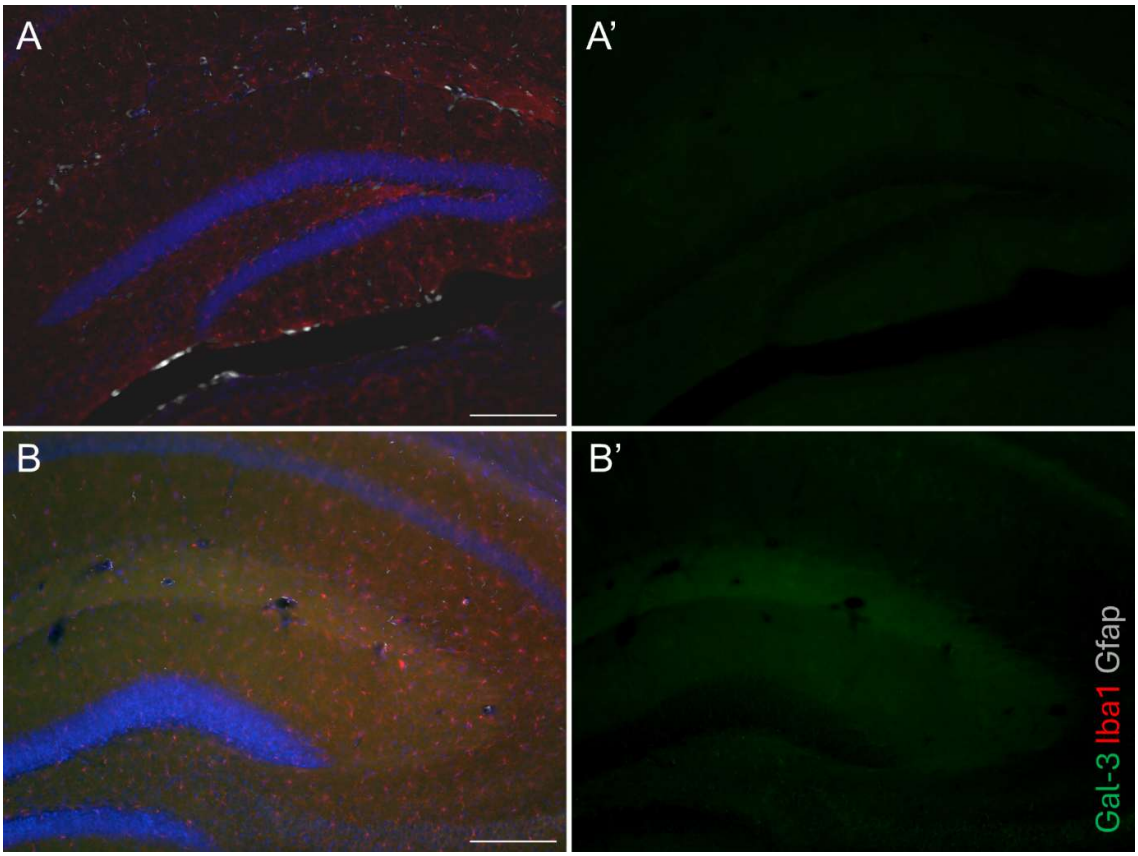


Figure 3.1.4: Galectin-3 is not expressed in the hippocampus of Galectin-3$^{-/-}$ mice in both young adult (A) and middle-aged (B) mice.

3.2 Galectin-3 decreases neural stem cell proliferation but does not affect differentiation *in vitro*

In the V-SVZ, Galectin-3 is mainly expressed by cells of the neural lineage, including GFAP+ NSCs and TAPs cells. However, in various mouse models of AD including 5xFAD (Boza-Serrano et al., 2019), APP/PS1 (Tao et al., 2020) and Tau22 (Siew et al., 2024) mice, Galectin-3 expression in the hippocampus is co-localised with IBA1, suggesting expression by microglia. In my hands, similar observations were made in C57Bl6 mice (Figures 3.1.2 and 3.1.3). During inflammation, Galectin-3 is secreted and can act as a feed-forward signal to further chemoattract microglia and macrophages (Sano et al., 2000). Hence, I asked if Galectin-3 or its inhibition has a direct effect on hippocampal neurogenesis.

3.2.1 Neural stem cell proliferation is decreased by Galectin-3, but is not affected by Galectin-3 inhibitor in medium

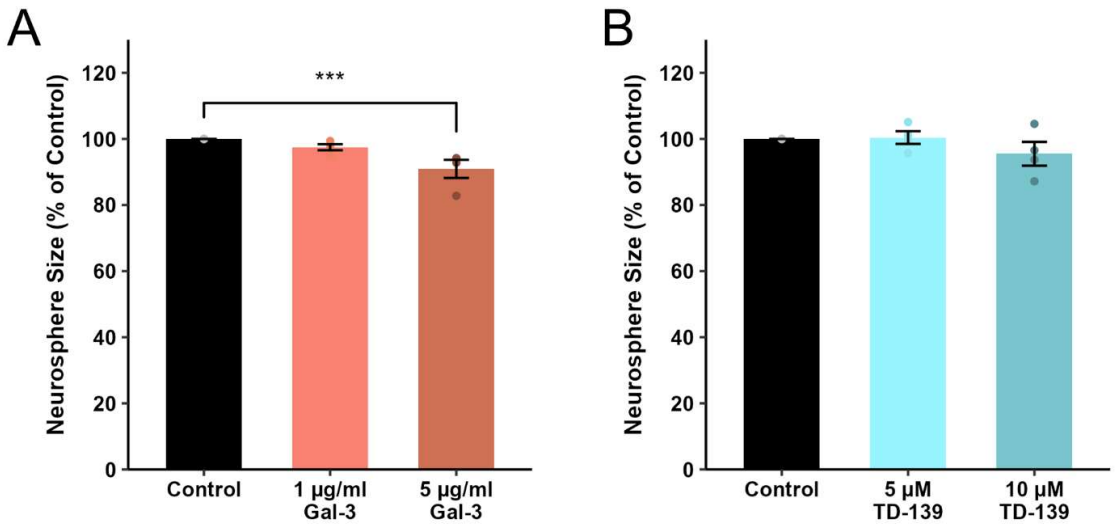


Figure 3.2.1: Galectin-3 decreased hippocampal neural stem cell proliferation *in vitro*. (A) SGZ-derived neurospheres treated with Galectin-3 had reduced diameters at day 5 when compared to control. (B) No significant changes in neurosphere size was observed when SGZ-derived neurospheres were treated with the Galectin-3 inhibitor TD-139.

n = 4, one-way ANOVA with Tukey HSD. Error bars show standard error of the mean (SEM).

After 5 days in treatment medium, the diameters of neurospheres were measured to determine if Galectin-3 affected the proliferative capacity of NSCs. As compared to control neurospheres, addition of Galectin-3 at both 1 µg/ml and 5 µg/ml decreased neurosphere diameter ($p = 0.010$, one-way ANOVA). Tukey Post-Hoc analysis revealed a dose-dependent effect of Galectin-3, with 1 µg/ml Galectin-3 showing no significant effect on neurosphere diameter ($p = 0.56$, Tukey HSD) and 5 µg/ml Galectin-3 showing a decrease in neurosphere diameter ($p = 0.0099$, Tukey HSD). 5 µg/ml Galectin-3 appears to decrease neurosphere diameter by approximately 9%, with the 95% CI being (0.87, 0.95).

Similarly, diameters of neurospheres after 5 days of treatment with the Galectin-3 inhibitor TD-139 were measured. Treatment with TD-139 at both 5μM and 10μM did not significantly affect neurosphere diameter. ($p = 0.3$, one-way ANOVA).

3.2.2 Neural stem cell differentiation is not affected by presence of Galectin-3 or Galectin-3 inhibitor in medium

To determine if Galectin-3 or the Galectin-3 inhibitor TD-139 affects NSC differentiation into astrocytes or neurons, the differentiation cultures were fixed 5 days after seeding and immunostained for GFAP (astrocytes/NSCs) and β-III-tubulin (neurons). The number of β-III-tubulin$^+$ and GFAP$^+$ cells were counted and expressed as a percentage of the total number of cells (DAPI$^+$).

The proportion of cells expressing either marker was quantified. There was no significant difference in the proportion of cells expressing either β-III-tubulin$^+$ (Figure 3.2.2.1; $p = 0.67$, $n=3$, one-way ANOVA) or GFAP ($p = 0.42$, $n=3$, one-way ANOVA).

Similarly, the presence of TD-139 in the medium did not affect the differentiation of neural stem cells into their β-III-tubulin$^+$ neurons (Figure 3.2.2.2; $p = 0.30$, $n=3$, one-way ANOVA) or GFAP$^+$ astrocytes ($p = 0.83$, $n=3$, one-way ANOVA).

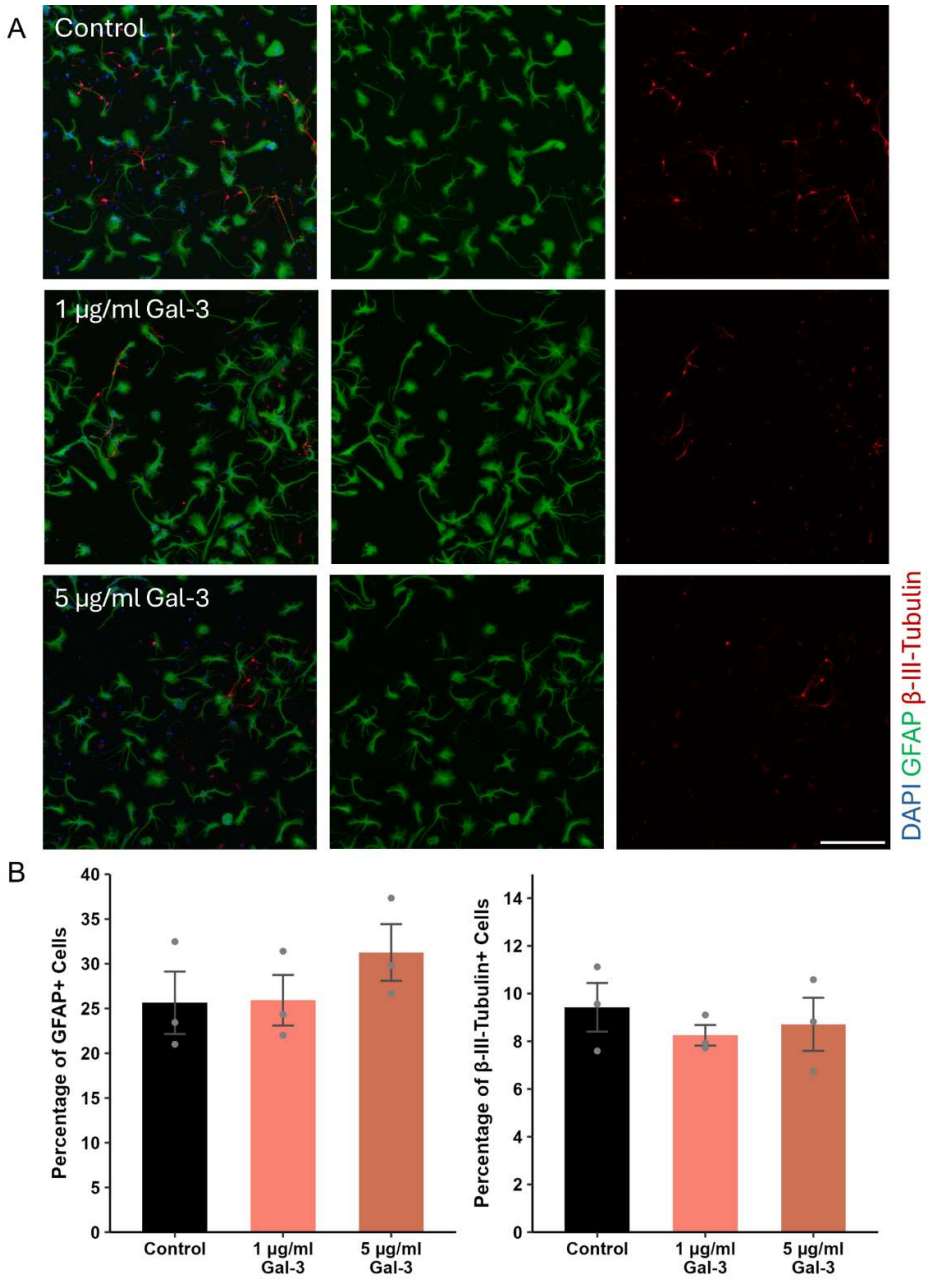


Figure 3.2.2.1: Galectin-3 did not affect neural stem cell differentiation *in vitro*. (A) GFAP and β-III-tubulin immunofluorescence staining of neural stem cells on day 5 of differentiation. Cells were treated with control, 1 µg/ml Galectin-3 or 5 µg/ml Galectin-3 in the differentiation medium. Scale bar represents 200 µm. (B) Proportion of cells expressing either GFAP or β-III-tubulin were compared. No significant difference in the proportion of cells expressing either β-III-tubulin^{+} ($p = 0.67$, n=3, one-way ANOVA) or GFAP ($p = 0.42$, $n = 3$, one-way ANOVA). Error bars represent SEM.

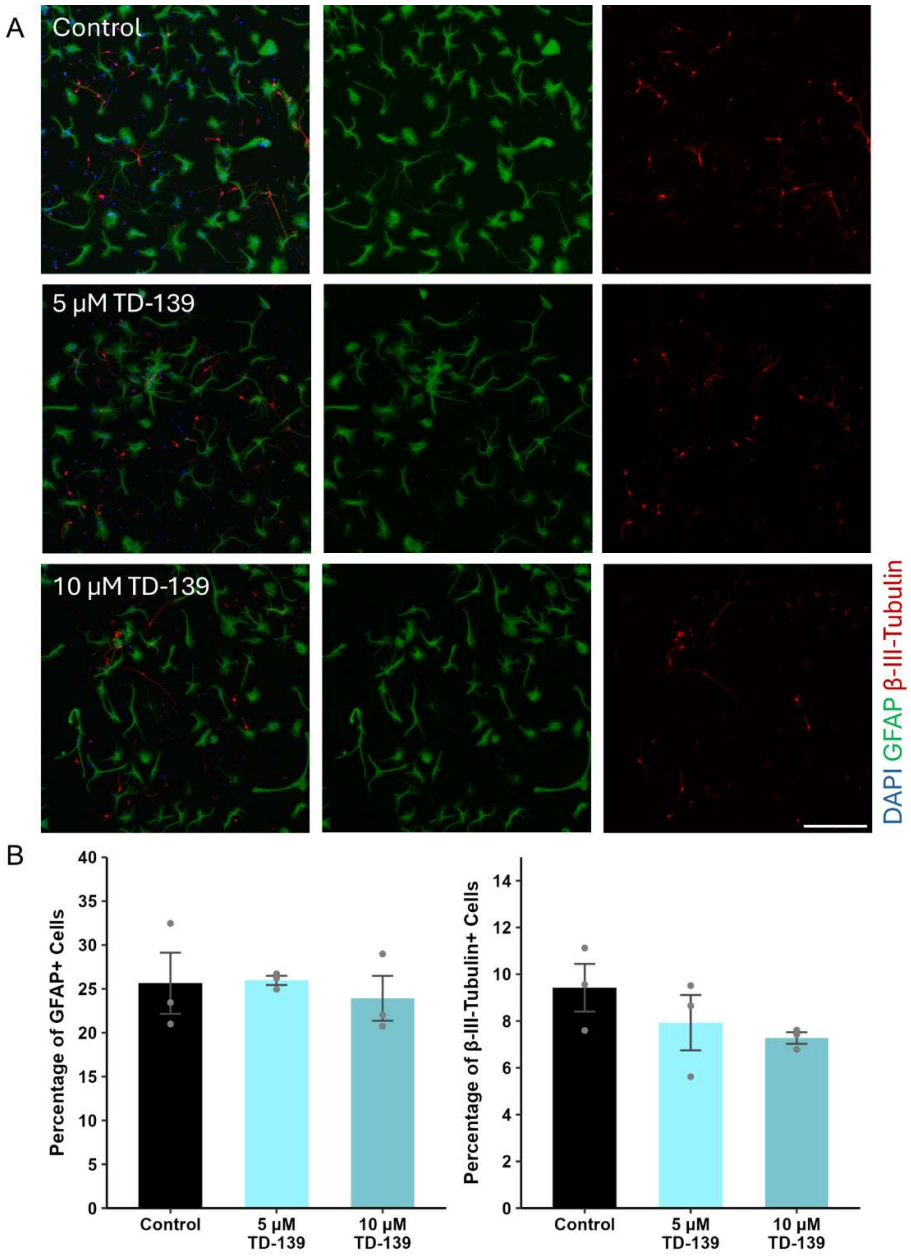


Figure 3.2.2.2: Pharmacological inhibition of Galectin-3 did not affect neural stem cell differentiation *in vitro*. (A) GFAP and β-III-tubulin immunofluorescence staining of neural stem cells on day 5 of differentiation. Cells were treated with control, 5 μM TD-139 or 10 μM TD-139 in the differentiation medium. Scale bar represents 200 μm. (B) Proportion of cells expressing either GFAP or β-III-tubulin were compared. No significant difference in the proportion of cells expressing either β-III-tubulin$^+$ ($p = 0.30$, n=3, one-way ANOVA) or GFAP$^+$ ($p = 0.83$, n=3, one-way ANOVA). Error bars represent SEM.

3.3 Galectin-3 knockout did not significantly alter adult hippocampal neurogenesis in young adult mice on a Sv129 background

Since addition of Galectin-3 decreased hippocampal neural stem cell proliferation *in vitro*, I sought to determine if Galectin-3 knockout would alter neurogenesis in adult mice. Neurogenesis in the SGZ starts with a radial glia like neural stem cell (NSC, $GFAP^+$) dividing and eventually differentiating into neuroblasts (DCX^+) and then maturing into post-mitotic neurons which reside in the dentate gyrus ($NeuN^+$). I investigated the effect of Galectin-3 knockout on all three populations.

3.3.1 Galectin-3 knockout did not affect the transient amplifying progenitor or neuroblast population in young adult mice

To investigate the effect of Galectin-3 knockout on the population of transient amplifying progenitors (TAPs) and neuroblasts, I immunostained hippocampal sections of coronally sectioned brains from Galectin-$3^{+/+}$ and Galectin-$3^{-/-}$ mice. No significant differences were observed between the TAP population ($p = 0.267$) or the neuroblast population ($p = 0.351$).

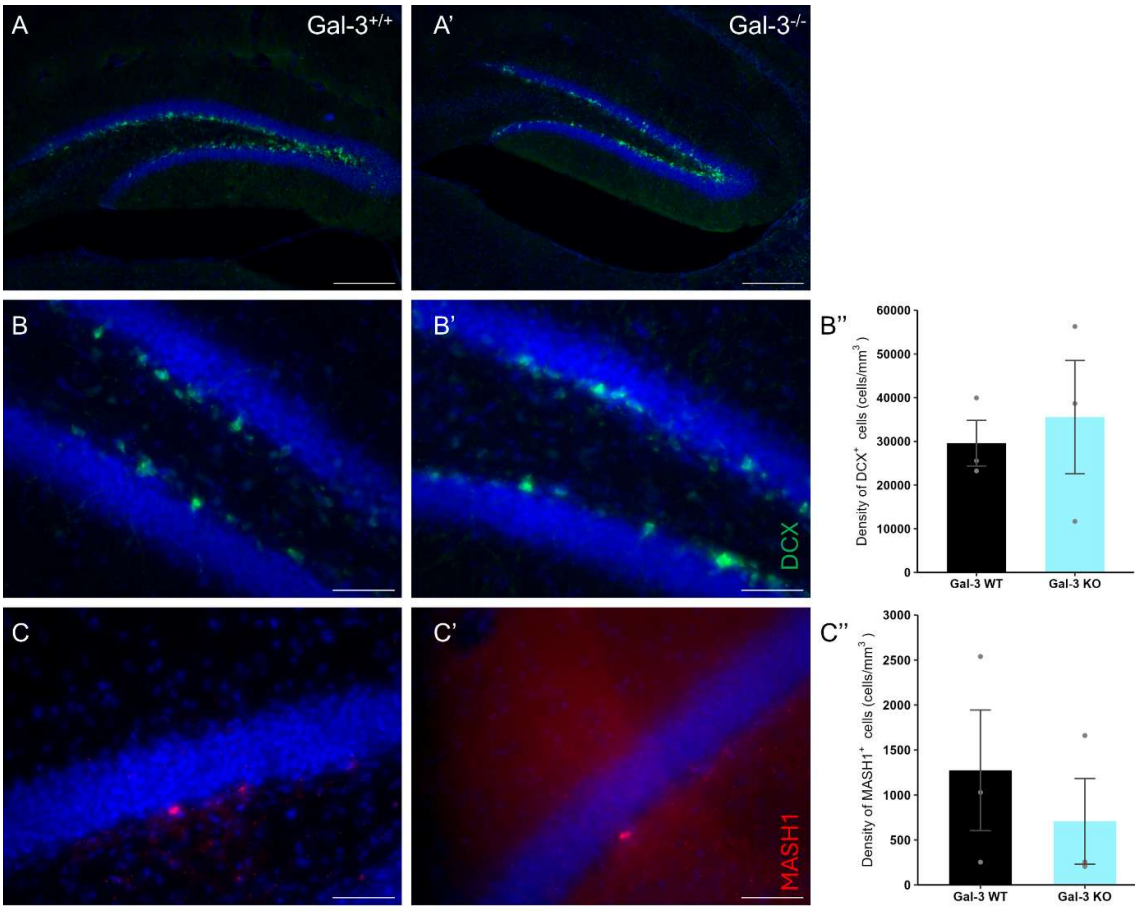


Figure 3.3.1: Galectin-3 knockout on a Sv129 background did not affect neuroblast or transient amplifying progenitor (TAP) cell populations. (A) Immunofluorescent labelling of DCX+ cells did not show a difference between the densities of neuroblasts in Galectin-$3^{+/+}$ and Galectin-$3^{-/-}$ mice. Scale bars represent 200 µm. (B) Quantification of DCX^+ cell density in the dentate gyrus did not show significant differences between Galectin-$3^{+/+}$ and Galectin-$3^{-/-}$ mice. (C) Quantification of $MASH1^+$ cell density in the dentate gyrus did not show significant differences in TAP population between Galectin-$3^{+/+}$ and Galectin-$3^{-/-}$ mice. Scale bars in B and C represent 50 µm.

n = 3 males, Student's t-test. Error bars represent SEM.

3.4 Galectin-3 knockout did not significantly alter hippocampal neurogenesis in young adult mice

To further investigate how Galectin-3 knockout may affect NSC proliferation and differentiation *in vivo*, I generated Galectin-$3^{-/-}$ and Galectin-$3^{+/+}$ mice from Galectin-$3^{+/-}$ x Galectin-$3^{+/-}$ matings. At 2 months, BrdU was given via I.P. injections for 10 consecutive days to label dividing cells. Mice were sacrificed by transcardiac perfusion either 10 days (neuroblast cohort, NB) or 30 days (label retaining cell cohort, LRC) after the last BrdU dose.

3.4.1 Galectin-3 knockout did not affect slow dividing label retaining cell

$GFAP^+$ NSCs which divided during the period of BrdU injections but did not further differentiate will retain their BrdU labelling (label retaining cells, LRCs). To determine if Galectin-3 knockout would increase the LRC population, the density of these double-labelled cells ($BrdU^+GFAP^+$) were quantified in Galectin-$3^{+/+}$ and Galectin-$3^{-/-}$ mice of the LRC cohort. In Galectin-$3^{+/+}$ mice, the density was 583.16 $\pm$ 136.30 cells/mm^3, (mean $\pm$ SEM), while in Galectin-$3^{-/-}$ mice the density was 311.67 $\pm$ 94.62 cells/mm^3. There was no significant difference between Galectin-$3^{+/+}$ and Galectin-$3^{-/-}$ animals ($p = 0.09$, Student's t-test).

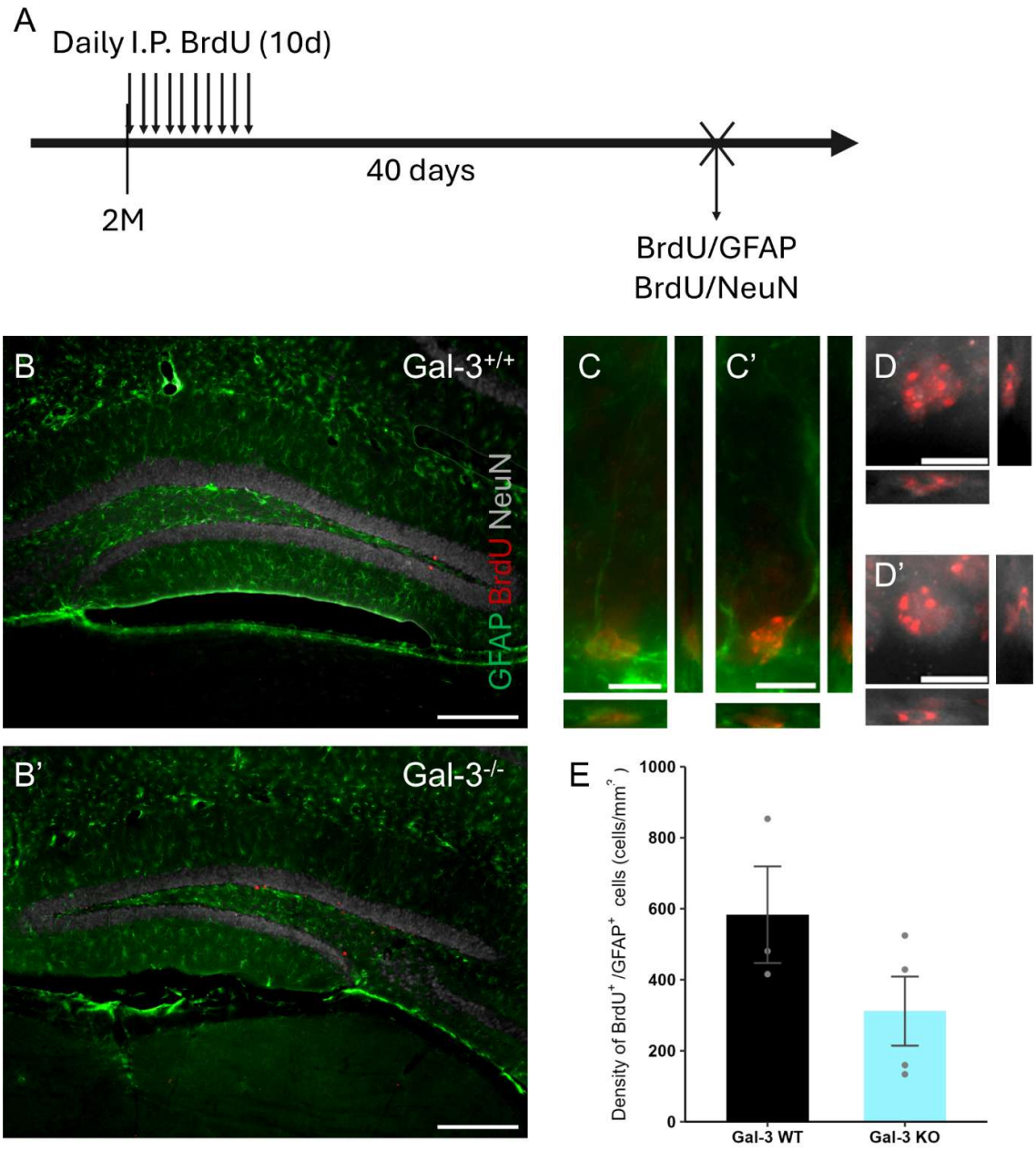


Figure 3.4.1: (A) BrdU regimen to identify label retaining cells (LRCs) and post-mitotic neurons. BrdU was injected daily via i.p. injections at 100mg/kg for 10 days. 30 days after the last BrdU injection, the mice were sacrificed. (B & C) Immunostaining of BrdU/NeuN and BrdU/GFAP cells in Galectin-$3^{+/+}$ and Galectin-$3^{-/-}$ hippocampi respectively, with examples of orthogonal projections of $BrdU^{+}GFAP^{+}$ (B') and $BrdU^{+}NeuN^{+}$ (B'' and C'') cells. Scale bars in (B) represent 200 µm, scale bars in (C) and (D) represent 10 µm. n = 4 Galectin-$3^{+/+}$ (3 males, 1 female), n = 5 Galectin-$3^{-/-}$ (1 male and 4 females); Student's t-test. Error bars represent SEM.

3.4.2 Galectin-3 knockout trended towards increased neuroblast generation in young adult mice

I generated the samples and collected them. Hannah Rosenheim sectioned 2 of the brains as part of her Master's rotation. Immunostaining was performed together and Hannah performed quantification of the images.

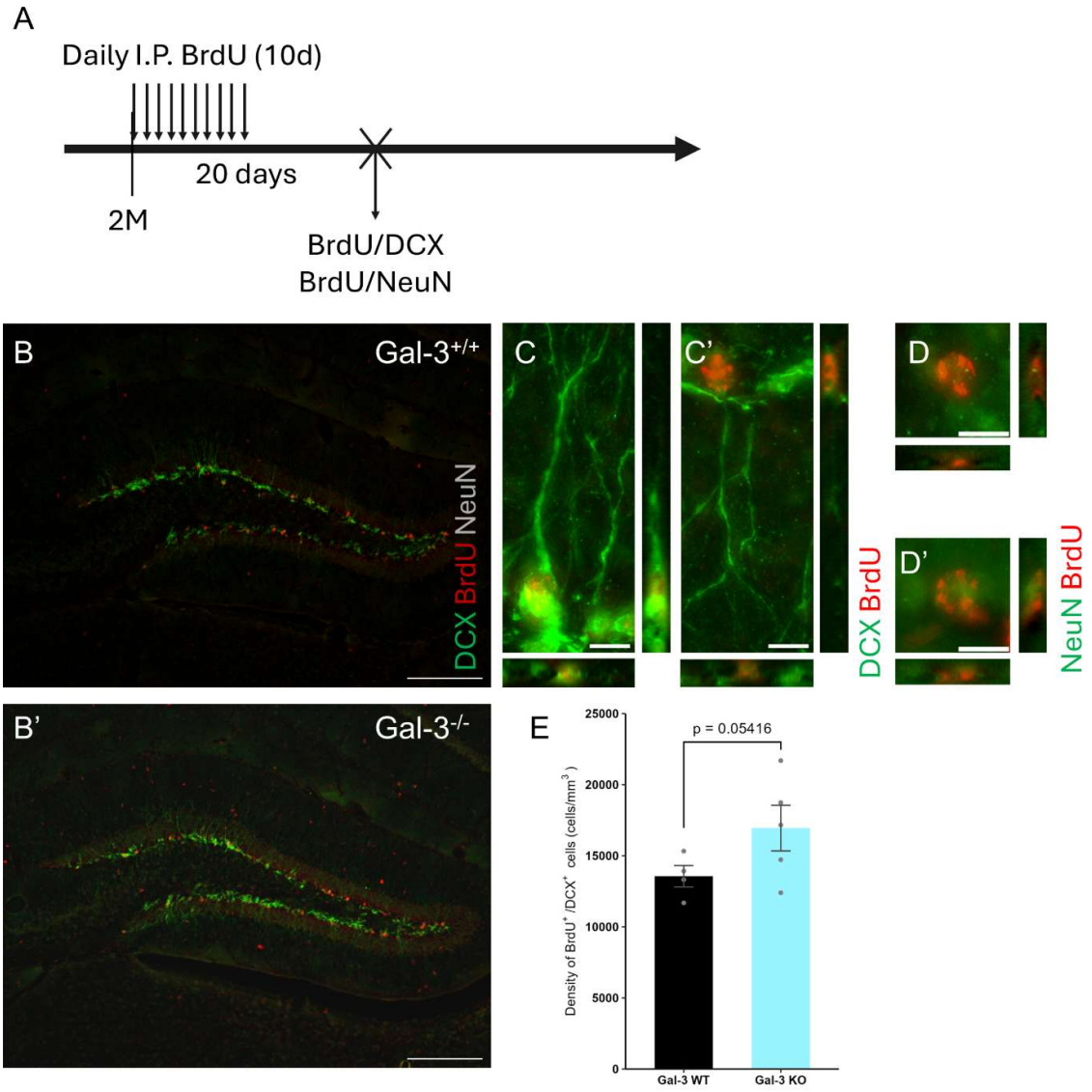


Figure 3.4.2. Figure Legend on the following page.

Figure 3.4.2. (A) BrdU regimen to identify neuroblasts and post-mitotic neurons. BrdU was injected daily via i.p. injections at 100mg/kg for 10 days. 10 days after the last BrdU injection, the mice were sacrificed. (B & C) Immunostaining of BrdU/DCX and BrdU/NeuN cells in Galectin-$3^{+/+}$ and Galectin-$3^{-/-}$ hippocampi respectively, with examples of orthogonal projections of $BrdU^+DCX^+$ (B') and $BrdU^+NeuN^+$ (B'' and C'') cells. Scale bars in (B) represent 200 μm, scale bars in (C) and (D) represent 10 μm. n = 4 Galectin-$3^{+/+}$ (3 males, 1 female), n = 6 Galectin-$3^{-/-}$ (2 males and 4 females); Student's t-test. Error bars represent SEM.

To determine if knockout of Galectin-3 alters the neuroblast population in the hippocampus, the number of $BrdU^+DCX^+$ neuroblasts per volume of dentate gyrus was quantified in both Galectin-$3^{+/+}$ and Galectin-$3^{-/-}$ mice of the NB cohort. In Galectin-$3^{+/+}$ mice, the density was 13564.36 $\pm$ 754.12 cells/mm^3 (mean $\pm$ SEM), while in Galectin-$3^{-/-}$ mice the density was 16946.83116 $\pm$ 1603.33 cells/mm^3. There was a strong trend towards increased neuroblast generation in the Galectin-$3^{-/-}$ mice ($p = 0.05416$, Student's t-test). However, interpretation of this is limited by the small sample size and the lack of stratification according to sex.

3.4.3 Galectin-3 knockout did not affect number of post-mitotic neurons generated

To determine if knockout of Galectin-3 alters the generation of post-mitotic neurons in the dentate gyrus, I quantified the number of $BrdU^+NeuN^+$ neurons per volume of dentate gyrus.

In the NB cohort, Galectin-$3^{+/+}$ mice had a density of 13860.16 $\pm$ 2308.21 (mean $\pm$ SEM) $BrdU^+NeuN^+$ cells/mm^3 of dentate gyrus while Galectin-$3^{-/-}$ mice had a density of 15797.81 $\pm$ 2521.09 $BrdU^+NeuN^+$ cells/mm^3 of dentate gyrus (Figure 3.4.3 A).

In the LRC cohort, Galectin-$3^{+/+}$ mice had a density of 7852.97 $\pm$ 683.83 $BrdU^+NeuN^+$ cells/mm^3 of dentate gyrus while Galectin-$3^{-/-}$ mice had a density of 6622.04 $\pm$ 351.11 $BrdU^+NeuN^+$ cells/mm^3 of dentate gyrus (Figure 3.4.3 B).

In both the NB and the LRC cohorts, no significant difference was observed between Galectin-$3^{+/+}$ and Galectin-$3^{-/-}$ mice ($p_{exact} = 0.2$) for both NB and LRC, Mann-Whitney Test).

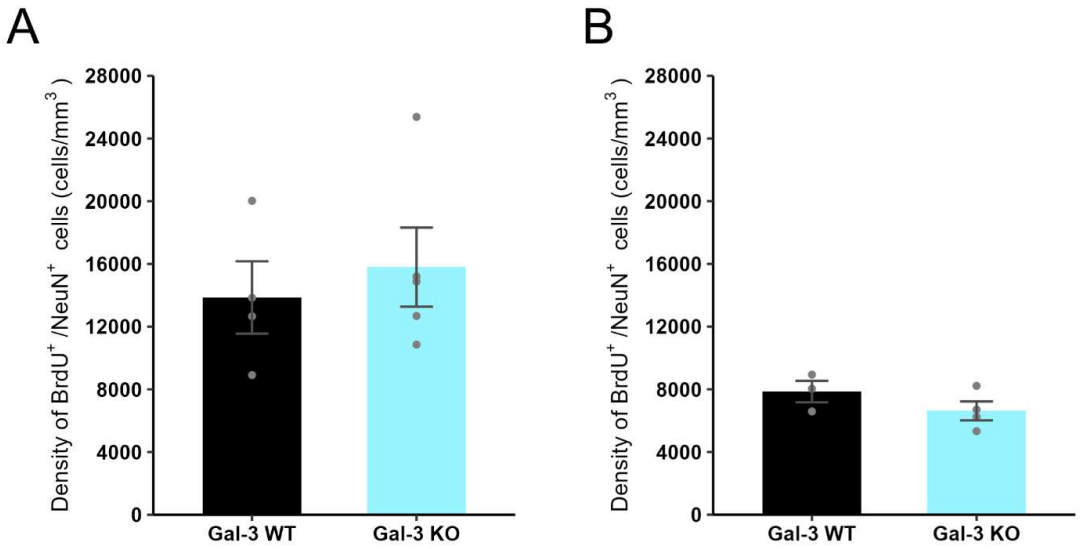


Figure 3.4.3: $BrdU^{+}NeuN^{+}$ cells densities in the DG of mice with 30 days between the last BrdU injection and fixation (A) and 10 days between the last injection and fixation (B). No significant differences between the density of post-mitotic neurons were observed in both cohorts.

(A) n = 4 Galectin-$3^{+/+}$ (3 males, 1 female), n = 6 Galectin-$3^{-/-}$ (2 males and 4 females); (B) n = 4 Galectin-$3^{+/+}$ (3 males, 1 female), n = 5 Galectin-$3^{-/-}$ (1 male and 4 females). Mann-Whitney Test. Error bars represent SEM.

3.4.4 Galectin-3 knockout did not affect location of $BrdU^{+}/NeuN^{+}$ cells within the DG

Granule cells of the dentate gyrus are generated in the SGZ and migrate a small distance into the GCL as they mature. To determine if knockout of Galectin-3 alters the position of the granule cells within the GCL, I quantified the proportion of $BrdU^{+}/NeuN^{+}$ cells which remained in the SGZ in Galectin-$3^{+/+}$ and Galectin-$3^{-/-}$ animals using a subset of the images for the above analysis. Cells are defined as being in the SGZ if no other cells separate it from the hilus of the DG, the remaining cells were defined as being in the GCL (Figure 3.4.4 A and B).

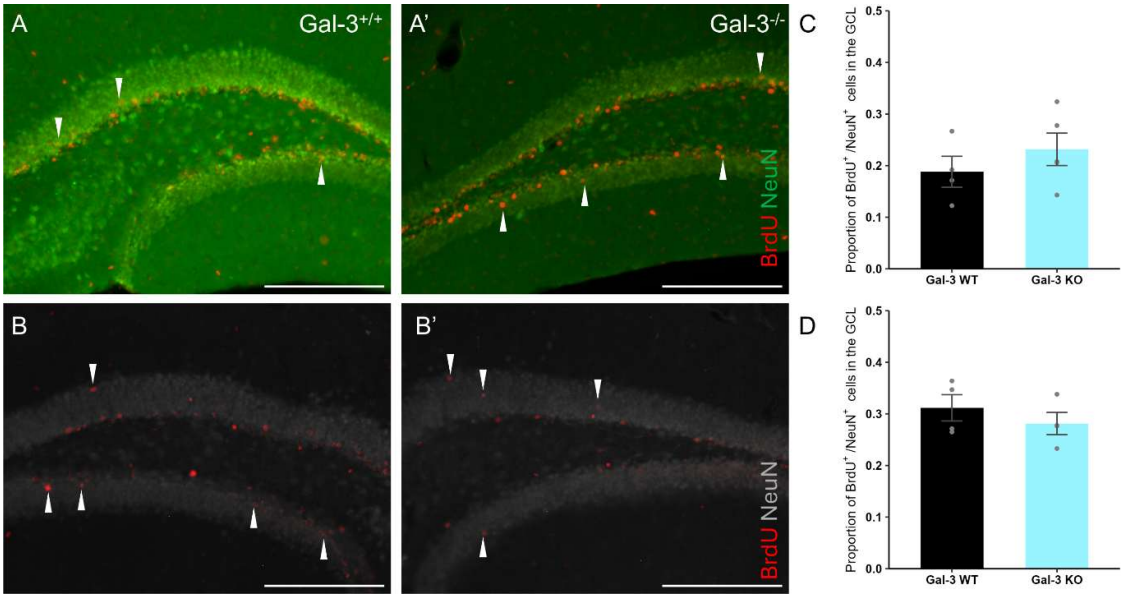


Figure 3.4.4: Galectin-3 knockout did not alter the location of $BrdU^+NeuN^+$ cells within the GCL. (A, B) $BrdU^+/NeuN^+$ cells in the dentate gyrus of Galectin-$3^{+/+}$ mice and Galectin-$3^{-/-}$ mice (A', B'); white arrowheads highlight cells which have migrated into the GCL. (C, D) Proportion of $BrdU^+/NeuN^+$ cells which have migrated into the GCL. Scale bars represent 200 µm.

(A) and (C) show data from the NB cohort; n = 4 Galectin-$3^{+/+}$ (3 males, 1 female), n = 6 Galectin-$3^{-/-}$ (2 males and 4 females); Student's t-test. Error bars represent SEM.

(B) and (D) show data from the LRC cohort; n = 4 Galectin-$3^{+/+}$ (3 males, 1 female), n = 5 Galectin-$3^{-/-}$ (1 male and 4 females); Student's t-test. Error bars represent SEM.

$BrdU^+/NeuN^+$ cells in the NB cohort which were sacrificed 10 days after the last BrdU injection, 18.81 $\pm$ 3.00 % (n = 4, Mean $\pm$ SEM) of $BrdU^+/NeuN^+$ cells had migrated into the GCL of Galectin-$3^{+/+}$ mice. Similarly, 23.16 $\pm$ 3.14 % (n = 5) of $BrdU^+/NeuN^+$ cells had migrated into the GCL of Galectin-$3^{-/-}$ mice. No significant difference was observed between the two groups ($p = 0.18$, Student's t-test).

In the LRC cohort which had 30 days between the last BrdU injection and sacrifice, Galectin-$3^{+/+}$ mice had 31.18 $\pm$ 2.55 % of $BrdU^+/NeuN^+$ cells in the GCL while Galectin-$3^{-/-}$ mice had 28.14 $\pm$ 2.16 % of $BrdU^+/NeuN^+$ cells in the GCL. Similarly, no significant difference was detected between the two groups ($p = 0.20$, Student's t-test).

Post-hoc ANOVA testing between the two populations showed that there was indeed an effect of cohort (LRC vs. NB) but no effect of genotype on the proportion of $BrdU^+/NeuN^+$ cells which migrated into the GCL.

3.5 Galectin-3 knockout in middle-aged mice did not alter generation of newborn neurons in WTs

Immunostaining and quantification was performed by Zubaida Mukthar as part of her Final Year Project (Biology department), under my supervision.

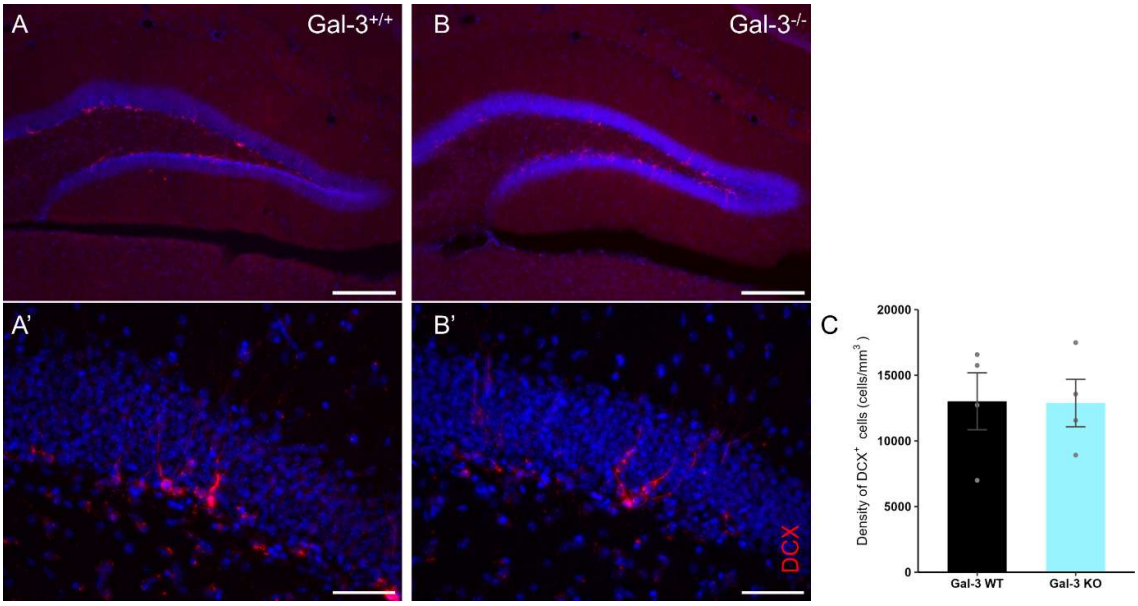


Figure 3.5: Galectin-3 knockout did not alter generation of neuroblasts in middle-aged mice. (A and B) DCX^+ cells in the dentate gyrus of 7-month old Galectin-$3^{+/+}$ (A) and Galectin-$3^{-/-}$ (B) mice. Scale bars represent 200 µm. Comparison of the density of DCX+ cells in the dentate gyrus reveal no significant differences between Galectin-$3^{+/+}$ and Galectin-$3^{-/-}$ mice (C). n = 5 males Galectin-$3^{+/+}$, n = 6 males Galectin-$3^{-/-}$; Student's t-test. Error bars show SEM.

Tao and colleagues showed robust Galectin-3 expression in 7-month old mice (Tao et al., 2020). I have also showed that in Galectin-3+/+ mice, middle-aged mice show more Galectin-3 reactivity as compared to young adults. As such, to determine if ageing modulates the effect that Galectin-3 has on adult hippocampal neurogenesis, these middle-aged mice were

immunostained for DCX (Mean age ± SEM were for Galectin-$3^{+/+}$: 7.4 ± 0.16, for Galectin-$3^{-/-}$: 7.6 ± 0.45; n = 4 each). No significant differences between the neuroblast populations were detected between Galectin-$3^{+/+}$ and Galectin-$3^{-/-}$ mice.

3.6 Discussion

3.6.1 Galectin-3 expression is detectable in the hippocampus and SGZ of C57Bl6 mice from 10 weeks.

To my knowledge, this is the first study showing expression of Galectin-3 in young adult mice. Previous studies have shown similar patterns of hippocampal Galectin-3 expression in older mice (Shin et al., 2025; Tao et al., 2020), with Galectin-3 expression being seen in the CA1 and the hilus of the dentate gyrus. However, these studies did not examine the neurogenic SGZ. Herein, I show that unlike in the SVZ where cells of the neural lineage express Galectin-3 (Comte et al., 2011), Galectin-3 is expressed by microglia in the SGZ. This suggests that Galectin-3 could be performing different roles in the SGZ as compared to in the SVZ.

3.6.2 On the use of recombinant Galectin-3 and TD-139 over Galectin-3 overexpression and silencing via nucleofection of plasmids

To identify the role of Galectin-3 in the SVZ, previous work in the lab nucleofected either Galectin-3-targeting short-hairpin or Galectin-3-overexpressing plasmids into neurospheres and *in vivo* postnatally (Al-Dalahmah, Campos Soares, et al., 2020; Al-Dalahmah, Nicholson, et al., 2020). In the SVZ, Galectin-3 was expressed in ependymal cells and some astrocyte-like stem cells. Hence, using nucleofection of constructs to increase or decrease Galectin-3 expression in neural stem cells to reveal the effects that Galectin-3 had on Wnt and BMP signalling in the neural lineage was relevant in the SVZ (Al-Dalahmah, Campos Soares, et al., 2020; Al-Dalahmah, Nicholson, et al., 2020). However, unlike cells of the neurogenic lineage in the SVZ, the neurogenic cells in the SGZ do not express Galectin-3. This is seen from the co-localisation of Galectin-3 with IBA1 in the SGZ and GCL of the DG. Similar observations

were made throughout the hippocampus in either young or middle-aged mice. Since Galectin-3$^+$ cells in the hippocampus were not of the neurogenic lineage, and almost all Galectin-3$^+$ cells were microglia, I decided that it would be more relevant to investigate the effects that secreted Galectin-3 had on neurogenesis by addition of recombinant Galectin-3.

In contexts of injury, astrocytes have been shown to upregulate Galectin-3 (Sirko et al., 2023). In the neurosphere assay, astrocytes are present. Hence, I added the Galectin-3 inhibitor TD-139 into the neurosphere medium to inhibit any Galectin-3 that would be present in the culture medium.

3.6.3 Galectin-3 effects on different neuronal populations

Galectin-3's role in SVZ neurogenesis and gliogenesis has been characterised by previous work in the Szele lab (Al-Dalahmah, Campos Soares, et al., 2020; Al-Dalahmah, Nicholson, et al., 2020; Comte et al., 2011). However, despite several experiments designed to shed light on this question, little was known about Galectin-3's effect on neurogenesis in the SGZ. Galectin-3 is upregulated in the hippocampus of various AD mouse models, but in addition to being pathologically relevant, Galectin-3 is expressed by microglia in the DG under homeostatic conditions, with levels of Galectin-3 also increasing with age (Shin et al., 2025). Hence, identifying the effects of Galectin-3 on neurogenesis in the SGZ may represent a potential pathway to modulate AHN.

In my hands, while Galectin-3 treated neurospheres showed reduced proliferation, I did not identify an effect of Galectin-3 knockout on the density of dividing NSCs in the hippocampus (Figure 3.4.1). While further interrogation of the neural lineage revealed slight increases in neuroblasts (Figure 3.4.2), no changes were observed in the densities of post-mitotic neurons (Figure 3.4.3). Furthermore, having investigated the density of post-mitotic neurons generated during a 10-day BrdU-dosing period at both an early (10 day washout) and late (30 day washout), the lack of difference between the densities of BrdU$^+$NeuN$^+$ cells at both time points suggest that Galectin-3 knockout also did not affect cell survival.

While Galectin-3 did not appear to significantly alter NSC division, or neuroblast and mature neuron generation in the SGZ, it could still affect the migration of neurons in the dentate gyrus. Cells in the dentate gyrus generated in the SGZ initially project into the inner molecular layer, but as they mature and migrate radially into the GCL, their dendrites project further into the molecular layer of the dentate gyrus (Radic et al., 2017). Ectopic migration of neurons into the hilus has been shown to affect their morphology and maturation (Scharfman et al., 2000). In the SVZ and the RMS, Galectin-3 increased neuroblast migration (Comte et al., 2011); I observed Galectin-3^{+} cells in the SGZ, hilus and molecular layer, and since Galectin-3 is known to be a secreted protein, it is likely that cells of the neural lineage in the GCL are exposed to Galectin-3. As such, the presence of Galectin-3 in the SGZ may affect the maturation of granule cells if it modulates the distribution of newly generated neurons in the GCL. Quantification of the proportion of $BrdU^{+}NeuN^{+}$ cells remaining in the SGZ also reveals no significant changes in the proportion of cells which have migrated into the GCL between Galectin-$3^{+/+}$ and Galectin-$3^{-/-}$ mice. In conclusion, while Galectin-3 was present in the dentate gyrus and SGZ of C57Bl6 mice from 10 weeks, I did not observe any significant effect of Galectin-3 knockout on neurogenesis (Soares et al., 2025).

3.6.4 Discrepancies between *in vitro* neurosphere assays and *in vivo* mouse models

In the neurosphere assays, a significant decrease in neural stem cell proliferation as measured by neurosphere diameter was observed. However, there were no significant changes to the density of the neural lineages in Galectin-$3^{-/-}$ mice compared to their Galectin-$3^{+/+}$ counterparts *in vivo*. This could be due to the lack of statistical power, low levels of Galectin-3 expression in the hippocampus, sex differences in neurogenesis or spatial differences in hippocampal neurogenesis.

Furthermore, human recombinant Galectin-3 was used for treatment of murine NSCs, whereas mouse NSCs in the DG would have been exposed to mGal-3 *in vivo*.

3.6.4.1 Lack of statistical power

In the proliferation assay where Galectin-3 treatment decreased neurosphere size, post-hoc calculation of statistical power revealed a 1 – β of 0.73, suggesting a slightly underpowered study and the possibility of a false positive. Here, one additional replicate would have increased the power to a 1 – β value of 0.9. Additionally, the sample sizes of the *in vivo* analyses were low, with between n = 3 to n = 5 animals per genotype for each of the analyses. This resulted in 1 – β values of under 0.6, suggesting they were all lacking statistical power. For the analysis of the change in neuroblast density, given the observed effect size, n = 10 per genotype would have been required to achieve the required statistical significance and power. Hence, future studies should include larger cohorts.

3.6.4.2 Low Galectin-3 expression in the hippocampus and DG in WT

While expression of Galectin-3 is detectable by immunohistochemistry in the hippocampus, and specifically in the neurogenic SGZ of the dentate gyrus, this was at much lower levels as compared to AD mouse models. Furthermore, the majority of the Galectin-3 expressing cells were observed in the CA1 region. Hence, the Galectin-3 knockout mouse models used did not appear to have strong differences in the levels of Galectin-3 in the hippocampus compared to their wildtype counterparts. The concentration of recombinant Galectin-3 used in the neurosphere assay was previously shown to rescue neural rosette formation in human embryonic stem cells (Soares et al., 2025). Taken together, these suggest that depletion of homeostatic levels of Galectin-3 in wildtype mice may not affect hippocampal neurogenesis.

Compared to healthy controls, AD patients have increased levels of Galectin-3. Various AD mouse models show similar increases in Galectin-3 compared to controls (Boza-Serrano et al., 2019; Siew et al., 2024; Tao et al., 2020). The same authors have also shown cognitive improvements with genetic ablation of Galectin-3 in AD mouse models, without direct evidence that this was due to increased hippocampal neurogenesis. While it would be possible to compare neurogenesis levels in these mice, Galectin-3 also affects tau aggregation and Aβ

plaque formation, both of which could confound the effects, if any, of Galectin-3 on neural stem cell proliferation and differentiation. Future studies could investigate the effects of Galectin-3 knockout on neurogenesis in geriatric mice (24M, where Galectin-3 is expressed at even higher levels compared to 12M – approximately twice as much in the hippocampus; (Shin et al., 2025)). Another approach could be to overexpress Galectin-3 in the hippocampus either via intrahippocampal injections of Galectin-3 or Galectin-3 overexpressing constructs. More targeted approaches such as the use of transgenic HexB-Cre driver lines to selectively overexpress Galectin-3 in microglia could better mimic the effects of disease on neurogenesis, as microglia are the major cell type producing Galectin-3 in neurodegenerative diseases.

3.6.4.3 Constitutive KO of Galectin-3 vs. inducible systems

In both the strains of Galectin-$3^{-/-}$ mice used, Galectin-3 was constitutively knocked out. This could result in compensatory levels of other Galectins. For instance, knockout of Galectin-1 has been shown to increase neurogenesis in the SGZ (Imaizumi et al., 2011). Hence, if the Galectin-$3^{-/-}$ mice had increased levels of Galectin-1, any changes in neurogenesis due to Galectin-3KO could be masked by concurrent increases in Galectin-1. To this end, inducible knockout models can be employed.

3.6.4.4 Sex differences in adult hippocampal neurogenesis

In the neurosphere assays, NSCs were derived from both male and female neonates.

Small molecules and genetic perturbations have shown sex-specific effects on SVZ neurogenesis (Ruddy et al., 2019; Vancamp et al., 2019).

I have included both sexes in my study. However, due to the small sample size, it was not possible to separately analyse the cohorts. Additionally, in the middle-aged cohort, only males were used. As discussed in Chapter 1, males and females have shown differences in characteristics of neurogenesis. Hence, future studies should aim to include a larger number of animals and to perform analyses both with the sexes combined and separately.

3.6.4.5 Dorso-ventral differences in expression of Galectin-3

In my work, I have only investigated the role of Galectin-3 on neurogenesis in the dorsal hippocampus of the mouse, which corresponds to the posterior hippocampus in primates. While the dorsal hippocampus is more involved in memory and cognitive functions (Fanselow & Dong, 2010), the ventral hippocampus is also affected in AD and mediates the emotional changes seen in AD (Spoleti et al., 2022; Xu et al., 2021). I did not investigate the distribution of Galectin-3 in the ventral hippocampus, nor did I investigate if Galectin-3 knockout altered neurogenesis in the ventral hippocampus. Previous studies have shown region-specific changes in neurogenesis after treatment with fluoxetine and JNK inhibitor (Mohammad et al., 2018; Zhou et al., 2016), both of which increased neurogenesis in the ventral but not the dorsal hippocampus. Hence, it will be important for future studies to identify if Galectin-3 knockout alters neurogenesis in the ventral hippocampus.

3.6.5 Use of two different mouse strains

Galectin-3$^{-/-}$ mice from two different strains (C57Bl6 and 129/SvJ), along with their WT littermates were used. This was to ensure that any effects of Galectin-3 knockout on neurogenesis was not due to either background strain differences, or targeting construct artefacts.

3.6.5.1 Background strain-dependent effects on AHN

Differences in baseline levels of AHN have been reported between C57BL/6 and 129/SvJ (Clark et al., 2011; Kim et al., 2017), with lower levels of hippocampal neurogenesis (DCX and BrdU/NeuN) in 129/SvJ mice (Clark et al., 2011; Kim et al., 2017). One study showed that on a C57BL/6 background, MOR-1 knockout enhanced hippocampal neurogenesis by decreasing apoptosis (Cominski et al., 2014). However, there was an opposite effect of MOR-1 KO on the 129S6 background (Cominski et al., 2014). Even for interventions which robustly increase neurogenesis across multiple mouse strains such as exercise, the magnitude of increase in neurogenesis differs greatly across mouse strains (Clark et al., 2011).

3.6.5.2 Targeting construct-dependent effects

The Lgals3^{tm1Poi} mutation replaced exons 2 – 4 of Galectin-3 with a neomycin cassette, resulting in loss of the coding region for the N-terminal and part of the CRD. The Lgals3^{tm1Ftl} mutation replaced 0.5kb between intron 4 and exon 5 with a neomycin cassette, disrupting the CRD. Targeting constructs may produce off-target effects and may result in production of truncated protein isoforms, both of which may confound results.

Truncated proteins may act as dominant negatives, and the effects seen may be due to gain-of-functions from the presence of the truncated protein rather than the loss-of-function of Galectin-3.

Nonetheless, both strains have previously been verified to lack Galectin-3 protein. In my hands, Galectin-3 is not immunohistochemically detected in the dorsal third ventricles in both strains, where ependymal cells strongly express Galectin-3 in WT mice. In the Galectin-3^{tm1Ftl} mice, western blots also showed no detectable levels of Galectin-3. Furthermore, the antibody chosen detects an epitope on the N-terminal. Taken together, these suggest that the presence of off-target effects arising from truncated Galectin-3 is unlikely to have a significant effect in my experiments.

3.6.6 Future directions

3.6.6.1 Galectin-3 and neurite outgrowth/maturation

As discussed in 3.6.4.2, low levels of Galectin-3 under homeostatic conditions could account for the lack of effect on hippocampal neurogenesis. However, most of the Galectin-3+ cells I observed were in the molecular layer of the CA1. Additionally, Galectin-3 knockout increased retention of fear memory (Chen et al., 2017) and CA1 neurons have been shown to mediate fear conditioning (Tronson et al., 2009). This, together with the fact that Galectin-3 is present in molecular layer of CA1 region, where dendrites of CA1 neurons project towards, suggest that Galectin-3 knockout may have improved fear retention and increased LTP by altering the synapses of CA1 neurons. Furthermore, microglia have been shown to aberrantly phagocytose synapses in the context of AD (De Schepper et al., 2023). If Galectin-3 could

induce aberrant phagocytosis of synapses, inhibition of Galectin-3 may be able to rescue cognitive deficits without having to increase neurogenesis. As stem cell pools diminish with age this could offer an alternative for AD therapy in addition to increasing AHN.

3.6.7 Conclusion

My work has shown that Galectin-3 potentially decreases proliferation of hippocampal neural stem cells without affecting their relative differentiation into neurons or astrocytes.

It is possible that the cognitive improvements observed from Galectin-3 ablation in a WT or AD background could in part be due to increases in neurogenesis. However, as Galectin-3 is mostly expressed in the CA1 region of the hippocampus, it is possible that the cognitive benefits observed from Galectin-3 knockout are also due to Galectin-3's effects on mature neurons in the hippocampus. Future work should aim to identify whether Galectin-3 knockout would alter the complexity of neuronal arborisation in the CA1 region.

Chapter 4: The effect of Galectin-3 on Glial cells

4.1 Introduction

4.1.1 Sholl analysis

Sholl analysis involves first tracing the processes of individual microglia and then quantifying the number of intersections at each radius from the soma (Sholl, 1953). Sholl analysis has been extensively used to characterise the morphology of neurons and microglia. By comparing the differences in branching complexity, inferences can be made about the morphology of microglia. While microglia exist on a continuum of states and morphology does not equate to function, Sholl analysis can provide an insight into how “activated” these microglia are.

I performed Sholl analysis using the Simple Neurite Tracer (SNT) plugin in ImageJ. In Galectin-$3^{+/+}$ mice, $IBA1^{+}$ microglial processes were traced from both Galectin-3 expressing (Galectin-3+) and non-expressing (Gal-3-) cells. Sholl analysis was performed and the number of intersections was plotted against the distance from soma. A mixed effects model analysis was used to compare the overall differences between the Sholl plots and the number of intersections at each radius (Zucco, 2018). A Student’s t-test was also performed for the total number of intersections, the soma area, the end radius, Schoenen Ramification Index (SRI), and the Sholl regression coefficients (Sholl decay, semi-log). All data passed normality checks except for the Sholl decay of 7M Galectin-$3^{-/-}$ mice, where a Mann-Whitney Test was used instead of a Student’s t-test. The Schoenen Ramification Index (SRI) (Schoenen, 1982) takes the maximum number of intersections at any radius over the number of primary branches, giving an overall idea of branching complexity. Usually, a higher SRI indicates more complex branching complexity. The Sholl regression coefficient (or Sholl decay) is the rate at which the branches decrease (or decay) with increasing distance from the soma; a higher coefficient suggests shorter, less complex branching while a lower coefficient usually suggests more complex arborisation.

4.1.2 Disease associated microglia genes

Galectin-3 was shown to be upregulated in DAM from 5xFAD mice (Keren-Shaul et al., 2017), and also specifically in microglia which have phagocytosed Aβ (Grubman et al., 2021). Given that Galectin-3 knockout decreased plaque burden *in vivo* and reduced inflammatory cytokine secretion *in vitro* (Boza-Serrano et al., 2019), I asked if Galectin-3 modulation could directly modulate expression levels of DAM genes. If Galectin-3 modulation is sufficient to regulate the expression of DAM genes, it could suggest that Galectin-3 may be an upstream regulator of DAM states *in vivo*.

4.1.3 Disease associated astrocyte genes

A subset of astrocytes identified near Aβ plaques the 5xFAD model showed upregulation of genes associated with inflammatory signalling and response to toxic compounds (Habib et al., 2020). Plaque-associated microglia upregulate Galectin-3 (Keren-Shaul et al., 2017), which may be secreted. Hence, I sought to determine if exogenous Galectin-3 could alter astrocytic expression of DAA genes.

4.2 Galectin-3 expressing microglia are not morphologically distinct from non-Galectin-3 expressing microglia

I first asked if Galectin-3 expressing (Gal-3+) microglia exhibit a different morphology as compared to non-Galectin-3 expressing (Gal-3-) microglia. I hypothesised that Galectin-3+ microglia would be more reactive and thus would have a less ramified morphology, with lower branching complexity when compared to neighbouring Gal-3- cells.

C57Bl6 mice and Galectin-3 knockout mice at young adult (Galectin-$3^{+/+}$: 2.6 $\pm$ 0.453 months, n = 2 males and n = 3 females; Galectin-$3^{-/-}$: 2.7 $\pm$ 0.407 months, n = 3 males and females) were used in these analyses.

In WT young adult mice, Galectin-3 expressing microglia are morphologically similar to non-Galectin-3 expressing microglia.

Overall comparisons of the Sholl plots of Gal-3+ microglia with that of Gal-3- microglia suggested a difference between the profiles ($p = 0.047$). Analysis of the number of intersections at each radius revealed differences at 10 and 14 µm, but was not significant after FDR adjustment of p-values. Additionally, no significant differences were found between the Sholl regression coefficient, soma area, end radius, SRI, or the total number of intersections of Gal-3+ cells and Gal-3- cells.

Data from statistical analyses can be found in the appendix (Supplementary table 4.2.1).

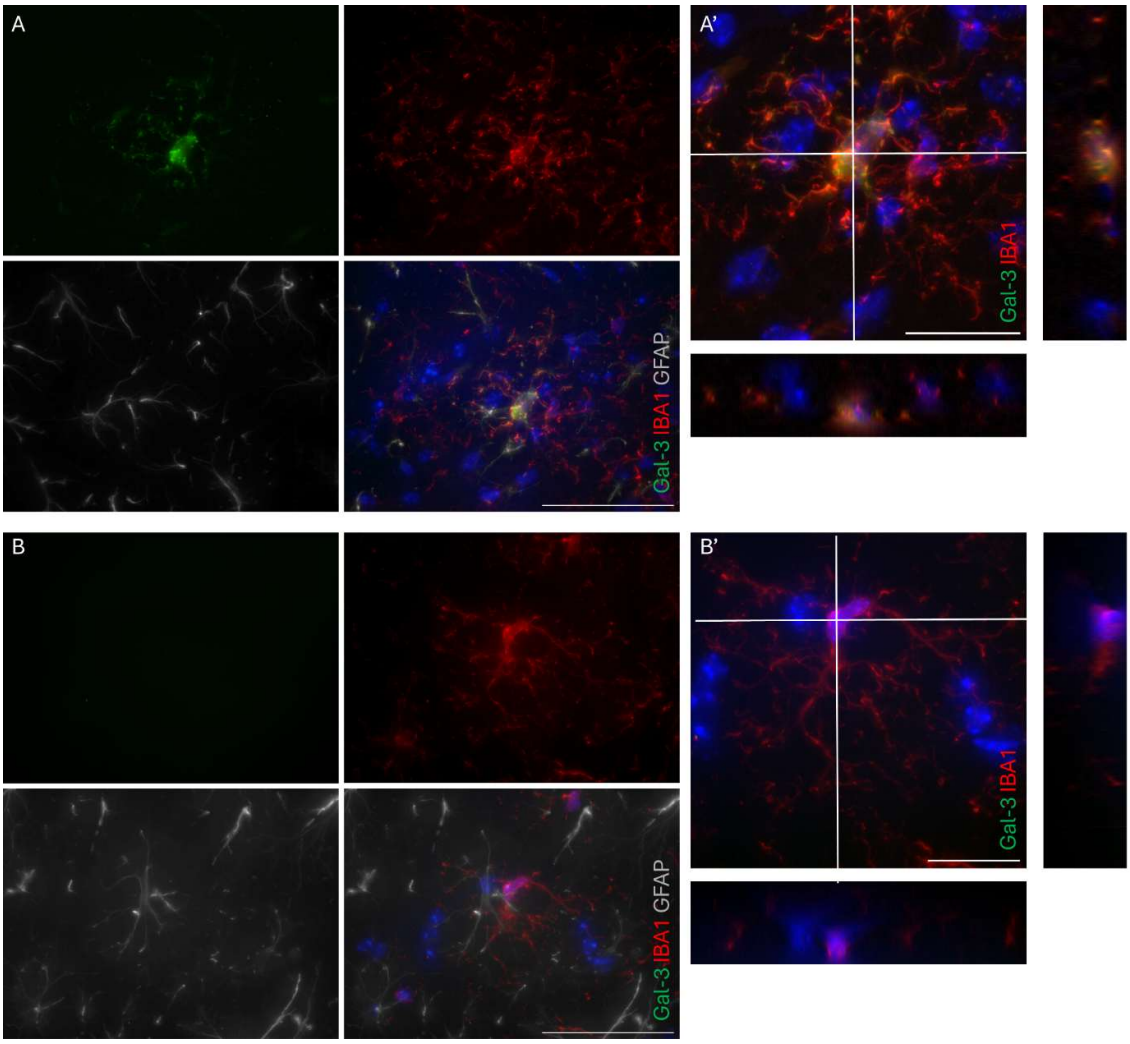


Figure 4.2.1: Morphology of Gal-3+ and Gal-3- microglia in young adult C57Bl6 mice. Gal-3+ (A) and Gal-3- (B) microglia can be observed in the hippocampus of young adult mice. (A') and (B') show orthogonal projections of a single microglia. Scale bars represent 50 µm (A and B) and 20 µm (A' and B').

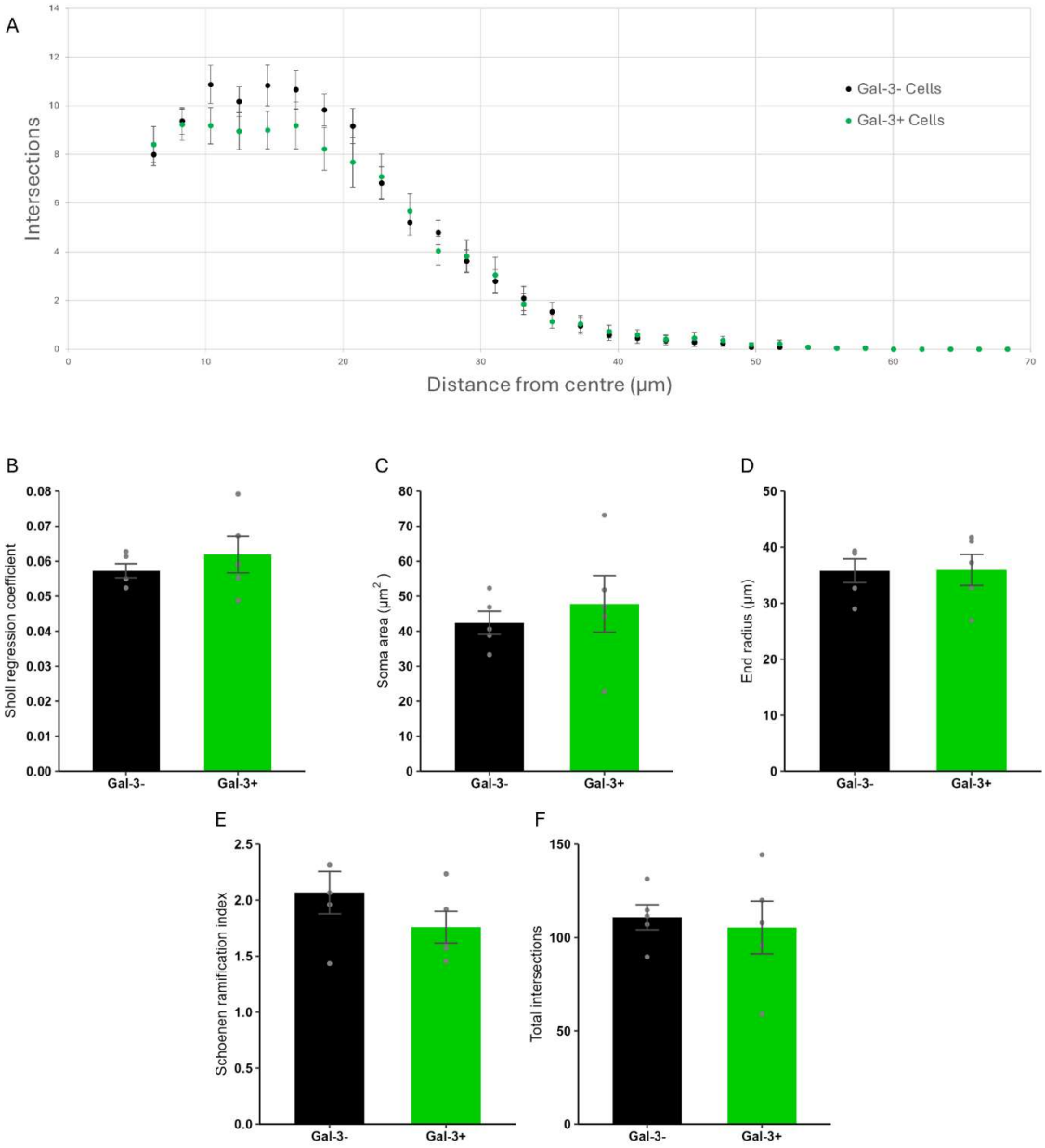


Figure 4.2.2: Sholl analysis of microglia in young adult C57Bl6 mice show no statistical differences between Gal-3- and Gal-3+ cells. (A) Sholl plot of Gal-3+ and Gal-3- microglia. No significant differences were observed at any of the radii sampled. (B – F) Statistical analysis of the Sholl decay, soma areas, end radii, Schoenen ramification indices and total intersections. 25 Gal-3+ cells and 21 Gal-3- cells were traced from 5 animals (3 males, 2 females). Mixed model analysis was used for the Sholl plots (Zucco, 2018) and Student's t-test was used for statistical analysis of Sholl decay, soma areas, end radii, Schoenen ramification indices and total intersections. Error bars show S.E.M.

In WT middle-aged male mice, Galectin-3 expressing microglia are morphologically similar to non-Galectin-3 expressing microglia.

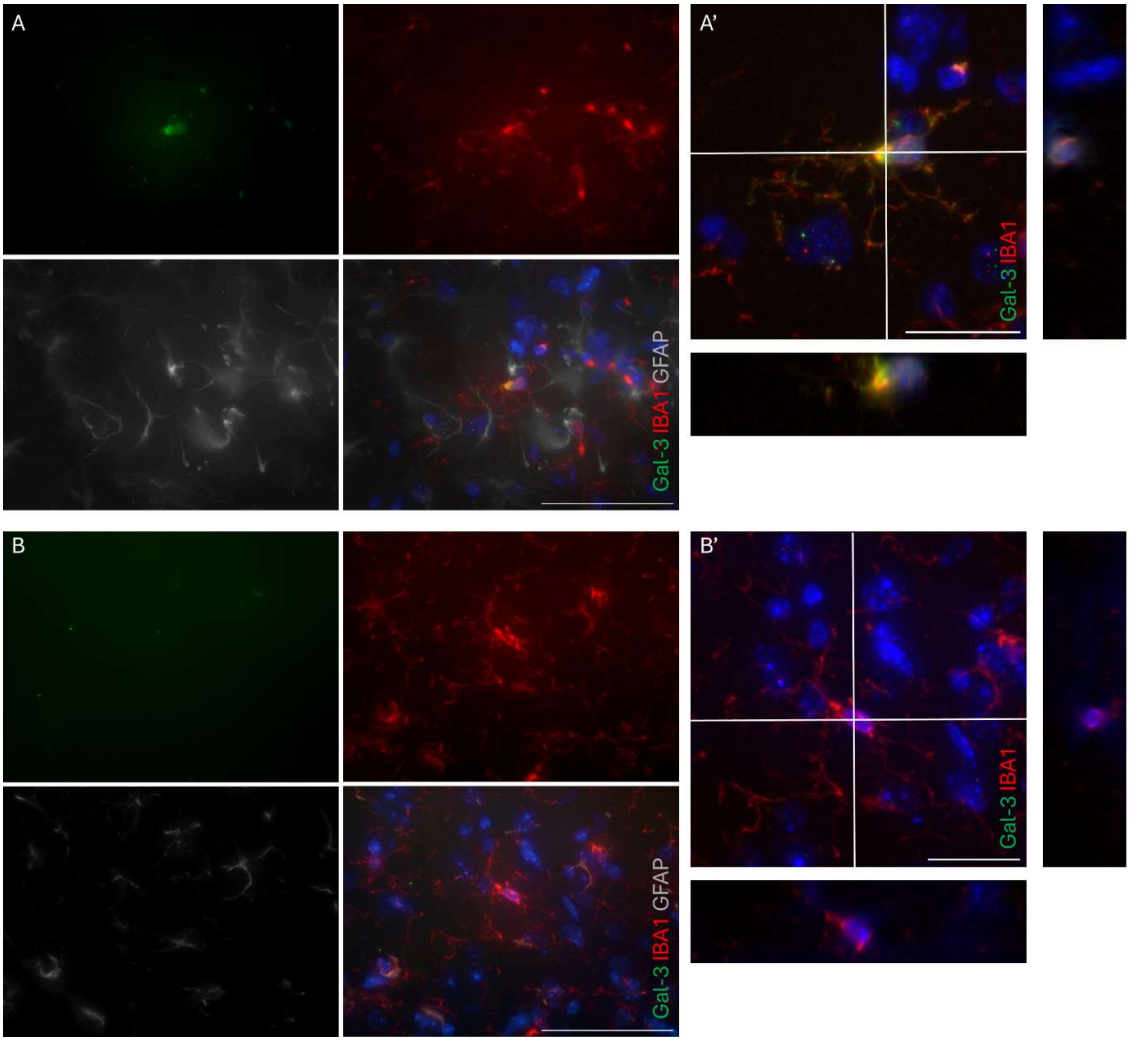


Figure 4.2.3: Morphology of Gal-3+ and Gal-3- microglia in middle-aged C57Bl6 mice. Gal-3+ (A) and Gal-3- (B) microglia can be observed in the hippocampus of middle-aged mice. (A') and (B') show orthogonal projections of a single microglia. Scale bars represent 50 µm (A and B) and 20 µm (A' and B').

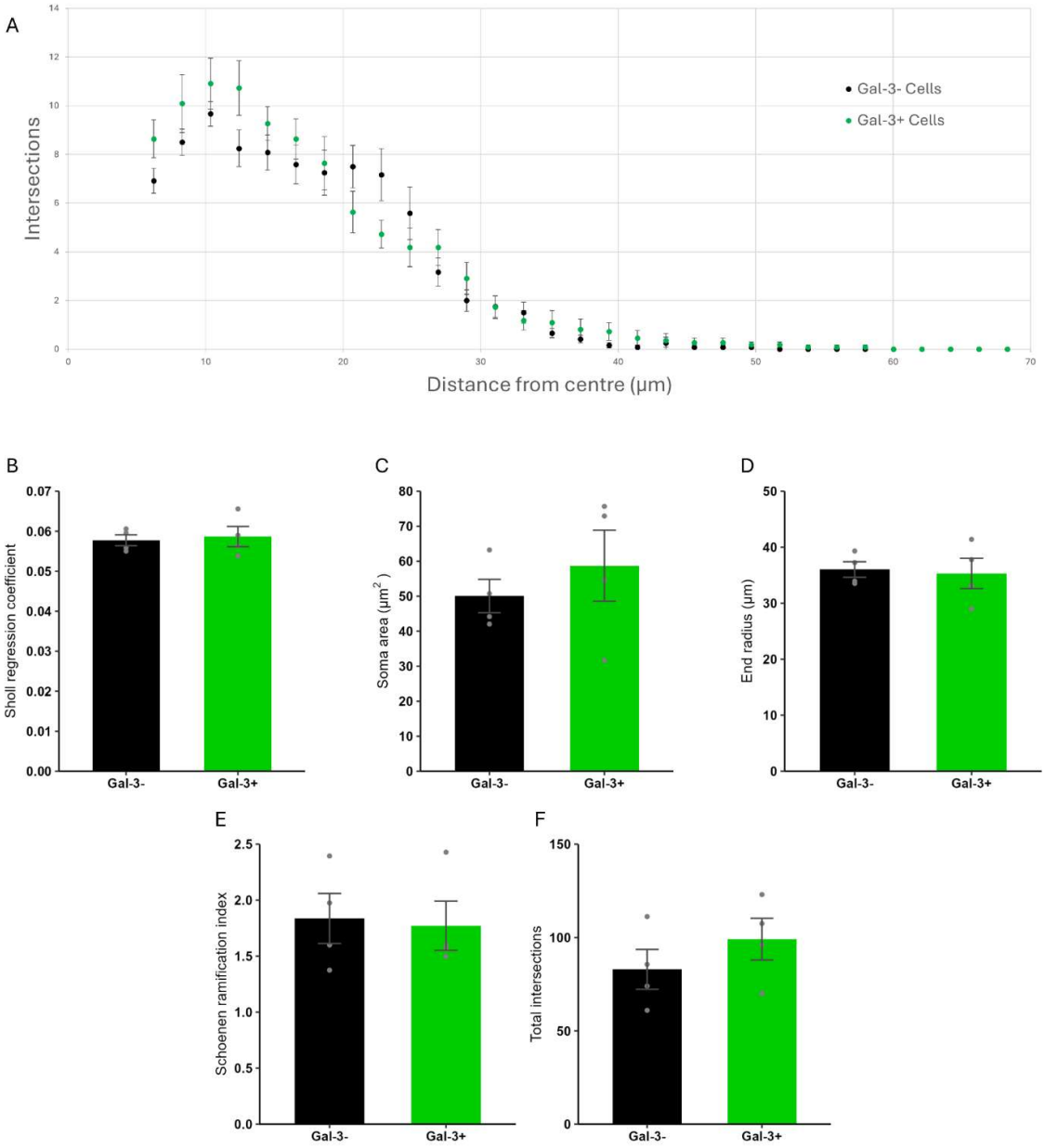


Figure 4.2.4: Sholl analysis of microglia in middle-aged C57Bl6 mice show no statistical differences between Gal-3- and Gal-3+ cells. (A) Sholl plot of Gal-3+ and Gal-3- microglia. No significant differences were observed at any of the radii sampled. (B – F) Statistical analysis of the Sholl decay, soma areas, end radii, Schoenen ramification indices and total intersections. 11 Gal-3+ cells and 12 Gal-3- cells were traced from 4 animals. Figure legend continued on the next page.

Figure 4.2.4: (continued from the previous page) Mixed model analysis was used for the Sholl plots (Zucco, 2018) and Student's t-test was used for statistical analysis of Sholl decay, soma areas, end radii, Schoenen ramification indices and total intersections. Error bars show S.E.M.

While overall comparison of the Sholl curves also suggested a difference ($p = 0.043$) between Gal-3+ and Gal-3- cells, with the number of intersections differing at 12 and 23 μm, FDR adjustments again made the difference in number of intersections not significant. As before, no significant differences were observed between the sholl decay, SRI, total intersections or the end radius of Gal-3+ and Gal-3- cells. Together, these suggest that in middle-aged WT male mice, microglia show similar morphology regardless of whether they express Galectin-3. Data from statistical analyses can be found in the appendix (Supplementary table 4.2.2).

4.3 In C57Bl6 mice, microglia from young mice do not significantly differ from microglia from middle-aged mice

With increasing age, levels of pro-inflammatory cytokines increase in the brain. Hence, I asked if there was a difference in microglial morphology between young C57Bl6 mice as compared to middle-aged mice. I hypothesised that with increased age, microglia would show a less ramified morphology.

A visual comparison of young and middle-aged C57Bl6 mice show that there is an increase in Galectin-3 immunoreactivity in the hippocampus of middle-aged compared to young C57Bl6 mice (Figures 3.2.2 and 3.2.3). This is mostly due to an increase in the number of Gal-3+ cells in the molecular layer of the CA1.

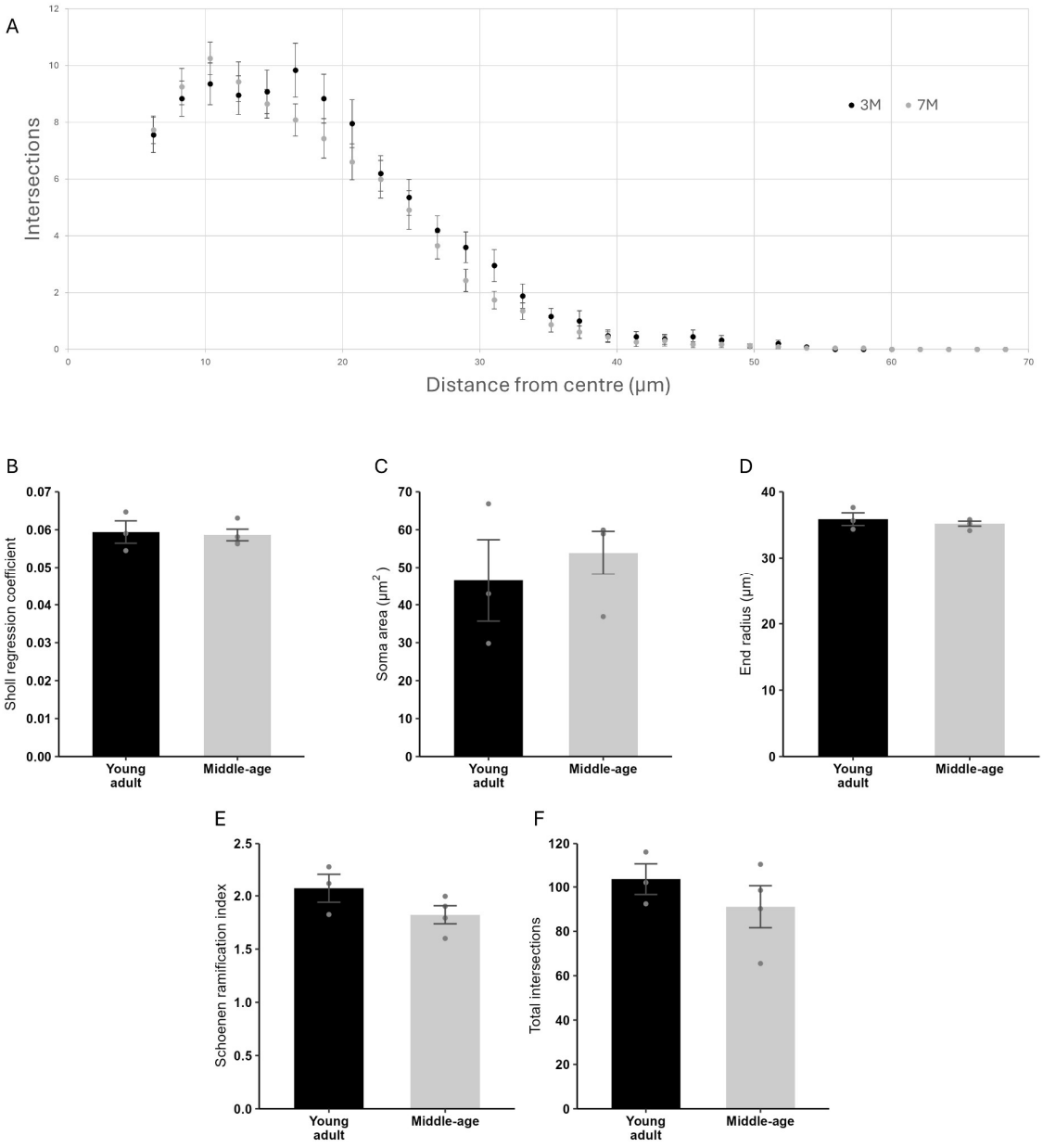


Figure 4.3: Sholl analysis of microglia in C57Bl6 mice show no statistical differences between microglia from young adult and microglia from middle-aged mice. (A) Sholl plot of microglia from young adult and middle-aged mice. No significant differences were observed at any of the radii sampled. (B – F) Statistical analysis of the Sholl decay, soma areas, end radii, Schoenen ramification indices and total intersections. Figure legend continued on the next page.

Figure 4.3: (continued from the previous page) 25 cells were traced from three 3M-old male mice and 23 cells were traced from four 7M-old male mice. Mixed model analysis was used for the Sholl plots (Zucco, 2018) and Student's t-test was used for statistical analysis of Sholl decay, soma areas, end radii, Schoenen ramification indices and total intersections. Error bars show S.E.M.

A Sholl plot of WT microglia from male mice at 3M and 7M reveals subtle differences, with 7M mice having an earlier peak of intersections as compared to 3M mice (Figure 4.2.4). This is accompanied with a sharper decline in the number of intersections between 20 – 30 μm from the soma. Mixed model analysis also shows an overall difference between the two populations ($p = 0.0041$), with a statistically significant difference between the number of intersections at 16 μm ($p = 0.0305$). However, after correction for multiple testing, this was no longer significant. Metrics from Sholl analysis do not show significant difference between microglia from young and middle-aged WT mice. Analysis of the area under the curve (AUC) of the Sholl profiles also did not show significant differences between microglia from young and middle-aged WT mice ($p = 0.3017$).

Data from statistical analyses can be found in the appendix (Supplementary table 4.3).

4.4 Microglia from Galectin-3$^{-/-}$ mice are more ramified than microglia from Galectin-3$^{+/+}$ mice

Next, I asked if knockout of Galectin-3 in WT mice would have a similar effect as in 5xFAD mice, with reduction in microglia inflammatory response. I hypothesised that Galectin-3$^{-/-}$ mice will have microglia with a more ramified morphology and higher branching complexity when compared to Galectin-3$^{+/+}$ mice. Middle-aged mice (Galectin-3$^{+/+}$: 7.6 $\pm$ 0.905 months, Galectin-3$^{-/-}$: 7.4 $\pm$ 0.330 months; n = 4 males each) were used for these analyses.

Galectin-3 knockout in young adult mice increased branching complexity.

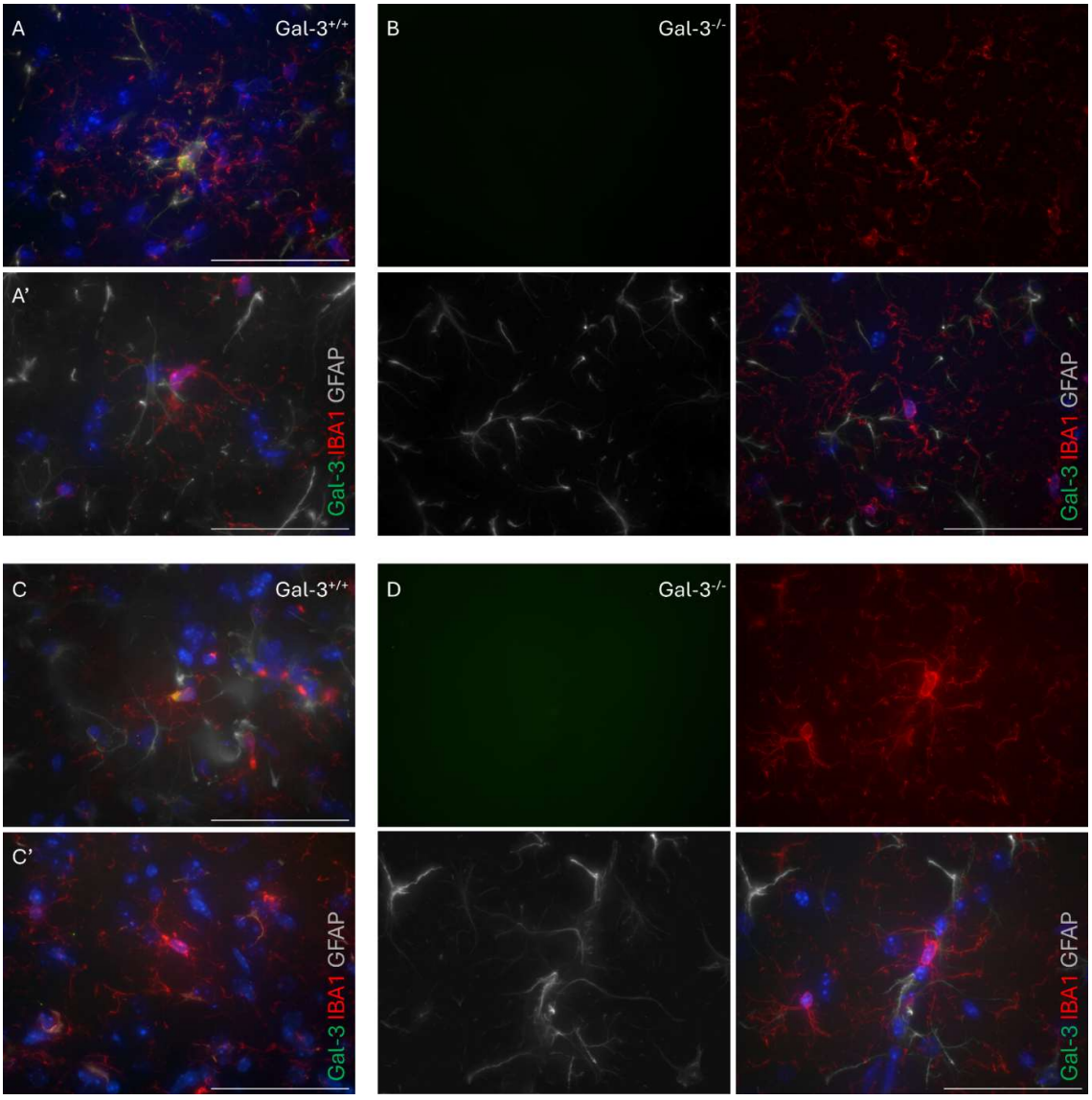


Figure 4.4.1: Representative immunofluorescent images of microglia in Galectin-$3^{+/+}$ and Galectin-$3^{-/-}$ mice. Gal-3+ (A) and Gal-3- (A') microglia in young adult Galectin-$3^{+/+}$ mice and microglia in Galectin-$3^{-/-}$ young adult mice (B). Gal-3+ (C) and Gal-3- (C') microglia in middle-aged Galectin-$3^{+/+}$ mice and microglia in Galectin-$3^{-/-}$ young adult mice (D). Scale bars represent 50 µm.

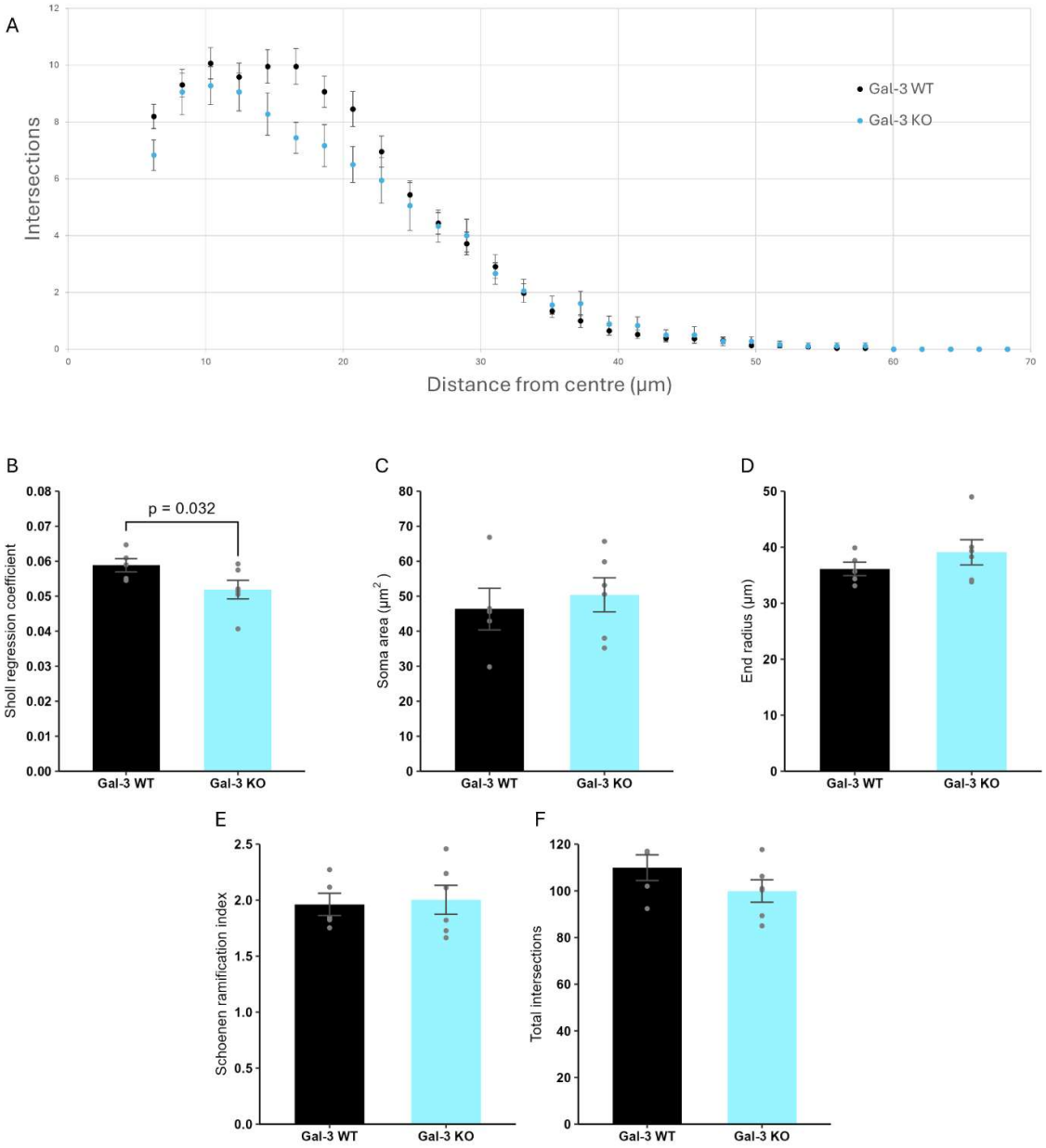


Figure 4.4.2: Sholl analysis of microglia in young adult mice show slight differences between microglia from the hippocampi of Galectin-$3^{+/+}$ and Galectin-$3^{-/-}$ young adult mice. (A) Sholl plot of microglia from Galectin-$3^{+/+}$ and Galectin-$3^{-/-}$ mice. No significant differences were observed at any of the radii sampled. (B – F) Statistical analysis of the Sholl decay, soma areas, end radii, Schoenen ramification indices and total intersections. Microglia from

Galectin-3$^{-/-}$ mice had smaller Sholl regression coefficients as compared to microglia from Galectin-3$^{+/+}$ mice. . Figure legend continued on the next page.

Figure 4.4.2: (continued from the previous page) 47 cells were traced from five Galectin-3$^{+/+}$ mice (3 males, 2 females) and 19 cells were traced from six Galectin-3$^{-/-}$ mice (3 males, 3 females). Mixed model analysis was used for the Sholl plots (Zucco, 2018) and Student's t-test was used for statistical analysis of Sholl decay, soma areas, end radii, Schoenen ramification indices and total intersections. Error bars show S.E.M.

Analysis of the merged Sholl curves of Galectin-3$^{-/-}$ and Galectin-3$^{+/+}$ mice reveal significant differences between microglia ($p = 0.0043$). While microglia from Galectin-3$^{-/-}$ mice show reduced number of intersections between 14 – 21 µm, this was not statistically significant after FDR corrections. Interestingly, this is reflected in the difference in Sholl regression coefficients, where microglia from Galectin-3$^{-/-}$ mice showed smaller Sholl decay compared to microglia of Galectin-3$^{+/+}$ mice ($p = 0.032$). While none of the other metrics were significantly different between Galectin-3$^{+/+}$ and Galectin-3$^{-/-}$, analysis of the microglia from male mice alone reveals even larger differences in Sholl decay. Together, these suggest that knockout of Galectin-3 in wildtype young adult mice may have a small effect on microglia morphology, with microglia from Galectin-3$^{-/-}$ mice having slightly more complex branching.

Data from statistical analyses can be found in the appendix (Supplementary table 4.4.1).

Galectin-3 knockout results in more ramified microglia morphology in middle-aged male mice.

The number of Galectin-3+ microglia increases in 7M mice as compared to 3M mice. Hence, I asked if there would be a greater effect of Galectin-3 knockout on microglia morphology in middle-aged mice. Mixed model analysis of the Sholl curves did not reveal a significant difference between microglia of Galectin-$3^{+/+}$ and Galectin$^{-/-}$ mice. While no significant difference were observed in the SRI and total number of intersections, microglia from Galectin-$3^{-/-}$ mice show decreased Sholl decay and increased end radii as compared to microglia from Galectin-$3^{+/+}$ mice ($p = 0.016$ and $p = 0.044$ respectively).

Data from statistical analyses can be found in the appendix (Supplementary table 4.4.2).

Figure 4.4.3 (Figure on next page): Sholl analysis of microglia in middle-aged mice show differences between morphology of microglia from Galectin-$3^{+/+}$ and Galectin-$3^{-/-}$ mice. (A) Sholl plot of microglia from Galectin-$3^{+/+}$ and Galectin-$3^{-/-}$ middle-aged mice. No significant differences were observed at any of the radii sampled. (B – F) Statistical analysis of the Sholl decay, soma areas, end radii, Schoenen ramification indices and total intersections. Microglia from Galectin-$3^{-/-}$ mice had smaller Sholl regression coefficients (B), decreased soma size (C), and increased terminal branch radii (D) as compared to microglia from Galectin-$3^{+/+}$ mice.

11 cells were traced from four Galectin-$3^{+/+}$ male mice and 12 cells were traced from four Galectin-$3^{-/-}$ male mice. Mixed model analysis was used for the Sholl plots (Zucco, 2018) and Student's t-test was used for statistical analysis of Sholl decay, soma areas, end radii, Schoenen ramification indices and total intersections. Error bars show S.E.M.

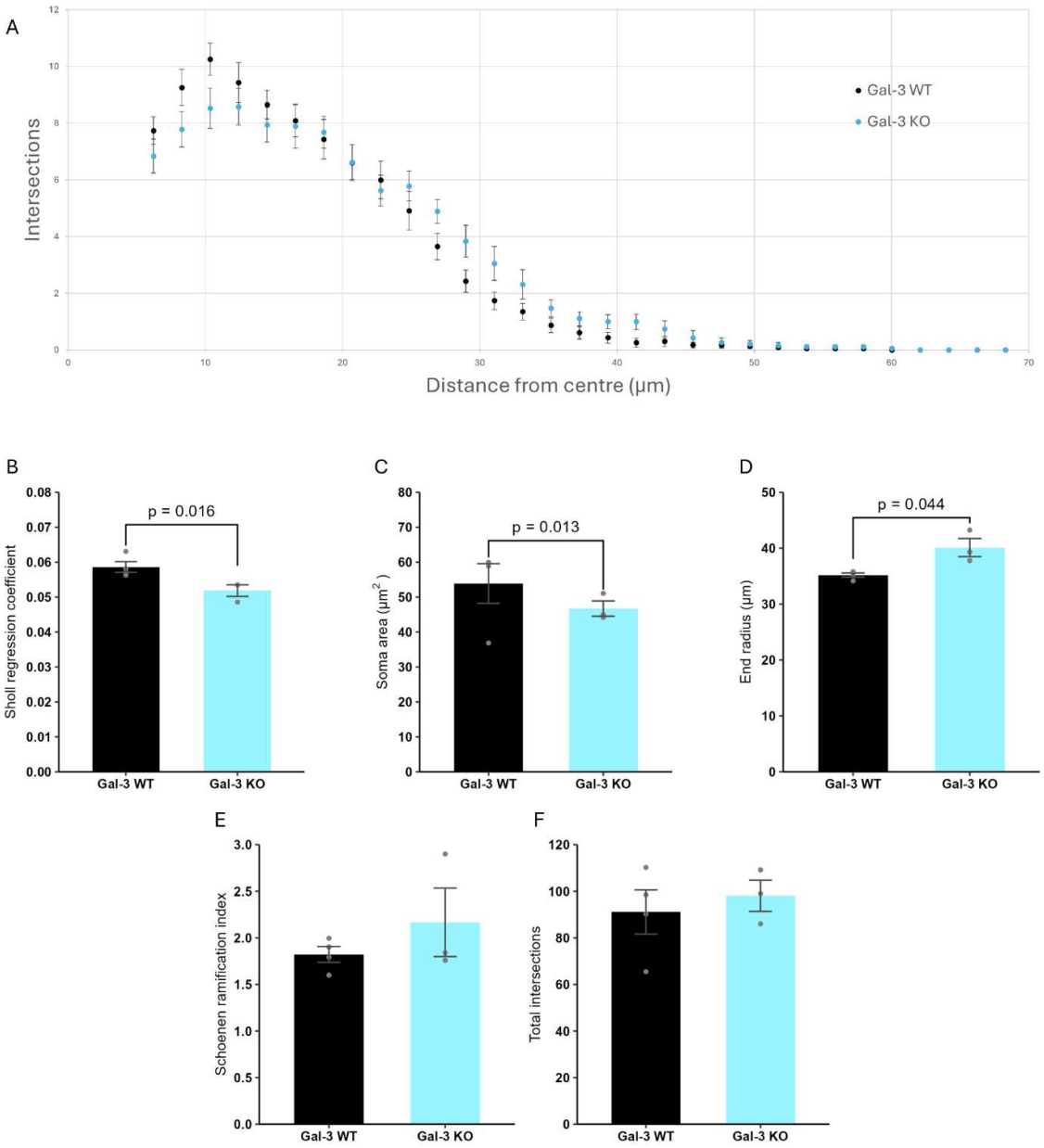


Figure 4.4.3: Sholl analysis of microglia in middle-aged mice show differences between morphology of microglia from Galectin-$3^{+/+}$ and Galectin-$3^{-/-}$ mice.

4.5 The effect of Galectin-3 knockout on DAM gene expression

4.5.1 Galectin-3 knockout did not alter DAM gene expression in primary murine microglia

Gene expression levels (relative to housekeeping genes beta-actin and Hprt) for various DAM genes, homeostatic microglia genes and pro-inflammatory cytokine genes were compared between Galectin-$3^{+/+}$ and Galectin-$3^{-/-}$ microglia. No significant differences were observed between genes upregulated in AD microglia (Tyrobp, Lpl and Cst7; Figure 4.5.1 A – C), genes downregulated in AD microglia (Hexb, P2ry12 and Cd33; Figure 4.5.1 D – F), or pro-inflammatory cytokine genes (Il6 and Tnfa; Figure 4.5.1 G and H). Other DAM genes were also compared and can be found in appendix (Supplementary figure 4.5).

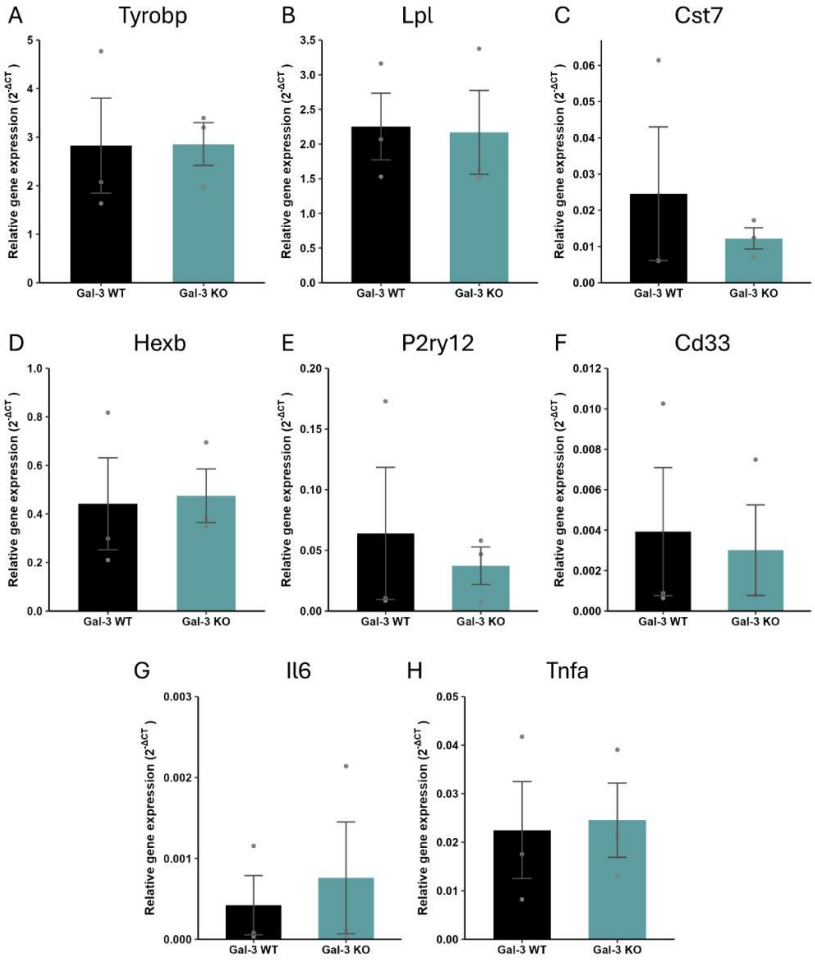


Figure 4.5.1 Gene expression levels of selected disease-associated and homeostatic genes in primary murine microglia. Relative gene expression levels of genes upregulated in DAM (A – C). No significant differences were observed between Galectin-3 WT and Galectin-3 KO microglia. Similarly, no significant differences were observed in the expression of homeostatic microglia genes (D – F). Levels of pro-inflammatory cytokine Il6 and Tnfa expression were also similar between Galectin-3 WT and Galectin-3 KO microglia.

n = 3, Student's t-test was used for statistical analyses. Error bars show S.E.M.

4.5.2 Treatment of BV2 microglia with Galectin-3 or TD-139 did not affect expression of DAM genes

Treatment of cells, purification of RNA and RT-qPCR was performed by Sofia Savastano as part of her Master's Thesis (department of Biochemistry) under my supervision.

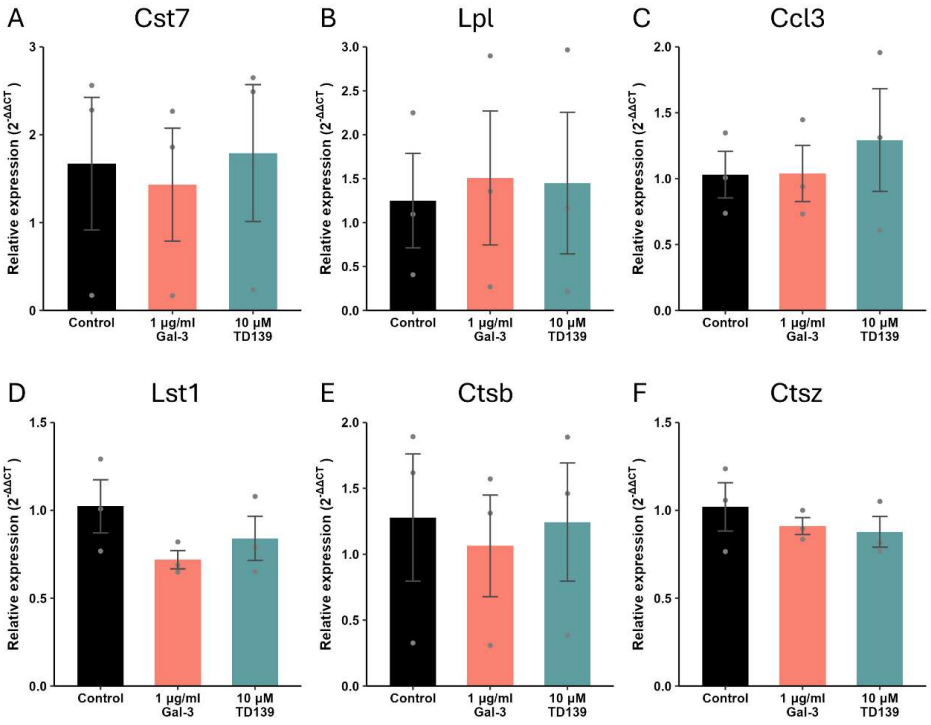


Figure 4.5.2: Treatment of BV2 microglia with Galectin-3 or its inhibitor TD-139 did not alter expression of disease associated microglial genes.

n = 3, one-way ANOVA was used for statistical analyses. Error bars show S.E.M.

To determine if exogenous Galectin-3 would affect levels of disease associated microglia (DAM) gene expression, the microglial cell line BV2 was used. BV2 microglia were treated with either Galectin-3 or Galectin-3 inhibitor TD-139 for 24 hours before the lysate was collected and RNA purified. qPCR was run for the DAM genes Cst7, Lpl, Apoe, Trem2, Ctsb and Ctsz (Figure 4.5.2). No significant differences were seen in expression of the genes. Other DAM genes were also compared and can be found in appendix (Supplementary figure 4.6).

4.6 The effect of Galectin-3 modulation on Disease Associated Astrocyte (DAA) gene expression

4.6.1 Exogenous Galectin-3 increased expression of a subset of DAA genes in primary murine astrocytes

While treatment with $A\beta O_{1-42}$ only significantly increased expression of Clu and *Gsn* ($p = 0.009$ and $p = 0.0004$ respectively), Galectin-3 treatment increased expression of Clu, Fxyd1, Gsn and Serpina3 ($p = 0.015$, $p = 0.038$, $p = 0.0002$, and $p = 0.019$ respectively).

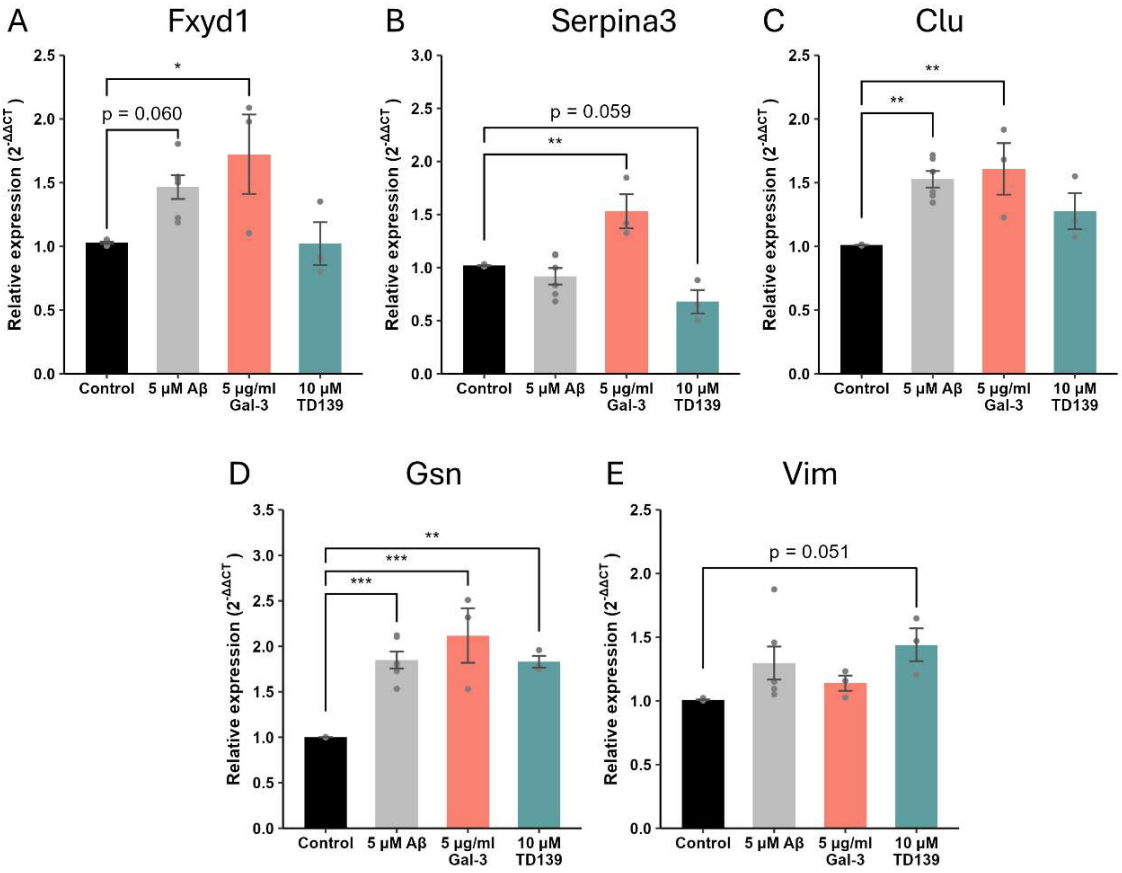


Figure 4.6.1: Treatment of primary murine astrocytes with Galectin-3 increased expression of a subset of Disease Associated Astrocyte genes.

n = 3. one-way ANOVA was used for statistical analyses. Error bars show S.E.M.

4.7 Discussion

4.7.1 Galectin-3 expression did not alter microglial morphology in young or middle-aged C57Bl6 mice

To my knowledge, this is the first quantitative analysis of the effect Galectin-3 has on microglia morphology in the mouse brain. Previously, work by Reichert and Rotshenker showed that Galectin-3 knockdown in primary murine microglia increased ramification of microglia while decreasing phagocytosis. In their work, Galectin-3$^{-/-}$ microglia, or microglia with Galectin-3 knockdown had almost five-fold smaller soma size, and a more ramified morphology (Reichert & Rotshenker, 2019). However, they had also previously reported not detecting Galectin-3 expression by microglia under homeostatic conditions (Reichert & Rotshenker, 1999).

In my hands, I saw expression of Galectin-3 by microglia under homeostatic conditions in the hippocampus. Interestingly, on a WT background, Galectin-3 expressing microglia in young adult or middle-aged mice are morphologically indistinguishable from non-Galectin-3 expressing microglia (Figures 4.2.2 and 4.2.4). Sholl analysis revealed that Gal-3+ and Gal-3- microglia have similar Sholl profiles. The Sholl regression coefficients were also not significantly different, showing that the density of processes as a function of distance from centre of the cell body (or the decay rate of the processes) did not change with Galectin-3 expression. Soma areas were also similar between Gal-3+ and Gal-3- microglia. The Schoen ramification index is the ratio between the maximum number of intersections and the number of primary branches, hence giving a measure of the maximum branching complexity arising from the primary branches. With decreased ramification suggestive of more reactive microglia, a lower SRI will hence be suggestive of microglia of a more reactive state. Since Gal-3+ and Gal-3- microglia had similar SRI, it suggests similar branching complexities. The end radii measures the length of the furthest process, while the total intersection measures the sum of all processes that intersect at the defined radii. The lack of change between these metrics

suggests that Gal-3+ and Gal-3- microglia have similar process lengths and amounts of branching.

In AD models such as the 5xFAD or APP/PS1, Gal-3+ microglia in mostly cluster around Aβ plaques, and appear with more amoeboid morphologies (Boza-Serrano et al., 2019; Tao et al., 2020). This contrasts with Gal-3+ microglia observed in my C57Bl6 mice. While I did not observe morphological changes between Gal-3+ and Gal-3- microglia, morphology does not inform of the exact functional state of microglia. Hence, it is possible that Gal-3+ microglia under homeostatic conditions may represent a different microglial state as compared to Gal-3+ under disease conditions. For instance, Gal-3+ microglia in the Tau22 model expressed CD68 at higher levels than Gal-3- microglia (Siew et al., 2024). Comparison of the proportion of CD68+ cells which are either Gal-3+ or Gal-3- may reveal if Galectin-3 expression has differing roles in pathology compared to under homeostatic conditions. Similarly, comparison of markers of more activated microglia such as Il-1β could reveal if Gal-3+ microglia are poised towards activation in WT mice.

4.7.2 Galectin-3 knockout increases microglial ramification in middle-aged male mice, and to a smaller extent in young adult male mice.

Classically, de-ramified microglia have been associated with a more reactive and phagocytic state. In both young adults and middle-aged mice, microglia from Galectin-$3^{-/-}$ mice show increased branching complexity as compared to microglia from Galectin-$3^{+/+}$ mice. Galectin-3 is classically considered to be pro-inflammatory and is upregulated in various neurodegenerative diseases where neuroinflammation is present. As there is an increase in the amount of Galectin-3-immunoreactivity between middle-age and young adult mice (Figures 3.1.2 and 3.1.3), this suggests that there could be more Galectin-3 present in middle-aged brains as compared to young adult brains, which could contribute towards a more pro-inflammatory environment. This is reflected in the comparison of morphology between middle-aged Galectin-$3^{+/+}$ and Galectin-$3^{-/-}$ mice, where the effect of Galectin-3 knockout on morphology is stronger.

In the 7-month old cohort, Galectin-3 knockout resulted in microglia with smaller Sholl regression coefficient, suggesting increased complexity of branching at larger distances from the cell body. Taken together with increased end radius, these suggest longer branches with more complex branching in the Galectin-3 knockouts. Lastly, microglia from Galectin-$3^{-/-}$ mice also have decreased soma area as compared to microglia from Galectin-$3^{+/+}$ mice. While the effect of Galectin-3 knockout on Sholl decay was underpowered ($1 - \beta = 0.56$), both the soma area and the end radii analyses had $1 - \beta > 0.8$, suggesting strong effect of Galectin-3 knockout on these metrics.

Taken together, my results suggest that the presence of Galectin-3 alters microglia morphology in a non-cell autonomous manner. Knockout of Galectin-3 resulted in microglia with more ramified, and less reactive morphology, hence supporting the model that Galectin-3 may promote increased microglial reactivity. However, morphology does not fully inform of the state of microglia *in vivo*. Further analysis such as quantification of the proportion of microglia expressing CD68 in Galectin-$3^{-/-}$ and Galectin-$3^{+/+}$ mice will provide better understanding of the effect that Galectin-3 has on microglial activation under homeostatic conditions.

4.7.3 Galectin-3 did not significantly alter disease associated microglial gene expression *in vitro*

If Galectin-3 were a primary upstream regulator of DAM gene expression, its manipulation would be expected to induce transcriptional changes. However, modulation of Galectin-3, either through genetic deletion or exogenous treatment, did not significantly alter the expression of DAM genes in primary murine microglia or BV2 cells. This suggests that Galectin-3 alone is not sufficient to drive DAM-like transcriptional signatures in microglia under normal culture conditions. This is consistent with previous findings in primary murine microglia from Galectin-$3^{+/+}$ and Galectin-$3^{-/-}$ mice which showed that microglia only exhibited significant changes in pro-inflammatory cytokine secretion when challenged with Aβ fibrils or with LPS (Boza-Serrano et al., 2019).

4.7.4 Galectin-3 altered expression of Disease Associated Astrocyte (DAA) genes *in vitro*

Serpina3 is a serine protease inhibitor. Interestingly, a polymorphic form of Serpina3 found in the SAMP8 mouse model which has characteristics of AD maintains Aβ in the more toxic oligomeric form (Akbor et al., 2021), with the normal variant also exhibiting similar, albeit weaker, effects.

In contrast to the lack of effect which Galectin-3 had in microglia, treatment of primary murine astrocytes with either Galectin-3 or TD-139 altered expression of DAA genes. Treatment of astrocytes with $A\beta O_{1\text{-}42}$ increased expression of several DAA genes including *Clusterin* and *Gelsolin*. However, while $A\beta O_{1\text{-}42}$ alone did not significantly increase expression of *Serpina3* or *Fxyd1*, Galectin-3 alone was sufficient to increase its expression. This suggests that a subset of the DAA genes could potentially be induced by Galectin-3 *in vitro* without exogenous Aβ.

Overall, these findings suggest that Galectin-3 can directly modulate expression of disease associated astrocytic genes seen in AD models such as 5xFAD. Given Galectin-3's role in inflammation, these results support a model in which Galectin-3 contributes to astrocytic activation.

However, this analysis does not conclude that Galectin-3 functionally activates astrocytes, nor that Galectin-3 can establish the induction of a full DAA phenotype. Changes in gene expression do not always correspond to protein level changes. Next, as compared to astrocytes *in vivo*, cultured astrocytes do not receive key environmental inputs including neuronal and microglial interactions. Hence, the observed DAA gene expression changes reflect partial, context-dependent activation of astrocytic pathways. Future work should first identify if Galectin-3 modulation can alter levels of DAA in the brain, and if Galectin-3 can alter astrocyte functions using electrophysiological measurements.

4.7.5 Limitations and future work

4.7.5.1 Use of BV2 microglia

The main advantage of using the BV2 cell line over primary microglia is the increased homogeneity of cultures. Primary murine microglia are derived from primary mixed glial cultures, which were in turn obtained from neonatal brain tissue. As such, they may have been exposed to varying levels of stimuli such as neuronal debris from the isolation process. While characterisation of the cultures was performed to show that microglial cultures comprised of IBA1 expressing cells, there may also be batch variations across cultures and contamination with other cell types. Lastly, microglia are also heterogeneous across brain regions, with region-specific transcriptional signatures (Tan et al., 2020). In contrast, BV2 cells are derived from murine microglia immortalised with retrovirus carrying *raf*/*v-myc* (Blasi et al., 1990). They are not exposed to debris from the cell extraction process and are a homogeneous population. However, microglia immortalised by inducible expression of oncogenes expressed lower levels of homeostatic genes (Yeh et al., 2025). BV2 cells are immortalised, and express higher levels of cell cycle and DNA damage related genes (He et al., 2018). Hence, they may represent less mature microglia compared to primary microglia. Furthermore, primary microglia exhibited a stronger response to pro-inflammatory stimuli and weaker chemotactic response to C5a as compared to BV2 microglia (He et al., 2018). Together, these suggest a baseline level of activation in BV2 microglia as compared to primary microglia. Hence, the effects of Galectin-3 modulation may have been masked by the high baseline level of activation in BV2 microglia. The lack of change in DAM gene expression in BV2 cells may not have been due to a lack of effect of Galectin-3 on the DAM transcriptional programme.

Nonetheless, the reduced variability of BV2 cells compared to primary microglia provides clearer detection of treatment effects, which can then be confirmed in other model systems. Additionally, BV2 cells are highly proliferative as compared to primary microglia, providing scalability while reducing animal use in research. Future work looking at the effects of

Galectin-3 in BV2 cells should be cross-validated in other model systems to ensure the robustness of the observed phenotype.

4.7.5.2 Limitations of *in vitro* gene expression analyses

Primary murine microglial cultures exhibit increased baseline levels of reactivity compared to microglia *in vivo* (Cadiz et al., 2022), with increased expression of DAM genes in cultured microglia compared to freshly isolated microglia (Cadiz et al., 2022). This pre-activated state may be less sensitive to Galectin-3 modulation, limiting the ability to detect changes in DAM gene expression. Consequently, while the results suggest that Galectin-3 is not sufficient to initiate DAM transcriptional signatures *in vitro*, it does not exclude a role for Galectin-3 in regulating microglial states *in vivo*. Future work should explore the use of TGFβ and decreasing the amount of sera present to decrease baseline reactivity of cultured microglia.

Primary astrocytic cultures have similar constraints as microglial cultures, including pre-activation and possible contamination with other cell types. The presence of other cell types may also confound interpretation of the results as Galectin-3 may have increased expression of DAA genes indirectly. To exclude this possibility, immunopanning or cell sorting should be employed in future studies. This can be performed at the first passage before the astrocytes are plated for treatments to obtain a purified astrocytic culture. Decreased serum levels, including serum-free culture conditions should also be explored for future work (Prah et al., 2019). Alternatively, stem-cell derived astrocytes can be generated from human iPSCs or ESCs and cultured under defined conditions to further improve relevance.

Chapter 5: Galectin-3 increases microglial phagocytosis of pHrodo-$A\beta_{1-42}$ via astrocyte secreted factors

5.1 Introduction

Galectin-3 has been shown to induce Aβ deposition in WT mice, and knockout of Galectin-3 has decreased Aβ plaque load in 5xFAD and APP/PS1 mouse models (Boza-Serrano et al., 2019; Tao et al., 2020). The authors have shown that Galectin-3 directly binds to Aβ and promoted the formation of Aβ fibrils (Tao et al., 2020). However, less is known about the effect that Galectin-3 has on clearance of Aβ. Microglia are responsible for Aβ clearance *in vivo*, and microglia in various models of AD have increased Galectin-3 expression (Keren-Shaul et al., 2017; Krasemann et al., 2017), and more specifically microglia from 5xFAD mice which have phagocytosed Aβ plaques also upregulate Galectin-3 (Grubman et al., 2021).

While intracellular Galectin-3 has been shown to promote phagocytosis in macrophages (Sano et al., 2003), extracellular Galectin-3 has not been shown to have a similar effect. While preliminary data from the Mead lab suggested that treatment of hiPSC-derived macrophages with Galectin-3 could decrease their phagocytic capacity for apoptotic neurons (Mead lab, personal communication), it has not been well characterised whether Galectin-3 would increase or decrease phagocytosis of Aβ. Hence, I asked if treatment of microglia with Galectin-3 or its inhibitor would alter phagocytosis of $A\beta O_{1\text{-}42}$.

5.2 Oligomerisation of Beta-Amyloid and Characterisation by western blot and transmission electron microscopy (TEM)

Oligomers of $A\beta_{1-42}$ ($A\beta O_{1-42}$) were prepared as described in Chapter 2. They were then used for treatment of cultures, or labelled with pHrodo-SE (pHrodo-$A\beta O_{1-42}$) for use in phagocytosis assays. To characterise the species of Aβ in my preparations, I sent an aliquot of the preparations for TEM. Samples sent were prepared in the same manner as those used in cultures (i.e. same number of freeze-thaw cycles).

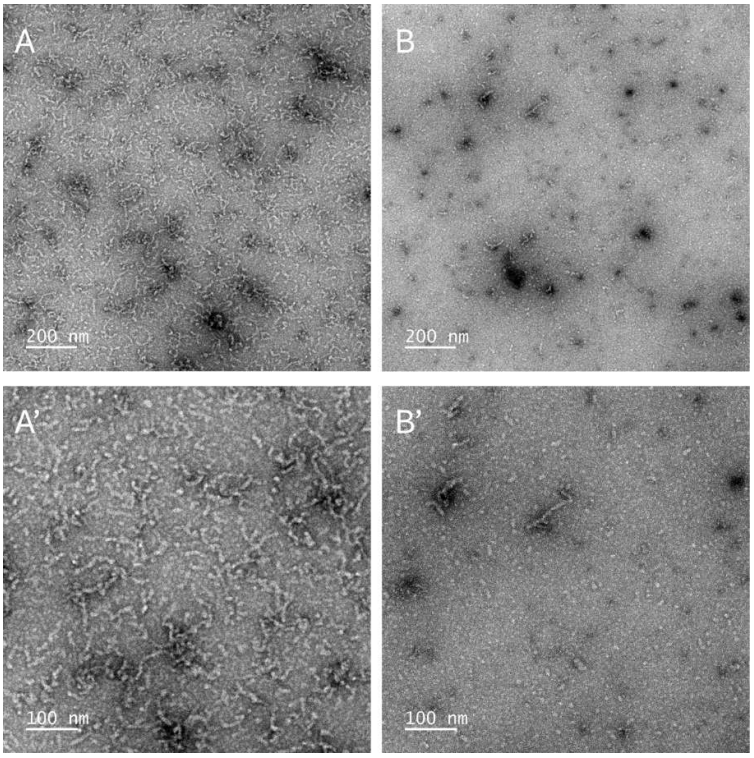


Figure 5.2 Transmission electron microscopy of $A\beta O_{1-42}$ (A) and pHrodo-$A\beta O_{1-42}$ (B). Oligomers and short fibrils can be seen in both unlabelled (A) and pHrodo-labelled (B) oligomers.

5.3 Addition of Galectin-3 or its inhibitor to microglial cultures did not alter phagocytosis of pHrodo-AβO$_{1-42}$

pHrodo-conjugated Aβ only fluoresces under low pH conditions and hence the presence of pHrodo signal suggests phagocytic uptake into lysosomes. The phagocytic index, defined as the pHrodo fluorescence area divided by cell area was plotted over 24 hours.

To determine if Galectin-3 treatment altered phagocytosis of AβO$_{1-42}$, I treated murine microglia with either:

1) 5 μM pHrodo-AβO$_{1-42}$ alone (5 μM Aβ)
2) pHrodo-AβO$_{1-42}$ + 5 μg/ml Galectin-3 (5 μM Aβ + 5 μg/ml Galectin-3), or
3) pHrodo-AβO$_{1-42}$ + 10 μM TD-139 (5 μM Aβ + 10 μM TD-139).

5.3.1 Galectin-3 did not alter phagocytosis of pHrodo-AβO$_{1-42}$ by BV2 microglia

Assays were performed by Sofia Savastano as part of her final year Biochemistry dissertation, under my supervision.

In the murine microglial cell line BV2, treatment with both Galectin-3 or its inhibitor TD-139 did not alter phagocytosis of pHrodo-AβO$_{1-42}$. This was seen both at the 24 hour endpoint ($p = 0.67$) and over 24 hours (AUC, $p = 0.72$).

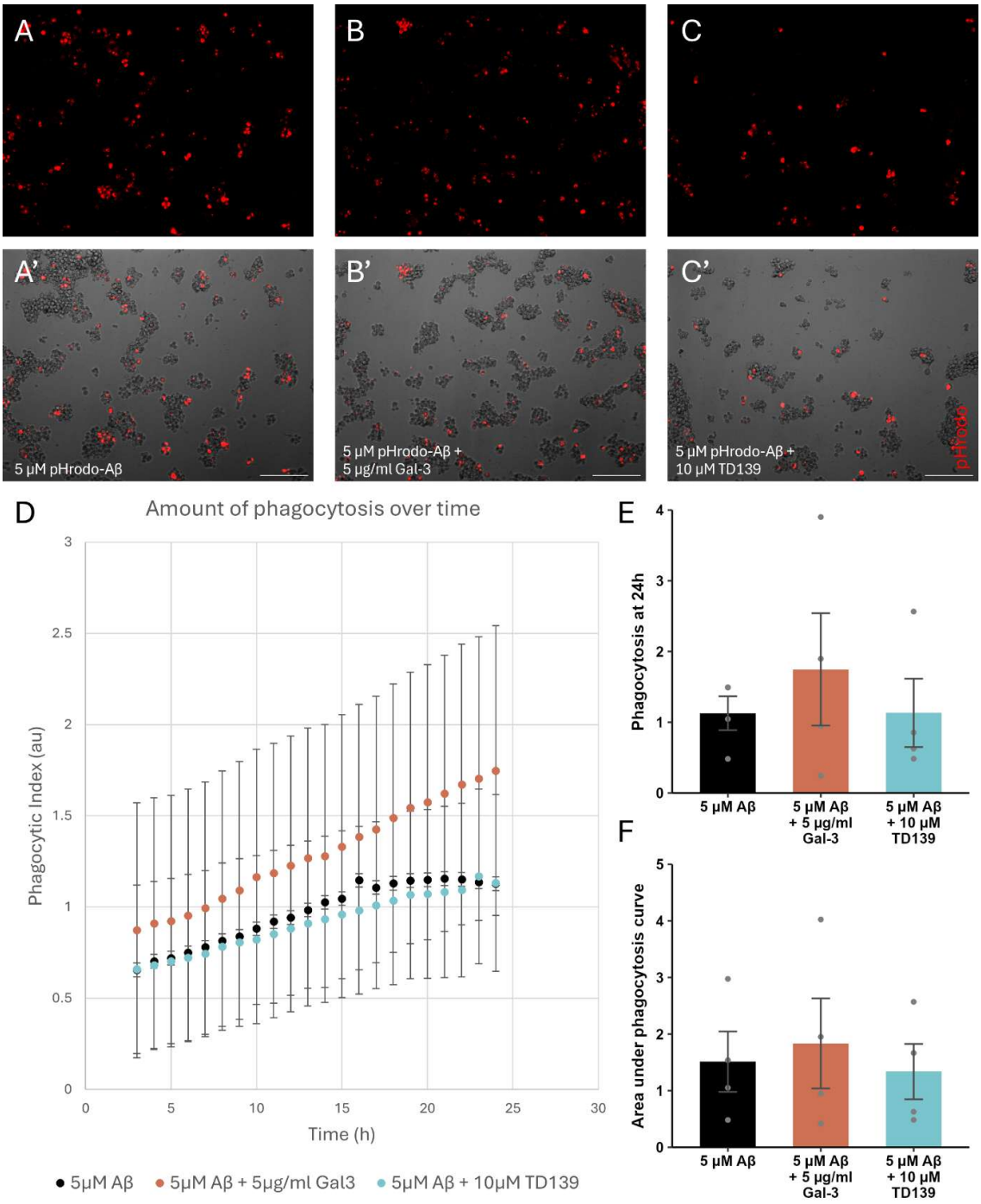


Figure 5.3.1 Addition of Galectin-3 or Galectin-3 inhibitor TD-139 did not alter phagocytosis of pHrodo-AβO_{1-42} in BV2 microglial cultures. Figure legend continued on next page.

Figure 5.3.1 Legend continued from previous page. (A – C) pHrodo fluorescence in BV2 microglia at 24 hours post treatment with 5 μM pHrodo-AβO_{1-42} (A), 5 μM pHrodo-AβO_{1-42} and 5 μg/ml Galectin-3 (B), and 5 μM pHrodo-AβO_{1-42} and 10 μM TD-139 (C). (A' – C') pHrodo is observed within the BV2 cells (brightfield). (D) Change in Phagocytic Index (pHrodo area/GFP area) over time. No significant difference was seen between the conditions. (E) Phagocytic index at 24 hours post treatment. One-way ANOVA showed no significant difference was observed between the conditions. (F) Area under curve analysis over 24 hours. No significant difference was seen between the conditions with one-way ANOVA. n = 4 replicates, scale bars represent 200 μm, and error bars show SEM.

5.3.2 Galectin-3 did not alter phagocytosis of pHrodo-AβO_{1-42} by primary murine microglia from Cx3cr1-GFP$^{+/-}$ mice

To determine if primary microglia responded differently than the microglial cell line, I then extracted glia from Cx3cr1-GFP$^{+/-}$ mice. At passage 1, the cultures were shaken on an orbital shaker, tapped, and then rinsed to isolate microglia, which were seeded at 50 k cells/cm^2. Cultures were rinsed with PBS the following day and treated with the same conditions as before. The phagocytic index at the end was compared to determine if there were differences in the amount of pHrodo in microglia at the endpoint, and the area under the curve was compared to determine changes to the amount of phagocytosis which occurred over 24 hours. No significant differences were observed in the amount of phagocytosis across the conditions at the endpoint or over 24 hours (one-way ANOVA, $p = 0.39$ and $p = 0.12$ respectively).

In conclusion, Galectin-3 or its inhibition did not significantly alter phagocytosis of Aβ oligomers in microglial cultures.

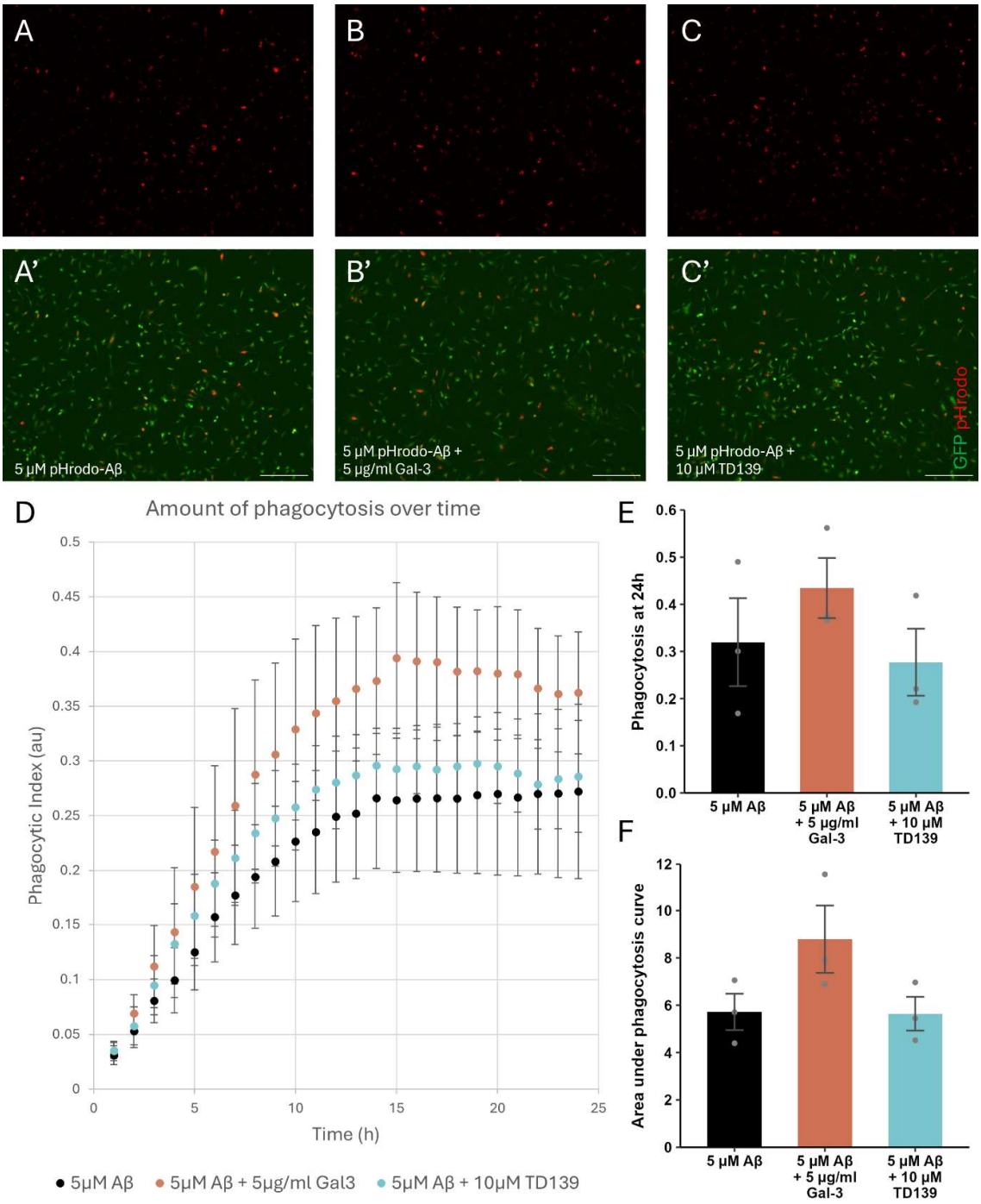


Figure 5.3.2 Addition of Galectin-3 or Galectin-3 inhibitor TD-139 did not alter phagocytosis of pHrodo-AβO_{1-42} in primary microglial cultures. Figure legend continued on next page.

Figure 5.3.2 Legend continued from previous page. (A – C) pHrodo fluorescence in CX3CR1-GFP$^{+/-}$ microglia at 24 hours post treatment with 5 μM pHrodo-AβO_{1-42} (A), 5 μM pHrodo-AβO_{1-42} and 5 μg/ml Galectin-3 (B), and 5 μM pHrodo-AβO_{1-42} and 10 μM TD-139 (C). (A' – C') pHrodo is observed within GFP^{+} cells. (D) Change in Phagocytic Index (pHrodo area/GFP area) over time. No significant difference was seen between the conditions. (E) Phagocytic index at 24 hours post treatment. One-way ANOVA showed no significant difference was observed between the conditions. (F) Area under curve analysis over 24 hours. No significant difference was seen between the conditions with one-way ANOVA. n = 3 replicates, scale bars represent 200 μm, and error bars show SEM.

5.4 Galectin-3 mediates microglial phagocytosis of pHrodo-AβO_{1-42} in mixed glial cultures

As astrocytes have been shown to contribute towards phagocytosis of Aβ *in vivo*, I asked if Galectin-3 or its inhibition would affect phagocytosis of AβO_{1-42} in cultures of microglia and astrocytes derived from Cx3cr1-GFP$^{+/-}$ mice. Using the same treatment parameters before, mixed glial cultures were treated either with 5 μM pHrodo-AβO_{1-42} alone (Figure 5.4A), or together with 5 μg/ml Galectin-3 (Figure 5.4B) or 5 μM pHrodo-AβO_{1-42} and 10 μM TD-139 (Figure 5.4C). The phagocytic index was plotted over 24 hours and a one-way ANOVA was performed on the phagocytic index at 24 hours and the amount of phagocytosis over 24 hours (AUC). A significant difference was observed between the groups at 24 hours (Figure 5.4E, $p = 0.0002$), with Tukey post-hoc test showing a significant decrease in phagocytosis between TD-139 treated cultures and Galectin-3 treated cultures ($p = 0.00002$), and between control and TD-139 treated cultures ($p = 0.0002$). Similarly, comparison of the amount of phagocytosis over 24 hours show a significant difference between groups (Figure 5.4F, $p = 0.03$), with significantly decreased phagocytosis in TD-139 treated cultures as compared to Galectin-3 treated cultures.

Furthermore, pHrodo was seen exclusively co-localising with GFP, suggesting that while astrocytes contributed towards the Galectin-3 mediated increase in phagocytosis, they did not themselves phagocytose detectable amounts of pHrodo-AβO_{1-42}. This suggests that Galectin-3 could have stimulated a contact-based astrocyte-microglia interaction or production of secreted factors from astrocytes.

Figure 5.4 Figure on following page. (A – C) pHrodo fluorescence in CX3CR1-GFP$^{+/-}$ mixed glia at 24 hours post treatment with 5 µM pHrodo-AβO_{1-42} (A), 5 µM pHrodo-AβO_{1-42} and 5 µg/ml Galectin-3 (B), and 5 µM pHrodo-AβO_{1-42} and 10 µM TD-139 (C). (A' – C') pHrodo is observed within GFP^{+} cells, suggesting phagocytosis occurred in microglia and not astrocytes. (D) Change in Phagocytic Index (pHrodo area/GFP area) over time. Galectin-3 treated cultures showed a higher amount of phagocytosis compared to control cultures, and TD-139 treated cultures showed lower amount of phagocytosis. (E) Phagocytic index at 24 hours post treatment. One-way ANOVA showed significant difference between the conditions, with Tukey post-hoc test showing that TD-139 treated cultures had decreased phagocytic index. (F) Area under curve analysis over 24 hours. Significant difference was seen between the conditions with one-way ANOVA, with Galectin-3 treated cultures showing increased phagocytosis over 24 hours as compared to TD-139 treated cultures. n = 3 replicates, scale bars represent 200 µm, and error bars show SEM.

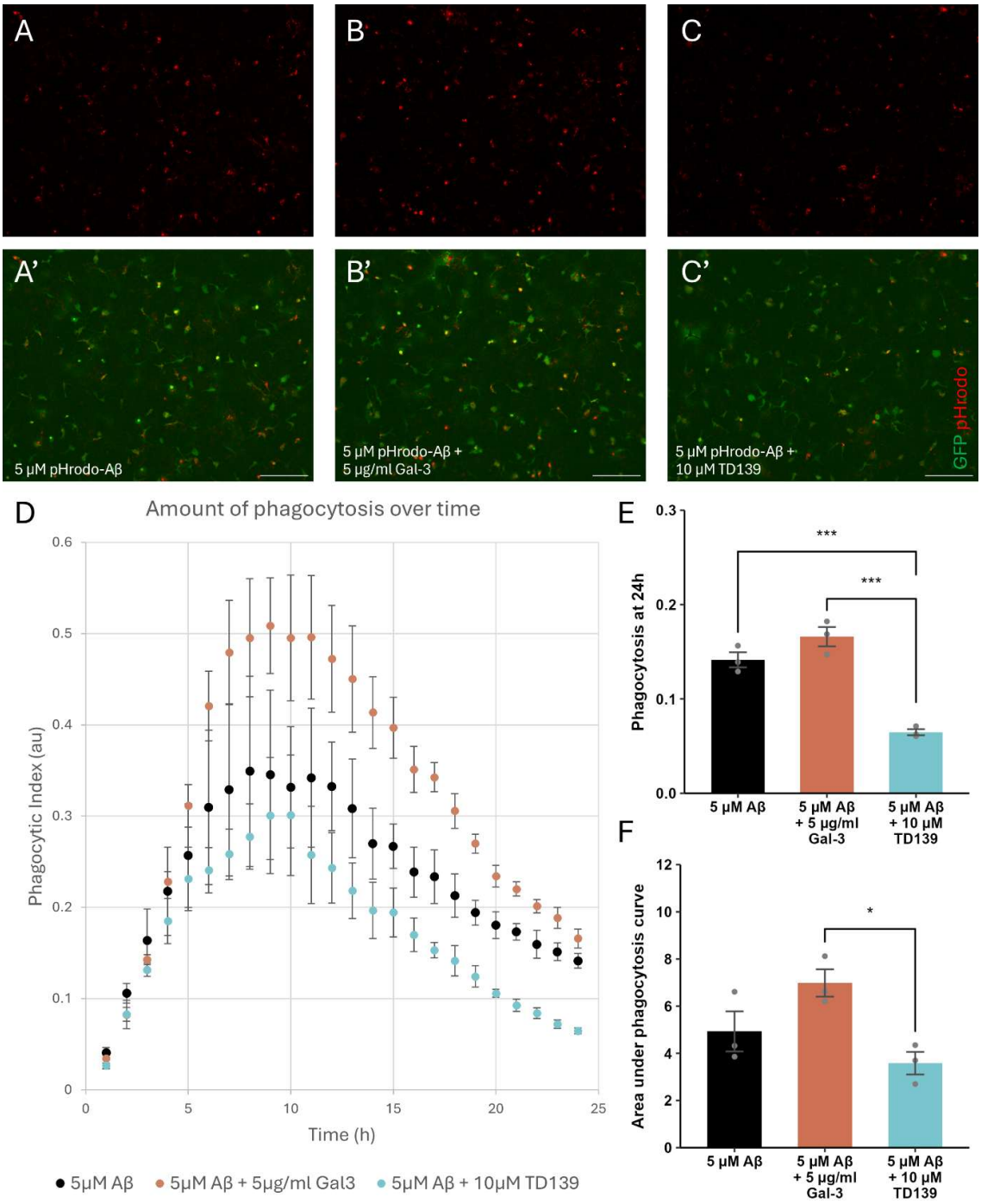


Figure 5.4 Addition of Galectin-3 increased, while addition of Galectin-3 inhibitor TD-139 decreased microglial phagocytosis of pHrodo-AβO_{1-42} in mixed glial cultures. Figure legend on previous page.

5.5 Galectin-3 increases microglial phagocytosis of pHrodo-$A\beta O_{1-42}$ through astrocyte secreted factors

The results from 5.3 and 5.4 when taken together suggest that microglia alone do not respond to the presence of exogenous Galectin-3 in the medium, but when in co-culture with astrocytes, exogenous Galectin-3 could have either increased secreted factors from astrocytes which aided microglial phagocytosis, or did so through a contact-based interaction. To determine if Galectin-3 induced astrocyte-secreted factors were sufficient to increase microglial phagocytosis of pHrodo-$A\beta O_{1-42}$, I first obtained primary astrocytes from Galectin-$3^{-/-}$ neonates and cultured them as before. At passage 1, cells were seeded onto 24-well plates at 200k cells/well and cultured for 1 day before medium was changed to the treatment medium. Astrocytes were treated with control astrocyte conditioned medium (CT Ast CM) or Galectin-3 (Galectin-3 Ast CM) for 24h and the CM was collected, aliquoted and frozen at –80°C until phagocytosis experiments. I then treated primary murine microglia with the following conditions for 24 hours:

1) 5 μM pHrodo-$A\beta O_{1-42}$ (5 μM Aβ)
2) 5 μM pHrodo-$A\beta O_{1-42}$ + 5 μg/ml Galectin-3 (5 μM Aβ + 5 μg/ml Galectin-3)
3) 5 μM pHrodo-$A\beta O_{1-42}$ in control astrocyte conditioned medium (5 μM Aβ + CT Ast CM)
4) 5 μM pHrodo-$A\beta O_{1-42}$ in 5 μg/ml Galectin-3 treated Ast CM (5 μM Aβ + Galectin-3 Ast CM)

A two-way ANOVA was used to analyse the data and Tukey post-hoc tests were used to perform pairwise comparisons between groups.

Microglia treated with Galectin-3 Ast CM showed increased phagocytosis as compared to the rest of the conditions (Figure 5.5E). At 24 hours, a significant difference was observed between Galectin-3 treated and non-Galectin-3 treated cultures ($p = 0.006$), between cultures treated with and without Ast CM ($p = 0.02$). There was also a significant effect of interaction between Galectin-3 treatment and Ast CM ($p = 0.02$).

Tukey post-hoc analysis showed that there was no significant difference between 5 μM pHrodo-AβO_{1-42} and 5 μM pHrodo-AβO_{1-42} + 5 μg/ml Galectin-3 ($p = 0.91$), firstly replicating the results seen in 5.3 and showing that Galectin-3 alone is not sufficient to increase microglial phagocytosis of AβO_{1-42}. Additionally, there was no significant difference between 5 μM pHrodo-AβO_{1-42} and 5 μM pHrodo-AβO_{1-42} + 10 μM TD-139 ($p = 1.00$), next showing that astrocyte conditioned medium alone was not sufficient to increase AβO_{1-42} phagocytosis. Tukey post-hoc tests comparing 5 μM Aβ + Galectin-3 Ast-CM with both 5 μM Aβ + CT Ast-CM ($p = 0.007$) and 5 μM Aβ + 5 μg/ml Galectin-3 ($p = 0.02$) show statistical difference (Figure 5.5F).

Similar results were obtained for the analysis of the area under curve (AUC) over 24 hours, with significant difference was observed with the effect of Galectin-3 ($p = 0.009$), Ast CM ($p = 0.04$), and interaction between Galectin-3 treatment and Ast CM ($p = 0.048$).

Again, no significant changes were detected with either addition of Galectin-3 alone or with the presence of control astrocyte CM ($p = 0.87$ and $p = 1.00$, respectively). However, when compared to either CT Ast CM or 5 μg/ml Galectin-3, Galectin-3 Ast CM from Galectin-3 treated astrocytes significantly increased phagocytosis over the 24 hour period ($p = 0.02$ and $p = 0.04$, respectively; Figure 5.5G).

In conclusion, both Galectin-3 or CT Ast CM alone was not sufficient to increase microglial phagocytosis of pHrodo-AβO_{1-42}, but when Galectin-3 treated astrocyte conditioned medium was added to microglia, phagocytosis of pHrodo-AβO_{1-42} was increased. Taken together, these results suggest that astrocytes secrete factors in response to Galectin-3 which was sufficient to increase microglial phagocytosis of pHrodo-AβO_{1-42}.

Figure 5.5 Figure on following page. (A – D) pHrodo fluorescence in CX3CR1-GFP$^{+/-}$ microglia at 24 hours post treatment with 5 μM pHrodo-AβO_{1-42} (A), 5 μM pHrodo-AβO_{1-42} and 5 μg/ml Galectin-3 (B), 5 μM pHrodo-AβO_{1-42} and CT astrocyte-conditioned medium (C), 5 μM pHrodo-AβO1-42 and Galectin-3 astrocyte-conditioned medium (D). (A' – D') pHrodo is observed within GFP^{+} cells. (E) Change in Phagocytic Index (pHrodo area/GFP area) over time. Microglia cultured in Galectin-3 astrocyte-conditioned medium showed increased phagocytosis over the rest of the conditions. (F – G) Phagocytic index at 24 hours post treatment (F) and Area under curve over 24 hours (G), with one-way ANOVA showed significant difference between the conditions. Multiple-testing corrections after t-testing showed significant differences between 5 μM pHrodo-AβO_{1-42} and 5 μg/ml Galectin-3 (B) and 5 μM pHrodo-AβO_{1-42} and Galectin-3 astrocyte-conditioned medium (D), and 5 μM pHrodo-AβO_{1-42} and CT astrocyte-conditioned medium (C) and 5 μM pHrodo-AβO_{1-42} and Galectin-3 astrocyte-conditioned medium (D).

n = 3 replicates, scale bars represent 200 μm, and error bars show SEM.

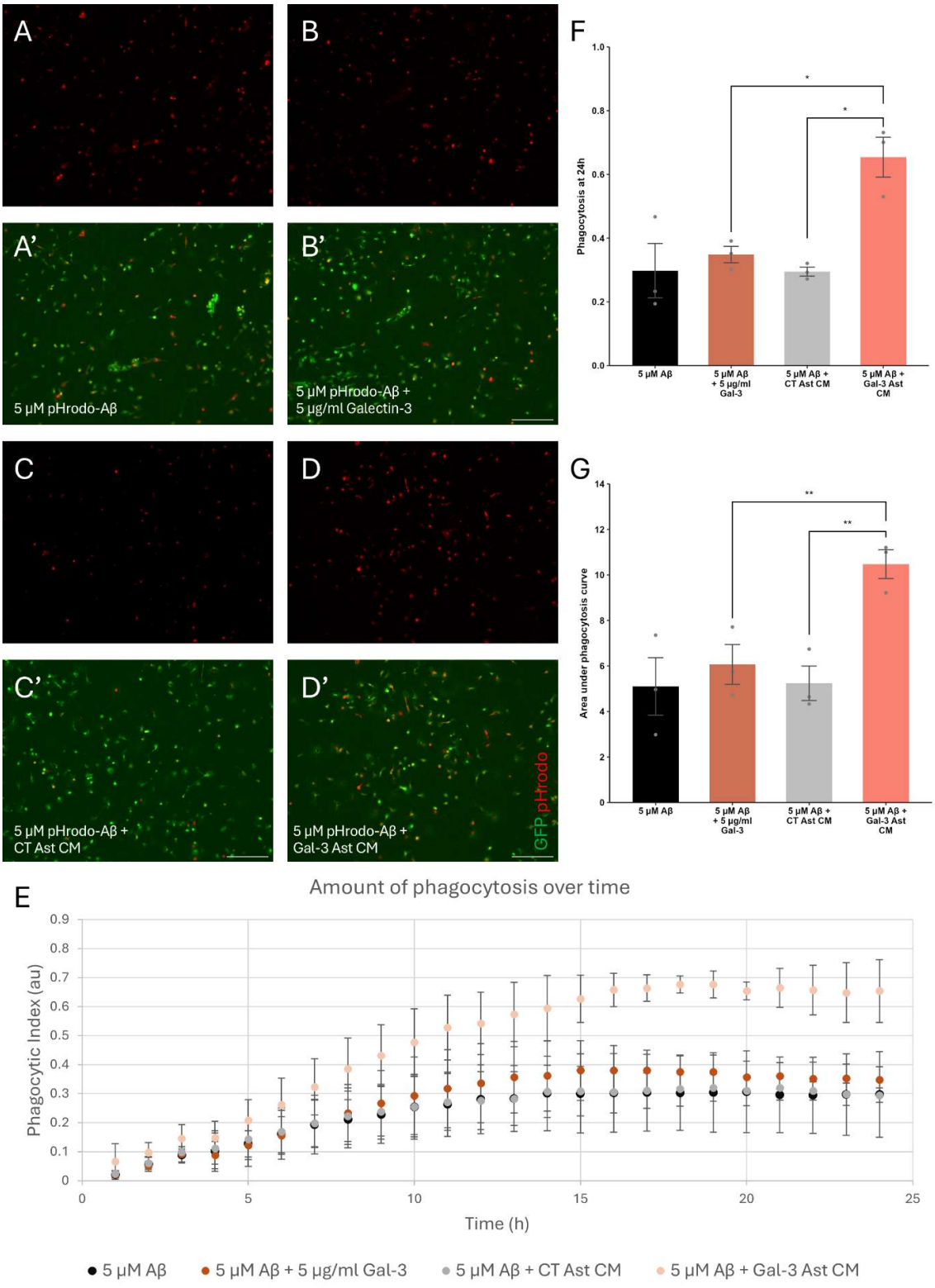


Figure 5.5 Galectin-3 treated astrocytes secrete factors which increased microglial phagocytosis of pHrodo-AβO_{1-42}. Legend on previous page.

5.6 Galectin-3 increases microglial phagocytosis of pHrodo-$A\beta O_{1-42}$ in mixed glial cultures via matrix metalloproteinases (MMPs)

To determine if the reduction in phagocytosis was indeed from decreased ADE secretion by astrocytes, the experiment was repeated with the MMP inhibitor Marimastat (BB 2516). Marimastat was a kind gift from Prof Daniel Anthony.

To determine the effects of MMP inhibition on phagocytosis of oligomeric amyloid beta 1-42 ($A\beta O_{1-42}$), I treated primary murine glial cells with the following conditions for 24 hours:

1) 5 µM pHrodo-$A\beta O_{1-42}$
2) 5 µM pHrodo-$A\beta O_{1-42}$ + 5 µM Marimastat
3) 5 µM pHrodo-$A\beta O_{1-42}$ + 10 µM Marimastat
4) 5 µM pHrodo-$A\beta O_{1-42}$ + 10 µM Marimastat + 5 µg/ml Galectin-3

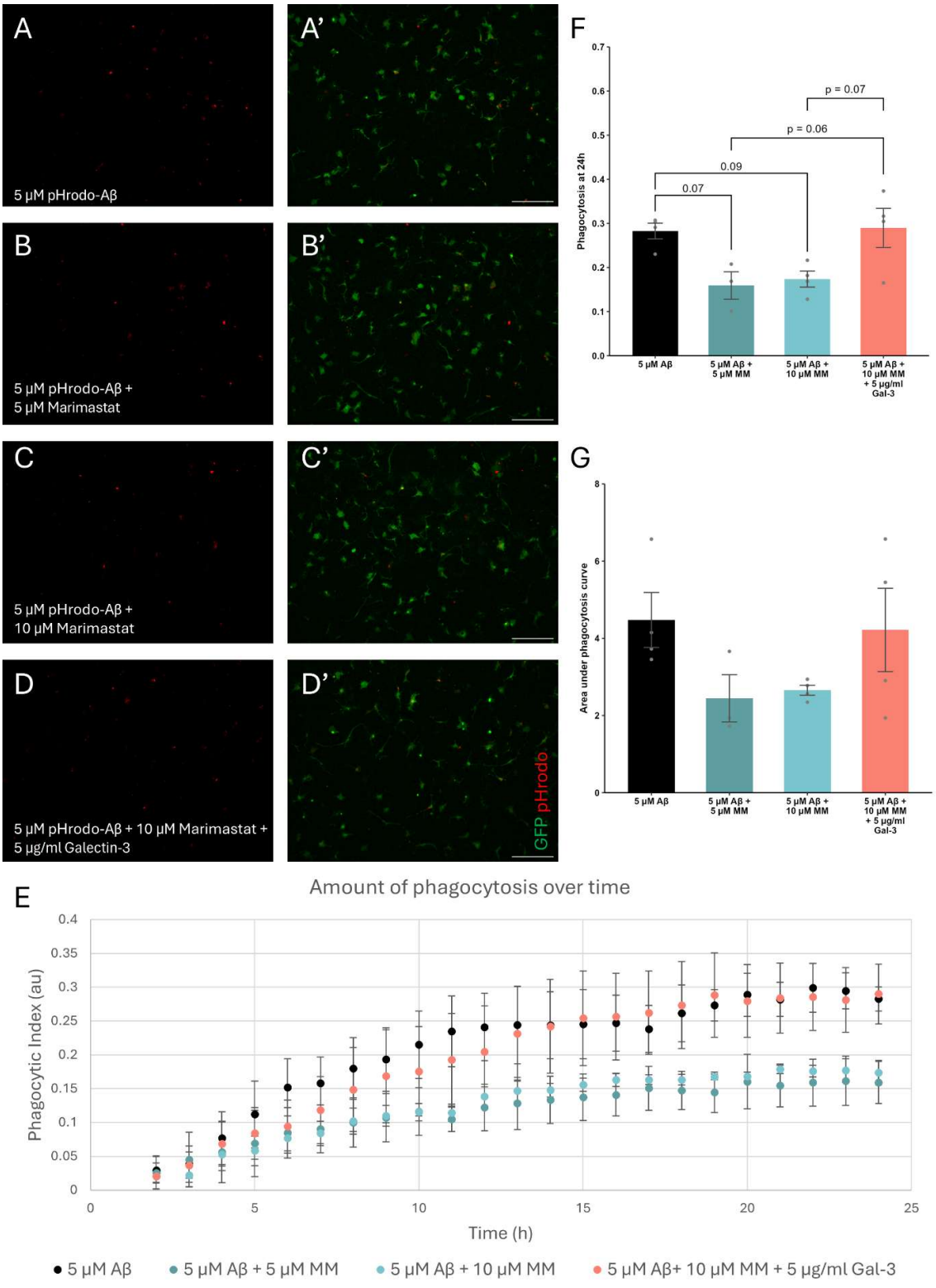


Figure 5.6 MMP inhibitor Marimastat decreased phagocytosis of pHrodo-AβO1-42 in mixed glial cultures. Figure legend continued on the following page.

Figure 5.6 Addition of MMP inhibitor Marimastat decreased microglial phagocytosis of pHrodo-$A\beta O_{1-42}$ in mixed glial cultures. (A – D) pHrodo fluorescence in CX3CR1-$GFP^{+/-}$ mixed glia at 24 hours post treatment with 5 μM pHrodo-$A\beta O_{1-42}$ (A), 5 μM pHrodo-$A\beta O_{1-42}$ and 5 μM Marimastat (B), 5 μM pHrodo-$A\beta O_{1-42}$ and 10 μM Marimastat (C) 5 μM pHrodo-$A\beta O_{1-42}$, 10 μM Marimastat and 5 μg/ml Galectin-3 (D). (A' – D') pHrodo is observed within GFP^{+} cells. (E) Change in Phagocytic Index (pHrodo area/GFP area) over time. Mixed glia treated with Marimastat showed decreased phagocytosis. (F) Phagocytic index at 24 hours post treatment. One-way ANOVA showed significant difference between the conditions, with Tukey post-hoc testing showing significant decrease of phagocytic index in cultures treated with Marimastat. (G) Area under curve of phagocytosis over 24 hours. No significant difference was observed between the conditions. n = 4 replicates, scale bars represent 200 μm, and error bars show SEM.

5.6.1 Addition of MMP inhibitor Marimastat to mixed glial cultures decreased microglial phagocytosis of pHrodo-AβO$_{1-42}$

At 24 hours, there was a significant effect between the treatment groups ($p = 0.02$, one-way ANOVA), however, analysis of the AUC over 24 hours revealed no significant differences between the groups ($p = 0.18$).

5.6.2 Addition of MMP inhibitor Marimastat to mixed glial cultures abrogated the Galectin-3 mediated increase in microglial phagocytosis of pHrodo-AβO$_{1-42}$

The initial lower rate of phagocytosis in cultures treated with Marimastat and Galectin-3 (5 – 13 hours post treatment) suggest that Marimastat may have had an initial effect on the MMPs which were present in the medium prior to treatment. After 13 hours post treatment, the amount of phagocytosis was comparable to that of control cultures, and there was no significant difference as compared to control cultures. A trend towards increased phagocytosis was seen when compared to cultures treated only with Marimastat (Figure 5.6F; $p = 0.068$, $1 - \beta = 0.854$).

5.7 Galectin-3 increased expression of amyloid degrading enzymes (ADEs) in astrocytes

To determine the effects of oligomeric Aβ 1-42 ($AβO_{1-42}$), Galectin-3 and its inhibitor TD-139 on astrocytic expression of amyloid-degrading enzymes (ADEs), I treated primary murine astrocytes with the following conditions for 24 hours:

1) DMSO Control
2) 5 μM $AβO_{1-42}$
3) 5 μg/ml Galectin-3
4) 10 μM TD-139

I then extracted and purified the RNA from the samples and performed qPCR with primers for the ADEs Mmp2, Mmp9, Scarb1, Ece1, Ide and Mme.

Treatment of astrocytes with $AβO_{1-42}$ significantly increased Ide and Mmp2 expression (Figure 5.7 B and D). Treatment of astrocytes with Galectin-3 alone significantly increased Mmp2, Mmp9 and Scarb1 expression (Figure 5.7 D – F).

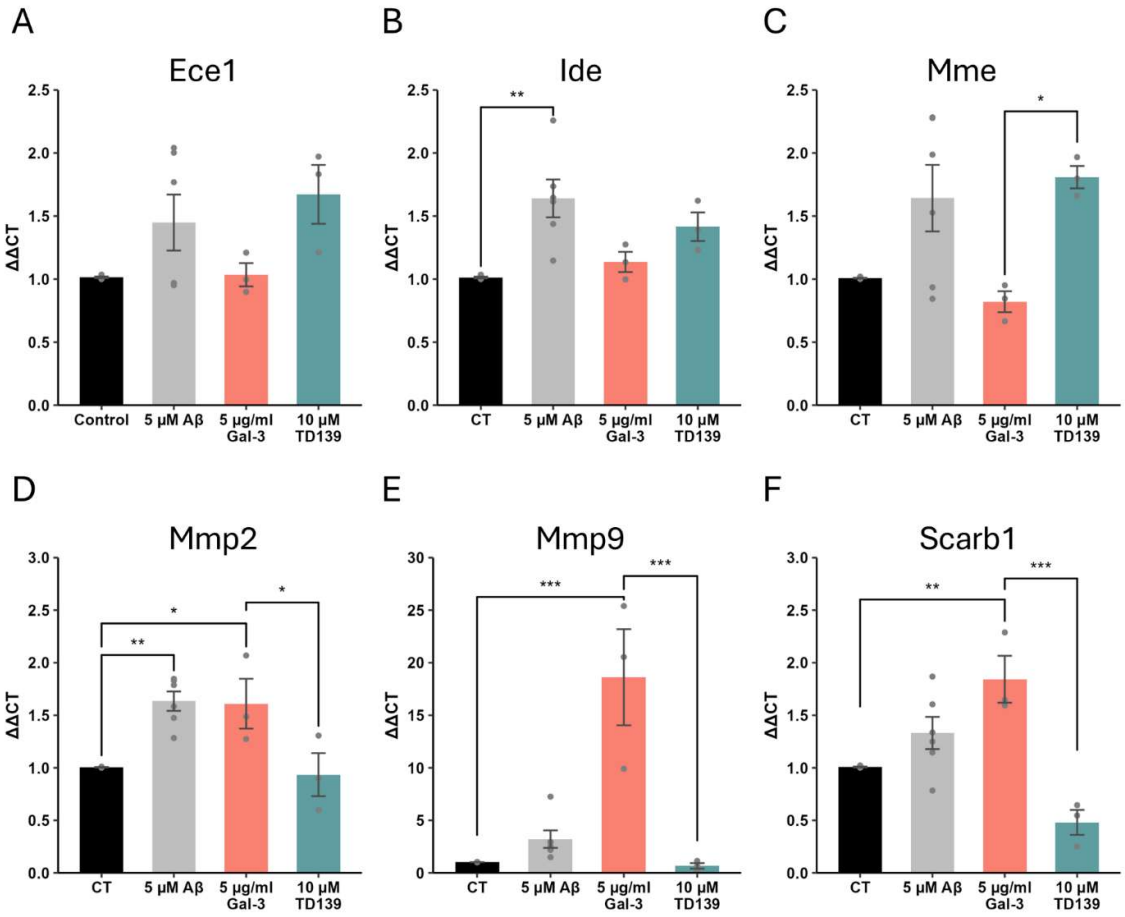


Figure 5.7: Changes to gene expression levels of amyloid degrading enzymes after treatment with 5 μM $AβO_{1-42}$, 5 μg/ml Galectin-3 or 10 μM TD-139. One-way ANOVA showed significant differences in Ide, Mme, Mmp2, Mmp9 and Scarb1. Significance levels in the plots represent results from Tukey post-hoc analyses, *: $p < 0.05$, **: $p < 0.01$, ***: $p < 0.001$.

n = 6 (CT and 5 μM Aβ), n = 3 (5 μg/ml Gal-3 and 10 μM TD-139). Error bars represent SEM.

5.8 Galectin-3 increased levels of pro-MMP9 and cleaved MMP9 in Galectin-$3^{+/+}$ and Galectin-$3^{-/-}$ primary murine glia

To determine if increased expression of Mmp9 in astrocytes translated to increased MMP9 protein levels, I treated Galectin-$3^{+/+}$ primary murine mixed glia over 24h with 5 µg/ml Galectin-3, using lipopolysaccharide (LPS) as a positive control. Previously, Yang and colleagues showed that LPS at concentrations between 2 ng/ml and 2 µg/ml induced expression of MMP9 in rat brain astrocytes (Yang et al., 2019). Hence, an LPS concentration of 100 ng/ml was chosen as a positive control for induction of MMP9 in my cultures. Concurrently, Galectin-$3^{-/-}$ glia were treated with either 5 µg/ml Galectin-3 or LPS. The cells were then lysed with RIPA + phosphatase and protease inhibitors and boiled with 4xLB before being run on a PAGE and immunoblotted for MMP9.

To quantify the changes in MMP9 expression, a western blot was performed. In Galectin-$3^{+/+}$ cultures, treatment with Galectin-3 did not reach statistical significance ($p = 0.055$). However, after removal of outliers, a significant effect was observed with Galectin-3 treatment (Figure 5.8A, $p = 0.02$). Galectin-3 also increased active MMP9 levels, with a significant difference between control and Galectin-3 cultures ($p = 0.03$). In Galectin-3-/- cultures, treatment with Galectin-3 significantly increased Pro-MMP9 levels ($p = 0.03$).

Figure 5.8: Figure on next page. (A) Western blot for MMP9 shows increased MMP9 on addition of Galectin-3, with LPS as a positive control. Galectin-3 treatment significantly increased protein levels of both Pro-MMP9 (B) and Active MMP9 (B') in WT mice. Galectin-3 also significantly increased protein levels of both Pro-MMP9 (C) and Active MMP9 (C') in Galectin-$3^{-/-}$ mice. n = 4 replicates, Student's t-test. Error bars represent SEM.

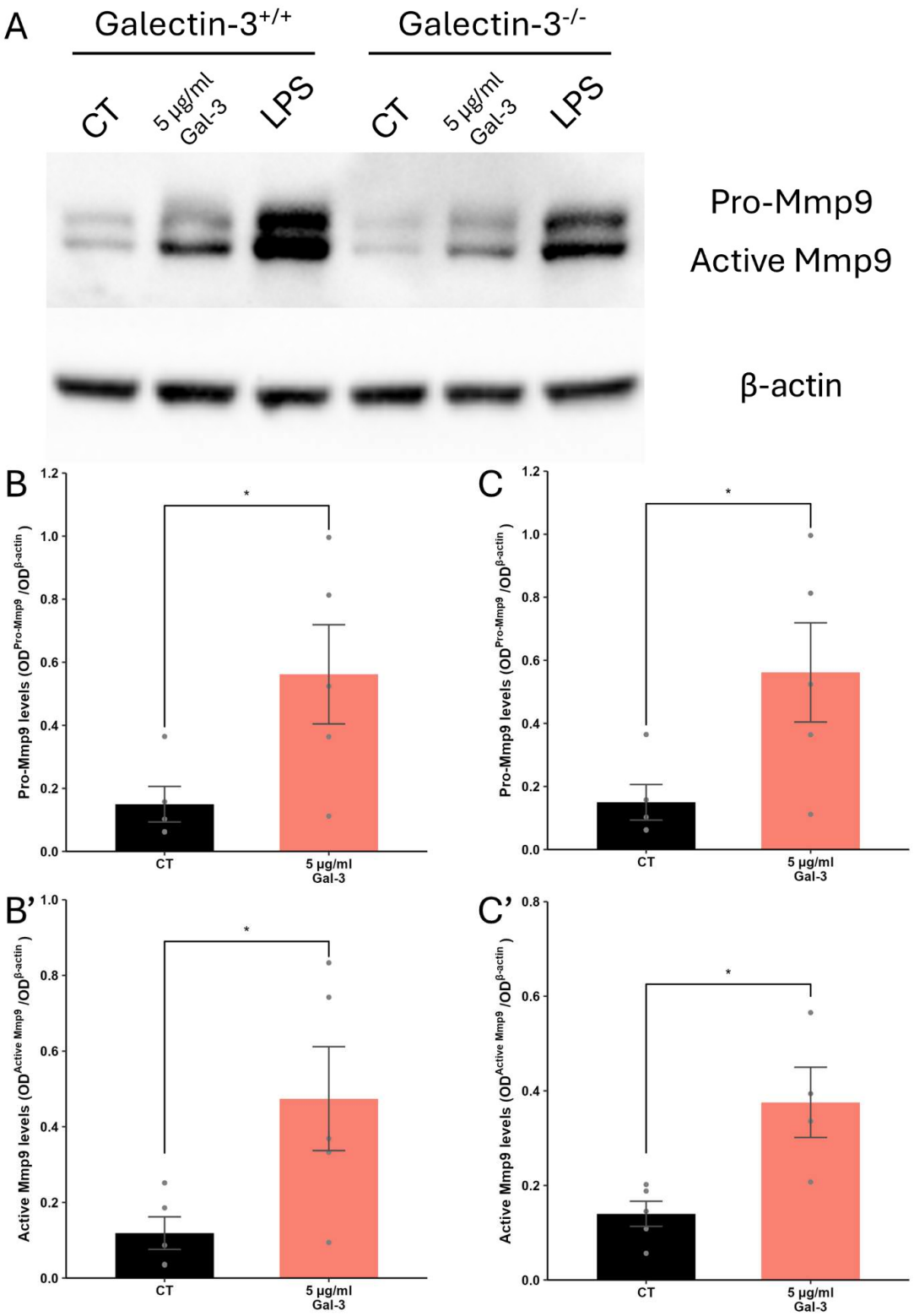


Figure 5.8: Galectin-3 increased MMP9 levels in Galectin-3$^{+/+}$ and Galectin-3$^{-/-}$ mixed glial cultures. Figure legend on previous page.

5.9 Discussion

In 5.4, I showed that addition of Galectin-3 increased microglial phagocytosis of pHrodo-AβO_{1-42} when astrocytes were present. When compared to the results in 5.3 where no significant changes to phagocytosis was observed either with addition of Galectin-3 or its inhibitor, this suggested that the effect of Galectin-3 was mediated by astrocytes. I then showed that direct contact between microglia and astrocytes was not required for this effect using astrocyte conditioned medium. In 5.6, I showed in fact that the MMP inhibitor Marimastat decreased phagocytosis, and that the addition of both Galectin-3 and Marimastat returned phagocytosis to levels similar to control cultures. I then showed upregulation of various ADEs by astrocytes when treated with Galectin-3 in 5.7; this corresponded with increased levels of both pro-MMP9 and active MMP9 in astrocytic cultures in the presence of Galectin-3.

Altogether, these showed that addition of exogenous Galectin-3 increased uptake of AβO_{1-42} by microglia in the presence of astrocyte secreted factors. However, these experiments do not show that MMP9 is sufficient to increase uptake of AβO_{1-42} by microglia. Addition of recombinant MMP9 together with AβO_{1-42} will need to be performed to determine if MMP9 can indeed increase AβO_{1-42} uptake by microglia.

5.9.1 Aβ uptake pathways in microglia

5.9.1.1 Macropinocytosis

In my work, I did not ascertain the pathway through which Aβ was internalised by microglia. Hence, it is possible that the increased pHrodo-AβO_{1-42} uptake was via other pathways including macropinocytosis or receptor-mediated endocytosis. One possibility was that the upregulation of ADEs resulted in extracellular degradation of Aβ, especially larger species such as fibrillar Aβ. This could result in increased soluble Aβ present and hence increase uptake of Aβ via macropinocytosis (Mandrekar et al., 2009).

Future experiments can determine if the increased Aβ uptake by microglia is due to increased phagocytosis of fibrillar Aβ or via increased macropinocytosis of soluble Aβ by including macropinocytosis inhibitors such as 5-(N-ethyl-N-isopropyl)amiloride (EIPA).

5.9.1.2 Receptor-mediated endocytosis

Galectin-3 has been shown to drive Clathrin-independent endocytosis in mammalian cells (Lakshminarayan et al., 2014). Hence, the presence of Galectin-3 may also drive Aβ uptake into endosomes via Clathrin-independent mechanisms.

5.9.1.3 Interactions between Galectin-3 and astrocytic factors

Another possibility is that interactions between Galectin-3 and secreted astrocytic factors could be required for the increased uptake of $A\beta O_{1\text{-}42}$. To this end, the assay described in 5.4 could be refined by pre-treatment with Galectin-3 or TD-139, followed by addition of $A\beta O_{1\text{-}42}$ in media without Galectin-3. Similarly, astrocyte-conditioned medium can also be collected from Galectin-3 pre-treated astrocytes by addition of fresh media after pre-treatment with Galectin-3. If similar results are obtained, it would suggest that the astrocyte secreted factors alone, without interaction with Galectin-3, are sufficient to increase microglial uptake of pHrodo-$A\beta O_{1\text{-}42}$.

5.9.1.4 Other astrocytic interactions

In my hands, Galectin-3 altered pHrodo-$A\beta O_{1\text{-}42}$ phagocytosis in microglia–astrocyte co-cultures but not in pure microglial cultures, suggesting astrocytes were mediating the increase. One possibility was that Galectin-3 increased phagocytosis of pHrodo-$A\beta O_{1\text{-}42}$ by astrocytes but not microglia; Galectin-3 may differentially affect astrocytic and microglial phagocytosis, as there are phagocytosis-regulating receptors unique to either microglia or astrocytes (Konishi et al., 2022). Additionally, previous studies have shown that astrocytes can also endocytose monomeric and oligomeric Aβ (Lee et al., 2015). However, I did not observe pHrodo signal outside of GFP^+ cells (Figures 5.4 and 5.6). This suggested that in my culture system, phagocytosis by astrocytes was negligible, and the increased phagocytosis from Galectin-3 treatment was likely due to an astrocytic-microglial interaction.

Next, astrocytes could be secreting signalling factors into the media which modulate microglial activation. To this end, I have shown that Galectin-3 treated astrocytes upregulated expression of Aβ-degrading enzymes Mmp2, Mmp9 and Scarb1, and that protein levels of Pro- and active MMP9 were increased after Galectin-3 treatment. However, these results do not exclude that other secreted factors may be increased after Galectin-3 treatment.

Another astrocyte-secreted molecule that could modulate phagocytosis of pHrodo-AβO_{1-42} by microglia is Il33 (Fu et al., 2016). Future work could aim to identify if astrocytic secretion of Il33 can also be regulated by Galectin-3.

Lastly, in the mixed glial cultures, microglia are in direct contact with the astrocytic monolayer. While Galectin-3 treated Ast CM was sufficient to increase microglial AβO_{1-42} phagocytosis, it does not exclude possible contact-based interactions between the microglia and astrocytes in addition to the secreted factors that may have increased AβO_{1-42} phagocytosis.

5.9.2 Possible pathways of MMP9 upregulation by Galectin-3 in astrocytes:

NF-κB pathway

MMP9 upregulation was mediated via NF-κB pathway in rat primary astrocytes treated with 2-chloroethanol (2-CE) (Wang et al., 2018), with increased IκBα phosphorylation on treatment with 2-CE. Pharmacological inhibition of IκBα phosphorylation or of activator protein 1 (AP1) decreased MMP9 expression, suggesting that MMP9 can be regulated via the NF-κB pathway. Galectin-3 has been shown to bind to TLR4 and activate TLR4–NF-κB signalling in other systems (Burguillos et al., 2015; Wang et al., 2024; Zhou et al., 2018).

CD147 clustering via Galectin-3 oligomerisation

In immortalised human corneal keratinocytes, Galectin-3 upregulated Mmp9 expression and MMP9 levels by clustering of CD147. Silencing of CD147, or truncation of Galectin-3 (Galectin-3C) muted the increase of MMP9 by Galectin-3 (Cruzat et al., 2018). Interestingly, in this model of wound healing, Galectin-3 is only seen at the leading edge where it appears to cluster

CD147 via its N-terminal polymerisation domain. This clustering of CD147 has previously been shown to induce Mmp synthesis (Mauris et al., 2014). Interestingly, in the brain, CD147 is expressed by both endothelial cells and astrocytes, and is strongly upregulated after ischemic injury (Patrizz et al., 2020). This suggests that Galectin-3 induced MMP9 upregulation could require the oligomerisation of Galectin-3 upon binding of CD147.

5.9.3 Use of WT Aβ over mutant Aβ

Mutations within the 42 aa sequence of $Aβ_{1-42}$ can result in increased aggregation kinetics (Hatami et al., 2017). I chose to focus on $Aβ_{1-42}$ with the WT sequence; this was firstly because while mutations in Aβ can result in familial AD, majority of AD cases are sporadic.

Furthermore, of the 452 FAD mutations in PSEN1, PS2 and APP evaluated, only 66 were in APP (Xiao et al., 2021); within these 66, only 20 were within $Aβ_{1-42}$ (Xiao et al., 2021). This suggests that the majority of FAD mutations are found either in PSEN1 or adjacent to $Aβ_{1-42}$ (Xiao et al., 2021). These mutations result in altered processing of Aβ and rather than changing how the monomers interact, they either increase the amount of Aβ or the Aβ42/Aβ40 ratio. Altogether, this suggests that the overwhelming majority of AD cases are not caused by mutations within the $Aβ_{1-42}$ sequence.

Nonetheless, it remains interesting how mutations within the $Aβ_{1-42}$ sequence may affect degradation and remains for future studies to identify whether mutations in Aβ will affect phagocytosis.

While fibrillar Aβ (fAβ) is the form of Aβ in plaques, there is little correlation between Aβ-plaque load and cognitive decline, suggesting that other forms of Aβ must be responsible for neurodegeneration. Increasing evidence is showing that prefibrillar species of Aβ such as oligomers (AβO) and protofibrils are more toxic than fAβ, with intracerebroventricular injections of fAβ not having effects on memory and learning but AβOs being detrimental (He et al., 2012).

5.9.4 Inhibition of Galectin-3 increased expression of Mme (Neprilysin)

Interestingly, inhibition of Galectin-3 had the opposite effect on Mme (encoding Neprilysin, NEP) as compared to other ADEs. Previously, work has shown that the decrease of NEP could contribute towards deposits of Aβ in cerebral blood vessels (Miners et al., 2006). Additionally, Tao and colleagues showed increased NEP expression in Galectin-3$^{-/-}$ mice (Tao et al., 2020). This suggests that paradoxically, Galectin-3 inhibition could also increase clearance of Aβ. However, it is worth noting that only MMP9 could degrade Aβ fibrils.

5.9.5 Limitations

5.9.5.1 Measurements of phagocytosis

In the phagocytosis experiments described in 5.3, BV2 cells were used. While care was taken to ensure even seeding of cells, BV2 cells are semi adherent and cell densities across the plate may not have been completely even. To account for this, experiments were performed in technical triplicates, and the area of pHrodo fluorescence was normalised to the cell area. However, in BV2 cultures, it was not possible to normalise the amount of pHrodo signal to the number of cells at each time point as the cells were not fluorescent and it was not possible to image brightfield and fluorescent channels simultaneously.

The use of Cx3cr1-GFP$^{+/-}$ microglia allowed firstly for more consistent cell densities as the primary microglia were adherent. The GFP fluorescence also allowed normalisation of pHrodo signal to the cell area at each time point. This was especially important in the mixed glia phagocytosis experiments, as GFP^{+}-microglia begin to proliferate once GFP^{-}-astrocytes have formed a confluent monolayer. While equal densities of total glia were seeded, the density of microglia in culture could vary across the biological replicates. Hence, comparison of the Phagocytic Index reduced the variability across replicates.

Additionally, only pHrodo-labelled Aβ was used as cargo in these experiments. Therefore, the current experimental design cannot determine whether the Galectin-3-mediated increase in microglial uptake is specific to Aβ or reflects a more general increase in microglial uptake.

Future experiments using alternative pHrodo-labelled cargo would help determine the cargo specificity of this phenotype.

5.9.5.2 Presence of endogenous levels of Galectin-3

As the Cx3cr1-GFP$^{+/-}$ model is not deficient in Galectin-3, microglia in the mixed glia cultures express Galectin-3 endogenously. Additionally, phagocytosis of Aβ has been shown to increase Galectin-3 expression (Grubman et al., 2021). Taken together, these suggest that even without addition of exogenous Galectin-3, microglia in the mixed glial cultures could be releasing Galectin-3 into the medium, in turn affecting gene expression of astrocytes. Additionally, astrocytes have been shown to express Galectin-3 in traumatic brain injury models (Sirko et al., 2015). Hence, it was possible that endogenous levels of Galectin-3 were present in the medium in the experiments described in 5.3, 5.4, 5.6 and 5.7. This likely explains why the addition of TD-139 in experiment 5.4 decreased phagocytosis. As a result, to ensure that no residual levels of Galectin-3 were in the CT Ast CM for the experiments outlined in 5.5, Galectin-3$^{-/-}$ astrocytes were used.

5.9.5.3 Aggregation state of AβO$_{1-42}$ in culture medium

In my experiments, I treated microglia and mixed glia with Galectin-3 directly. I and others have shown that Galectin-3 can promote Aβ oligomerisation and deposition (Chapter 7; and (Boza-Serrano et al., 2019; Tao et al., 2020)). While the pHrodo-AβO$_{1-42}$ used in my phagocytosis assays were pre-oligomerised, a few factors regarding the culture conditions may have affected the aggregation state of Aβ during the assays. Firstly, the presence of Galectin-3 in the culture medium may still bind and result in further aggregation of Aβ. Next, the medium used for cell culture was not fully defined due to presence of fetal bovine serum (FBS). There is a possibility that factors present in FBS may also affect aggregation of Aβ. Lastly, the high concentration of Aβ used may also have promoted further aggregation during the assays. Future assays could employ Galectin-3$^{-/-}$ glia which ensures that Galectin-3 is not present in the medium, and pre-treatment of cells with Galectin-3 followed by addition of pHrodo-AβO$_{1-42}$ in medium without Galectin-3 or FBS.

Alternatively, investigation of pHrodo-AβO_{1-42} phagocytosis by induced pluripotent stem cell (iPSC)-derived microglia would also provide strong evidence that this effect can be replicated in human cells. iPSC-derived glia models will also allow for better control of the microglia to astrocyte ratio.

5.9.5.4 Degradation of AβO_{1-42}

While I showed alterations to uptake of AβO_{1-42} by microglia, the results cannot determine if the increased AβO_{1-42} internalised by microglia is degraded. Microglia may uptake Aβ but can fail to degrade it, resulting in the secretion of Aβ back into the extracellular space (Chung et al., 1999). To determine the fate of the AβO_{1-42} internalised by microglia, future work can incorporate a washout step after the phagocytosis assay. Enzyme-linked immunosorbent assays (ELISAs) measuring Aβ levels in the lysate (intracellular) and media (extracellular) will inform if the increased uptake of Aβ corresponds with increased degradation.

Chapter 6: Galectin-3 increases MMP9 *in vitro*

6.1 Introduction

In Chapter 5, I showed that Galectin-3 increased Mmp9 expression and MMP9 levels. Specifically in section 5.8, I showed that LPS was able to increase MMP9 levels in both Galectin-$3^{+/+}$ and Galectin-$3^{-/-}$ mixed glial cultures. However, there appeared to be differences in the extent to which MMP9 was upregulated (Figure 5.8). One possible mechanism through which LPS increases MMP9 levels is via the TLR4-NfκB pathway and that Galectin-3 binds and signals through the TLR4 pathway. Taken with the fact that Galectin-3 alone was sufficient to increase levels of both Pro-MMP9 and Active MMP9 (Figure 5.8 B and C), all these suggest that modulation of Galectin-3 could affect how glial cells respond to pro-inflammatory stimuli such as LPS. Hence, I first asked if Galectin-$3^{-/-}$ glia had a diminished response to LPS stimuli as compared to Galectin-$3^{+/+}$ glia.

6.2 Galectin-3 knockout decreased LPS-mediated increase in MMP9 levels in primary murine glia

Quantification of Pro-MMP9 and Active-MMP9 levels reveal that Galectin-$3^{-/-}$ glia had decreased MMP9 levels as compared to Galectin-$3^{+/+}$ glia. This was true for both Pro-MMP9 ($p = 0.030$) and Active MMP-9 ($p = 0.041$).

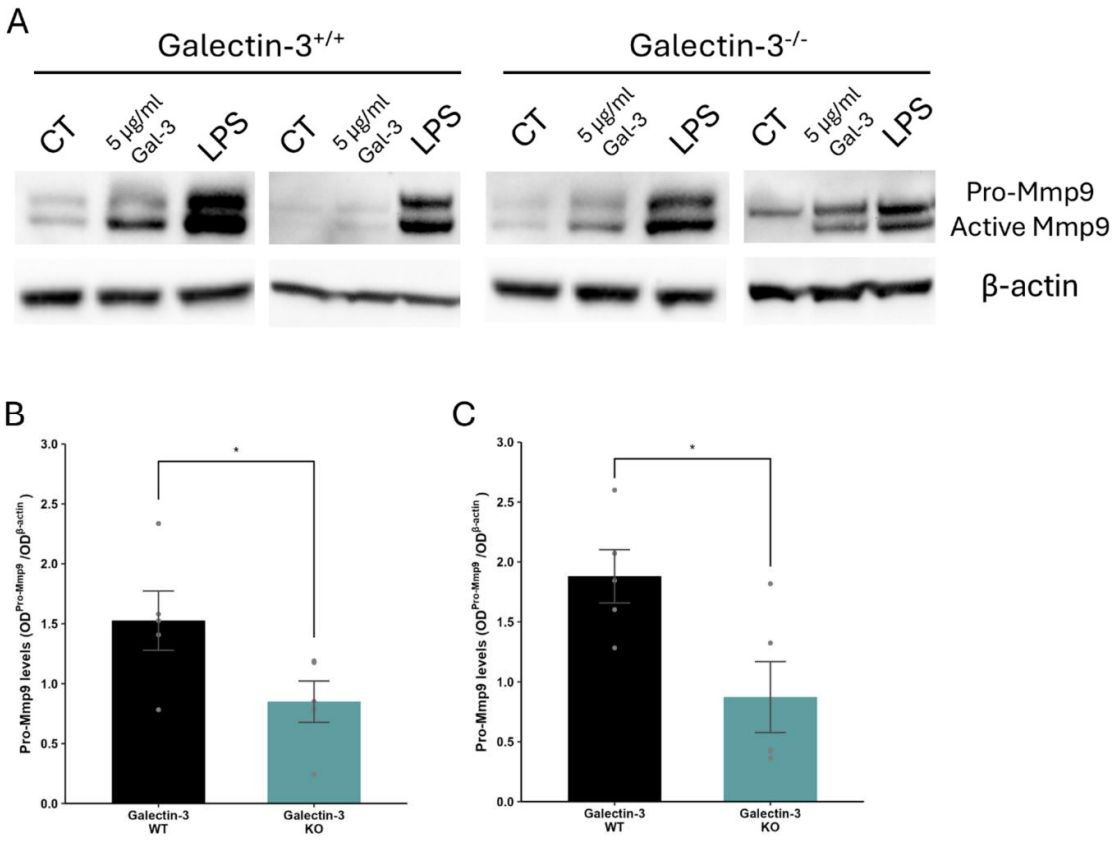


Figure 6.2: Galectin-3 knockout decreased LPS-induced MMP9 levels in mixed glial cultures. (A) Western blot for MMP9 show a stronger increase in MMP9 protein levels after LPS treatment in Galectin-$3^{+/+}$ glia as compared to Galectin-$3^{-/-}$. (B – C) Decreased levels of Pro-MMP9 (B) and active MMP9 (C) in LPS-treated Galectin-$3^{-/-}$ glia compared to Galectin-$3^{+/+}$ glia. Student's t-test, n = 4. Error bars show SEM.

6.3 LPS and Galectin-3 knockout have sex dependent effects on MMP9 levels

i.p. injections, mice sacrifice, and brain collection were performed by Dr Daniel Rand. I received frozen half-brains and processed the brains thereafter.

To determine if the reduction in LPS-induced MMP9 levels by Galectin-3 knockout could be replicated *in vivo*, Galectin-$3^{+/+}$ and Galectin-$3^{-/-}$ mice were given i.p. injections of either saline or LPS. The brains were then collected and processed for WB. The levels of MMP9 and Galectin-3 were normalised to β-actin and a two-way ANOVA was used to determine if there was a statistical difference in the response to LPS based on the genotype of the mice.

Figure 6.3: Figure on next page. Galectin-3 knockout had a sex-dependent effect on LPS-induced MMP9 levels. (A and B) Western blot of Galectin-$3^{+/+}$ and Galectin-$3^{-/-}$ mice treated with saline or LPS. Both female (A) and male (B) mice were used. (C and D) MMP9 levels in whole brain lysates, normalised to β-actin levels. Two-way ANOVA showed an increase in MMP9 levels after LPS treatment for both females (C, $p = 0.021$) and males (D, $p = 0.015$). (E and F) Galectin-3 levels in whole brain lysates, normalised to β-actin levels. Two-way ANOVA showed increase in Galectin-3 levels after LPS treatment in males (F, $p = 0.006$) but not females (E, $p = 0.33$). n = 3 animals per sex, genotype and condition, error bars represent SEM.

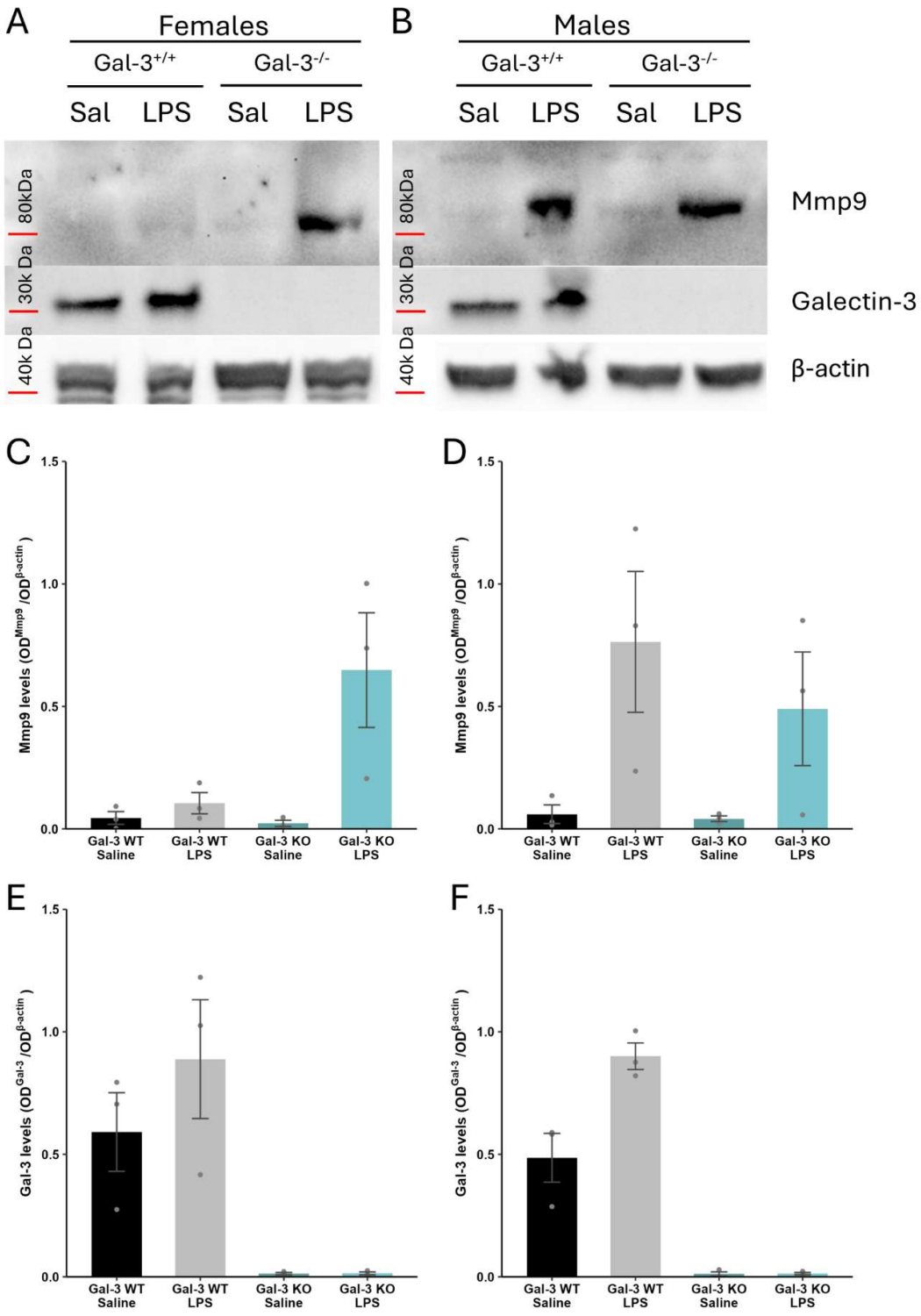


Figure 6.3: Galectin-3 knockout had sex-dependent effect on LPS-induced MMP9 levels.

Figure legend continued on previous page.

6.3.1 Peripheral LPS increased MMP9 levels in the brain

While I and others have shown that LPS induced MMP9 expression and protein levels in cultured astrocytes (Chapter 5.7 and 5.8, and (Yang et al., 2019)), there are mixed reports about whether LPS crosses the blood brain barrier (BBB) (Banks & Robinson, 2010; Vargas-Caraveo et al., 2017).

LPS treatment increased MMP9 levels in both Galectin-$3^{+/+}$ and Galectin-$3^{-/-}$ mice of both sexes (Figure 6.3 A and B). Analysis of MMP9 protein levels in the brain (optical density, $OD_{MMP9}/OD_{\beta\text{-actin}}$) shows that mice treated with LPS show increased MMP9 levels as compared to saline treated controls (Figure 6.3 C and D). This was true for both male and female mice ($p = 0.015$ and $p = 0.021$ respectively, two-way ANOVA). Hence, peripheral LPS was able to induce MMP9 expression in the brain in both Galectin-$3^{+/+}$ and Galectin-$3^{-/-}$ mice.

6.3.2 Galectin-3 knockout in males did not have a significant effect on LPS-induced MMP9 levels

In males, while MMP9 levels appeared slightly lower in Galectin-$3^{-/-}$ mice as compared to Galectin-$3^{+/+}$ mice, this difference was not statistically significant. This was true when the effect of Galectin-3 knockout was compared overall (two-way ANOVA, $p = 0.46$), or when saline-treated mice were compared separately from LPS-treated mice ($p = 1$ and $p = 0.73$, Tukey post-hoc).

Additionally, Galectin-3 knockout did not affect the response to LPS (two-way ANOVA, interaction: $p = 0.51$). Detailed ANOVA results can be found in the appendix (Supplementary Table 6.3.1)

6.3.3 Galectin-3 knockout in females increased LPS-mediated increase in MMP9 levels

In females, MMP9 levels also appeared slightly lower in saline-treated Galectin-$3^{-/-}$ mice as compared to saline-treated Galectin-$3^{+/+}$ mice, although this difference was not statistically significant ($p = 1$, Tukey post-hoc). Surprisingly, when comparing LPS-treated mice, MMP9 levels were significantly increased in Galectin-$3^{-/-}$ as compared to Galectin-$3^{+/+}$ mice (Tukey post-hoc, $p = 0.0499$). This was also reflected as an effect of Galectin-3 knockout on the response to LPS (two-way ANOVA interaction, $p = 0.046$).

Detailed ANOVA results can be found in the appendix (Supplementary Table 6.3.2)

6.3.4 LPS increased Galectin-3 levels in male mice

In Galectin-$3^{+/+}$ male mice, LPS treatment increased Galectin-3 levels significantly (Figure 6.3F, $p = 0.004$). However, while there was a slight increase of Galectin-3 levels in LPS-treated females, this was not significantly different from saline-treated females (Figure 6.3E, $p = 0.5$). Hence, this shows that peripheral inflammation induced via LPS can increase Galectin-3 levels in brains of male mice.

6.4 Discussion

In the previous Chapter, I showed that Galectin-3 alone was sufficient to increase levels of MMP9 in primary murine glial cells. In this Chapter, I first show that knockout of Galectin-3 resulted in decreased levels of both Pro- and active MMP9 after treatment with LPS (Figure 6.2). I then showed that *in vivo*, a peripheral inflammatory challenge with LPS was able to induce Galectin-3 expression in the brain (Figure 6.3 E and F), with a significant increase in Galectin-3 levels in males but not in females. Concurrently, I show that brain MMP9 levels was increased with peripheral LPS (Figure 6.3 C and D). In males, we see a slight lowering of MMP9 with Galectin-3 knockout (Figure 6.3 D). Interestingly, it appears that female Galectin-$3^{+/+}$ mice had a muted response to LPS as compared to male Galectin-$3^{+/+}$ mice, however, this was not statistically significant after adjustment for multiple testing (B-H adjusted p = 0.13). Contrastingly, Galectin-3 knockout in females strongly increased MMP9 levels after peripheral LPS (Figure 6.3 C). With two-way ANOVA analyses, while male mice only show an effect of treatment (saline vs. LPS; p = 0.01), females show an effect of treatment (p = 0.02) and interaction between genotype and treatment (p = 0.046).

6.4.1 Possible mechanisms of interaction between Galectin-3 and LPS to induce MMP9 levels

Galectin-3 has been shown to bind to LPS and potentiate response of neutrophils to LPS (Fermino et al., 2011), and Galectin-3 knockout decreased secretion of TNFα, interferon gamma (IFNγ) and IL-4 proinflammatory cytokines by BV2 microglia in response to LPS (Burguillos et al., 2015), suggesting that Galectin-3 could lead to increased pro-inflammatory response. As discussed in the previous Chapter, Galectin-3 is a TLR4 ligand and can activate NFκB signalling (Zhou et al., 2018) through which these inflammatory signals are mediated. Hence, knockout of Galectin-3 could be mediating the levels of MMP9 via the same pathways.

6.4.2 Sex difference in LPS-induced MMP9 levels *in vivo*

In Galectin-$3^{+/+}$ mice, while male mice show a strong increase in MMP9 levels after peripheral LPS (Figure 6.3 B and D), female mice do not show a strong induction of MMP9 (Figure 6.3A and C). This could be due to a lower cell surface expression of TLR4 by females compared with males (Marriott & Huet-Hudson, 2006). *In vivo*, LPS elicited a higher inflammatory response in males than in females, with higher sera Il6 levels post i.p. injection of LPS (Marriott & Huet-Hudson, 2006). This is the same pathway through which MMP9 is regulated by TLR4, suggesting that the trend towards decreased MMP9 expression could be regulated along the same LPS-TLR4-NFkB axis as IL6. Hence, it is not entirely surprising that upon peripheral LPS challenge, females showed decreased upregulation of MMP9 when compared to males.

6.4.3 Sex difference in how Galectin-3 knockout alters LPS-induced MMP9 levels *in vivo*

In vitro, I observed decreased LPS-induced MMP9 levels in Galectin-$3^{-/-}$ glia. This was somewhat mirrored in male mice, where slightly lower levels of MMP9 levels were observed in Galectin-$3^{-/-}$ mice treated with LPS as compared to Galectin-$3^{+/+}$ mice. Surprisingly, female mice had a completely opposite reaction, with Galectin-3 knockout increasing the effect of LPS-induced MMP9 levels.

6.4.4 Peripheral Galectin-3 vs. brain Galectin-3

The finding that females respond to Galectin-3 knockout differently than males raises more interesting questions. Firstly, was this an effect of peripheral Galectin-3, or Galectin-3 in the brain? Galectin-3 has evolutionarily conserved roles in binding pathogen associated molecular patterns (PAMPs) and is mainly secreted by macrophages in the periphery. Since the Galectin-$3^{-/-}$ mice were used, the effects I observed can be due to either peripheral or central Galectin-3, or a combination of both.

One possibility was that the suppression of Galectin-3 peripherally altered proinflammatory cytokine levels in the circulation. Inflammatory cytokines such as IL6, Il-1β and TNFα have been shown to induce MMP9 (Hu et al., 2025; Lin et al., 2007; Song et al., 2015), and elegant experiments using mice with bone marrow lacking Mmp2/MMP9 show that leukocyte-derived Tnfα crosses the BBB and increases MMP9 in astrocytes (Song et al., 2015). This model would suggest that in males, Galectin-3 knockout either had no effect, or decreased pro-inflammatory cytokine levels in the periphery (Chen et al., 2015), while in females, Galectin-3 in the periphery would be suppressing pro-inflammatory cytokine levels under LPS challenge, and Galectin-3 knockout would increase levels of pro-inflammatory cytokines. The altered levels of pro-inflammatory cytokines would then translate to changes in MMP9 production by astrocytes. To this end, serum of the mice in this experiment have been collected and can be run on a multiplex panel of cytokines such as the Luminex Assay kit.

The other possibility would be that reduction of peripheral Galectin-3 did not affect pro-inflammatory cytokine levels, but that the reduction of Galectin-3 in the brain altered the response of astrocytes to the pro-inflammatory cytokines. Given that both male and female mice show presence of Galectin-3 in the brain, this suggests that Galectin-3 is performing opposite functions in the male brain as compared to the female brain. In this model, Galectin-3 in the brain of male mice would increase MMP9 levels, while in females, Galectin-3 would be suppressing MMP9 production by astrocytes. To this end, modified citrus pectin (MCP), an inhibitor of Galectin-3, has been shown to inhibit MMP9 production in endothelial cells in a model of subarachnoid haemorrhage (Nishikawa et al., 2018). Unfortunately, the study only used male mice; nonetheless, this corroborates my findings that in male mice, MMP9 levels were lower in Galectin-$3^{-/-}$ than Galectin-$3^{+/+}$ after LPS treatment (Figure 6.3).

Regardless of whether the effect seen here was due to peripheral or brain Galectin-3, understanding if and how Galectin-3 differentially regulates in a sex-dependent manner peripheral cytokine production, brain MMP9 or both, will be highly important.

6.4.5 Implications for AD

While the peripheral LPS model is not exactly a model of AD, chronic LPS has been shown to be associated with increased neuroinflammation and cognitive decline (Zhu et al., 2014). Although one study suggested that MMP9 could be protective against LPS-induced inflammation in osteoclasts (Zhang et al., 2020), multiple studies have shown that MMP9 contributes to BBB breakdown after stroke (Turner & Sharp, 2016). Galectin-3 inhibitors have been in clinical trials for various systemic diseases including lung and liver fibrosis, and for AD. However, pre-clinical models (including studies targeting Galectin-3) continue to neglect the importance of sex differences in AD and favour male mice over the use of both sexes (Liu et al., 2025; Yin et al., 2020). Since I have shown that Galectin-3 inhibition elicits a different response in males as compared to females, my work strongly suggests that both sexes need to be included in pre-clinical studies.

6.4.6 Limitations and future work

6.4.6.1 Subregional differences in MMP9 levels

As seen from my work in Chapter 3 and 4, Galectin-3 is expressed by different cells in the hippocampus as compared to the SVZ, suggesting that it could be playing different roles in different brain regions. Here, proteins from entire half-brains were extracted from mice treated with LPS; this included the hippocampus, cortex, SVZ and hindbrain. In future experiments, the brain could be dissected into subregions, firstly allowing for deeper understanding of how Galectin-3 may be altered in these subregions in response to peripheral LPS. This will also allow us to identify which regions are responsible for the change in MMP9 levels upon LPS challenge, further informing us on which regions are susceptible to BBB damage associated with peripheral inflammatory challenges.

6.4.6.2 Peripheral vs. Brain Galectin-3 knockout

As discussed in 6.4.4, my Galectin-3 knockout model does not allow us to distinguish between the peripheral or central effects of Galectin-3 knockout on MMP9 levels. Future work should

consider using targeting approaches to remove central Galectin-3 such as intrahippocampal injections of MCP (Nishikawa et al., 2018), or by targeting microglial Galectin-3 using a $HexB^{CreERT2}$ driver line crossed with a $Galectin\text{-}3^{flox/flox}$ line. Inhibition of peripheral Galectin-3 can be achieved with MCP given in drinking water or via i.p. injections.

Chapter 7: Galectin-3 Promotes Beta Amyloid deposition *in vivo*

7.1 Introduction

Boza-Serrano and colleagues did not observe Aβ deposition when Aβ alone was injected intrahippocampally (Boza-Serrano et al., 2019). I replicated their experiments with a few modifications.

7.2 Galectin-3 Promotes Aβ Deposition *in vivo*

I performed all surgeries and sample collection. One set of four brains (PBS, Aβ only, Aβ + Galectin-3 and Aβ + Galectin-3C) was sectioned and immunostained by Zubaida Mukthar as part of her Master's dissertation (Department of Biology) under my careful guidance.

7.2.1 Injections of Aβ alone do not result in deposit formation

The collected brains were sectioned to generate 8 sets of five evenly spaced sections between approximately -1.25mm AP w.r.t. Bregma and -2.45mm AP relative to Bregma. No Galectin-3 or Aβ immunoreactivity was detected (Figure 7.1.1); to ensure that no deposits were present, every other section was immunostained for Galectin-3, Aβ and IBA1 (a compilation of tile scans of every other slice from one animal is provided in the appendix). A 5xFAD sample was included as a positive control. Additionally, the D3V of WT mice are immunoreactive for Galectin-3, which serves as an internal positive control.

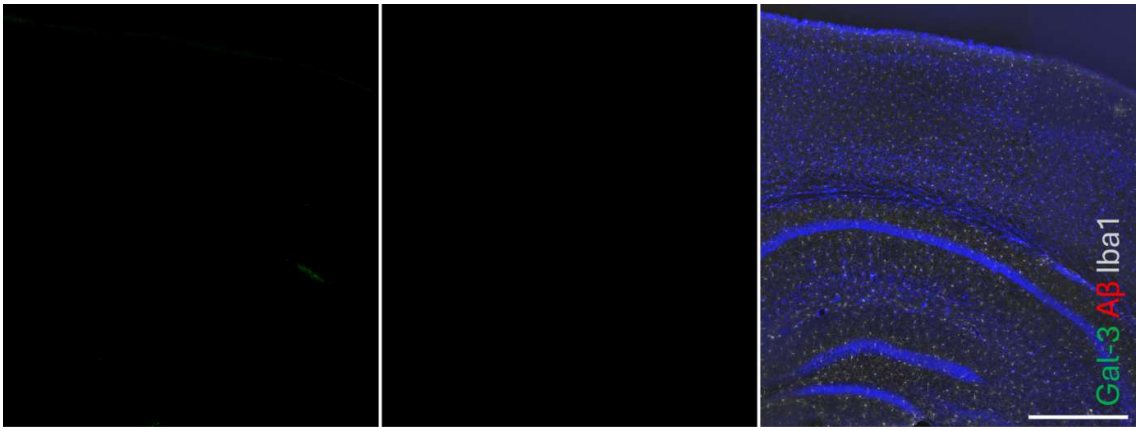


Figure 7.2.1: Injection of Aβ alone did not induce formation of deposits. Scale bar represents 500 µm.

A total of 6 mice were used across 2 cohorts (n = 1 male, n = 5 female).

7.2.2 Co-injections of Aβ with Galectin-3 result in deposits

When Galectin-3 was co-injected with Aβ, Aβ deposition was observed (Figure 7.2.2). I also observed that in addition to the presence of Galectin-3 in the Aβ-immunoreactive deposits, Galectin-3 expressing cells are also seen in the vicinity of the deposits.

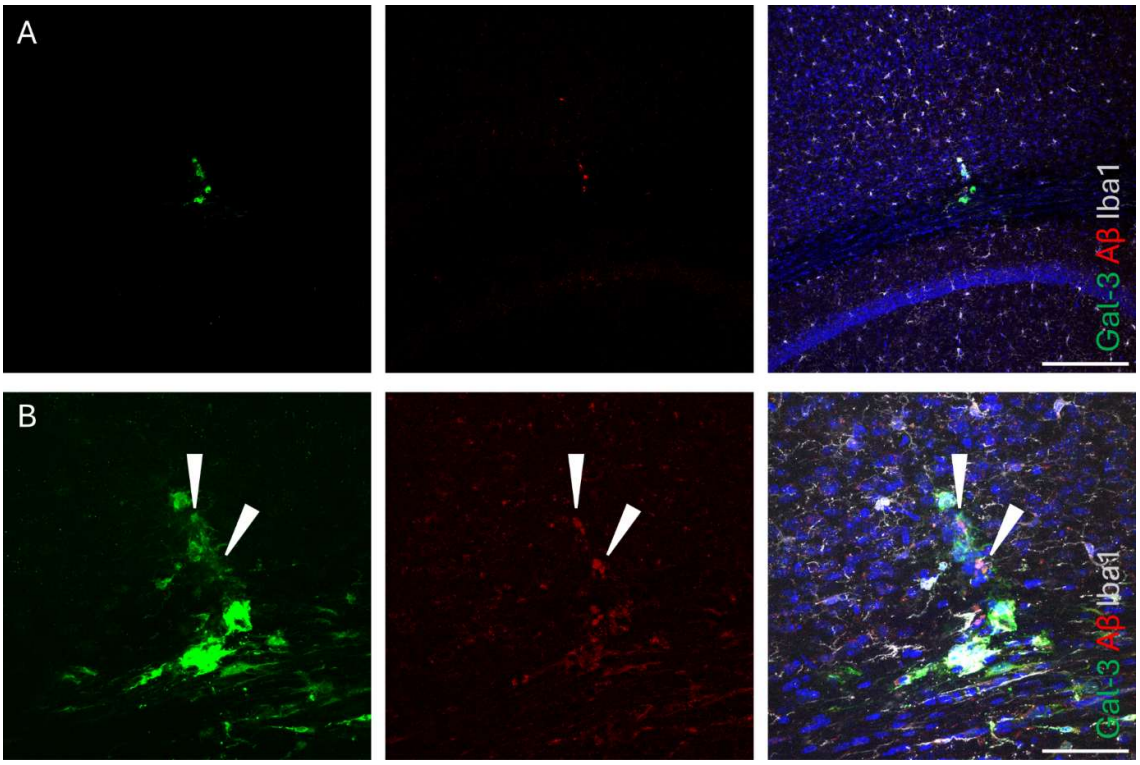


Figure 7.2.2: Injection of Beta Amyloid with full length Galectin-3 induced formation of deposits. (A) Aβ deposits could be seen in the hippocampus. Scale bar represents 200 μm. (B) Higher magnification shows Aβ is colocalised with Galectin-3, but also that microglia surrounding the deposits express Galectin-3. Scale bar represents 50 μm.

A total of 7 mice were used across 2 cohorts (n = 3 male, n = 4 female).

7.2.3 Co-injections of Aβ with Galectin-3C result in deposits

The N-terminal of Galectin-3 mediates its oligomerisation (Zhao et al., 2021). I hypothesised that by removing the N-terminus, it could abrogate the ability of Galectin-3 to promote Aβ oligomerisation and deposition. To this end, I co-injected Aβ with Galectin-3C, a truncated form of Galectin-3 with only the C-terminal CRD. Interestingly, deposits of Aβ were still detected.

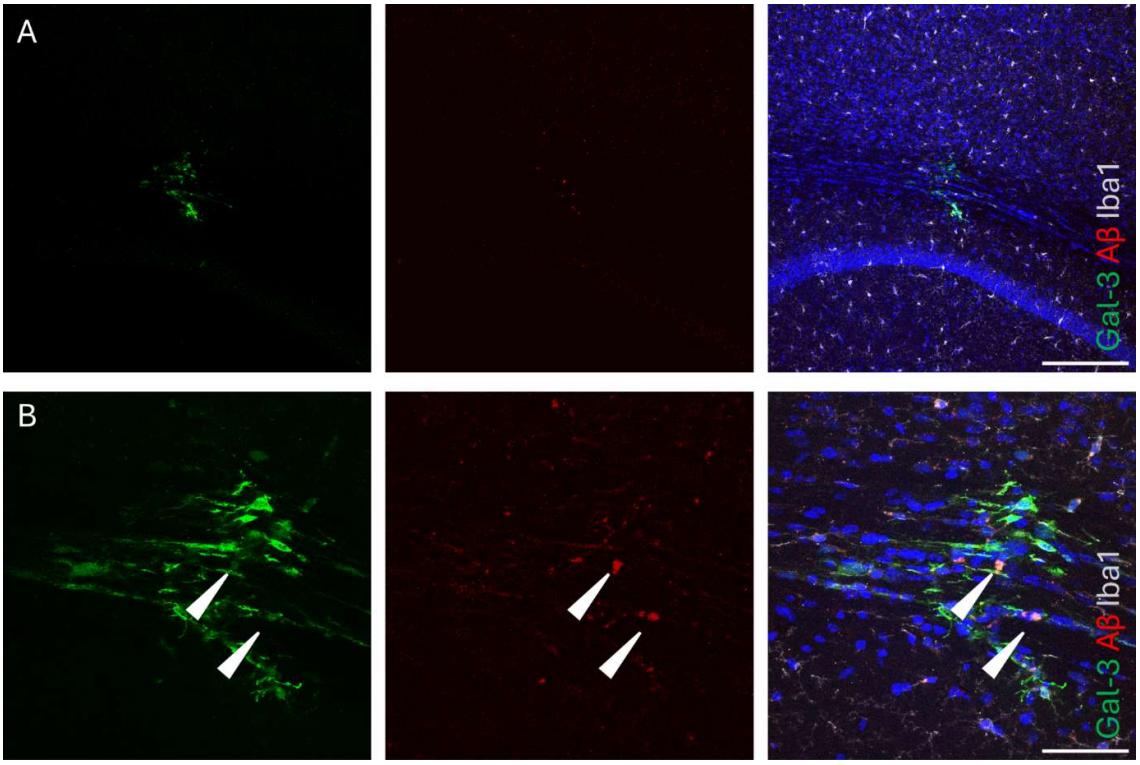


Figure 7.2.3: Injection of Aβ with Galectin-3 Carbohydrate Recognition Domain (Galectin-3C) induced formation of deposits. Since the Galectin-3 antibody used (clone M3/38) only detects full length Galectin-3, this suggests Galectin-3 immunoreactivity is host-derived. (A) Aβ deposits could be seen in the hippocampus. Scale bar represents 200 μm. (B) Higher magnification shows Aβ is colocalised with Galectin-3, but also that microglia surrounding the deposits express Galectin-3. Scale bar represents 50 μm.

A total of 6 mice were used across 2 cohorts (n = 1 male, n = 5 female).

The presence of extracellular Galectin-3 suggests the incorporation of Galectin-3 into the Aβ deposits, while presence of intracellular Galectin-3 suggests that the microglia surrounding the deposits upregulated Galectin-3. Additionally, the antibody used for Galectin-3 detection (clone M3/38) was purported to be against an epitope in the N-terminus of Galectin-3. This suggests that all the Galectin-3 immunoreactivity in the Galectin-3C + Aβ was solely against Galectin-3 produced by the host. In the Galectin-3C + Aβ injected WT mice, Galectin-3 co-localised with Aβ and no IBA1 was observed. This suggests that host Galectin-3 was incorporated into the deposits.

Upon MMP9 cleavage, Galectin-3 has limited hemagglutination and self-association potential (Ochieng et al., 1998), suggesting that the C-terminal CRD has reduced oligomerisation potential as compared to full length Galectin-3.

Since there were still deposits seen in the Galectin-3C + Aβ, and in these we see extracellular Galectin-3 which is co-localised with Aβ, this suggests that host Galectin-3 could be in part mediating the deposition of Aβ. To this end, the injections were repeated in Galectin-3KO mice.

Injection of Aβ with either Galectin-3, Galectin-3C or alone into Galectin-$3^{-/-}$ mice not only allows us to understand the role that host Galectin-3 plays in mediating Aβ deposition but also allows us to observe the host response to plaques which are formed in the absence of endogenous Galectin-3 expression.

7.3 Exogenous Galectin-3, without host Galectin-3, is sufficient to promote Aβ deposition

To determine if recombinant Galectin-3 was sufficient to promote Aβ deposition without the presence of host Galectin-3, I performed the same surgeries as before, but injecting into Galectin-$3^{-/-}$ mice.

7.3.1 Injections of Aβ alone into Galectin-$3^{-/-}$ mice did not result in Aβ deposits

Similar to the experiment outlined in 7.2.1, no deposition was observed in the hippocampus or surrounding regions of the brain (Figure 7.3.1). As before, every other section was immunostained to ensure that there were indeed no deposits.

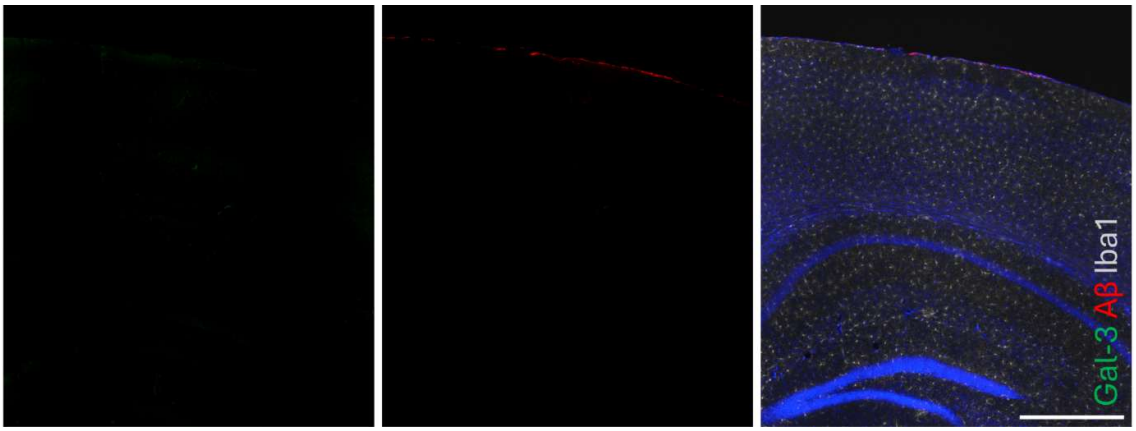


Figure 7.3.1: Injection of Aβ alone into Galectin-$3^{-/-}$ mice did not result in the formation of Aβ deposits. Scale bar represents 500 μm.

A total of 4 mice were used across 2 cohorts (n = 2 male, n = 2 female).

7.3.2 Injections of Aβ with Galectin-3 into Galectin-3$^{-/-}$ mice resulted in Aβ deposition

To determine if host Galectin-3 is required to promote Aβ deposition, I co-injected the same preparations of Aβ and Galectin-3 as before, but into Galectin-3$^{-/-}$ mice. Here, I observed that recombinant Galectin-3 alone, without upregulation of host Galectin-3, was sufficient to induce deposition of Aβ (Figure 7.3.2).

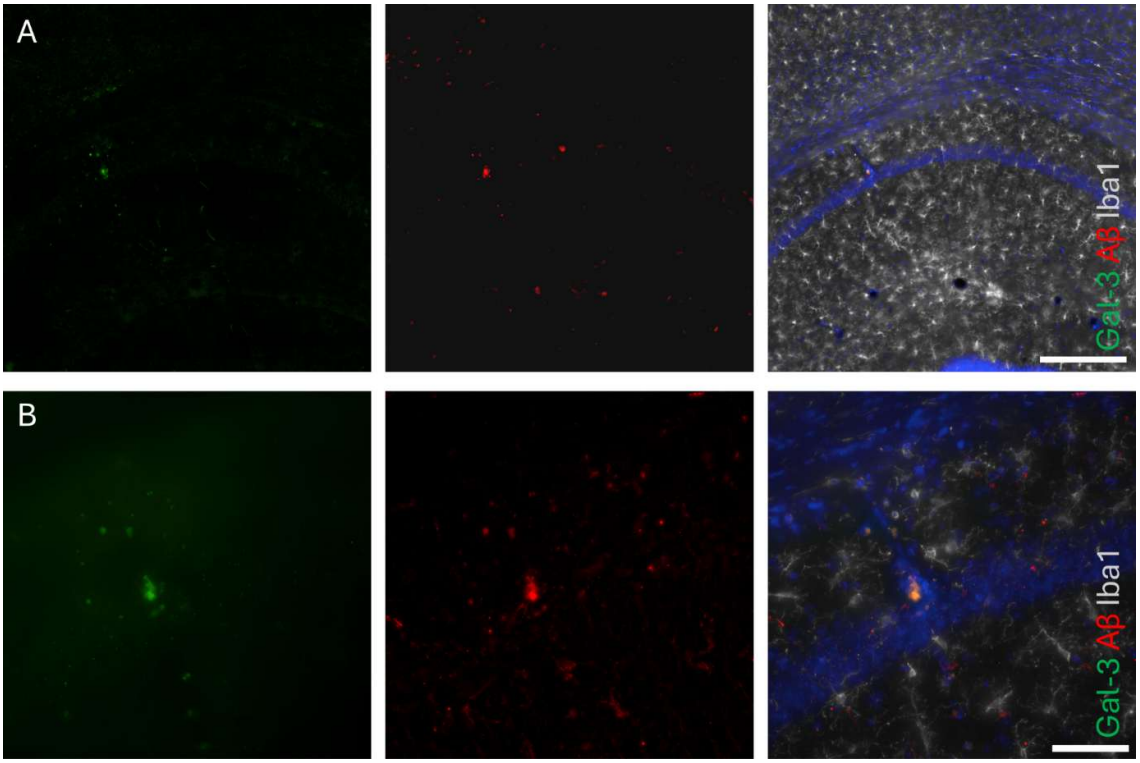


Figure 7.3.2: Injection of Aβ together with the full length Galectin-3 into Galectin-3$^{-/-}$ mice resulted in the formation of Aβ deposits. (A) Deposits were seen in the hippocampus (CA1). Scale bar represents 200 μm. (B) Higher magnification of the deposits show colocalization with Galectin-3. Scale bar represents 50 μm.

A total of 5 mice were used across 2 cohorts (n = 3 male, n = 2 female).

7.3.3 Injections of Aβ and Galectin-3C did not result in formation of Aβ deposits

In the previous experiment, Galectin-3C together with Aβ induced host Galectin-3 expression. Performing the same experiment in Galectin-3$^{-/-}$ I now did not observe deposits of Aβ (Figure 7.3.3), suggesting that the upregulation of host Galectin-3 was necessary to promote Aβ deposition when only the CRD of Galectin-3 was co-injected with Aβ.

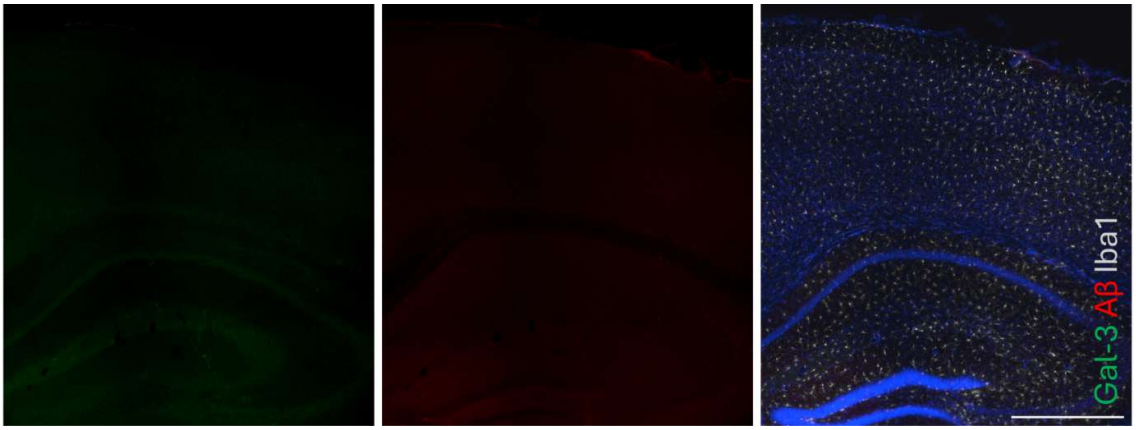


Figure 7.3.3: Injection of Aβ together with the C-terminal carbohydrate recognition domain of Galectin-3 into Galectin-3$^{-/-}$ mice did not result in the formation of Aβ deposits. Scale bar represents 500 µm.

A total of 6 mice were used across 2 cohorts (n = 3 male, n = 3 female).

7.4 Galectin-3 promotes Aβ oligomerisation *in vitro*

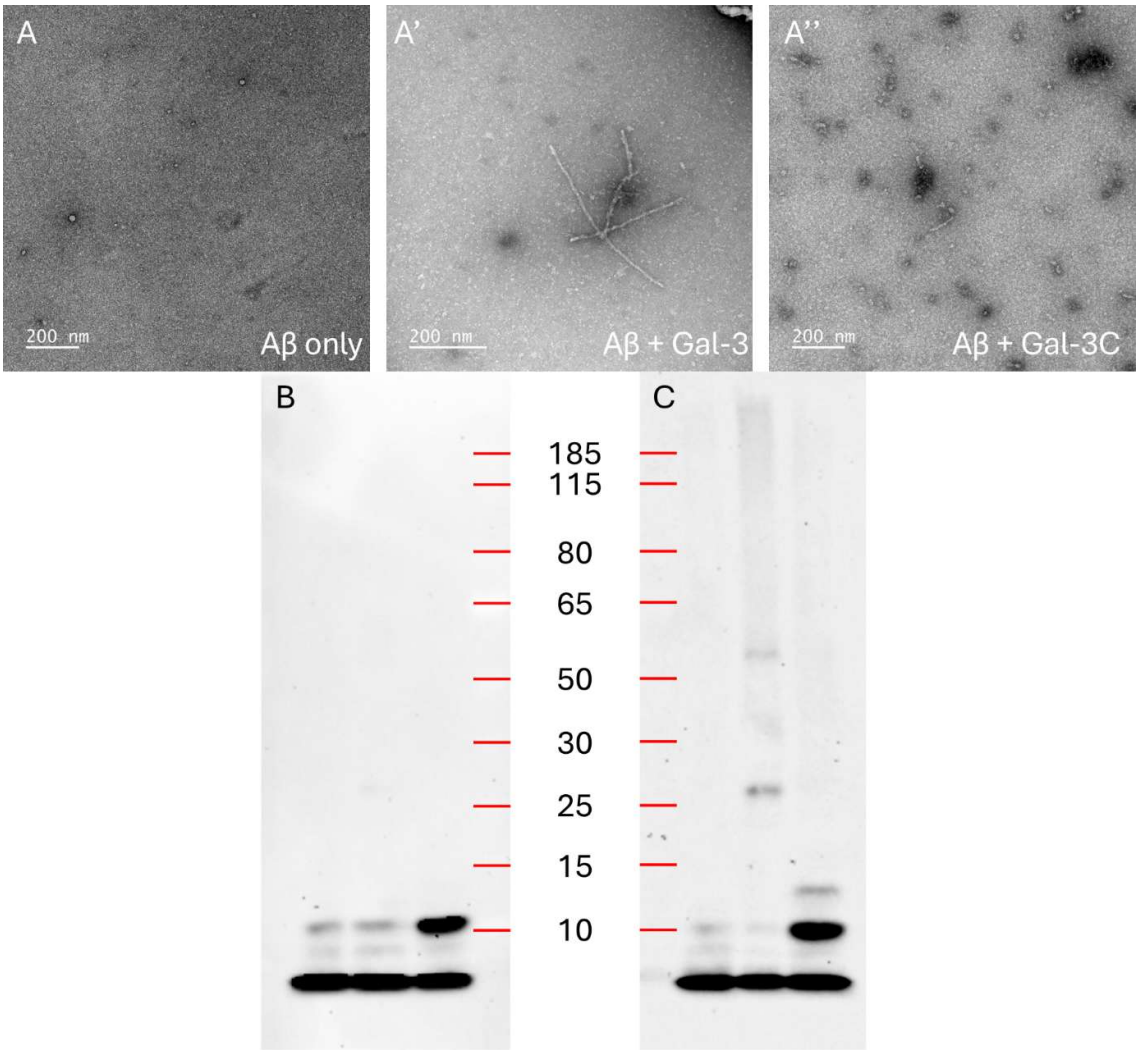


Figure 7.4: Galectin-3, but not Galectin-3C promoted the formation of high molecular weight (HMW) oligomers of Aβ. Incubation for 1 hour at 37 °C did not produce detectable oligomers when only Aβ was present (A), but produced large oligomers/protofibrils when Galectin-3 was added with Aβ (A'). Incubation of Aβ with Galectin-3C produced smaller oligomers of Aβ (A''). Western blot of Aβ, Aβ + Galectin-3 and Aβ + Galectin-3C before incubation (B) and after incubation (C). No HMW aggregates were detected pre-incubation (B), and HMW aggregates were only detected in Aβ + Galectin-3.

7.4.1 Amyloid Beta oligomerisation is induced by incubation with Galectin-3

Previously, I showed that incubation of Aβ alone at 4 °C overnight was able to induce formation of oligomers. These were characterised by TEM and appeared as oligomers of about 5 – 20 nm in diameter.

To determine the species of Aβ which I had injected, I prepared samples as I would for surgeries and sent them to be characterised by transmission electron microscopy (TEM). Aβ alone did not aggregate significantly (Figure 7.4A), but larger structures could be observed when Aβ was incubated with Galectin-3 (Figure 7.4A'). When only the CRD of Galectin-3 was incubated with Aβ, only small, possibly oligomeric structures could be observed (Figure 7.4A'').

I then boiled more of the same samples without reducing buffers for western blotting. Not using reducing conditions prevented the loss of disulfide bonds, retaining any oligomeric or fibrillar structures of Aβ. Incubation of Aβ by itself at 37 °C for 1 hour resulted in a sample which resolved into three bands. The lowest molecular weight band (~5 kDa) likely corresponds to monomers of Aβ while the other two likely correspond to di- to tetramers of Aβ (Figure 7.4). While incubation of Aβ alone did not induce formation of high molecular weight oligomers, incubation of Aβ with Galectin-3 under the same conditions resulted in the formation of high molecular weight oligomers larger than 50 kDa, which can be observed as a smear that runs beyond 185 kDa (Figure 7.4C).

7.4.2 Incubation with Galectin-3C does not promote formation of high molecular weight oligomers of Aβ

When Galectin-3C was added to Aβ, a strong increase in low molecular weight multimers can be seen even before incubation (Figure 7.4B). However, even after incubation at 37 °C for 1 hour, no high molecular weight aggregates were observed (Figure 7.4C), suggesting that the CRD of Galectin-3 was not sufficient to promote aggregation of Aβ into HMW aggregates.

7.4.3 Thioflavin T assay shows increased aggregation with Galectin-3 but not Galectin-3C

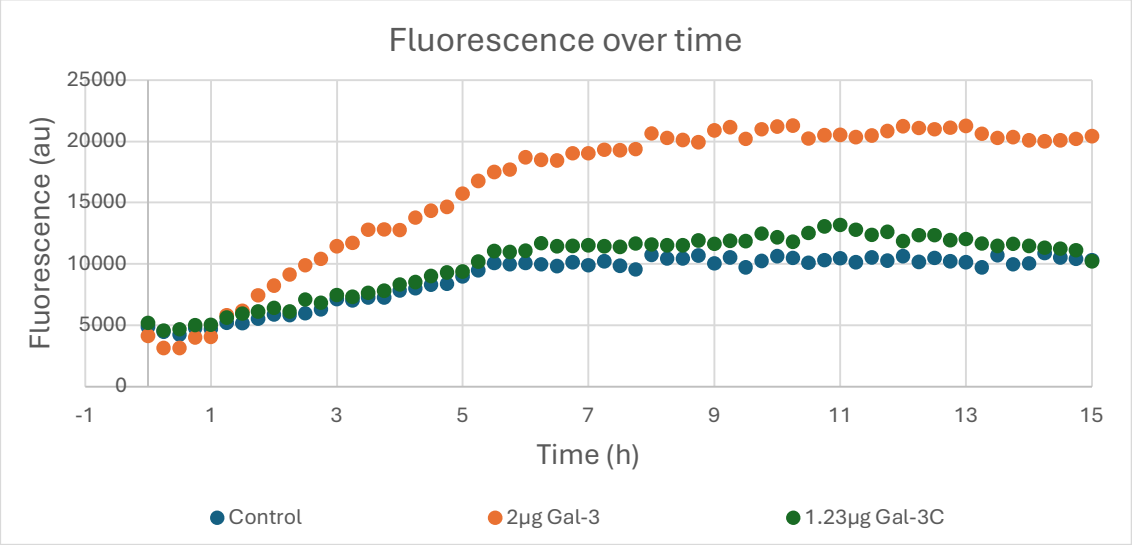


Figure 7.4.3 Aβ aggregation assay using Thioflavin T. While Galectin-3 increased aggregation of Aβ, Galectin-3C did not alter the aggregation of Aβ as compared to control.

n = 1 replicates.

To determine if Galectin-3 and Galectin-3C could alter aggregation of Aβ, I performed a Thioflavin T (ThT) assay. ThT shows a shift in emission to 480 nm after binding to beta sheet structures. Hence, it is suitable for studying how Aβ aggregates. As before, as the molecular weight of Galectin-3C was smaller than that of Galectin-3, a smaller mass of Galectin-3C was added. The number of moles of Galectin-3C was equal to the number of moles of Galectin-3.

While no difference in fluorescence was seen when Galectin-3C was added to Aβ, addition of Galectin-3 to Aβ increased fluorescence. Hence, Galectin-3C was not sufficient to promote aggregation of Aβ.

7.5 Discussion

7.5.1 Key differences between previous work on the role of Galectin-3 and Aβ aggregation

While both Boza-Serrano and colleagues (Boza-Serrano et al., 2019) and Tao and colleagues (Tao et al., 2020) show that Galectin-3 promoted Aβ deposition, it is worth noting the key differences between how Galectin-3 was introduced and the results obtained. In the former, Aβ monomers were pre-incubated either alone or with Galectin-3 before intrahippocampal injections into WT mice. Immunohistochemical detection of Galectin-3 and Aβ after two months showed deposits only in co-injected mice (Boza-Serrano et al., 2019).

In the latter, Aβ monomers alone were injected into both WT and Galectin-$3^{-/-}$ mice. Western blot analysis of hippocampal lysates shows presence of HMW Aβ oligomers as soon as 48 hours after injection in both WT and Galectin-$3^{-/-}$ mice, with the amount of HMW Aβ oligomers reduced in the knockout mice. Furthermore, injections of Aβ alone increased HMW Aβ oligomers over time. Tao and colleagues also injected Galectin-3OE plasmids into WT mice, followed by Aβ monomer injections 2 hours later (Tao et al., 2020). Western blot analysis 48 hours post-injections showed increased HMW oligomers in the Galectin-3OE plasmid injected mice.

One key difference between the findings of the two experiments was whether Aβ oligomerisation was detected when it was injected in isolation into WT mice. While Tao and colleagues saw increased HMW Aβ oligomers over NH_4OH controls, Boza-Serrano and colleagues did not detect Thioflavin S (ThioS)-reactivity in their Aβ only injected animals. Two methodological differences may explain their seemingly contrasting findings. While Boza-Serrano and colleagues employed immunohistochemical detection of ThioS+ plaques, Tao and colleagues used western blots to show the presence of HMW Aβ oligomers. It is possible

that HMW oligomers were present in the Aβ injected hippocampi that were not detected by ThioS. Another possible explanation for this difference could be the time between injections and detection. While Tao and colleagues sacrificed their mice 48 hpi, the longer time between Aβ injection and sacrifice by Boza-Serrano and colleagues could have allowed for the clearance of these oligomers.

7.5.2 Galectin-3C together with Aβ was sufficient to induce host expression of Galectin-3

As there are only 2 studies to date directly showing the role of Galectin-3 in Aβ, and both had employed different methodologies as discussed in the previous section, it is important for me to replicate the results of the experiments. In my experiments, I elected to use immunohistochemical methods for detection as this preserves the spatial information on Galectin-3 and Aβ. I showed that intrahippocampal injections of Aβ were able to form deposits when pre-incubated with both full length Galectin-3 and Galectin-3C. Using Aβ antibodies for detection, I did not observe immunoreactivity from the animals injected with Aβ alone, suggesting that if there were any non-fibrillary Aβ present in these mice, they were under the limit of detection by immunohistochemistry (IHC).

Next, I showed that mice injected with Aβ alone did not have increased Galectin-3 immunoreactivity one month post injection. In contrast, mice injected with Galectin-3 and Aβ showed increased Galectin-3 immunoreactivity. A similar observation was made with animals injected with Galectin-3C + Aβ, showing Galectin-3 reactivity around the injection site. However, the Galectin-3 antibody used was raised against an epitope on the N-terminus which did not detect the purified Galectin-3C. Additionally, the Galectin-3 immunoreactivity in both Galectin-3 + Aβ and Galectin-3C + Aβ were mostly intracellular and co-localised with IBA1, suggesting that it was host-derived.

Hence, my experiments show that both Galectin-3 and its CRD, in combination with Aβ, were sufficient to induce prolonged ectopic expression of host Galectin-3 in a manner that Aβ alone was not.

7.5.3 Galectin-3C did not result in HMW oligomers of Aβ.

Next, I showed that *in vitro*, Galectin-3C did not drive the formation of HMW oligomers, but was sufficient to induce low molecular weight (LMW) oligomers. In contrast, full length Galectin-3 promoted HMW oligomer formation *in vitro*. Further characterisation of samples prepared in an identical manner to those injected into mice reveals presence of oligomers and short fibrils in Galectin-3 + Aβ but only small oligomers in Galectin-3C + Aβ. Furthermore, ThT assay showed that only full length Galectin-3 was able to promote aggregation of Aβ towards fibrils. This suggests that Galectin-3C alone was not sufficient to fully promote aggregation of Aβ.

Taken together with the finding that Galectin-3C and Aβ co-injection was sufficient to drive formation of long-lasting Aβ deposits, this suggests that the LMW oligomers promoted by Galectin-3CRD was sufficient to induce prolonged host-derived Galectin-3 expression. However, this confounded with the original question of whether Galectin-3CRD alone was sufficient to promote Aβ deposition, as the increased host Galectin-3 could have initiated a feed-forward cycle, resulting in a similar effect as an injection with full length Galectin-3. Furthermore, it is unclear whether this increase in Galectin-3 expression by the host was due to LMW Aβ oligomers alone, the presence of Galectin-3CRD, or a combination of both.

By performing the same injections into Galectin-$3^{-/-}$ mice, I showed that Galectin-3 in combination with Aβ was still able to induce formation of Aβ deposits detectable by immunohistochemistry. This suggests that while host-derived Galectin-3 may have contributed to Aβ deposition in WT mice, the exogenous Galectin-3 was sufficient to result in Aβ deposition.

7.5.4 Full length Galectin-3, but not Galectin-3C, was sufficient to promote Aβ deposition in Galectin-3$^{-/-}$ mice.

As seen from the presence of deposits in Galectin-3$^{-/-}$ mice injected with Aβ + Galectin-3 (Figure 7.3.2), Galectin-3 was able to induce Aβ deposition even in the absence of host Galectin-3. This is in contrast to Galectin-3C, where injection of Aβ + Galectin-3C into Galectin-3$^{-/-}$ mice did not induce Aβ deposits. One possible explanation is that in Galectin-3$^{+/+}$ mice, the small molecular weight oligomers or Galectin-3C induced expression of Galectin-3 in microglia. When secreted, host-derived Galectin-3 then caused further oligomerisation of Aβ into larger molecular weight oligomers and then deposition; in the Galectin-3$^{-/-}$ mice, without the production of host Galectin-3, deposition of Aβ was no longer observed. Hence, I have shown that the N-terminal oligomerisation domain of Galectin-3 is necessary for the ability of Galectin-3 to promote Aβ aggregation *in vitro*, and to promote Aβ deposition *in vivo*. Furthermore, I showed that recombinant Galectin-3 alone without host Galectin-3 is sufficient to induce Aβ deposition.

Altogether, these suggest that the HMW oligomers promoted by full length Galectin-3 were sufficient to induce long-lasting deposits of Aβ.

7.5.5 Limitations

7.5.5.1 in vitro aggregation assays

While the thioflavin T assay can rapidly determine β-sheet fibril formation in Aβ preparations, it is ultimately a reductionist approach which does not fully recapitulate the physiological conditions of Aβ aggregation in AD. Firstly, the *in vitro* assays used high concentrations of Galectin-3 and Aβ which may force interactions that do not usually occur *in vivo*. Next, these assays lack physiological binding partners of Aβ which may also interact with Galectin-3 or Aβ to stabilise various states of Aβ; these include ApoE, Clusterin and other extracellular matrix (ECM) proteins. Furthermore, these assays are acellular. Both microglia and astrocytes are crucial in amyloid processing and have been shown to alter how Aβ aggregates (Baligacs et

al., 2024; Sollvander et al., 2016). The interactions between Galectin-3, Aβ and cellular degradation mechanisms cannot be recapitulated in these assays.

Furthermore, the ThT aggregation assay was only a single technical replicate. As such, more validation needs to be performed to ensure that the effect observed can be replicated robustly. Lastly, the thioflavin T assay cannot detect oligomer formation. Hence, conditions which promote oligomerisation but not fibrilisation will not alter the kinetics of the thioflavin T assay.

7.5.5.2 Potential artefact of in vivo injections

I observed both Galectin-3 and Aβ reactivity in the hippocampus after injections of Galectin-3 + Aβ and Galectin-3C + Aβ. While this could have been due to Galectin-3 inducing Aβ oligomerisation and deposition, there are other potential artefacts which may have resulted in the presence of Aβ deposits. Firstly, the mechanical injury associated with injection may have induced a local inflammatory response. Hence, rather than being a Galectin-3 dependent effect, the deposition may also have required other factors derived from reactive glia in the injection region. Concurrently, a high concentration of Aβ was injected. Hence, the observed deposition could also be due to the clearance mechanisms being overwhelmed. Additionally, Galectin-3 was also introduced at supraphysiological concentrations. As with the *in vitro* oligomerisation assays, placing high concentrations of Galectin-3 and Aβ may artificially force interactions that may not be present under physiological conditions. As such, the aggregated species arising from Galectin-3 and Aβ in these assays may not represent those observed in disease.

Lastly, there could have been a host response due to the recognition of non-self antigens. The injected Galectin-3 (both full length and CRD), and Aβ were human recombinant proteins. Since Galectin-3 functions as a Pattern Recognition Receptor, the increased host-derived Galectin-3 expression could reflect a general immune response against foreign antigens. Furthermore, the full length Galectin-3 was expressed in E. coli, and there could be endotoxins which could also trigger host immune response.

Future work could either test the preparations for endotoxins, or use recombinant proteins expressed in other systems (e.g. human embryonic kidney, HEK cells) or of synthetic origin. Furthermore, the use of mouse recombinant Galectin-3 could also ascertain that the host immune response to recombinant Galectin-3 is not due to cross species differences.

7.5.5.3 Limited quantification of deposits

In my work, assessment of Aβ deposition is largely based on histological observation, which is inherently qualitative or semi-quantitative. While this approach allows localisation of deposits, it limits the ability to accurately quantify differences in Aβ load between conditions. Future work should incorporate more quantitative biochemical approaches. Western blotting of brain homogenates can be used to detect Aβ species across different molecular weights, allowing comparison of soluble versus insoluble fractions and providing insight into the distribution of oligomeric and higher-order aggregates. ELISAs and Homologous Time Resolved Fluorescence (HTRF)-based assays offer greater sensitivity and specificity for quantifying total Aβ levels. Sequential extraction protocols (e.g., PBS-, detergent-, and formic acid–soluble fractions) can further distinguish between soluble and insoluble Aβ pools, enabling a more detailed characterisation of aggregation state. This would allow determination of whether observed differences in deposition reflect increased total Aβ. Quantitative analyses would strengthen conclusions by providing objective measures of Aβ burden and enabling more precise evaluation of the effects of Galectin-3 on aggregation and deposition *in vivo*.

Chapter 8: Final discussion

8.1 Overview and mechanistic model

This thesis investigated whether Galectin-3 acts as a regulator of hippocampal neurogenesis, glial activation, Aβ uptake, and Aβ aggregation. The findings support a model in which Galectin-3 does not act through a single linear pathway, but instead functions as a context-dependent mediator linking glial biology, extracellular protease activity, and amyloid aggregation.

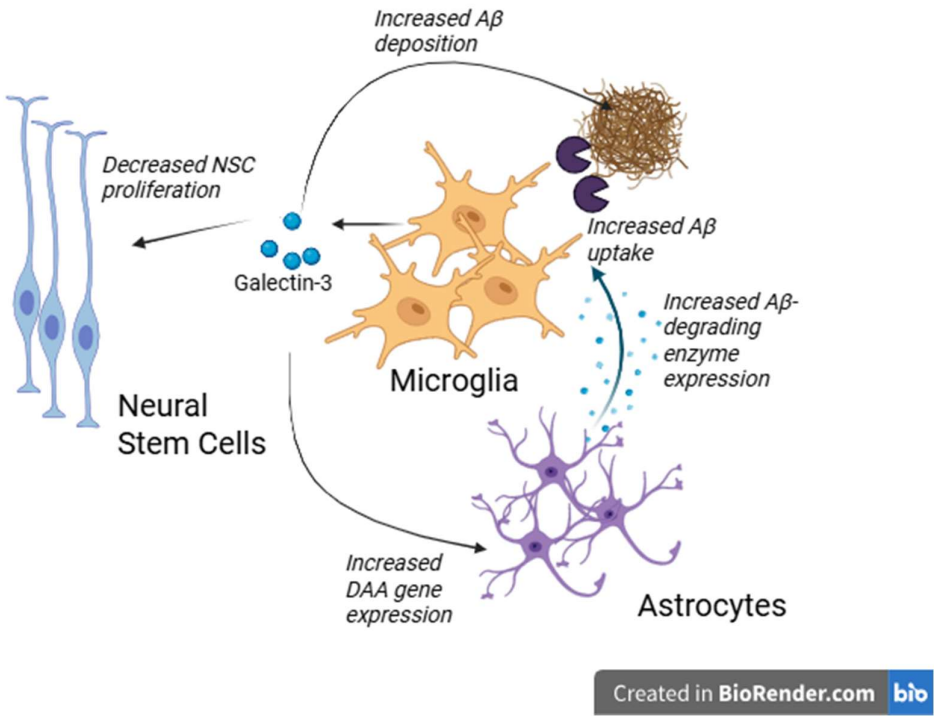


Figure 8.1: Central model integrating Galectin-3, Aβ and glial biology.

The central model arising from my work is that Galectin-3 can influence Alzheimer's disease-relevant biology through two partially separable mechanisms. First, Galectin-3 can act directly on Aβ, promoting the formation of high molecular weight oligomers and facilitating deposition. Second, Galectin-3 can act on glial cells, particularly astrocytes, to alter expression of amyloid-degrading enzymes, including MMP9, thereby modifying Aβ processing and subsequent

microglial uptake. These mechanisms converge on Aβ accumulation and clearance, while also providing a route through which Galectin-3 may indirectly affect the neurogenic niche.

This framework reconciles the major findings of the thesis: Galectin-3 reduced neural stem cell proliferation *in vitro* but did not significantly alter hippocampal neurogenesis in healthy adult mice; Galectin-3 knockout altered microglial morphology but did not induce broad changes in DAM gene expression; Galectin-3 altered astrocytic DAA-associated gene expression and increased MMP9; Galectin-3 enhanced microglial Aβ uptake only in the presence of astrocytes; and full-length Galectin-3, but not Galectin-3C alone, promoted Aβ oligomerisation and deposition.

Altogether, these findings suggest that Galectin-3 is best understood as a multicellular and context-dependent regulator rather than as a direct driver of one isolated pathological pathway.

8.2 Galectin-3 and hippocampal neurogenesis

One aim of my thesis was to determine whether Galectin-3 regulates hippocampal neurogenesis. This was motivated by previous work showing that Galectin-3 regulates postnatal SVZ neurogenesis and gliogenesis (Al-Dalahmah, Campos Soares, et al., 2020), together with evidence that adult hippocampal neurogenesis is altered in Alzheimer's disease (discussed in chapter 1). *in vitro*, recombinant Galectin-3 reduced neurosphere size without altering differentiation into neurons or astrocytes. This suggests that Galectin-3 can directly suppress neural stem cell proliferation under simplified culture conditions. However, this effect was not clearly reproduced *in vivo*. Galectin-3 knockout did not significantly alter the density of label-retaining neural stem cells, neuroblasts, or post-mitotic neurons in the adult hippocampus. Similarly, Galectin-3 knockout did not significantly alter the distribution of newly generated neurons within the granule cell layer. These findings indicate that, under homeostatic conditions, endogenous Galectin-3 is not a major regulator of adult hippocampal neurogenesis.

The discrepancy between the *in vitro* and *in vivo* findings is important. *in vitro* neurosphere assays isolate neural progenitors from their niche and expose them to defined concentrations

of recombinant Galectin-3. In contrast, *in vivo* hippocampal neurogenesis occurs within a complex environment shaped by astrocytes, microglia, vasculature, extracellular matrix, neuronal activity, and systemic factors. It is therefore possible that Galectin-3 can act directly on neural progenitors, but that this effect is buffered *in vivo* by the surrounding niche.

A second explanation is that Galectin-3 expression in the healthy adult hippocampus may be too low to exert a strong effect on neurogenesis. Galectin-3 expression is markedly increased in Alzheimer's disease models and after inflammatory stimulation, suggesting that its effects on the neurogenic niche may become more relevant under pathological conditions. Thus, the absence of a strong phenotype in healthy mice does not exclude a role for Galectin-3 in regulating neurogenesis in disease, where Galectin-3 levels, glial activation, and inflammatory signalling are substantially altered.

This interpretation positions neurogenesis as a downstream and context-dependent endpoint of Galectin-3 activity. Galectin-3 may affect neural progenitors directly, but its more physiologically relevant effects may occur indirectly through modulation of glial cells, inflammatory mediators, and amyloid pathology.

8.3 Galectin-3 and glial biology

Galectin-3 is strongly associated with glial activation in AD, where it is upregulated in plaque-associated microglia and disease-associated microglial populations (Grubman et al., 2021; Keren-Shaul et al., 2017). It has also been implicated in inflammatory signalling, including responses to Aβ and LPS (Burguillos et al., 2015). Based on this literature, Galectin-3 was expected to influence microglial activation and disease-associated gene expression.

The findings of my thesis complicate this view. Firstly, microglia expressing Galectin-3 were not morphologically distinct from non-expressing microglia in WT mice, suggesting that Galectin-3 expression alone is not sufficient to define a morphologically reactive microglial state under homeostatic conditions. However, Galectin-3 knockout increased microglial ramification, particularly in middle-aged mice, indicating that endogenous Galectin-3 can influence microglial morphology. While increased ramification may reflect reduced activation,

microglial morphology does not directly define function and morphological analysis alone cannot establish inflammatory phenotype. Therefore, while the morphology data support a role for Galectin-3 in shaping microglial state, it should not be overinterpreted as proof of altered microglial function.

At the transcriptional level, Galectin-3 modulation did not significantly alter selected DAM-associated genes in primary microglia or BV2 cells. This suggests that Galectin-3 alone is not sufficient to induce a DAM-like state *in vitro*. DAM states arise in complex disease environments involving chronic Aβ exposure, plaque proximity, astrocytic interactions, and tissue-level inflammatory cues. Simplified *in vitro* monoculture systems cannot reproduce this environment. Hence, this negative result does not rule out a role for Galectin-3 in DAM biology *in vivo*.

In contrast, Galectin-3 altered DAA-associated gene expression in astrocytes. This suggests that astrocytes may be more transcriptionally responsive than microglia to Galectin-3 under these experimental conditions. However, as with DAM markers, DAA-associated gene expression should not be equated with a full disease-associated astrocyte state. Nevertheless, this suggests that Galectin-3 may regulate glial biology less by directly inducing microglial DAM identity, and more by altering astrocytic state and astrocyte-mediated control of microglial function.

8.4 Astrocyte–microglia crosstalk and Aβ uptake

One of the key findings of my thesis is that Galectin-3 increased microglial uptake of pHrodo-labelled Aβ in mixed glial cultures, but not in BV2 microglia or purified primary microglia. This indicates that the increased uptake is not purely cell-autonomous to microglia. Instead, astrocytes are required for the Galectin-3-mediated increase in Aβ uptake. Astrocyte conditioned medium experiments further support this interpretation, as Galectin-3-treated astrocyte-conditioned medium increased microglial Aβ uptake. This suggests that soluble astrocyte-derived factors are sufficient to mediate at least part of the effect. However, direct contact-dependent mechanisms cannot be fully excluded in mixed cultures, and the pHrodo

assay itself measures acidification rather than uptake alone. Lastly, I did not ascertain whether the Aβ was degraded by microglia, or merely accumulated in lysosomes. Therefore, the effect should be described as increased Aβ uptake-associated pHrodo signal, rather than increased degradation.

This finding supports a multicellular model in which Galectin-3 acts on astrocytes, which then modify the extracellular environment and influence microglial Aβ uptake. This is consistent with the broader literature showing that astrocytes and microglia reciprocally regulate each other's activation states in neurodegenerative disease.

The mixed glia culture data also help reconcile the lack of DAM gene induction. In this case, microglial Aβ uptake was altered only when astrocytes were present, suggesting that the effect of Galectin-3 may occur through astrocyte-derived signalling rather than through a cell-intrinsic DAM program.

8.5 MMP9 as part of a broader protease network

The data in my thesis identify MMP activity as a potential mediator of Galectin-3-dependent Aβ uptake. Galectin-3 increased the expression of amyloid-degrading enzymes in astrocytes, including Mmp2, Mmp9, and Scarb1, and increased both pro-MMP9 and active MMP9 protein levels in mixed glial cultures. Inhibition of MMP activity with Marimastat reduced Aβ uptake in mixed glial cultures and attenuated the Galectin-3-mediated increase in pHrodo signal. Together, these findings support a model in which Galectin-3 acts on astrocytes to modify the extracellular environment, thereby influencing the form of Aβ encountered by microglia and hence microglial uptake.

MMP9 may contribute to this by cleaving Aβ, thus altering its aggregation state or modifying receptor accessibility. In this model, astrocytes alter the form of Aβ that microglia encounter via secreted amyloid degrading enzymes. However, since Marimastat is a broad-spectrum MMP inhibitor, and astrocytes express multiple amyloid-degrading enzymes, MMP9 may not be the sole regulator of this process. Therefore, MMP activity contributes to the Galectin-3-

mediated increase in Aβ uptake, with MMP9 representing one component of a broader astrocyte-derived protease network. Further work would be required to establish whether MMP9 is necessary and sufficient. Such experiments could include selective MMP9 inhibition, Mmp9 knockout astrocytes, recombinant MMP9 rescue, or direct biochemical analysis of Aβ species after exposure to Galectin-3-treated astrocyte-conditioned medium.

8.6 MMP9 as a context-dependent modulator of Aβ processing and neurodegeneration

In the central nervous system (CNS), MMP9 has roles in neural development, synaptic plasticity, angiogenesis, and neural progenitor migration (Cai et al., 2017; Dziembowska & Wlodarczyk, 2012; Gore et al., 2021; Kang et al., 2008). In the context of AD, MMP9 is also relevant because it can degrade Aβ, including fibrillar Aβ, and has been detected in association with Aβ pathology (Py et al., 2014; Yan et al., 2006).

In this thesis, I show that Galectin-3-mediated upregulation of astrocytic MMP9 could plausibly alter Aβ by proteolytic cleavage, which could lead to altered aggregation states, changes in solubility, or changes in receptor accessibility prior to microglial uptake. However, it is crucial that MMP9 should not be presented as a solely protective mediator. Although MMP9 can contribute to Aβ degradation, its role in AD is likely context dependent.

8.6.1 MMP9 can contribute to AD pathologies

Bruno and Cuello show that Mmp9 degrades mature NGF (Bruno & Cuello, 2006), and that NGF is altered in AD patients alongside an upregulation of Mmp9 levels and activity (Bruno et al., 2009). Nerve Growth Factor (NGF) is essential for the survival and function of basal forebrain cholinergic neurons (BFCN), with heterozygous NGF mutants showing reduced Choline acetyltransferase^{+} cell numbers and size, along with cognitive defects (Chen et al., 1997). In AD, BFCNs are especially vulnerable, with loss of BFCN activity being characteristic.

In addition, MMP9 can cleave Tau into fragments with increased pro-aggregatory properties (Frost et al., 2009; Nubling et al., 2012).

8.6.2 MMP9 leads to blood brain barrier (BBB) breakdown in AD and other neurological conditions

Aβ deposits around arteries are commonly seen in AD patients which can lead to cerebral amyloid angiopathy (CAA) (Jellinger, 2002). Both matrix metalloproteinase 2 (MMP2) and MMP9 are observed in CAA vessels in AD patients and mouse models, with levels higher in haemorrhagic brain regions (Hernandez-Guillamon et al., 2012). Work by Mulder and colleagues (2012) has shown that primary human astrocytes upregulate amyloid degrading enzymes including MMPs 2/9 when exposed to Aβ (Mulder et al., 2012). Together, these show that Aβ pathology could induce expression of MMPs 2/9, which could lead to degradation of the BBB, resulting in complications such as haemorrhagic bleeds.

Mmp9 levels are upregulated after cerebral ischemic stroke (Turner & Sharp, 2016) and has been shown to lead to BBB breakdown (Asahi et al., 2001; Mun-Bryce & Rosenberg, 1998), with increasing levels of Mmp9 correlating with poor outcomes (Inzitari et al., 2013). Additionally, knockout of Mmp9 protected postnatal mice from BBB breakdown after hypoxia-ischemia (Svedin et al., 2007).

Taken together, these suggest that the upregulation of MMP9 in AD can contribute to BBB breakdown. Since inhibition of MMP9 after hypoxia-ischemia is BBB-protective, MMP9 inhibition may also be beneficial in AD where BBB breakdown is seen. To this end, knockout of MMP9 has been shown to rescue cognitive deficits in both Aβ injected mice (Mizoguchi et al., 2009) and in 5xFAD mice (Ringland et al., 2021).

Altogether, Galectin-3-dependent induction of MMP9 may contribute to Aβ clearance in one context while promoting other pathological processes in another.

8.7 Galectin-3, inflammation, and MMP9 *in vivo*

The *in vivo* LPS experiments described in my work extend the Galectin-3–MMP9 axis into an inflammatory context. In primary cultures, Galectin-3 knockout reduced the LPS-induced increase in MMP9, suggesting that endogenous Galectin-3 contributes to inflammatory regulation of MMP9 *in vitro*. This is consistent with the broader role of Galectin-3 as an inflammatory mediator and with the ability of LPS to induce Galectin-3 expression in microglia and brain tissue.

However, the *in vivo* findings were more complex. Peripheral LPS increased MMP9 levels in the brain, but the effect of Galectin-3 knockout differed between sexes. In males, Galectin-3 knockout showed a trend towards reducing LPS-induced MMP9, broadly aligning with the *in vitro* glial culture findings. In females, the effect was reversed, with Galectin-3 knockout increasing the LPS-mediated MMP9 response. This indicates that Galectin-3 may not regulate MMP9 uniformly across biological contexts. However, the small sample size (n = 3 per condition and sex) limits interpretation of the results.

These findings have two major implications. First, they support the idea that Galectin-3 participates in inflammatory regulation of MMP9. Second, they show that this regulation is sex-dependent and context-sensitive. Galectin-3 should therefore not be described simply as a positive regulator of MMP9. Its effect likely depends on cellular composition, inflammatory stimulus, sex, and the balance between central and peripheral immune signalling.

This complexity is important in the context of AD. MMP9 has potentially beneficial effects through Aβ degradation, but also potentially harmful effects through Tau cleavage, NGF degradation, extracellular matrix remodelling, and BBB disruption. Thus, whether Galectin-3-mediated regulation of MMP9 is protective or detrimental may depend on disease stage and tissue context. For example, increased MMP9 could support Aβ clearance in a glial environment where proteolytic degradation is dominant, but contribute to vascular instability or neuronal vulnerability where BBB breakdown, CAA, or Tau pathology are prominent.

Lastly, if Galectin-3 inhibition reduces MMP9 in one sex or context but increases it in another, targeting Galectin-3 may not produce uniform downstream effects. Further understanding of how Galectin-3 may differentially regulate MMP9 levels in a sex-dependent manner will allow us to stratify patients based on sex and improve therapeutic outcomes. This is particularly relevant for AD, where sex differences in disease prevalence, immune responses, and glial biology have been described. My data therefore strengthen the mechanistic link between Galectin-3 and inflammatory MMP9 regulation, but also indicate that Galectin-3-targeted therapies would require careful consideration of sex, inflammatory state, and disease stage.

Overall, these findings position MMP9 as a context-dependent downstream mediator within the broader Galectin-3 network. Rather than acting as a simple linear pathway, Galectin-3 appears to sit at the intersection of amyloid processing and glial reactivity. This supports the central model of the thesis: Galectin-3 links Aβ aggregation and glial biology through multiple interacting mechanisms, with MMP9 acting as one important but non-exclusive component.

8.8 Galectin-3 and Aβ aggregation

The final component of the mechanistic model concerns the direct effect of Galectin-3 on Aβ aggregation. *In vivo*, Aβ alone did not induce detectable deposits after intrahippocampal injection, whereas co-injection of Aβ with full-length Galectin-3 induced Aβ deposition. Importantly, full-length Galectin-3 also induced Aβ deposition in Galectin-3 knockout mice, demonstrating that exogenous full-length Galectin-3 was sufficient to promote deposition without host-derived Galectin-3.

The Galectin-3 Carbohydrate recognition domain (Galectin-3C) experiments refine this conclusion. In WT mice, Aβ co-injected with Galectin-3C produced deposits, but Galectin-3 immunoreactivity appeared to be host-derived. In Galectin-3 knockout mice, Aβ with Galectin-3C did not induce deposition. Therefore, Galectin-3C alone was not sufficient to promote Aβ deposition under these conditions. Instead, the WT Galectin-3C result is best interpreted as a host-response effect, in which Galectin-3C and/or Aβ induced endogenous full-length Galectin-3, which then contributed to deposition.

The *in vitro* aggregation assays support this interpretation. Full-length Galectin-3 promoted the formation of high molecular weight Aβ oligomers and increased Thioflavin T signal, whereas Galectin-3C did not promote comparable high molecular weight oligomer formation. These findings suggest that the N-terminal oligomerisation domain of Galectin-3 is required for its ability to promote high-order Aβ assembly.

This provides a direct biochemical arm of the model: full-length Galectin-3 can promote Aβ oligomerisation and deposition through its oligomerisation capacity. This mechanism is distinct from, but potentially interacts with, the glial mechanism described above. Galectin-3 may both promote Aβ aggregation directly and alter Aβ uptake indirectly through astrocyte-mediated changes in protease activity.

This raises the question of Galectin-3's role in Aβ oligomerisation, whether this is an intrinsic function of Galectin-3, or a byproduct of Galectin-3 biology. Galectin-3 has been shown to promote phagocytosis of glycosylated cargo by acting as an opsonin. In this model, it binds to MerTK on microglia as well as its cargo to promote clearance of neuronal debris, myelin, and bacteria (Cockram et al., 2019; Reichert et al., 1994; Yip et al., 2017). It is possible that Galectin-3 intrinsically binds to Aβ, acting as a damage associated molecular pattern to promote clearance of Aβ amongst other debris. Unlike other cargo that Galectin-3 recognizes, Aβ has the potential to aggregate into cytotoxic forms. This is also observed in the case of Tau, where Galectin-3 also promotes its aggregation (Siew et al., 2024). As such, it is likely that while the intrinsic role of Galectin-3 is to opsonise debris for clearance by immune cells, the role of Galectin-3 in Aβ oligomerisation is extrinsic.

8.9 Integrating Galectin-3, Aβ aggregation, MMP9, and neurogenesis

The findings support an integrated model in which Galectin-3 links amyloid pathology, glial biology, and neurogenesis through both direct and indirect mechanisms.

At the molecular level, full-length Galectin-3 promotes Aβ oligomerisation and deposition. This effect requires the N-terminal oligomerisation domain, as Galectin-3C alone was insufficient to promote high molecular weight Aβ oligomers or deposition in Galectin-3 knockout mice.

At the cellular level, Galectin-3 acts on astrocytes to alter expression of DAA-associated genes and amyloid-degrading enzymes, including MMP9. This changes the extracellular environment in which microglia encounter Aβ. Increased MMP activity may alter Aβ structure, solubility, or receptor accessibility, thereby affecting uptake by microglia. The fact that Galectin-3 increased pHrodo-Aβ signal only in mixed glial cultures indicates that astrocyte–microglia crosstalk is central to this mechanism. Galectin-3 also acts on neural stem cells, decreasing proliferation directly but not differentiation.

At the tissue level, these glial and amyloid-related processes may influence the hippocampal neurogenic niche. Galectin-3 directly reduced neural stem cell proliferation *in vitro*, but its knockout did not significantly alter hippocampal neurogenesis in healthy adult mice. This suggests that Galectin-3 may have the capacity to influence neurogenesis, but that its effects are context-dependent *in vivo*. In Alzheimer's disease, where Galectin-3, Aβ, glial activation, and inflammatory proteases are all elevated, hippocampal neurogenesis may be diminished by a combination of these factors.

Thus, Galectin-3 may affect neurogenesis in disease less as a direct stem-cell regulator and more as a modifier of the inflammatory and amyloid-rich niche. This model links the neurogenesis findings with the glial and Aβ aggregation findings, rather than treating them as separate outcomes.

8.10 Galectin-3 and ageing

Serum Galectin-3 levels increase with age in the general population (de Boer et al., 2012), and multiple diseases have been associated with increased levels of Galectin-3.

Oxidized phosphatidylcholines (OxPCs) are neurotoxic lipid byproducts of oxidative stress that accumulate with age (Dong & Yong, 2022). In ageing mouse spinal cord, increased Galectin-3 is correlated with neurodegeneration. Co-injection of Galectin-3 with OxPC exacerbated

OxPC induced neuroinflammation and neurodegeneration, and the converse is true where Galectin-3$^{-/-}$ mice show reduced OxPC-mediated damage (Xue et al., 2023). This suggests that Galectin-3 may synergise with other age-associated markers, further increasing disease phenotypes.

Galectin-3 has also been proposed as a biomarker of frailty. Increased Galectin-3 was correlated with higher frailty scores, C-reactive protein and IL-6 levels (Ji et al., 2023), suggesting that Galectin-3 could be promoting macrophage inflammatory signalling, which could result in inflammaging.

Hence, in aged tissues, Galectin-3 adopts a more pro-inflammatory role, contributing to chronic inflammation. This contrasts with developing tissues where Galectin-3 has other roles including cell adhesion and apical basal polarity (Soares et al., 2025).

8.11 Galectin-3 in AD patients

Single-cell RNA-sequencing analyses of patient samples show stronger upregulation of Galectin-3 in monocytes and astrocytes as compared to microglia (Olah et al., 2020). In mice, Galectin-3 is also expressed in ependymal cells (Comte et al., 2011). One possible explanation is that mouse models of AD tend to exhibit more severe pathologies, which may account for the robust increase of microglial Galectin-3 observed in these systems. In these models, we see Galectin-3 expressing microglia around Aβ plaques. A similar observation was made in human AD brain samples (Boza-Serrano et al., 2019). Hence, the relatively low detection of microglia expressing Galectin-3 in human single cell RNA sequencing studies could reflect that the Galectin-3-expressing population is enriched in plaque adjacent microglia and is consequently under-represented in single-cell RNA sequencing analyses.

Importantly, Galectin-3 can be secreted and has been shown to be upregulated in patient CSF and sera (Ashraf & Baeesa, 2018; Boza-Serrano et al., 2022), suggesting that extracellular Galectin-3 may play a more significant role in disease progression. Consistent with this, I show that Galectin-3 treatment of murine astrocytes increased expression of disease-associated genes and ECM remodelling enzymes. Hence, while Galectin-3 expression by microglia as

detected by scRNAseq studies may appear low, increased Galectin-3 levels in patient serum and CSF supports the relevance of Galectin-3 in AD. Future work employing spatial transcriptomics can determine if Galectin-3 expressing microglia are enriched around Aβ plaques.

8.12 Implications for Galectin-3 as a therapeutic target

The data presented in this thesis support Galectin-3 as a plausible therapeutic target in Alzheimer's disease, but also indicate that its functions are complex. Inhibition of Galectin-3 may reduce Aβ aggregation directly by preventing Galectin-3-mediated oligomerisation. It may also alter glial responses, including astrocyte activation and MMP9 regulation. These effects could be beneficial if they reduce pathological aggregation or excessive neuroinflammatory signalling.

However, my findings also indicate that Galectin-3 inhibition may have context-dependent consequences. Galectin-3 increased microglial Aβ uptake in mixed glial cultures through astrocyte-derived factors, suggesting that Galectin-3 can also enhance aspects of Aβ clearance or processing. Complete inhibition of Galectin-3 could therefore have both beneficial and detrimental effects depending on disease stage, cell type, and local pathology.

This is particularly important for MMP9. MMP9 may contribute to Aβ degradation and uptake, but it can also participate in inflammatory tissue remodelling and blood–brain barrier disruption. Therefore, Galectin-3-dependent regulation of MMP9 should not be assumed to be uniformly protective or harmful. Instead, the therapeutic value of targeting Galectin-3 likely depends on whether the dominant disease process is Aβ aggregation, impaired clearance, glial inflammation, or vascular dysfunction.

8.12.1 Clinical trials with Galectin-3 as a target

Human patients with liver fibrosis show increased Galectin-3 expression associated with cirrhotic nodules, and this is also seen in the CCl_4 model of liver fibrosis in rats (Henderson et al., 2006). Crucially, while Galectin-3 knockout did not alter the initial injury caused by CCl_4,

small interfering RNA (siRNA) inhibition of Galectin-3 decreased hepatic stellate cell (HSC) activation as evidenced by decreased alpha-smooth muscle actin (α-SMA) (Henderson et al., 2006).

Administration of adenoviral-TGF-β1 into mice induced fibrosis of the lung, with interstitial areas showing increased collagen (Mackinnon et al., 2012). Immunohistochemical staining reveal expression of Galectin-3 by alveolar macrophages, with increases in Galectin-3 levels in the bronchoalveolar lavage fluid (Mackinnon et al., 2012). In Galectin-$3^{-/-}$ mice, the effect of adenoviral-TGF-β1 was ameliorated (Mackinnon et al., 2012).

Similar effects of Galectin-3 modulation were observed in other fibrotic conditions including renal fibrosis and arteriosclerosis (Henderson et al., 2008; MacKinnon et al., 2013).

As such, inhibitors of Galectin-3 have been tested in clinical trials for treatment of fibrotic conditions. Inhaled TD-139/GB0139 was tested for treatment of idiopathic pulmonary fibrosis (NCT03832946) and GR-MD-02 was tested for treatment of liver fibrosis (Harrison et al., 2018). However, while these showed promise in pre-clinical models, clinical trials were terminated after a lack of efficacy.

In AD, TrueBinding had an ongoing clinical trial (NCT05476783) for TB006, an α-Galectin-3 monoclonal antibody (mAb). Unfortunately, the trial was prematurely terminated due to resource constraints. Nonetheless, it highlights the potential for Galectin-3 as a target in AD, and my work suggests several processes that Galectin-3 is involved in that can be targeted by using Galectin-3 inhibitors in AD treatment.

8.12.2 Galectin-3 inhibition as a BBB protective therapy

In Chapter 6, I show that treatment of primary murine astrocytes with Galectin-3 increases MMP9 levels. This was previously observed in other cell types. I also show that Galectin-$3^{-/-}$ astrocytes have a diminished response to LPS in terms of MMP9 secretion. As it is well known that MMP9 contributes to the breakdown of the BBB, this is of great interest as it highlights how Galectin-3 inhibition could potentially protect against BBB breakdown both in ageing (as Galectin-3 is increased with age, and could potentially increase MMP9 levels) and in disease.

Furthermore, Galectin-3 also appears to increase microglial reactivity, with the increase in Galectin-3 in WT 7M mice, there was a bigger difference between microglia from Galectin-$3^{+/+}$ and Galectin-$3^{-/-}$ mice at middle-age than there was in young mice, suggesting that the increased Galectin-3 could have a role in this.

Altogether, these seem to highlight a potential for inhibition of Galectin-3 as protective against the effects of ageing in addition to being a possible target in AD (Knox et al., 2022).

8.12.3 Galectin-3 inhibition could reduce neuroinflammation

In Chapter 4, I have shown that knockout of Galectin-3 *in vivo* increased ramification of microglia, even in healthy young adult mice and more so in middle-aged mice (Figures 4.4.2 and 4.4.3). In disease, Galectin-3 is upregulated and could have a stronger effect on microglial state. Furthermore, treatment of primary murine astrocytes with exogenous Galectin-3 induced expression of the disease-associated astrocyte (DAA) genes Clu, Gsn in a similar manner as treatment with $A\beta O_{1-42}$ did. Galectin-3 also increased expression of Fxyd1 and Serpina3 independent of $A\beta O_{1-42}$. Hence, inhibition of Galectin-3 could be beneficial by reducing the expression of disease associated glial genes, and groups are already identifying BBB-penetrant molecules which can inhibit Galectin-3 (Liu et al., 2025).

8.12.4 Galectin-3 inhibition could increase neurogenesis

In Chapter 3, I showed that addition of Galectin-3 to neurosphere cultures decreased proliferation of neural stem cells (Figure 3.2.1). While in healthy WT mice knockout of Galectin-3 did not significantly alter neurogenesis, I have shown that Galectin-3 is mostly detected in the CA1 in the hippocampus under homeostatic conditions. In AD, Aβ plaques are found in the dentate gyrus in both human patients (Thal et al., 2002) and mouse models of AD. Galectin-3 has been shown to colocalise with Aβ plaques and has been correlated with cognitive decline (Boza-Serrano et al., 2022). As there are increased levels of Galectin-3 in AD, inhibition of Galectin-3 may also increase neurogenesis in these conditions.

8.13 Limitations of current work

8.13.1 Cx3cr1-GFP mice

In my phagocytosis assays, I used primary glial cells extracted from Cx3cr1-GFP$^{+/-}$ pups. Previously, I highlighted that microglia proliferate once the astrocytic layer is confluent. As such, if I had used WT glia, I would not have been able to distinguish if the phagocytosis was occurring in microglia or astrocytes. Using Cx3cr1-GFP$^{+/-}$ glia allowed me to address this. However, Cx3cr1 knockout mice have previously been shown to have increased phagocytosis of Aβ (Liu et al., 2010). This was also true of their microglia *in vitro*, where the authors showed increased $A\beta_{1\text{-}42}$ uptake by Cx3cr1$^{-/-}$ microglia (Liu et al., 2010). While other work has also shown that Cx3cr1-GFP$^{+/-}$ mice are significantly different from Cx3cr1-GFP$^{-/-}$ mice in terms of phagocytosis (Zabel et al., 2016), knockdown of Cx3cr1 in APP/PS1 mice (Cx3cr1$^{+/-}$) have been shown to increase Aβ phagocytosis (Hickman et al., 2019; Lee et al., 2010). While I showed that Galectin-3 increased phagocytosis by microglia via astrocytic secretion of MMPs, it was possible that Cx3cr1-GFP$^{+/-}$ microglia had increased capacity for phagocytosis of Aβ, and in WTs, the upregulation of MMP9 would not have altered phagocytosis by microglia. One possible improvement would be to use WT microglia stained with CellTracker Green (Invitrogen, C7025) in the conditioned media experiments. To improve on this further, I believe that using the hiPSC models I discussed previously may recapitulate human disease more so than primary murine cells.

8.13.2 Primary glial cultures

In Chapters 4 and 5, I performed gene expression and functional analyses on primary glia under various conditions – in monoculture, with astrocyte conditioned medium, and in co-cultures.

8.13.2.1 Sources of glial cultures

The primary glial cells used in my experiments were isolated from neonates. In adult microglia, regional differences in gene expression and morphology have been noted by multiple studies (Tan et al., 2020). Since Aβ plaques are observed mostly in the hippocampus in early phases of the disease, it is possible that glia in different brain regions may have different plaque clearing abilities. In addition to regional heterogeneity of microglia, neonates also have a subpopulation of microglia in a highly activated state (Hammond et al., 2019). Hence, care was taken during the dissection of the brain to only include the cortex and hippocampus. However, the possibility that other brain regions were present in the cultures cannot be excluded.

8.13.2.2 Purified glial cultures

To obtain cultures of purified microglia and astrocytes, microglia were dissociated from mixed glial cultures derived from whole mouse forebrains by mechanical shaking. Firstly, such mechanical methods may result in contamination by other cell types. Next, while purified glial cultures provide a controlled system to assess cell-autonomous responses, they represent a highly reductionist model of glial biology. By isolating microglia or astrocytes, these systems remove confounding influences from other cell types, allowing direct interrogation of whether Galectin-3 acts intrinsically on a specific population. However, glial cells *in vivo* exist within a complex network of bidirectional signalling involving astrocytes, microglia, neurons, amongst other cells. In the absence of these interactions, purified glia lack key regulatory inputs and may adopt altered activation states, which can lead to both false-negative and misleading interpretations.

8.13.2.3 Mixed glial cultures

In mixed glial cultures, both astrocytes and microglia may contribute to the observed outcomes, making it difficult to resolve the cellular source of specific effects. As a result, changes such as increased Aβ uptake cannot be definitively attributed to a direct

microglial response to Galectin-3, astrocyte-mediated signalling, or a combination of both. For example, the enhanced Aβ uptake observed in chapter 5 may arise from astrocyte-secreted factors, alterations in Aβ processing, or changes in microglial reactivity due to glial crosstalk. This lack of cellular resolution limits mechanistic interpretation and complicates the identification of the primary driver of the observed phenotype.

The mixed glial cultures may also not accurately reflect physiological microglia-to-astrocyte ratios. As a result, the balance of signalling between these cell types is likely altered, potentially amplifying paracrine interactions. Consequently, effects arising from astrocyte–microglia crosstalk, such as changes in Aβ uptake, may be exaggerated under these conditions and may not scale proportionally in the intact brain. This limits the extent to which findings from mixed cultures can be directly extrapolated to *in vivo* glial dynamics.

8.13.2.4 Conclusions

Future work can use immunopanning or cell sorting to ensure that purified cultures do not contain any contaminating cells. This can also allow more precise control of microglia-to-astrocyte ratios to better recapitulate physiological ratios. Another possible improvement would be the use of human cells. In addition to the control of cellular ratios, hiPSC-microglia and hiPSC-astrocyte media can be fully defined and serum-free (Canals et al., 2018; van Wilgenburg et al., 2013), reducing differences between cultures in the long term.

Alternatively, *ex vivo* organotypic cultures can also be used to replicate the cellular ratios and incorporate signals from other neural cells. Thereafter, immunocytochemical or immunohistochemical analysis can be used to identify the effects of treatments on each cell type by co-labelling with cell-specific markers, or cell sorting prior to qPCR

or western blotting will provide better resolution as to the relative contribution of each cell population to the observed effects.

8.13.3 Use of human rGalectin-3 and $A\beta_{1-42}$ in murine models

In my work, I have used human recombinant proteins (Galectin-3, Galectin-3C and $A\beta_{1-42}$). These may affect murine cells and brains differently than mouse proteins would.

Importantly, I showed that human Galectin-3 interacts with human $A\beta_{1-42}$ to promote its aggregation (Chapter 7). However, it is important to note that these experiments were performed either *in vitro* (ThT aggregation assay) or within the murine brain (stereotaxic injections). In the latter, the exogenous (human) proteins may have different interactions with the host (murine) proteins.

Galectin-3 has multiple binding partners involved in various cellular mechanisms including phagocytosis (triggering receptor expressed on myeloid cells 2, TREM2) (Boza-Serrano et al., 2019), immune signalling (TLR4) (Burguillos et al., 2015). Since Galectin-3 binds to β-galactoside-containing glycans, and glycosylation sites may have cross-species differences, the human isoform of Galectin-3 may have altered affinities to the murine binding partners. If so, the differences in the strength of interaction between Galectin-3 and its binding partners may exaggerate or dampen downstream signalling responses. This could lead to murine microglia and astrocytes having different responses as compared to human microglia and astrocytes. However, it is important to note that mouse and human Galectin-3 are highly conserved, and especially so for the carbohydrate recognition domain, as discussed in chapter 1.

8.13.4 Aβ-galectin-3 pre-incubation conditions

For experiments involving injections of $A\beta_{1-42}$, Aβ monomers dissolved in PBS were incubated for an hour at 37 °C either alone, with full length Galectin-3, or with C-terminal truncated Galectin-3 (Galectin-3C). As with the *in vitro* aggregation assays, pre-incubation at relatively high concentrations of Aβ and Galectin-3 imposes artificial

interaction conditions that may not reflect physiological levels. This may promote non-physiological binding and aggregation, potentially exaggerating the extent of Galectin-3–Aβ interactions and subsequent deposition. In addition, pre-incubation occurs in the absence of physiological binding partners, such as lipoproteins, extracellular matrix components, and other Aβ-interacting proteins. As a result, Galectin-3 and Aβ interact in a simplified environment that does not recapitulate the competitive and regulatory conditions present *in vivo*.

8.13.5 Limitations of pHrodo labelled Aβ

8.13.5.1 pHrodo measures acidification

While pHrodo labelling of Aβ provides a convenient readout of Aβ uptake by microglia, it does not directly measure uptake but rather the acidification of the environment surrounding pHrodo-labelled Aβ. Consequently, increases in pHrodo signal may reflect enhanced lysosomal acidification, more rapid trafficking of Aβ to acidic compartments, or increased uptake. Hence, treatments which alter lysosomal pH or metabolic state may also result in changes to pHrodo signal independent of the uptake of pHrodo-Aβ. In addition, impaired degradation of Aβ leading to accumulation within lysosomes can also increase pHrodo signal. Furthermore, pHrodo labelling does not provide information on the pathway of Aβ internalisation and does not capture early stages of uptake prior to acidification. To address these limitations, future work could employ pH-insensitive fluorescent labelling of Aβ in combination with co-localisation studies using endosomal and lysosomal markers to distinguish uptake from intracellular processing.

8.13.5.2 pHrodo labelling may alter receptor-ligand interactions

pHrodo-SE labels proteins via covalent reaction with free amine groups. Since pHrodo-SE has a molecular weight of 650 g/mol and $A\beta_{1\text{-}42}$ monomers are 4514 g/mol, a single pHrodo molecule represents over 14% of the mass of an Aβ monomer. Labelling monomers prior to oligomerisation therefore has the potential to interfere with aggregation, possibly altering the

kinetics or leading to off-pathway oligomer species. In addition, oligomerisation involves the formation of secondary structures, while pHrodo-SE labelling occurs through covalent modification of free amino groups. In monomeric $A\beta_{1-42}$, these amino groups are accessible; however, following oligomerisation, some labelled residues may become buried within the oligomeric structure. This could introduce variability in fluorescence signal independent of acidification. To minimise these effects, Aβ was labelled after oligomer formation, thereby reducing potential interference with aggregation and improving consistency in both oligomer structure and labelling efficiency.

However, pHrodo labelling of AβO may still result in changes to interactions between Aβ and its receptors due to alterations to the amine residues. Such changes may affect receptor-mediated uptake pathways and can alter how Aβ is internalised by microglia.

8.13.6 Sex-dependent effects

8.13.6.1 Sex-dependent effects in cell cultures

Both the neurosphere and primary glial cultures were derived from a mixture of male and female neonates, without stratification or tracking of sex. Previous work has shown that primary microglia isolated from adult male mice exhibit a more reactive phenotype than those from females (Villa et al., 2018). Similarly, while astrocytes from both sexes upregulate inflammatory markers such as IL6, IP10, TNFα and IL1β in response to LPS, male-derived astrocytes show a stronger transcriptional response (Santos-Galindo et al., 2011).

As the cultures used in this study contained glia from both sexes, variation in the male-to-female ratio across replicates may have introduced additional variability, particularly if responses to Galectin-3 are sex-dependent. Moreover, if male and female glia differ in the magnitude or direction of their responses, mixed-sex cultures may obscure or attenuate treatment effects, leading to underestimation or masking of biologically relevant differences. Hence, separation of the neonates into males and females before glia isolation will allow assessment of any sex-specific responses and determine whether the effects of Galectin-3 on glial function are sex-dependent.

8.13.6.2 *in vivo* experiments

In the neurogenesis experiments, both male and female mice were used; however, the sample size was insufficient to allow stratified analysis by sex. To minimise confounding factors, all female mice used were virgins, as pregnancy is known to alter hippocampal neurogenesis in rodents (Pawluski & Galea, 2007). However, while the oestrus cycle and estrogen have been shown to affect hippocampal neurogenesis (Tanapat et al., 1999), the oestrus cycles of female mice were not monitored in this study. As a result, variability in neurogenesis arising from hormonal cycling may have contributed to the observed data. Consequently, potential effects of Galectin-3 knockout on hippocampal neurogenesis may have been obscured or attenuated by uncontrolled differences in oestrus stage among female mice.

Male microglia have differing transcriptomic signature from female microglia *in vivo* (Villa et al., 2018). These could contribute to the sex differences in pro-inflammatory cytokine levels observed with inflammatory challenges (Erickson et al., 2018). In the experiments examining the effect of Galectin-3 knockout on LPS-induced MMP9 levels, stratification of the animals by sex revealed interactions between sex and the effect of Galectin-3 knockout. In females, a lower response to LPS was observed in WT mice, with LPS inducing more MMP9 in Galectin-3 knockout mice. However, this effect was the opposite in males. However, as with the neurogenesis experiments, the oestrus cycle of female mice was not monitored. Given that fluctuations in circulating hormones can influence inflammatory responses, variability in oestrus stage may have contributed to the observed differences and confounded interpretation. Consequently, while the data suggest sex-dependent regulation of MMP9 by Galectin-3, the lack of control for hormonal state limits the extent to which these effects can be clearly attributed to sex alone.

8.13.6.3 Conclusions

The experiments here lack robust sex-stratified analyses and hence may have missed any sex-dependent effects. Furthermore, due to the lack of oestrus monitoring, the sex differences observed in the LPS-induced models may have been confounded by oestrus stage. Future work should continue to include female mice, but larger sample sizes along with monitoring of oestrus cycles will allow better identification of any sex-dependent effects of Galectin-3 on neurogenesis and neuroinflammation.

Chapter 9: References

Akbor, M. M., Kurosawa, N., Nakayama, H., Nakatani, A., Tomobe, K., Chiba, Y., Ueno, M., Tanaka, M., Nomura, Y., & Isobe, M. (2021). Polymorphic SERPINA3 prolongs oligomeric state of amyloid beta. *PLOS ONE*, *16*(3), e0248027. https://doi.org/10.1371/journal.pone.0248027

Al-Dalahmah, O., Campos Soares, L., Nicholson, J., Draijer, S., Mundim, M., Lu, V. M., Sun, B., Tyler, T., Adorjan, I., O'Neill, E., & Szele, F. G. (2020). Galectin-3 modulates postnatal subventricular zone gliogenesis. *Glia*, *68*(2), 435–450. https://doi.org/10.1002/glia.23730

Al-Dalahmah, O., Nicholson, J., Draijer, S., Soares, L. C., & Szele, F. G. (2020). Galectin-3 diminishes Wnt signaling in the postnatal subventricular zone. *Stem Cells*, *38*(9), 1149–1158. https://doi.org/10.1002/stem.3202

Alonso-Moreno, M. C., Gallardo-Caballero, M., Pradanos-Senen, A. V., & Llorens-Martin, M. (2025). Human adult hippocampal neurogenesis in health and disease. *Aging Brain*, *8*, 100145. https://doi.org/10.1016/j.nbas.2025.100145

Amber, S., Sumera, Mirza, F. J., Asif, M., Hassan, D., Ahmed, T., & Zahid, S. (2020). Amyloid-beta induced neurotoxicity impairs cognition and adult hippocampal neurogenesis in a mouse model for Alzheimer's disease. *Current Alzheimer Research*, *17*(11), 1033–1042. https://doi.org/10.2174/1567205017666201224162730

Asahi, M., Wang, X., Mori, T., Sumii, T., Jung, J. C., Moskowitz, M. A., Fini, M. E., & Lo, E. H. (2001). Effects of matrix metalloproteinase-9 gene knock-out on the proteolysis of blood-brain barrier and white matter components after cerebral ischemia. *Journal of Neuroscience*, *21*(19), 7724–7732. https://doi.org/10.1523/JNEUROSCI.21-19-07724.2001

Ashraf, G. M., & Baeesa, S. S. (2018). Investigation of Gal-3 expression pattern in serum and cerebrospinal fluid of patients suffering from neurodegenerative disorders. *Frontiers in Neuroscience*, *12*, 430. https://doi.org/10.3389/fnins.2018.00430

Baglietto-Vargas, D., Sanchez-Mejias, E., Navarro, V., Jimenez, S., Trujillo-Estrada, L., Gomez-Arboledas, A., Sanchez-Mico, M., Sanchez-Varo, R., Vizuete, M., Davila, J. C., Garcia-Verdugo, J. M., Vitorica, J., & Gutierrez, A. (2017). Dual roles of Abeta in proliferative processes in an amyloidogenic model of Alzheimer's disease. *Scientific Reports*, *7*(1), 10085. https://doi.org/10.1038/s41598-017-10353-7

Baik, S. H., Kang, S., Son, S. M., & Mook-Jung, I. (2016). Microglia contributes to plaque growth by cell death due to uptake of amyloid beta in the brain of Alzheimer's disease mouse model. *Glia*, *64*(12), 2274–2290. https://doi.org/10.1002/glia.23074

Baligacs, N., Albertini, G., Borrie, S. C., Serneels, L., Pridans, C., Balusu, S., & De Strooper, B. (2024). Homeostatic microglia initially seed and activated microglia later reshape amyloid plaques in Alzheimer's disease. *Nature Communications*, *15*(1), 10634. https://doi.org/10.1038/s41467-024-54779-w

Banks, W. A., & Robinson, S. M. (2010). Minimal penetration of lipopolysaccharide across the murine blood-brain barrier. *Brain, Behavior, and Immunity*, *24*(1), 102–109. https://doi.org/10.1016/j.bbi.2009.09.001

Blasi, E., Barluzzi, R., Bocchini, V., Mazzolla, R., & Bistoni, F. (1990). Immortalization of murine microglial cells by a v-raf/v-myc carrying retrovirus. *Journal of Neuroimmunology*, *27*(2–3), 229–237. https://doi.org/10.1016/0165-5728(90)90073-v

Boza-Serrano, A., Ruiz, R., Sanchez-Varo, R., Garcia-Revilla, J., Yang, Y., Jimenez-Ferrer, I., Paulus, A., Wennstrom, M., Vilalta, A., Allendorf, D., Davila, J. C., Stegmayr, J., Jimenez, S., Roca-Ceballos, M. A., Navarro-Garrido, V., Swanberg, M., Hsieh, C. L., Real, L. M., Englund, E., . . . Deierborg, T. (2019). Galectin-3, a novel endogenous TREM2 ligand, detrimentally regulates inflammatory response in Alzheimer's disease. *Acta Neuropathologica*, *138*(2), 251–273. https://doi.org/10.1007/s00401-019-02013-z

Boza-Serrano, A., Vrillon, A., Minta, K., Paulus, A., Camprubi-Ferrer, L., Garcia, M., Andreasson, U., Antonell, A., Wennstrom, M., Gouras, G., Dumurgier, J., Cognat, E., Molina-Porcel, L., Balasa, M., Vitorica, J., Sanchez-Valle, R., Paquet, C., Venero, J. L., Blennow, K., & Deierborg, T. (2022). Galectin-3 is elevated in CSF and is associated with Abeta deposits and tau aggregates in brain tissue in Alzheimer's disease. *Acta Neuropathologica*, *144*(5), 843–859. https://doi.org/10.1007/s00401-022-02469-6

Bruno, M. A., & Cuello, A. C. (2006). Activity-dependent release of precursor nerve growth factor, conversion to mature nerve growth factor, and its degradation by a protease cascade. *Proceedings of the National Academy of Sciences of the United States of America*, *103*(17), 6735–6740. https://doi.org/10.1073/pnas.0510645103

Bruno, M. A., Leon, W. C., Fragoso, G., Mushynski, W. E., Almazan, G., & Cuello, A. C. (2009). Amyloid beta-induced nerve growth factor dysmetabolism in Alzheimer disease. *Journal of Neuropathology and Experimental Neurology*, *68*(8), 857–869. https://doi.org/10.1097/NEN.0b013e3181aed9e6

Burguillos, M. A., Svensson, M., Schulte, T., Boza-Serrano, A., Garcia-Quintanilla, A., Kavanagh, E., Santiago, M., Viceconte, N., Oliva-Martin, M. J., Osman, A. M., Salomonsson, E., Amar, L., Persson, A., Blomgren, K., Achour, A., Englund, E., Leffler, H., Venero, J. L., Joseph, B., & Deierborg, T. (2015). Microglia-secreted Galectin-3 acts as a Toll-like receptor 4 ligand and contributes to microglial activation. *Cell Reports*, *10*(9), 1626–1638. https://doi.org/10.1016/j.celrep.2015.02.012

Cadiz, M. P., Jensen, T. D., Sens, J. P., Zhu, K., Song, W. M., Zhang, B., Ebbert, M., Chang, R., & Fryer, J. D. (2022). Culture shock: microglial heterogeneity, activation, and disrupted single-cell microglial networks in vitro. *Molecular Neurodegeneration*, *17*(1), 26. https://doi.org/10.1186/s13024-022-00531-1

Cai, H., Ma, Y., Jiang, L., Mu, Z., Jiang, Z., Chen, X., Wang, Y., Yang, G. Y., & Zhang, Z. (2017). Hypoxia response element-regulated MMP-9 promotes neurological recovery via glial scar degradation and angiogenesis in delayed stroke. *Molecular Therapy*, *25*(6), 1448–1459. https://doi.org/10.1016/j.ymthe.2017.03.020

Callahan, L. M., & Coleman, P. D. (1995). Neurons bearing neurofibrillary tangles are responsible for selected synaptic deficits in Alzheimer's disease. *Neurobiology of Aging*, *16*(3), 311–314. https://doi.org/10.1016/0197-4580(95)00035-d

Canals, I., Ginisty, A., Quist, E., Timmerman, R., Fritze, J., Miskinyte, G., Monni, E., Hansen, M. G., Hidalgo, I., Bryder, D., Bengzon, J., & Ahlenius, H. (2018). Rapid and efficient induction of functional astrocytes from human pluripotent stem cells. *Nature Methods*, *15*(9), 693–696. https://doi.org/10.1038/s41592-018-0103-2

Cao, Y., Liu, P., Bian, H., Jin, S., Liu, J., Yu, N., Cui, H., Sun, F., Qian, X., Qiu, W., & Ma, C. (2024). Reduced neurogenesis in human hippocampus with Alzheimer's disease. *Brain Pathology*, *34*(3), e13225. https://doi.org/10.1111/bpa.13225

Chen, K. S., Nishimura, M. C., Armanini, M. P., Crowley, C., Spencer, S. D., & Phillips, H. S. (1997). Disruption of a single allele of the nerve growth factor gene results in atrophy of basal forebrain cholinergic neurons and memory deficits. *Journal of Neuroscience*, *17*(19), 7288–7296. https://doi.org/10.1523/JNEUROSCI.17-19-07288.1997

Chen, S. S., Sun, L. W., Brickner, H., & Sun, P. Q. (2015). Downregulating galectin-3 inhibits proinflammatory cytokine production by human monocyte-derived dendritic cells via RNA interference. *Cellular Immunology*, *294*(1), 44–53. https://doi.org/10.1016/j.cellimm.2015.01.017

Chen, T. B., Lee, Y. J., Lin, S. Y., Chen, J. P., Hu, C. J., Wang, P. N., & Cheng, I. H. (2019). Plasma Abeta42 and total tau predict cognitive decline in amnestic mild cognitive impairment. *Scientific Reports*, *9*(1), 13984. https://doi.org/10.1038/s41598-019-50315-9

Chen, Y. C., Ma, Y. L., Lin, C. H., Cheng, S. J., Hsu, W. L., & Lee, E. H. (2017). Galectin-3 negatively regulates hippocampus-dependent memory formation through inhibition of integrin signaling and Galectin-3 phosphorylation. *Frontiers in Molecular Neuroscience*, *10*, 217. https://doi.org/10.3389/fnmol.2017.00217

Chen, Z., & Palmer, T. D. (2013). Differential roles of TNFR1 and TNFR2 signaling in adult hippocampal neurogenesis. *Brain, Behavior, and Immunity*, *30*, 45–53. https://doi.org/10.1016/j.bbi.2013.01.083

Chung, H., Brazil, M. I., Soe, T. T., & Maxfield, F. R. (1999). Uptake, degradation, and release of fibrillar and soluble forms of Alzheimer's amyloid beta-peptide by microglial cells. *Journal of Biological Chemistry*, *274*(45), 32301–32308. https://doi.org/10.1074/jbc.274.45.32301

Clark, P. J., Kohman, R. A., Miller, D. S., Bhattacharya, T. K., Brzezinska, W. J., & Rhodes, J. S. (2011). Genetic influences on exercise-induced adult hippocampal neurogenesis across 12 divergent mouse strains. *Genes, Brain, and Behavior*, *10*(3), 345–353. https://doi.org/10.1111/j.1601-183X.2010.00674.x

Cockram, T. O. J., Puigdellivol, M., & Brown, G. C. (2019). Calreticulin and Galectin-3 opsonise bacteria for phagocytosis by microglia. *Frontiers in Immunology*, *10*, 2647. https://doi.org/10.3389/fimmu.2019.02647

Cominski, T. P., Ansonoff, M. A., Turchin, C. E., & Pintar, J. E. (2014). Loss of the mu opioid receptor induces strain-specific alterations in hippocampal neurogenesis and spatial learning. *Neuroscience*, *278*, 11–19. https://doi.org/10.1016/j.neuroscience.2014.07.039

Comte, I., Kim, Y., Young, C. C., van der Harg, J. M., Hockberger, P., Bolam, P. J., Poirier, F., & Szele, F. G. (2011). Galectin-3 maintains cell motility from the subventricular zone to the olfactory bulb. *Journal of Cell Science*, *124*(Pt 14), 2438–2447. https://doi.org/10.1242/jcs.079954

Cruzat, A., Gonzalez-Andrades, M., Mauris, J., AbuSamra, D. B., Chidambaram, P., Kenyon, K. R., Chodosh, J., Dohlman, C. H., & Argueso, P. (2018). Colocalization of Galectin-3 with CD147 is associated with increased gelatinolytic activity in ulcerating human corneas. *Investigative Ophthalmology & Visual Science*, *59*(1), 223–230. https://doi.org/10.1167/iovs.17-23196

Dar, N. J., & Glazner, G. W. (2020). Deciphering the neuroprotective and neurogenic potential of soluble amyloid precursor protein alpha (sAPPalpha). *Cellular and Molecular Life Sciences*, *77*(12), 2315–2330. https://doi.org/10.1007/s00018-019-03404-x

de Boer, R. A., van Veldhuisen, D. J., Gansevoort, R. T., Muller Kobold, A. C., van Gilst, W. H., Hillege, H. L., Bakker, S. J., & van der Harst, P. (2012). The fibrosis marker galectin-3 and outcome in the general population. *Journal of Internal Medicine*, *272*(1), 55–64. https://doi.org/10.1111/j.1365-2796.2011.02476.x

De Schepper, S., Ge, J. Z., Crowley, G., Ferreira, L. S. S., Garceau, D., Toomey, C. E., Sokolova, D., Rueda-Carrasco, J., Shin, S. H., Kim, J. S., Childs, T., Lashley, T., Burden, J. J., Sasner, M., Sala Frigerio, C., Jung, S., & Hong, S. (2023). Perivascular cells induce microglial phagocytic states and synaptic engulfment via SPP1 in mouse models of Alzheimer's disease. *Nature Neuroscience*, *26*(3), 406–415. https://doi.org/10.1038/s41593-023-01257-z

Dong, Y., & Yong, V. W. (2022). Oxidized phospholipids as novel mediators of neurodegeneration. *Trends in Neurosciences*, *45*(6), 419–429. https://doi.org/10.1016/j.tins.2022.03.002

Dziembowska, M., & Wlodarczyk, J. (2012). MMP9: a novel function in synaptic plasticity. *The International Journal of Biochemistry & Cell Biology*, *44*(5), 709–713. https://doi.org/10.1016/j.biocel.2012.01.023

Erickson, M. A., Liang, W. S., Fernandez, E. G., Bullock, K. M., Thysell, J. A., & Banks, W. A. (2018). Genetics and sex influence peripheral and central innate immune responses and blood-brain barrier integrity. *PLOS ONE*, *13*(10), e0205769. https://doi.org/10.1371/journal.pone.0205769

Espinosa-Oliva, A. M., Garcia-Miranda, P., Alonso-Bellido, I. M., Carvajal, A. E., Gonzalez-Rodriguez, M., Carrillo-Jimenez, A., Temblador, A. J., Felices-Navarro, M., Garcia-Dominguez, I., Roca-Ceballos, M. A., Vazquez-Carretero, M. D., Garcia-Revilla, J., Santiago, M., Peral, M. J., Venero, J. L., & de Pablos, R. M. (2021). Galectin-3 deletion reduces LPS and acute colitis-induced pro-inflammatory microglial activation in the ventral mesencephalon. *Frontiers in Pharmacology*, *12*, 706439. https://doi.org/10.3389/fphar.2021.706439

Fanselow, M. S., & Dong, H. W. (2010). Are the dorsal and ventral hippocampus functionally distinct structures? *Neuron*, *65*(1), 7–19. https://doi.org/10.1016/j.neuron.2009.11.031

Faucher, P., Mons, N., Micheau, J., Louis, C., & Beracochea, D. J. (2015). Hippocampal injections of oligomeric amyloid beta-peptide (1-42) induce selective working memory deficits and long-lasting alterations of ERK signaling pathway. *Frontiers in Aging Neuroscience*, *7*, 245. https://doi.org/10.3389/fnagi.2015.00245

Fermino, M. L., Polli, C. D., Toledo, K. A., Liu, F. T., Hsu, D. K., Roque-Barreira, M. C., Pereira-da-Silva, G., Bernardes, E. S., & Halbwachs-Mecarelli, L. (2011). LPS-induced galectin-3 oligomerization results in enhancement of neutrophil activation. *PLOS ONE*, *6*(10), e26004. https://doi.org/10.1371/journal.pone.0026004

Franjic, D., Skarica, M., Ma, S., Arellano, J. I., Tebbenkamp, A. T. N., Choi, J., Xu, C., Li, Q., Morozov, Y. M., Andrijevic, D., Vrselja, Z., Spajic, A., Santpere, G., Li, M., Zhang, S., Liu, Y., Spurrier, J., Zhang, L., Gudelj, I., . . . Sestan, N. (2022). Transcriptomic taxonomy and neurogenic trajectories of adult human, macaque,

and pig hippocampal and entorhinal cells. *Neuron*, *110*(3), 452–469.e14. https://doi.org/10.1016/j.neuron.2021.10.036

Frost, B., Jacks, R. L., & Diamond, M. I. (2009). Propagation of tau misfolding from the outside to the inside of a cell. *Journal of Biological Chemistry*, *284*(19), 12845–12852. https://doi.org/10.1074/jbc.M808759200

Fu, A. K., Hung, K. W., Yuen, M. Y., Zhou, X., Mak, D. S., Chan, I. C., Cheung, T. H., Zhang, B., Fu, W. Y., Liew, F. Y., & Ip, N. Y. (2016). IL-33 ameliorates Alzheimer's disease-like pathology and cognitive decline. *Proceedings of the National Academy of Sciences of the United States of America*, *113*(19), E2705–2713. https://doi.org/10.1073/pnas.1604032113

Giuffrida, M. L., Caraci, F., Pignataro, B., Cataldo, S., De Bona, P., Bruno, V., Molinaro, G., Pappalardo, G., Messina, A., Palmigiano, A., Garozzo, D., Nicoletti, F., Rizzarelli, E., & Copani, A. (2009). Beta-amyloid monomers are neuroprotective. *Journal of Neuroscience*, *29*(34), 10582–10587. https://doi.org/10.1523/JNEUROSCI.1736-09.2009

Gomez-Murcia, V., Sandau, U., Ferry, B., Parrot, S., Laurent, C., Basquin, M., Buee, L., Boison, D., & Blum, D. (2020). Hyperexcitability and seizures in the THY-Tau22 mouse model of tauopathy. *Neurobiology of Aging*, *94*, 265–270. https://doi.org/10.1016/j.neurobiolaging.2020.06.004

Gore, S. V., James, E. J., Huang, L. C., Park, J. J., Berghella, A., Thompson, A. C., Cline, H. T., & Aizenman, C. D. (2021). Role of matrix metalloproteinase-9 in neurodevelopmental deficits and experience-dependent plasticity in Xenopus laevis. *eLife*, *10*, Article e62147. https://doi.org/10.7554/eLife.62147

Gotz, J., Chen, F., van Dorpe, J., & Nitsch, R. M. (2001). Formation of neurofibrillary tangles in P301L tau transgenic mice induced by Abeta 42 fibrils. *Science*, *293*(5534), 1491–1495. https://doi.org/10.1126/science.1062097

Grubman, A., Choo, X. Y., Chew, G., Ouyang, J. F., Sun, G., Croft, N. P., Rossello, F. J., Simmons, R., Buckberry, S., Landin, D. V., Pflueger, J., Vandekolk, T. H., Abay, Z., Zhou, Y., Liu, X., Chen, J., Larcombe, M., Haynes, J. M., McLean, C., . . . Polo, J. M. (2021). Transcriptional signature in microglia associated with Abeta plaque phagocytosis. *Nature Communications*, *12*(1), 3015. https://doi.org/10.1038/s41467-021-23111-1

Habib, N., McCabe, C., Medina, S., Varshavsky, M., Kitsberg, D., Dvir-Szternfeld, R., Green, G., Dionne, D., Nguyen, L., Marshall, J. L., Chen, F., Zhang, F., Kaplan, T., Regev, A., & Schwartz, M. (2020). Disease-associated astrocytes in Alzheimer's disease and aging. *Nature Neuroscience*, *23*(6), 701–706. https://doi.org/10.1038/s41593-020-0624-8

Hammond, T. R., Dufort, C., Dissing-Olesen, L., Giera, S., Young, A., Wysoker, A., Walker, A. J., Gergits, F., Segel, M., Nemesh, J., Marsh, S. E., Saunders, A., Macosko, E., Ginhoux, F., Chen, J., Franklin, R. J. M., Piao, X., McCarroll, S. A., & Stevens, B. (2019). Single-cell RNA sequencing of microglia throughout the mouse lifespan and in the injured brain reveals complex cell-state changes. *Immunity*, *50*(1), 253–271.e6. https://doi.org/10.1016/j.immuni.2018.11.004

Haney, M. S., Bohlen, C. J., Morgens, D. W., Ousey, J. A., Barkal, A. A., Tsui, C. K., Ego, B. K., Levin, R., Kamber, R. A., Collins, H., Tucker, A., Li, A., Vorselen, D., Labitigan, L., Crane, E., Boyle, E., Jiang, L., Chan, J., Rincon, E., . . . Bassik, M. C. (2018). Identification of phagocytosis regulators using magnetic genome-wide CRISPR

screens. *Nature Genetics*, *50*(12), 1716–1727. https://doi.org/10.1038/s41588-018-0254-1

Harrison, S. A., Dennis, A., Fiore, M. M., Kelly, M. D., Kelly, C. J., Paredes, A. H., Whitehead, J. M., Neubauer, S., Traber, P. G., & Banerjee, R. (2018). Utility and variability of three non-invasive liver fibrosis imaging modalities to evaluate efficacy of GR-MD-02 in subjects with NASH and bridging fibrosis during a phase-2 randomized clinical trial. *PLOS ONE*, *13*(9), e0203054. https://doi.org/10.1371/journal.pone.0203054

Hashimoto, T., Serrano-Pozo, A., Hori, Y., Adams, K. W., Takeda, S., Banerji, A. O., Mitani, A., Joyner, D., Thyssen, D. H., Bacskai, B. J., Frosch, M. P., Spires-Jones, T. L., Finn, M. B., Holtzman, D. M., & Hyman, B. T. (2012). Apolipoprotein E, especially apolipoprotein E4, increases the oligomerization of amyloid beta peptide. *Journal of Neuroscience*, *32*(43), 15181–15192. https://doi.org/10.1523/JNEUROSCI.1542-12.2012

Hatami, A., Monjazeb, S., Milton, S., & Glabe, C. G. (2017). Familial Alzheimer's disease mutations within the amyloid precursor protein alter the aggregation and conformation of the amyloid-beta peptide. *Journal of Biological Chemistry*, *292*(8), 3172–3185. https://doi.org/10.1074/jbc.M116.755264

He, Y., Yao, X., Taylor, N., Bai, Y., Lovenberg, T., & Bhattacharya, A. (2018). RNA sequencing analysis reveals quiescent microglia isolation methods from postnatal mouse brains and limitations of BV2 cells. *Journal of Neuroinflammation*, *15*(1), 153. https://doi.org/10.1186/s12974-018-1195-4

He, Y., Zheng, M. M., Ma, Y., Han, X. J., Ma, X. Q., Qu, C. Q., & Du, Y. F. (2012). Soluble oligomers and fibrillar species of amyloid beta-peptide differentially affect cognitive functions and hippocampal inflammatory response. *Biochemical and Biophysical Research Communications*, *429*(3–4), 125–130. https://doi.org/10.1016/j.bbrc.2012.10.129

Henderson, N. C., Mackinnon, A. C., Farnworth, S. L., Kipari, T., Haslett, C., Iredale, J. P., Liu, F. T., Hughes, J., & Sethi, T. (2008). Galectin-3 expression and secretion links macrophages to the promotion of renal fibrosis. *American Journal of Pathology*, *172*(2), 288–298. https://doi.org/10.2353/ajpath.2008.070726

Henderson, N. C., Mackinnon, A. C., Farnworth, S. L., Poirier, F., Russo, F. P., Iredale, J. P., Haslett, C., Simpson, K. J., & Sethi, T. (2006). Galectin-3 regulates myofibroblast activation and hepatic fibrosis. *Proceedings of the National Academy of Sciences of the United States of America*, *103*(13), 5060–5065. https://doi.org/10.1073/pnas.0511167103

Hernandez-Guillamon, M., Martinez-Saez, E., Delgado, P., Domingues-Montanari, S., Boada, C., Penalba, A., Boada, M., Pagola, J., Maisterra, O., Rodriguez-Luna, D., Molina, C. A., Rovira, A., Alvarez-Sabin, J., Ortega-Aznar, A., & Montaner, J. (2012). MMP-2/MMP-9 plasma level and brain expression in cerebral amyloid angiopathy-associated hemorrhagic stroke. *Brain Pathology*, *22*(2), 133–141. https://doi.org/10.1111/j.1750-3639.2011.00512.x

Hickman, S. E., Allison, E. K., Coleman, U., Kingery-Gallagher, N. D., & El Khoury, J. (2019). Heterozygous CX3CR1 deficiency in microglia restores neuronal beta-amyloid clearance pathways and slows progression of Alzheimer's like-disease in PS1-APP mice. *Frontiers in Immunology*, *10*, 2780. https://doi.org/10.3389/fimmu.2019.02780

Ho, M. K., & Springer, T. A. (1982). Mac-2, a novel 32,000 Mr mouse macrophage subpopulation-specific antigen defined by monoclonal antibodies. *The Journal of Immunology*, *128*(3), 1221–1228. https://doi.org/10.4049/jimmunol.128.3.1221

Hu, C., Li, H., Cui, J., Li, Y., Zhang, F., Li, H., Luo, X., & Hao, Y. (2025). Integrative analysis identifies IL-6/JUN/MMP-9 pathway destroyed blood-brain-barrier in autism mice via machine learning and bioinformatic analysis. *Translational Psychiatry*, *15*(1), 239. https://doi.org/10.1038/s41398-025-03452-x

Hu, J., Akama, K. T., Krafft, G. A., Chromy, B. A., & Van Eldik, L. J. (1998). Amyloid-beta peptide activates cultured astrocytes: morphological alterations, cytokine induction and nitric oxide release. *Brain Research*, *785*(2), 195–206. https://doi.org/10.1016/s0006-8993(97)01318-8

Imaizumi, Y., Sakaguchi, M., Morishita, T., Ito, M., Poirier, F., Sawamoto, K., & Okano, H. (2011). Galectin-1 is expressed in early-type neural progenitor cells and down-regulates neurogenesis in the adult hippocampus. *Molecular Brain*, *4*, 7. https://doi.org/10.1186/1756-6606-4-7

Inzitari, D., Giusti, B., Nencini, P., Gori, A. M., Nesi, M., Palumbo, V., Piccardi, B., Armillis, A., Pracucci, G., Bono, G., Bovi, P., Consoli, D., Guidotti, M., Nucera, A., Massaro, F., Micieli, G., Orlandi, G., Perini, F., Tassi, R., . . . Group, M. S. (2013). MMP9 variation after thrombolysis is associated with hemorrhagic transformation of lesion and death. *Stroke*, *44*(10), 2901–2903. https://doi.org/10.1161/STROKEAHA.113.002274

Jellinger, K. A. (2002). Alzheimer disease and cerebrovascular pathology: an update. *Journal of Neural Transmission*, *109*(5–6), 813–836. https://doi.org/10.1007/s007020200068

Ji, X., Jiang, Z., Qiu, Y., Yu, J., Zhang, Y., Wang, J., Ye, B., Huang, Y., Gu, W., Huang, Y., Chen, J., & Bao, Z. (2023). High blood galectin-3 level associated with risk of frailty in aging. *Frontiers in Endocrinology*, *14*, 1189192. https://doi.org/10.3389/fendo.2023.1189192

Jin, M., Shiwaku, H., Tanaka, H., Obita, T., Ohuchi, S., Yoshioka, Y., Jin, X., Kondo, K., Fujita, K., Homma, H., Nakajima, K., Mizuguchi, M., & Okazawa, H. (2021). Tau activates microglia via the PQBP1-cGAS-STING pathway to promote brain inflammation. *Nature Communications*, *12*(1), 6565. https://doi.org/10.1038/s41467-021-26851-2

Kang, S. S., Kook, J. H., Hwang, S., Park, S. H., Nam, S. C., & Kim, J. K. (2008). Inhibition of matrix metalloproteinase-9 attenuated neural progenitor cell migration after photothrombotic ischemia. *Brain Research*, *1228*, 20–26. https://doi.org/10.1016/j.brainres.2008.06.056

Kang, W., & Hebert, J. M. (2015). FGF signaling is necessary for neurogenesis in young mice and sufficient to reverse its decline in old mice. *Journal of Neuroscience*, *35*(28), 10217–10223. https://doi.org/10.1523/JNEUROSCI.1469-15.2015

Keren-Shaul, H., Spinrad, A., Weiner, A., Matcovitch-Natan, O., Dvir-Szternfeld, R., Ulland, T. K., David, E., Baruch, K., Lara-Astaiso, D., Toth, B., Itzkovitz, S., Colonna, M., Schwartz, M., & Amit, I. (2017). A unique microglia type associated with restricting development of Alzheimer's disease. *Cell*, *169*(7), 1276–1290.e17. https://doi.org/10.1016/j.cell.2017.05.018

Kim, J. W., Nam, S. M., Yoo, D. Y., Jung, H. Y., Kim, I. Y., Hwang, I. K., Seong, J. K., & Yoon, Y. S. (2017). Comparison of adult hippocampal neurogenesis and susceptibility to treadmill exercise in nine mouse strains. *Neural Plasticity*, *2017*, 5863258. https://doi.org/10.1155/2017/5863258

Knox, E. G., Aburto, M. R., Clarke, G., Cryan, J. F., & O'Driscoll, C. M. (2022). The blood-brain barrier in aging and neurodegeneration. *Molecular Psychiatry*, *27*(6), 2659–2673. https://doi.org/10.1038/s41380-022-01511-z

Konishi, H., Koizumi, S., & Kiyama, H. (2022). Phagocytic astrocytes: Emerging from the shadows of microglia. *Glia*, *70*(6), 1009–1026. https://doi.org/10.1002/glia.24145

Krasemann, S., Madore, C., Cialic, R., Baufeld, C., Calcagno, N., El Fatimy, R., Beckers, L., O'Loughlin, E., Xu, Y., Fanek, Z., Greco, D. J., Smith, S. T., Tweet, G., Humulock, Z., Zrzavy, T., Conde-Sanroman, P., Gacias, M., Weng, Z., Chen, H., . . . Butovsky, O. (2017). The TREM2-APOE pathway drives the transcriptional phenotype of dysfunctional microglia in neurodegenerative diseases. *Immunity*, *47*(3), 566–581.e9. https://doi.org/10.1016/j.immuni.2017.08.008

Lakshminarayan, R., Wunder, C., Becken, U., Howes, M. T., Benzing, C., Arumugam, S., Sales, S., Ariotti, N., Chambon, V., Lamaze, C., Loew, D., Shevchenko, A., Gaus, K., Parton, R. G., & Johannes, L. (2014). Galectin-3 drives glycosphingolipid-dependent biogenesis of clathrin-independent carriers. *Nature Cell Biology*, *16*(6), 595–606. https://doi.org/10.1038/ncb2970

Lee, S., Varvel, N. H., Konerth, M. E., Xu, G., Cardona, A. E., Ransohoff, R. M., & Lamb, B. T. (2010). CX3CR1 deficiency alters microglial activation and reduces beta-amyloid deposition in two Alzheimer's disease mouse models. *American Journal of Pathology*, *177*(5), 2549–2562. https://doi.org/10.2353/ajpath.2010.100265

Lee, S. J., Seo, B. R., & Koh, J. Y. (2015). Metallothionein-3 modulates the amyloid beta endocytosis of astrocytes through its effects on actin polymerization. *Molecular Brain*, *8*(1), 84. https://doi.org/10.1186/s13041-015-0173-3

Li, S., Hong, S., Shepardson, N. E., Walsh, D. M., Shankar, G. M., & Selkoe, D. (2009). Soluble oligomers of amyloid Beta protein facilitate hippocampal long-term depression by disrupting neuronal glutamate uptake. *Neuron*, *62*(6), 788–801. https://doi.org/10.1016/j.neuron.2009.05.012

Lin, T., Zhang, W., Fan, Y., & Mulholland, M. (2007). Interleukin-1beta and interleukin-6 stimulate matrix metalloproteinase-9 secretion in cultured myenteric glia. *Journal of Surgical Research*, *137*(1), 38–45. https://doi.org/10.1016/j.jss.2006.05.043

Liu, X., Xu, J., Zheng, S., Yang, Y., Xie, Y., Liu, J., Zhong, J., Zhang, H., Chen, J., Dai, C., Wang, D., Luo, J., Chen, X., Zhong, F., & Ye, Z. C. (2025). AI-driven discovery of brain-penetrant Galectin-3 inhibitors for Alzheimer's disease therapy. *Pharmacological Research*, *218*, 107834. https://doi.org/10.1016/j.phrs.2025.107834

Liu, Z., Condello, C., Schain, A., Harb, R., & Grutzendler, J. (2010). CX3CR1 in microglia regulates brain amyloid deposition through selective protofibrillar amyloid-beta phagocytosis. *Journal of Neuroscience*, *30*(50), 17091–17101. https://doi.org/10.1523/JNEUROSCI.4403-10.2010

Lopez-Otin, C., Blasco, M. A., Partridge, L., Serrano, M., & Kroemer, G. (2023). Hallmarks of aging: An expanding universe. *Cell*, *186*(2), 243–278. https://doi.org/10.1016/j.cell.2022.11.001

Mackinnon, A. C., Gibbons, M. A., Farnworth, S. L., Leffler, H., Nilsson, U. J., Delaine, T., Simpson, A. J., Forbes, S. J., Hirani, N., Gauldie, J., & Sethi, T. (2012). Regulation of transforming growth factor-beta1-driven lung fibrosis by galectin-3. *American Journal of Respiratory and Critical Care Medicine*, *185*(5), 537–546. https://doi.org/10.1164/rccm.201106-0965OC

MacKinnon, A. C., Liu, X., Hadoke, P. W., Miller, M. R., Newby, D. E., & Sethi, T. (2013). Inhibition of galectin-3 reduces atherosclerosis in apolipoprotein E-deficient mice. *Glycobiology*, *23*(6), 654–663. https://doi.org/10.1093/glycob/cwt006

Mandrekar, S., Jiang, Q., Lee, C. Y., Koenigsknecht-Talboo, J., Holtzman, D. M., & Landreth, G. E. (2009). Microglia mediate the clearance of soluble Abeta through fluid phase macropinocytosis. *Journal of Neuroscience*, *29*(13), 4252–4262. https://doi.org/10.1523/JNEUROSCI.5572-08.2009

Maphis, N., Xu, G., Kokiko-Cochran, O. N., Jiang, S., Cardona, A., Ransohoff, R. M., Lamb, B. T., & Bhaskar, K. (2015). Reactive microglia drive tau pathology and contribute to the spreading of pathological tau in the brain. *Brain*, *138*(Pt 6), 1738–1755. https://doi.org/10.1093/brain/awv081

Marriott, I., & Huet-Hudson, Y. M. (2006). Sexual dimorphism in innate immune responses to infectious organisms. *Immunologic Research*, *34*(3), 177–192. https://doi.org/10.1385/IR:34:3:177

Mattson, M. P., Cheng, B., Davis, D., Bryant, K., Lieberburg, I., & Rydel, R. E. (1992). beta-Amyloid peptides destabilize calcium homeostasis and render human cortical neurons vulnerable to excitotoxicity. *Journal of Neuroscience*, *12*(2), 376–389. https://doi.org/10.1523/JNEUROSCI.12-02-00376.1992

Mauris, J., Woodward, A. M., Cao, Z., Panjwani, N., & Argueso, P. (2014). Molecular basis for MMP9 induction and disruption of epithelial cell-cell contacts by galectin-3. *Journal of Cell Science*, *127*(Pt 14), 3141–3148. https://doi.org/10.1242/jcs.148510

Meyer-Luehmann, M., Spires-Jones, T. L., Prada, C., Garcia-Alloza, M., de Calignon, A., Rozkalne, A., Koenigsknecht-Talboo, J., Holtzman, D. M., Bacskai, B. J., & Hyman, B. T. (2008). Rapid appearance and local toxicity of amyloid-beta plaques in a mouse model of Alzheimer's disease. *Nature*, *451*(7179), 720–724. https://doi.org/10.1038/nature06616

Miners, J. S., Van Helmond, Z., Chalmers, K., Wilcock, G., Love, S., & Kehoe, P. G. (2006). Decreased expression and activity of neprilysin in Alzheimer disease are associated with cerebral amyloid angiopathy. *Journal of Neuropathology and Experimental Neurology*, *65*(10), 1012–1021. https://doi.org/10.1097/01.jnen.0000240463.87886.9a

Mizoguchi, H., Takuma, K., Fukuzaki, E., Ibi, D., Someya, E., Akazawa, K. H., Alkam, T., Tsunekawa, H., Mouri, A., Noda, Y., Nabeshima, T., & Yamada, K. (2009). Matrix metalloprotease-9 inhibition improves amyloid beta-mediated cognitive impairment and neurotoxicity in mice. *Journal of Pharmacology and Experimental Therapeutics*, *331*(1), 14–22. https://doi.org/10.1124/jpet.109.154724

Mohammad, H., Marchisella, F., Ortega-Martinez, S., Hollos, P., Eerola, K., Komulainen, E., Kulesskaya, N., Freemantle, E., Fagerholm, V., Savontaus, E., Rauvala, H., Peterson, B. D., van Praag, H., & Coffey, E. T. (2018). JNK1 controls adult hippocampal neurogenesis and imposes cell-autonomous control of anxiety

behaviour from the neurogenic niche. *Molecular Psychiatry*, *23*(2), 362–374. https://doi.org/10.1038/mp.2016.203

Monje, M. L., Toda, H., & Palmer, T. D. (2003). Inflammatory blockade restores adult hippocampal neurogenesis. *Science*, *302*(5651), 1760–1765. https://doi.org/10.1126/science.1088417

Moreno-Jimenez, E. P., Flor-Garcia, M., Terreros-Roncal, J., Rabano, A., Cafini, F., Pallas-Bazarra, N., Avila, J., & Llorens-Martin, M. (2019). Adult hippocampal neurogenesis is abundant in neurologically healthy subjects and drops sharply in patients with Alzheimer's disease. *Nature Medicine*, *25*(4), 554–560. https://doi.org/10.1038/s41591-019-0375-9

Mulder, S. D., Veerhuis, R., Blankenstein, M. A., & Nielsen, H. M. (2012). The effect of amyloid associated proteins on the expression of genes involved in amyloid-beta clearance by adult human astrocytes. *Experimental Neurology*, *233*(1), 373–379. https://doi.org/10.1016/j.expneurol.2011.11.001

Mun-Bryce, S., & Rosenberg, G. A. (1998). Gelatinase B modulates selective opening of the blood-brain barrier during inflammation. *American Journal of Physiology*, *274*(5), R1203–1211. https://doi.org/10.1152/ajpregu.1998.274.5.R1203

Nichols, E., Steinmetz, J. D., Vollset, S. E., Fukutaki, K., Chalek, J., Abd-Allah, F., Abdoli, A., Abualhasan, A., Abu-Gharbieh, E., Akram, T. T., Al Hamad, H., Alahdab, F., Alanezi, F. M., Alipour, V., Almustanyir, S., Amu, H., Ansari, I., Arabloo, J., Ashraf, T., . . . Vos, T. (2022). Estimation of the global prevalence of dementia in 2019 and forecasted prevalence in 2050: an analysis for the Global Burden of Disease Study 2019. *The Lancet Public Health*, *7*(2), e105–e125. https://doi.org/10.1016/S2468-2667(21)00249-8

Nicolas, M., & Hassan, B. A. (2014). Amyloid precursor protein and neural development. *Development*, *141*(13), 2543–2548. https://doi.org/10.1242/dev.108712

Nishikawa, H., Liu, L., Nakano, F., Kawakita, F., Kanamaru, H., Nakatsuka, Y., Okada, T., & Suzuki, H. (2018). Modified citrus pectin prevents blood-brain barrier disruption in mouse subarachnoid hemorrhage by inhibiting Galectin-3. *Stroke*, *49*(11), 2743–2751. https://doi.org/10.1161/STROKEAHA.118.021757

Nomura, K., Vilalta, A., Allendorf, D. H., Hornik, T. C., & Brown, G. C. (2017). Activated microglia desialylate and phagocytose cells via neuraminidase, Galectin-3, and Mer tyrosine kinase. *The Journal of Immunology*, *198*(12), 4792–4801. https://doi.org/10.4049/jimmunol.1502532

Nubling, G., Levin, J., Bader, B., Israel, L., Botzel, K., Lorenzl, S., & Giese, A. (2012). Limited cleavage of tau with matrix-metalloproteinase MMP-9, but not MMP-3, enhances tau oligomer formation. *Experimental Neurology*, *237*(2), 470–476. https://doi.org/10.1016/j.expneurol.2012.07.018

Ochieng, J., Green, B., Evans, S., James, O., & Warfield, P. (1998). Modulation of the biological functions of galectin-3 by matrix metalloproteinases. *Biochimica et Biophysica Acta*, *1379*(1), 97–106. https://doi.org/10.1016/s0304-4165(97)00086-x

Oddo, S., Caccamo, A., Shepherd, J. D., Murphy, M. P., Golde, T. E., Kayed, R., Metherate, R., Mattson, M. P., Akbari, Y., & LaFerla, F. M. (2003). Triple-transgenic model of Alzheimer's disease with plaques and tangles: intracellular Abeta and synaptic dysfunction. *Neuron*, *39*(3), 409–421. https://doi.org/10.1016/s0896-6273(03)00434-3

Ohline, S. M., Chan, C., Schoderboeck, L., Wicky, H. E., Tate, W. P., Hughes, S. M., & Abraham, W. C. (2022). Effect of soluble amyloid precursor protein-alpha on adult hippocampal neurogenesis in a mouse model of Alzheimer's disease. *Molecular Brain*, *15*(1), 5. https://doi.org/10.1186/s13041-021-00889-1

Olah, M., Menon, V., Habib, N., Taga, M. F., Ma, Y., Yung, C. J., Cimpean, M., Khairallah, A., Coronas-Samano, G., Sankowski, R., Grun, D., Kroshilina, A. A., Dionne, D., Sarkis, R. A., Cosgrove, G. R., Helgager, J., Golden, J. A., Pennell, P. B., Prinz, M., . . . De Jager, P. L. (2020). Single cell RNA sequencing of human microglia uncovers a subset associated with Alzheimer's disease. *Nature Communications*, *11*(1), 6129. https://doi.org/10.1038/s41467-020-19737-2

Olivieri, F., Prattichizzo, F., Grillari, J., & Balistreri, C. R. (2018). Cellular senescence and inflammaging in age-related diseases. *Mediators of Inflammation*, *2018*, 9076485. https://doi.org/10.1155/2018/9076485

Ong, J., Wu, Q., Sasaki, K., Isoda, H., & Szele, F. G. (2025). Nutraceuticals: using food to enhance brain health by modulating postnatal neurogenesis in animal models and patient populations. *Stem Cells Translational Medicine*, *14*(5), Article szaf006. https://doi.org/10.1093/stcltm/szaf006

Patrizz, A., Doran, S. J., Chauhan, A., Ahnstedt, H., Roy-O'Reilly, M., Lai, Y. J., Weston, G., Tarabishy, S., Patel, A. R., Verma, R., Staff, I., Kofler, J. K., Li, J., Liu, F., Ritzel, R. M., & McCullough, L. D. (2020). EMMPRIN/CD147 plays a detrimental role in clinical and experimental ischemic stroke. *Aging*, *12*(6), 5121–5139. https://doi.org/10.18632/aging.102935

Pawluski, J. L., & Galea, L. A. (2007). Reproductive experience alters hippocampal neurogenesis during the postpartum period in the dam. *Neuroscience*, *149*(1), 53–67. https://doi.org/10.1016/j.neuroscience.2007.07.031

Prah, J., Winters, A., Chaudhari, K., Hersh, J., Liu, R., & Yang, S. H. (2019). A novel serum free primary astrocyte culture method that mimic quiescent astrocyte phenotype. *Journal of Neuroscience Methods*, *320*, 50–63. https://doi.org/10.1016/j.jneumeth.2019.03.013

Py, N. A., Bonnet, A. E., Bernard, A., Marchalant, Y., Charrat, E., Checler, F., Khrestchatisky, M., Baranger, K., & Rivera, S. (2014). Differential spatio-temporal regulation of MMPs in the 5xFAD mouse model of Alzheimer's disease: evidence for a pro-amyloidogenic role of MT1-MMP. *Frontiers in Aging Neuroscience*, *6*, 247. https://doi.org/10.3389/fnagi.2014.00247

Radic, T., Jungenitz, T., Singer, M., Beining, M., Cuntz, H., Vlachos, A., Deller, T., & Schwarzacher, S. W. (2017). Time-lapse imaging reveals highly dynamic structural maturation of postnatally born dentate granule cells in organotypic entorhino-hippocampal slice cultures. *Scientific Reports*, *7*, 43724. https://doi.org/10.1038/srep43724

Reichert, F., & Rotshenker, S. (1999). Galectin-3/MAC-2 in experimental allergic encephalomyelitis. *Experimental Neurology*, *160*(2), 508–514. https://doi.org/10.1006/exnr.1999.7229

Reichert, F., & Rotshenker, S. (2019). Galectin-3 (MAC-2) controls microglia phenotype whether amoeboid and phagocytic or branched and non-phagocytic by regulating the cytoskeleton. *Frontiers in Cellular Neuroscience*, *13*, 90. https://doi.org/10.3389/fncel.2019.00090

Reichert, F., Saada, A., & Rotshenker, S. (1994). Peripheral nerve injury induces Schwann cells to express two macrophage phenotypes: phagocytosis and the galactose-specific lectin MAC-2. *Journal of Neuroscience*, *14*(5 Pt 2), 3231–3245. https://doi.org/10.1523/JNEUROSCI.14-05-03231.1994

Ringland, C., Schweig, J. E., Eisenbaum, M., Paris, D., Ait-Ghezala, G., Mullan, M., Crawford, F., Abdullah, L., & Bachmeier, C. (2021). MMP9 modulation improves specific neurobehavioral deficits in a mouse model of Alzheimer's disease. *BMC Neuroscience*, *22*(1), 39. https://doi.org/10.1186/s12868-021-00643-2

Ruddy, R. M., Adams, K. V., & Morshead, C. M. (2019). Age- and sex-dependent effects of metformin on neural precursor cells and cognitive recovery in a model of neonatal stroke. *Science Advances*, *5*(9), eaax1912. https://doi.org/10.1126/sciadv.aax1912

Sano, H., Hsu, D. K., Apgar, J. R., Yu, L., Sharma, B. B., Kuwabara, I., Izui, S., & Liu, F. T. (2003). Critical role of galectin-3 in phagocytosis by macrophages. *The Journal of Clinical Investigation*, *112*(3), 389–397. https://doi.org/10.1172/JCI17592

Sano, H., Hsu, D. K., Yu, L., Apgar, J. R., Kuwabara, I., Yamanaka, T., Hirashima, M., & Liu, F. T. (2000). Human galectin-3 is a novel chemoattractant for monocytes and macrophages. *The Journal of Immunology*, *165*(4), 2156–2164. https://doi.org/10.4049/jimmunol.165.4.2156

Santos-Galindo, M., Acaz-Fonseca, E., Bellini, M. J., & Garcia-Segura, L. M. (2011). Sex differences in the inflammatory response of primary astrocytes to lipopolysaccharide. *Biology of Sex Differences*, *2*, 7. https://doi.org/10.1186/2042-6410-2-7

Sarkar, B., Das, A. K., & Maiti, S. (2013). Thermodynamically stable amyloid-beta monomers have much lower membrane affinity than the small oligomers. *Frontiers in Physiology*, *4*, 84. https://doi.org/10.3389/fphys.2013.00084

Sasaki, K., Davies, J., Doldan, N. G., Arao, S., Ferdousi, F., Szele, F. G., & Isoda, H. (2019). 3,4,5-Tricaffeoylquinic acid induces adult neurogenesis and improves deficit of learning and memory in aging model senescence-accelerated prone 8 mice. *Aging*, *11*(2), 401–422. https://doi.org/10.18632/aging.101748

Scharfman, H. E., Goodman, J. H., & Sollas, A. L. (2000). Granule-like neurons at the hilar/CA3 border after status epilepticus and their synchrony with area CA3 pyramidal cells: functional implications of seizure-induced neurogenesis. *Journal of Neuroscience*, *20*(16), 6144–6158. https://doi.org/10.1523/JNEUROSCI.20-16-06144.2000

Schirmbeck, G. H., Seady, M., Froes, F. T., Taday, J., Da Re, C., Souza, J. M., Goncalves, C. A., & Leite, M. C. (2023). Long-term LPS systemic administration leads to memory impairment and disturbance in astrocytic homeostasis. *Neurotoxicology*, *99*, 322–331. https://doi.org/10.1016/j.neuro.2023.11.009

Schoenen, J. (1982). The dendritic organization of the human spinal cord: the dorsal horn. *Neuroscience*, *7*(9), 2057–2087. https://doi.org/10.1016/0306-4522(82)90120-8

Schubert, D., Soucek, T., & Blouw, B. (2009). The induction of HIF-1 reduces astrocyte activation by amyloid beta peptide. *European Journal of Neuroscience*, *29*(7), 1323–1334. https://doi.org/10.1111/j.1460-9568.2009.06712.x

Shin, H. J., Lee, S. J., An, H. S., Choi, H. N., Jeong, E. A., Lee, J., Kim, K. E., Choi, B. H., Yun, S. P., Kang, D., Kang, S. S., & Roh, G. S. (2025). Microglial galectin-3

increases with aging in the mouse hippocampus. *Korean Journal of Physiology & Pharmacology*, *29*(2), 215–225. https://doi.org/10.4196/kjpp.24.196

Sholl, D. A. (1953). Dendritic organization in the neurons of the visual and motor cortices of the cat. *Journal of Anatomy*, *87*(4), 387–406.

Sidoryk-Wegrzynowicz, M., Gerber, Y. N., Ries, M., Sastre, M., Tolkovsky, A. M., & Spillantini, M. G. (2017). Astrocytes in mouse models of tauopathies acquire early deficits and lose neurosupportive functions. *Acta Neuropathologica Communications*, *5*(1), 89. https://doi.org/10.1186/s40478-017-0478-9

Siew, J. J., Chen, H. M., Chiu, F. L., Lee, C. W., Chang, Y. M., Chen, H. L., Nguyen, T. N. A., Liao, H. T., Liu, M., Hagar, H. T., Sun, Y. C., Lai, H. L., Kuo, M. H., Blum, D., Buee, L., Jin, L. W., Chen, S. Y., Ko, T. M., Huang, J. R., . . . Chern, Y. (2024). Galectin-3 aggravates microglial activation and tau transmission in tauopathy. *The Journal of Clinical Investigation*, *134*(2), Article e165523. https://doi.org/10.1172/JCI165523

Sirko, S., Irmler, M., Gascón, S., Bek, S., Schneider, S., Dimou, L., Obermann, J., De Souza Paiva, D., Poirier, F., Beckers, J., Hauck, S. M., Barde, Y. A., & Götz, M. (2015). Astrocyte reactivity after brain injury: The role of galectins 1 and 3. *Glia*, *63*(12), 2340–2361. https://doi.org/10.1002/glia.22898

Sirko, S., Schichor, C., Della Vecchia, P., Metzger, F., Sonsalla, G., Simon, T., Burkle, M., Kalpazidou, S., Ninkovic, J., Masserdotti, G., Sauniere, J. F., Iacobelli, V., Iacobelli, S., Delbridge, C., Hauck, S. M., Tonn, J. C., & Gotz, M. (2023). Injury-specific factors in the cerebrospinal fluid regulate astrocyte plasticity in the human brain. *Nature Medicine*, *29*(12), 3149–3161. https://doi.org/10.1038/s41591-023-02644-6

Soares, L. C., Huang, N., Bernhardova, H., Macarelli, V., Chan, M., Nikel, L., Bandiera, S., Yan, D., Gupta, D., Cruz, E. M., Vasaturo-Kolodner, T., Hillis, J. M., Wood, M., Salman, M., Molnar, Z., O'Neill, E., & Szele, F. G. (2025). Galectin-3 induces neurodevelopmental apical-basal polarity and regulates gyrification. *Science Advances*, *11*(36), eadt5859. https://doi.org/10.1126/sciadv.adt5859

Sollvander, S., Nikitidou, E., Brolin, R., Soderberg, L., Sehlin, D., Lannfelt, L., & Erlandsson, A. (2016). Accumulation of amyloid-beta by astrocytes result in enlarged endosomes and microvesicle-induced apoptosis of neurons. *Molecular Neurodegeneration*, *11*(1), 38. https://doi.org/10.1186/s13024-016-0098-z

Song, J., Wu, C., Korpos, E., Zhang, X., Agrawal, S. M., Wang, Y., Faber, C., Schafers, M., Korner, H., Opdenakker, G., Hallmann, R., & Sorokin, L. (2015). Focal MMP-2 and MMP-9 activity at the blood-brain barrier promotes chemokine-induced leukocyte migration. *Cell Reports*, *10*(7), 1040–1054. https://doi.org/10.1016/j.celrep.2015.01.037

Sorrells, S. F., Paredes, M. F., Cebrian-Silla, A., Sandoval, K., Qi, D., Kelley, K. W., James, D., Mayer, S., Chang, J., Auguste, K. I., Chang, E. F., Gutierrez, A. J., Kriegstein, A. R., Mathern, G. W., Oldham, M. C., Huang, E. J., Garcia-Verdugo, J. M., Yang, Z., & Alvarez-Buylla, A. (2018). Human hippocampal neurogenesis drops sharply in children to undetectable levels in adults. *Nature*, *555*(7696), 377–381. https://doi.org/10.1038/nature25975

Spalding, K. L., Bergmann, O., Alkass, K., Bernard, S., Salehpour, M., Huttner, H. B., Bostrom, E., Westerlund, I., Vial, C., Buchholz, B. A., Possnert, G., Mash, D. C.,

Druid, H., & Frisen, J. (2013). Dynamics of hippocampal neurogenesis in adult humans. *Cell*, *153*(6), 1219–1227. https://doi.org/10.1016/j.cell.2013.05.002

Spoleti, E., Krashia, P., La Barbera, L., Nobili, A., Lupascu, C. A., Giacalone, E., Keller, F., Migliore, M., Renzi, M., & D'Amelio, M. (2022). Early derailment of firing properties in CA1 pyramidal cells of the ventral hippocampus in an Alzheimer's disease mouse model. *Experimental Neurology*, *350*, 113969. https://doi.org/10.1016/j.expneurol.2021.113969

Stine, W. B., Jr., Dahlgren, K. N., Krafft, G. A., & LaDu, M. J. (2003). In vitro characterization of conditions for amyloid-beta peptide oligomerization and fibrillogenesis. *Journal of Biological Chemistry*, *278*(13), 11612–11622. https://doi.org/10.1074/jbc.M210207200

Svedin, P., Hagberg, H., Savman, K., Zhu, C., & Mallard, C. (2007). Matrix metalloproteinase-9 gene knock-out protects the immature brain after cerebral hypoxia-ischemia. *Journal of Neuroscience*, *27*(7), 1511–1518. https://doi.org/10.1523/JNEUROSCI.4391-06.2007

Sydow, A., Van der Jeugd, A., Zheng, F., Ahmed, T., Balschun, D., Petrova, O., Drexler, D., Zhou, L., Rune, G., Mandelkow, E., D'Hooge, R., Alzheimer, C., & Mandelkow, E. M. (2011). Tau-induced defects in synaptic plasticity, learning, and memory are reversible in transgenic mice after switching off the toxic Tau mutant. *Journal of Neuroscience*, *31*(7), 2511–2525. https://doi.org/10.1523/JNEUROSCI.5245-10.2011

Tan, Y. L., Yuan, Y., & Tian, L. (2020). Microglial regional heterogeneity and its role in the brain. *Molecular Psychiatry*, *25*(2), 351–367. https://doi.org/10.1038/s41380-019-0609-8

Tanapat, P., Hastings, N. B., Reeves, A. J., & Gould, E. (1999). Estrogen stimulates a transient increase in the number of new neurons in the dentate gyrus of the adult female rat. *Journal of Neuroscience*, *19*(14), 5792–5801. https://doi.org/10.1523/JNEUROSCI.19-14-05792.1999

Tao, C. C., Cheng, K. M., Ma, Y. L., Hsu, W. L., Chen, Y. C., Fuh, J. L., Lee, W. J., Chao, C. C., & Lee, E. H. Y. (2020). Galectin-3 promotes Abeta oligomerization and Abeta toxicity in a mouse model of Alzheimer's disease. *Cell Death and Differentiation*, *27*(1), 192–209. https://doi.org/10.1038/s41418-019-0348-z

Thal, D. R., Rub, U., Orantes, M., & Braak, H. (2002). Phases of A beta-deposition in the human brain and its relevance for the development of AD. *Neurology*, *58*(12), 1791–1800. https://doi.org/10.1212/wnl.58.12.1791

Tobin, M. K., Musaraca, K., Disouky, A., Shetti, A., Bheri, A., Honer, W. G., Kim, N., Dawe, R. J., Bennett, D. A., Arfanakis, K., & Lazarov, O. (2019). Human hippocampal neurogenesis persists in aged adults and Alzheimer's disease patients. *Cell Stem Cell*, *24*(6), 974–982.e3. https://doi.org/10.1016/j.stem.2019.05.003

Tomic, J. L., Pensalfini, A., Head, E., & Glabe, C. G. (2009). Soluble fibrillar oligomer levels are elevated in Alzheimer's disease brain and correlate with cognitive dysfunction. *Neurobiology of Disease*, *35*(3), 352–358. https://doi.org/10.1016/j.nbd.2009.05.024

Trompet, S., Jukema, W., Mooijaart, S. P., Ford, I., Stott, D. J., Westendorp, R. G., & de Craen, A. J. (2012). Genetic variation in galectin-3 gene associates with cognitive function at old age. *Neurobiology of Aging*, *33*(9), 2232.e1–2232.e9. https://doi.org/10.1016/j.neurobiolaging.2012.05.001

Tronson, N. C., Schrick, C., Guzman, Y. F., Huh, K. H., Srivastava, D. P., Penzes, P., Guedea, A. L., Gao, C., & Radulovic, J. (2009). Segregated populations of hippocampal principal CA1 neurons mediating conditioning and extinction of contextual fear. *Journal of Neuroscience*, *29*(11), 3387–3394. https://doi.org/10.1523/JNEUROSCI.5619-08.2009

Turner, R. J., & Sharp, F. R. (2016). Implications of MMP9 for blood brain barrier disruption and hemorrhagic transformation following ischemic stroke. *Frontiers in Cellular Neuroscience*, *10*, 56. https://doi.org/10.3389/fncel.2016.00056

van Wilgenburg, B., Browne, C., Vowles, J., & Cowley, S. A. (2013). Efficient, long term production of monocyte-derived macrophages from human pluripotent stem cells under partly-defined and fully-defined conditions. *PLOS ONE*, *8*(8), e71098. https://doi.org/10.1371/journal.pone.0071098

Vancamp, P., Gothie, J. D., Luongo, C., Sebillot, A., Le Blay, K., Butruille, L., Pagnin, M., Richardson, S. J., Demeneix, B. A., & Remaud, S. (2019). Gender-specific effects of transthyretin on neural stem cell fate in the subventricular zone of the adult mouse. *Scientific Reports*, *9*(1), 19689. https://doi.org/10.1038/s41598-019-56156-w

Vargas-Caraveo, A., Sayd, A., Maus, S. R., Caso, J. R., Madrigal, J. L. M., Garcia-Bueno, B., & Leza, J. C. (2017). Lipopolysaccharide enters the rat brain by a lipoprotein-mediated transport mechanism in physiological conditions. *Scientific Reports*, *7*(1), 13113. https://doi.org/10.1038/s41598-017-13302-6

Villa, A., Gelosa, P., Castiglioni, L., Cimino, M., Rizzi, N., Pepe, G., Lolli, F., Marcello, E., Sironi, L., Vegeto, E., & Maggi, A. (2018). Sex-specific features of microglia from adult mice. *Cell Reports*, *23*(12), 3501–3511. https://doi.org/10.1016/j.celrep.2018.05.048

Walter, S., Letiembre, M., Liu, Y., Heine, H., Penke, B., Hao, W., Bode, B., Manietta, N., Walter, J., Schulz-Schuffer, W., & Fassbender, K. (2007). Role of the toll-like receptor 4 in neuroinflammation in Alzheimer's disease. *Cellular Physiology and Biochemistry*, *20*(6), 947–956. https://doi.org/10.1159/000110455

Wang, G., Li, R., Feng, C., Li, K., Liu, S., & Fu, Q. (2024). Galectin-3 is involved in inflammation and fibrosis in arteriogenic erectile dysfunction via the TLR4/MyD88/NF-kappaB pathway. *Cell Death Discovery*, *10*(1), 92. https://doi.org/10.1038/s41420-024-01859-x

Wang, P., & Ye, Y. (2021). Filamentous recombinant human Tau activates primary astrocytes via an integrin receptor complex. *Nature Communications*, *12*(1), 95. https://doi.org/10.1038/s41467-020-20322-w

Wang, T., Jin, X., Liao, Y., Sun, Q., Luo, C., Wang, G., Zhao, F., & Jin, Y. (2018). Association of NF-kappaB and AP-1 with MMP-9 overexpression in 2-chloroethanol exposed rat astrocytes. *Cells*, *7*(8), Article 96. https://doi.org/10.3390/cells7080096

Wang, X., Zhang, S., Lin, F., Chu, W., & Yue, S. (2015). Elevated Galectin-3 levels in the serum of patients with Alzheimer's disease. *American Journal of Alzheimer's Disease and Other Dementias*, *30*(8), 729–732. https://doi.org/10.1177/1533317513495107

Woodbury, M. E., & Ikezu, T. (2014). Fibroblast growth factor-2 signaling in neurogenesis and neurodegeneration. *Journal of Neuroimmune Pharmacology*, *9*(2), 92–101. https://doi.org/10.1007/s11481-013-9501-5

Wu, X., Gao, Y., Shi, C., Tong, J., Ma, D., Shen, J., Yang, J., & Ji, M. (2023). Complement C1q drives microglia-dependent synaptic loss and cognitive impairments in a mouse model of lipopolysaccharide-induced neuroinflammation. *Neuropharmacology*, *237*, 109646. https://doi.org/10.1016/j.neuropharm.2023.109646

Xiao, X., Liu, H., Liu, X., Zhang, W., Zhang, S., & Jiao, B. (2021). APP, PSEN1, and PSEN2 variants in Alzheimer's disease: Systematic re-evaluation according to ACMG guidelines. *Frontiers in Aging Neuroscience*, *13*, 695808. https://doi.org/10.3389/fnagi.2021.695808

Xu, F., Ono, M., Ito, T., Uchiumi, O., Wang, F., Zhang, Y., Sun, P., Zhang, Q., Yamaki, S., Yamamoto, R., & Kato, N. (2021). Remodeling of projections from ventral hippocampus to prefrontal cortex in Alzheimer's mice. *Journal of Comparative Neurology*, *529*(7), 1486–1498. https://doi.org/10.1002/cne.25032

Xue, S., Lozinski, B. M., Ghorbani, S., Ta, K., D'Mello, C., Yong, V. W., & Dong, Y. (2023). Elevated Galectin-3 is associated with aging, multiple sclerosis, and oxidized phosphatidylcholine-induced neurodegeneration. *Journal of Neuroscience*, *43*(25), 4725–4737. https://doi.org/10.1523/JNEUROSCI.2312-22.2023

Yan, P., Hu, X., Song, H., Yin, K., Bateman, R. J., Cirrito, J. R., Xiao, Q., Hsu, F. F., Turk, J. W., Xu, J., Hsu, C. Y., Holtzman, D. M., & Lee, J. M. (2006). Matrix metalloproteinase-9 degrades amyloid-beta fibrils in vitro and compact plaques in situ. *Journal of Biological Chemistry*, *281*(34), 24566–24574. https://doi.org/10.1074/jbc.M602440200

Yang, C. C., Lin, C. C., Hsiao, L. D., Kuo, J. M., Tseng, H. C., & Yang, C. M. (2019). Lipopolysaccharide-induced matrix metalloproteinase-9 expression associated with cell migration in rat brain astrocytes. *International Journal of Molecular Sciences*, *21*(1), Article 259. https://doi.org/10.3390/ijms21010259

Yeh, H., De Cruz, M. A., You, Y., Ikezu, S., & Ikezu, T. (2025). Development and characterization of in vitro inducible immortalization of a murine microglia cell line for high throughput studies. *Scientific Reports*, *15*(1), 3207. https://doi.org/10.1038/s41598-025-87543-1

Yin, Q., Chen, J., Ma, S., Dong, C., Zhang, Y., Hou, X., Li, S., & Liu, B. (2020). Pharmacological inhibition of Galectin-3 ameliorates diabetes-associated cognitive impairment, oxidative stress and neuroinflammation in vivo and in vitro. *Journal of Inflammation Research*, *13*, 533–542. https://doi.org/10.2147/JIR.S273858

Yip, P. K., Carrillo-Jimenez, A., King, P., Vilalta, A., Nomura, K., Chau, C. C., Egerton, A. M., Liu, Z. H., Shetty, A. J., Tremoleda, J. L., Davies, M., Deierborg, T., Priestley, J. V., Brown, G. C., Michael-Titus, A. T., Venero, J. L., & Burguillos, M. A. (2017). Galectin-3 released in response to traumatic brain injury acts as an alarmin orchestrating brain immune response and promoting neurodegeneration. *Scientific Reports*, *7*, 41689. https://doi.org/10.1038/srep41689

Zabel, M. K., Zhao, L., Zhang, Y., Gonzalez, S. R., Ma, W., Wang, X., Fariss, R. N., & Wong, W. T. (2016). Microglial phagocytosis and activation underlying photoreceptor degeneration is regulated by CX3CL1-CX3CR1 signaling in a mouse model of retinitis pigmentosa. *Glia*, *64*(9), 1479–1491. https://doi.org/10.1002/glia.23016

Zaheer, A., Zaheer, S., Thangavel, R., Wu, Y., Sahu, S. K., & Yang, B. (2008). Glia maturation factor modulates beta-amyloid-induced glial activation,

inflammatory cytokine/chemokine production and neuronal damage. *Brain Research*, *1208*, 192–203. https://doi.org/10.1016/j.brainres.2008.02.093

Zhang, H., Liu, L., Jiang, C., Pan, K., Deng, J., & Wan, C. (2020). MMP9 protects against LPS-induced inflammation in osteoblasts. *Innate Immunity*, *26*(4), 259–269. https://doi.org/10.1177/1753425919887236

Zhao, Z., Xu, X., Cheng, H., Miller, M. C., He, Z., Gu, H., Zhang, Z., Raz, A., Mayo, K. H., Tai, G., & Zhou, Y. (2021). Galectin-3 N-terminal tail prolines modulate cell activity and glycan-mediated oligomerization/phase separation. *Proceedings of the National Academy of Sciences of the United States of America*, *118*(19), Article e2021074118. https://doi.org/10.1073/pnas.2021074118

Zheng, M., Liu, J., Ruan, Z., Tian, S., Ma, Y., Zhu, J., & Li, G. (2013). Intrahippocampal injection of Abeta1-42 inhibits neurogenesis and down-regulates IFN-gamma and NF-kappaB expression in hippocampus of adult mouse brain. *Amyloid*, *20*(1), 13–20. https://doi.org/10.3109/13506129.2012.755122

Zhou, Q. G., Lee, D., Ro, E. J., & Suh, H. (2016). Regional-specific effect of fluoxetine on rapidly dividing progenitors along the dorsoventral axis of the hippocampus. *Scientific Reports*, *6*, 35572. https://doi.org/10.1038/srep35572

Zhou, W., Chen, X., Hu, Q., Chen, X., Chen, Y., & Huang, L. (2018). Galectin-3 activates TLR4/NF-kappaB signaling to promote lung adenocarcinoma cell proliferation through activating lncRNA-NEAT1 expression. *BMC Cancer*, *18*(1), 580. https://doi.org/10.1186/s12885-018-4461-z

Zhu, B., Wang, Z. G., Ding, J., Liu, N., Wang, D. M., Ding, L. C., & Yang, C. (2014). Chronic lipopolysaccharide exposure induces cognitive dysfunction without affecting BDNF expression in the rat hippocampus. *Experimental and Therapeutic Medicine*, *7*(3), 750–754. https://doi.org/10.3892/etm.2014.1479

Zucco, A. (2018). *adrigabzu/sholl_analysis_in_R: AUC calculation and stats*. In Zenodo.

Chapter 10: Appendix

Origin	Target		Application	Dilution	Company	Catalogue number
Rat	Galectin-3 (M3/38)	Monoclonal	IHC/ICC	1 in 100	Santa Cruz	sc23938
Mouse	Beta-Amyloid (W0-2)	Monoclonal	IHC	1 in 300	Sigma-Aldrich	MABN10
Goat	Iba1	Polyclonal	IHC/ICC	1 in 300	Abcam	ab5076
Mouse	Mash1	Monoclonal	IHC	1 in 100	Invitrogen	14-5794-82
Rabbit	Doublecortin	Polyclonal	IHC/ICC	1 in 400	Cell Signaling Technology	4604S
Mouse	Beta-III-Tubulin	Monoclonal	ICC	1 in 500	Abcam	ab78078
Rabbit	GFAP	Polyclonal	IHC/ICC	1 in 100	Sigma-Aldrich	G9269
Rat	GFAP (2.2B10)	Monoclonal	ICC	1 in 100	Sigma-Aldrich	13-0300

Supplemental Table 2.4: List of antibodies used for immunofluorescence and their concentrations

Origin	Target		Application	Dilution	Company	Catalogue number
Rabbit	Mmp9 (RM1020)	Multiclonal	WB	1 in 400	Abcam	ab283575
Mouse	Beta-Actin	Monoclonal	WB	1 in 20 000	Proteintech	66009-1-IG
Mouse	Beta-Amyloid (W0-2)	Monoclonal	WB	1 in 300	Sigm-Aldrich	MABN10
Rat	Galectin-3 (M3/38)	Monoclonal	WB	1 in 200	Santa Cruz	sc23938

Supplemental Table 2.7: List of antibodies used for western blot and their concentrations

Gene		Sequence	Concentration	Efficiency (%)
Lst1	F	CGGTTCAGTCAGAGAGTGAAGA	0.1 μM	92.8
Lst1	R	GATGCATAGTGGGGCTCCTG	0.1 μM	92.8
Il17ra	F	AGTTCCCAAGCCAGTTGCAG	0.5 μM	92.5
Il17ra	R	GTGATCAGGAACTGGGCGAA	0.5 μM	92.5
Clec4a3	F	GAATGCATTTTCTGTCCGCGA	0.1 μM	95.7
Clec4a3	R	TTCTTCCTTTGGGGAGCTGGC	0.1 μM	95.7
Cst7	F	TGCCTTGAAGCGGACTCTAT	0.1 μM	105.8
Cst7	R	AGTGGGGAAAACACGAGTGG	0.1 μM	105.8
Lpl	F	TCGTCATCGAGAGGATCCGA	0.1 μM	100.5
Lpl	R	TGTTTGTCCAGTGTCAGCCA	0.1 μM	100.5
Lgals3	F	TAATCAGGTGAGCGGCACAG	0.5 μM	96.8
Lgals3	R	GCTAAGGCATCGTTAAGCGAAA	0.5 μM	96.8
P2ry12	F	TACCCTACAGAAACACTCAAGGC	0.1 μM	83.3
P2ry12	R	CCCAGGGGAGAAGGTGGTAT	0.1 μM	83.3
Cxcl10	F	CCACGTGTTGAGATCATTGCC	0.1 μM	83.8
Cxcl10	R	GAGGCTCTCTGCTGTCCATC	0.1 μM	83.8
Ccl5	F	GTGCCCACGTCAAGGAGTAT	0.1 μM	93
Ccl5	R	TCGAGTGACAAACACGACTG	0.1 μM	93
Il6	F	CGGCCTTCCCTACTTCACAA	0.1 μM	88.6
Il6	R	TTGCCATTGCACAACTCTTTTC	0.1 μM	88.6
Tnfa	F	CCCACGTCGTAGCAAACCA	0.1 μM	101.4
Tnfa	R	ACAAGGTACAACCCATCGGC	0.1 μM	101.4
HexB	F	AACTCAAGTGTTTGGGCCTGT	0.1 μM	100.9
HexB	R	GTTTGGATTTGATGCCCAACAT	0.1 μM	100.9
Tyrobp	F	CTGATTGCCCTGGCTGTGTA	0.1 μM	85.5

Tyrobp	R	TGTTGTTTCCGGGTCCCTTC	0.1 μM	85.5
Cd33	F	TTCTTGGGCTCTGTCTCGTG	0.1 μM	92.7
Cd33	R	GTGATCGCTTCCTGCCTCTTG	0.1 μM	92.7
Rab7b	F	ACCAAAACCGTTTGCGTTCT	0.1 μM	98.8
Rab7b	R	GGTCTTTCCCACGCCAAGT	0.1 μM	98.8
Ccl3	F	GCAACCAAGTCTTCTCAGCG	0.5 μM	86.6
Ccl3	R	TCTCTTAGTCAGGAAAATGACACC	0.5 μM	86.6
Ccl4	F	CTGTGCAAACCTAACCCCGA	0.5 μM	112.3
Ccl4	R	AGGGTCAGAGCCCATTGGT	0.5 μM	112.3
CtsB	F	ATTCACACCAATGGCCGAGT	0.5 μM	100.5
CtsB	R	TAGCCACCATTACAGCCGTC	0.5 μM	100.5
CtsD	F	GCAGTGCCTCTTATCCAGGG	0.1 μM	112.3
CtsD	R	CACCCTGCGATACCTTGAGTA	0.1 μM	112.3
CtsZ	F	CTGGGGCGCAGGACTTATC	0.1 μM	101.3
CtsZ	R	GTACGGACAGCAGGATGGAG	0.1 μM	101.3
Hprt	F	CAGTCCCAGCGTCGTGATTA	0.1 μM	109.5
Hprt	R	TGGCCTCCCATCTCCTTCAT	0.1 μM	109.5
ActB	F	CACTGTCGAGTCGCGTCC	0.1 μM	91.1
ActB	R	TCATCCATGGCGAACTGGTG	0.1 μM	91.1

Supplemental Table 2.8: Sequences of primers used

Galectin-3 expressing (Gal-3+) v.s. non-expressing (Gal-3-) cells in 3M C57Bl6 mice											
	Sholl Decay										
	Gal-3+		Gal-3-							p-value	
	Average	Stdev	Average	Stdev	t-stat	df	Cohen d	lower	upper	t-test	p-exact
Males	0.060	0.020	0.056	0.009	0.956	2.357	0.781	-0.043	0.026	0.213	
Combined	0.059	0.016	0.057	0.009	0.819519	5.147806	0.518309	-0.01894	0.009724	0.224378	
	Ramification Index										
	Gal-3+		Gal-3-							p-value	
	Average	Stdev	Average	Stdev	t-stat	df	Cohen d	lower	upper	t-test	p-exact
Males	1.910	0.708	2.327	0.601	1.713028	3.825358	1.398681	-0.30624	1.247949	0.082562	
Combined	1.781	0.593	2.126	0.602	1.307	7.413	0.826	-0.243	0.859	0.115	
	Sum intersections										
	Gal-3+		Gal-3-							p-value	
	Average	Stdev	Average	Stdev	t-stat	Df	Cohen d	lower	upper	t-test	p-exact
Males	101.75	41.28201	110.5385	30.23689	1.091	2.063	0.891157	-55.178	94.189	0.193	
Combined	109.5714	41.93635	115.56	31.8827	0.351467	5.725516	0.222288	-33.1933	44.17778	0.368904	
	End Radius										
	Gal-3+		Gal-3-							p-value	
	Average	Stdev	Average	Stdev	t-stat	Df	Cohen d	lower	upper	t-test	p-exact
Males	35.88	10.56727	36.62308	7.385802	0.733484	2.905066	0.598888	-12.2321	19.3851	0.258985	
Combined	37.55571	10.37658	36.5976	8.27396	0.041	7.478	0.025911	-8.268	7.983	0.484	
	Soma Size										
	Gal-3+		Gal-3-							p-value	
	Average	Stdev	Average	Stdev	t-stat	Df	Cohen d	lower	upper	t-test	p-exact
Males	57.26417	36.73525	42.08193	12.25715	0.392775	2.587599	0.3207	-49.4773	37.21346	0.36228	
Combined	46.32767	21.07337	50.39908	7.36175	0.620	5.298	0.392398	-27.417	16.610	0.280344	

Supplementary Table 4.2.1: Statistical analysis of Gal-3+ v.s. Gal-3- microglia in young adult WT mice

Galectin-3 expressing (Gal-3+) v.s. non-expressing (Gal-3-) cells in 7M C57Bl6 mice											
	Sholl Decay										
	Gal-3+		Gal-3-							p-value	
	Average	Stdev	Average	Stdev	t-stat	df	Cohen d	lower	upper	t-test	p-exact
Males	0.057616	0.00957	0.057698	0.00701	0.323514	4.600706	0.228759	-0.00852	0.006657	0.380244	
	Ramification Index										
	Gal-3+		Gal-3-							p-value	
	Average	Stdev	Average	Stdev	t-stat	df	Cohen d	lower	upper	t-test	p-exact
Males	1.660311	0.498352	2.06875	0.88677	0.204512	5.998361	0.144612	-0.70303	0.831257	0.422358	0.442857
	Sum intersections										
	Gal-3+		Gal-3-							p-value	
	Average	Stdev	Average	Stdev	t-stat	Df	Cohen d	lower	upper	t-test	p-exact
Males	102.0909	27.68557	93.25	26.08422	1.046789	5.987446	0.740192	-54.0039	21.65395	0.167802	
	End Radius										
	Gal-3+		Gal-3-							p-value	
	Average	Stdev	Average	Stdev	t-stat	Df	Cohen d	lower	upper	t-test	p-exact
Males	36.69545	10.01721	34.5	6.968658	0.229698	4.465474	0.162421	-7.40984	8.807095	0.414235	
	Soma Size										
	Gal-3+		Gal-3-							p-value	
	Average	Stdev	Average	Stdev	t-stat	Df	Cohen d	lower	upper	t-test	p-exact
Males	66.74064	23.64635	48.697	9.458294	0.77319	4.259215	0.546728	-39.0695	21.72965	0.240044	

Supplementary Table 4.2.2: Statistical analysis of Gal-3+ v.s. Gal-3- microglia in middle-aged WT mice

3M v.s. 7M Galectin-3$^{+/+}$ mice											
	Sholl Decay										
	Gal-3+		Gal-3-							p-value	
	Average	Stdev	Average	Stdev	t-stat	df	Cohen d	lower	upper	t-test	p-exact
Males	0.058158	0.014721	0.057659	0.008136	0.233443	3.076596	0.193519	-0.00965	0.011199	0.415046	
	Ramification Index										
	Gal-3+		Gal-3-							p-value	
	Average	Stdev	Average	Stdev	t-stat	df	Cohen d	lower	upper	t-test	p-exact
Males	2.126768	0.675216	1.87341	0.741342	1.592015	3.607511	1.276779	-0.20443	0.702163	0.097116	
	Sum intersections										
	Gal-3+		Gal-3-							p-value	
	Average	Stdev	Average	Stdev	t-stat	Df	Cohen d	lower	upper	t-test	p-exact
Males	106.32	35.47267	97.47826	26.62683	1.059882	4.942967	0.752628	-17.8101	42.65354	0.169109	
	End Radius										
	Gal-3+		Gal-3-							p-value	
	Average	Stdev	Average	Stdev	t-stat	Df	Cohen d	lower	upper	t-test	p-exact
Males	36.2664	8.865627	35.55	8.435026	0.66614	2.618951	0.571324	-2.85855	4.221122	0.279627	
	Soma Size										
	Gal-3+		Gal-3-							p-value	
	Average	Stdev	Average	Stdev	t-stat	Df	Cohen d	lower	upper	t-test	p-exact
Males	49.08912	27.04569	57.71882	19.85272	0.602873	3.093364	0.499204	-45.6718	30.91466	0.293967	

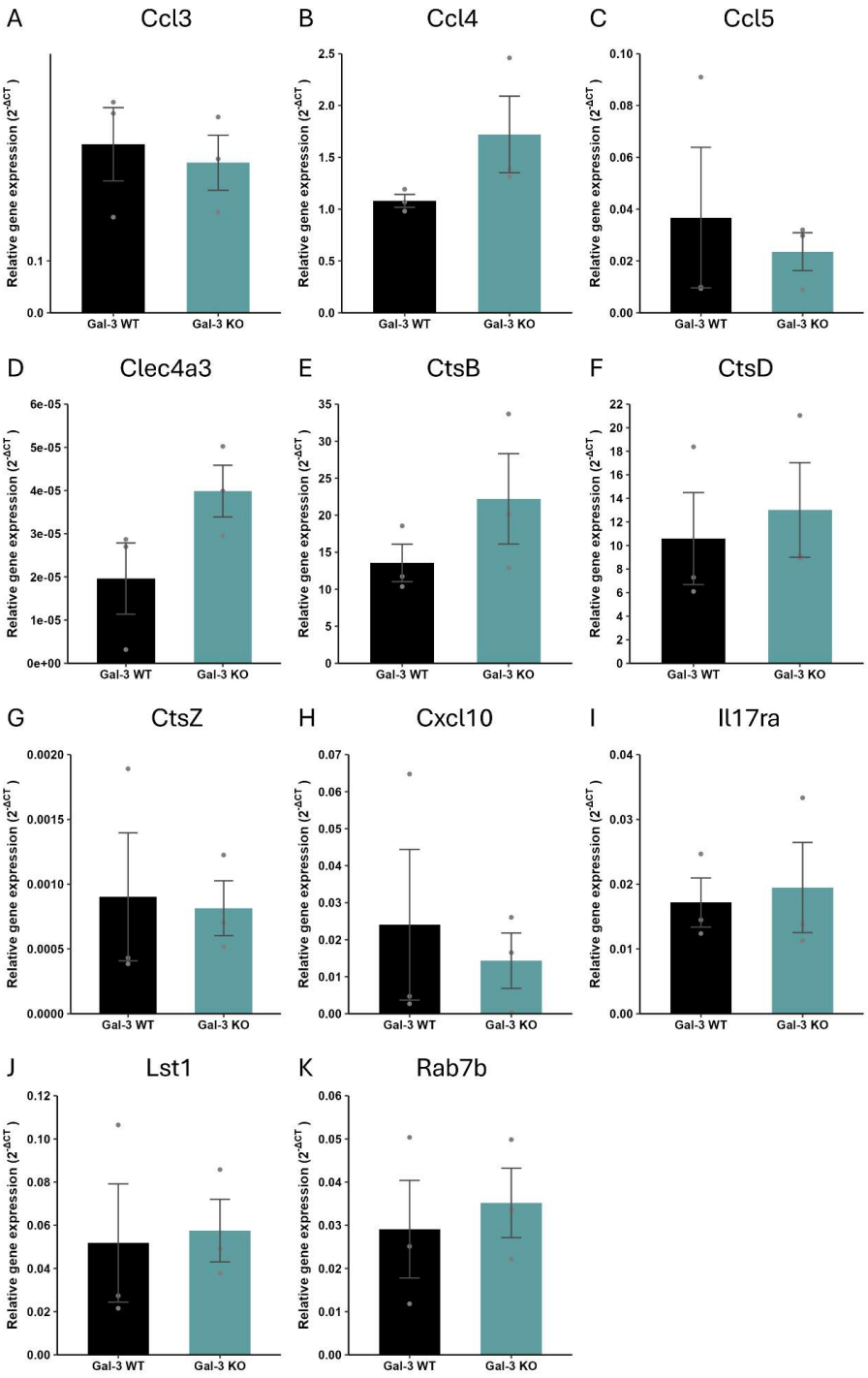
Supplementary Table 4.3: Statistical analysis of microglia between young adult and middle-aged WT mice

Galectin-3 WT (Galectin-3$^{+/+}$) v.s. KO (Galectin-3$^{-/-}$) microglia in 3M mice											
	Sholl Decay										
	Gal-3+		Gal-3-							p-value	
	Average	Stdev	Average	Stdev	t-stat	df	Cohen d	lower	upper	t-test	p-exact
Males	0.058158	0.014721	0.04723	0.010416	2.513	3.863	2.052	-0.001	0.025	0.034	
Combined	0.058	0.013	0.052	0.012	2.125615	8.587469	1.235381	-0.0005	0.014389	0.031957	
	Ramification Index										
	Gal-3+		Gal-3-							p-value	
	Average	Stdev	Average	Stdev	t-stat	df	Cohen d	lower	upper	t-test	p-exact
Males	2.126768	0.675216	2.054167	0.353076	0.112043	3.345565	0.091483	-0.77425	0.718573	0.45859	
Combined	1.968237	0.615983	1.959369	0.653115	0.253	8.811	0.148	-0.410	0.328	0.403	
	Sum intersections										
	Gal-3+		Gal-3-							p-value	
	Average	Stdev	Average	Stdev	t-stat	Df	Cohen d	lower	upper	t-test	p-exact
Males	106.32	35.47267	102.875	13.97383	0.080	3.885	0.065438	-29.306	31.027	0.470	
Combined	112.8261	36.50833	100.2222	23.21905	1.368029	8.478482	0.832159	-6.68275	26.65436	0.10323	
	End Radius										
	Gal-3+		Gal-3-							p-value	
	Average	Stdev	Average	Stdev	t-stat	Df	Cohen d	lower	upper	t-test	p-exact
Males	36.2664	8.865627	42.9525	8.694704	1.899633	2.327887	1.551044	-19.5592	6.454808	0.089826	
Combined	37.035	9.197762	38.87	8.536469	1.165	7.490	0.663066	-8.919	2.979	0.140	
	Soma Size										
	Gal-3+		Gal-3-							p-value	
	Average	Stdev	Average	Stdev	t-stat	Df	Cohen d	lower	upper	t-test	p-exact
Males	49.08912	27.04569	54.50456	10.27626	0.713811	2.25898	0.582824	-51.2037	35.23151	0.270947	
Combined	46.32767	13.28367	50.39908	11.95342	0.530	8.224	0.324104	-13.573	21.716	0.305199	

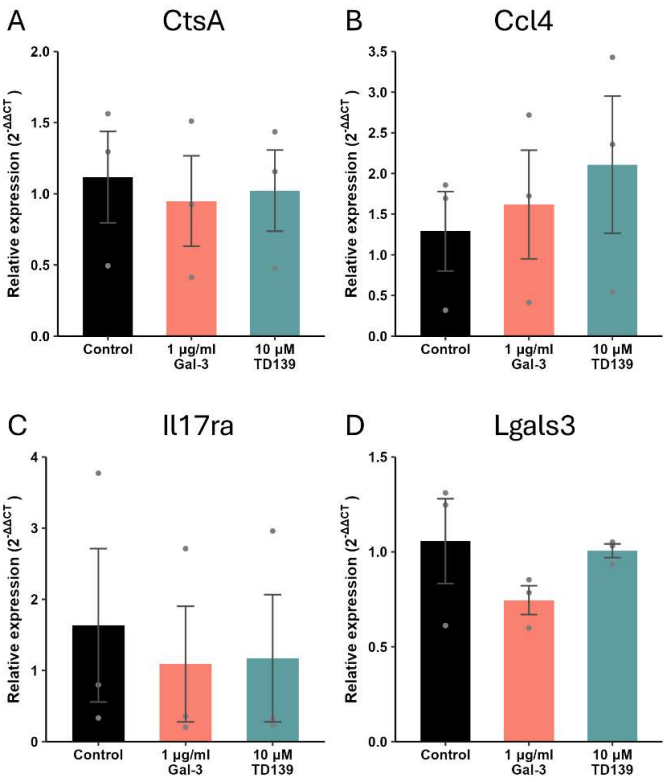
Supplementary Table 4.4.1: Statistical analysis of microglia from Galectin-3$^{+/+}$ and Galectin-3$^{-/-}$ mice in young adult mice

Galectin-3 WT (Galectin-3$^{+/+}$) v.s. KO (Galectin-3$^{-/-}$) microglia in 7M mice											
	Sholl Decay										
	Gal-3+		Gal-3-							p-value	
	Average	Stdev	Average	Stdev	t-stat	df	Cohen d	lower	upper	t-test	p-exact
Males	0.057659	0.008136	0.051165	0.007932	3.009982	4.643725	2.270689	0.000852	0.01268	0.01634	0.028571
	Ramification Index										
	Gal-3+		Gal-3-							p-value	
	Average	Stdev	Average	Stdev	t-stat	df	Cohen d	lower	upper	t-test	p-exact
Males	1.87341	0.741342	2.32477	1.267896	0.910732	2.215319	0.811057	-1.82489	1.137614	0.225212	
	Sum intersections										
	Gal-3+		Gal-3-							p-value	
	Average	Stdev	Average	Stdev	t-stat	Df	Cohen d	lower	upper	t-test	p-exact
Males	97.47826	26.62683	99.47368	21.48738	0.599073	4.910764	0.423688	-36.9357	23.03572	0.287843	
	End Radius										
	Gal-3+		Gal-3-							p-value	
	Average	Stdev	Average	Stdev	t-stat	Df	Cohen d	lower	upper	t-test	p-exact
Males	35.55	8.435026	40.85526	8.275459	2.947446	2.211977	2.625795	-11.4681	1.639401	0.043646	
	Soma Size										
	Gal-3+		Gal-3-							p-value	
	Average	Stdev	Average	Stdev	t-stat	Df	Cohen d	lower	upper	t-test	p-exact
Males	59.57218	0.578697	46.72613	3.786048	5.809377	2.093401	4.743336	3.7272	21.96492	0.012756	0.05

Supplementary Table 4.4.2: Statistical analysis of microglia from Galectin-3$^{+/+}$ and Galectin-3$^{-/-}$ mice in middle-aged mice



Supplemental Figure 4.5: Further genes in qPCR analysis between Galectin-$3^{+/+}$ and Galectin-$3^{-/-}$ primary murine microglia.



Supplemental figure 4.6: Further genes in qPCR analysis between BV2 microglia treated with Galectin-3 or TD-139

	Saline	LPS	
Galectin-3 WT	0.015777	0.235827	
Galectin-3 WT	0.028097	0.829607	
Galectin-3 WT	0.135835	1.224987	
Galectin-3 KO	0.021911	0.057075	
Galectin-3 KO	0.041221	0.850613	
Galectin-3 KO	0.061586	0.563406	

COUNT	Saline	LPS	balanced
Galectin-3 WT	3	3	6
Galectin-3 KO	3	3	6
	6	6	12

MEAN

	Saline	LPS	
Galectin-3 WT	0.059899	0.763474	0.411686
Galectin-3 KO	0.041574	0.490364	0.265967
	0.050734	0.626919	0.338827

VARIANCE

	Saline	LPS	
Galectin-3 WT	0.004363	0.247897	0.249407
Galectin-3 KO	0.000393	0.161427	0.125153
	0.002003	0.186103	0.176045

Two Factor Anova

ANOVA Alpha 0.05

	SS	*df*	*MS*	*F*	*p-value*	*p eta-sq*
Rows	0.063702	1	0.063702	0.615371	0.455371	0.071427
Columns	0.995967	1	0.995967	9.621175	0.014626	0.546001
Inter	0.048685	1	0.048685	0.470303	0.512228	0.055524
Within	0.828146	8	0.103518			
Total	1.9365	11	0.176045			

Supplementary Table 6.3.1: Two-way ANOVA of Galectin-$3^{+/+}$ and Galectin-$3^{-/-}$ **male** mice treated with saline or LPS.

	CT	LPS
Galectin-3 WT	0.09190 1	0.18814 2
Galectin-3 WT	0.03949 1	0.08348 3
Galectin-3 WT	0.00204 4	0.04336 2
Galectin-3 KO	0.04702 6	1.00186 1
Galectin-3 KO	0.01459 9	0.73798 6
Galectin-3 KO	0.00593 8	0.20550 1

COUNT

	CT	LPS	balanced
Galectin-3 WT	3	3	6
Galectin-3 KO	3	3	6
	6	6	12

MEAN

	CT	LPS	
Galectin-3 WT	0.04447 9	0.10499 6	0.07473 7
Galectin-3 KO	0.02252 1	0.64844 9	0.33548 5
	0.0335	0.37672 3	0.20511 1

VARIANCE

	CT	LPS	
Galectin-3 WT	0.00203 7	0.00558 7	0.00414 9
Galectin-3 KO	0.00046 9	0.16456	0.18354 7
	0.00114 7	0.15666 2	0.10385 9

Two Factor Anova

ANOVA				Alpha	0.05	
	SS	*df*	*MS*	*F*	*p-value*	*p eta-sq*
Rows	0.203969	1	0.203969	4.725505	0.061451	0.371341
Columns	0.353405	1	0.353405	8.187617	0.021106	0.505795
Inter	0.239768	1	0.239768	5.554882	0.046183	0.409807
Within	0.345307	8	0.043163			
Total	1.142449	11	0.103859			

Supplementary Table 6.3.2: Two-way ANOVA of Galectin-3$^{+/+}$ and Galectin-3$^{-/-}$ **female** mice treated with saline or LPS.